

**Biochemical and structural characterization of
Sirtuins from mammals and *Thermotoga maritima***

DISSERTATION

To obtain the degree

Doktor der Naturwissenschaften (Dr. rer. nat.)

Fakultät für Biologie, Chemie und Geowissenschaften,

Universität Bayreuth

Submitted by

Mahadevan Lakshminarasimhan

Bayreuth, 2012

This doctoral thesis was prepared at the Department of Physiological Chemistry, Ruhr-University Bochum, Germany and at the Department of Biochemistry, University of Bayreuth, Germany, in affiliations with International Max Planck Research School in Chemical Biology (IMPRS-CB) Ph.D. program, Max Planck Institute of Molecular Physiology, Dortmund Germany, and Elite Network of Bavaria, BioMedTech International graduate School of Science (BIGSS) Ph.D. program, University of Bayreuth, Germany from December 2008 until March 2012 supervised by Prof. Dr. Clemens Steegborn.

This is a full reprint of the dissertation submitted to attain the academic degree of Doctor of Natural Sciences (Dr. rer. nat.) and approved by the Faculty of Biology, Chemistry and Geosciences of the University of Bayreuth.

Acting dean: Prof. Dr. Beate Lohnert

Date of submission: 7th March, 2012

Date of defense: 11th May, 2012

Doctoral Committee:

Prof Dr. Clemens Steegborn 1st reviewer

Prof Dr. Wulf Blankenfeldt 2nd reviewer

Prof. Dr. Paul Rösch Chairman

Prof. Dr. Rainer Schobert

Dedicated to

Gina and my parents

Acknowledgements

There is a famous saying: “Behind every successful man is a great woman”, but in my case there are two (my mom and Gina) and I dedicate this thesis to them and also to my dad. Without their support, help and encouragement, I wouldn’t be where I’m now. They are my constant source of energy and inspiration and have always helped me pursue my dreams. I’m really fortunate to have such people in my life.

I’m also grateful to my family and friends for their constant support and encouragement.

I thank my research adviser Prof. Dr. Clemens Steegborn, for providing me the opportunity to work in his laboratory with exciting research topics, for his constant support and excellent scientific discussions.

I would also like to thank all the members of the biochemistry department, University of Bayreuth, Germany for all the support and a good working atmosphere.

I also thank Prof. Dr. Wulf Blankenfeldt (Department of Biochemistry, University of Bayreuth, Germany), Prof. Dr. Olaf Stemmann (Department of genetics, University of Bayreuth, Germany), Prof. Dr. Mike Schutkowski (University of Halle, Germany), Dr. Ute Curth (Hannover Medical school, Germany), Dr. Dirk Wolters (Ruhr University, Bochum, Germany) and Dr. Stefan Raunser (Max Planck Institute of Molecular Physiology, Dortmund, Germany) for fruitful discussions and collaborations.

Thanks also to Prof. Dr. Roger Goody, Prof. Dr. Martin Engelhard, Dr. Waltraud Hofmann-Goody and Ms. Christa Hornemann from the Max Planck Institute of Molecular Physiology, Dortmund, Germany for helping me with the IMPRS-CB (International Max Planck Research School in Chemical Biology) PhD program and supporting my scientific endeavors.

I also thank Prof. Dr. Paul Rösch, PD. Dr. Stephan Schwarzingler and Ms. Violaine Zigan for helping me with the ENB (Elite Network of Bavaria)/BIGSS (BioMedTec International Graduate School of Science) Ph.D. program at the University of Bayreuth, Germany.

I thank the IMPRS-CB Ph.D. program, MPI, Dortmund, Germany and ENB (Elite Network of Bavaria)/BIGSS (BioMedTec International Graduate School of Science) Ph.D. program, University of Bayreuth, Germany, for funding and financial support to carry out my research.

Publications and presentations pertaining to this work

Peer reviewed publications:

Christine Schlicker, Gina Boanca, Mahadevan Lakshminarasimhan, Clemens Steegborn (2011) Structure-based Development of Novel Sirtuin Inhibitors. *Aging*. 3: 852-872.

Mahadevan Lakshminarasimhan, Clemens Steegborn (2010) Emerging mitochondrial signaling mechanisms in physiology, aging processes, and as drug targets. *Exp. Gerontol.* 46: 174-177.

Manuscripts submitted and in preparation:

Frank Fischer, Melanie Gertz, Benjamin Suenkel, Mahadevan Lakshminarasimhan, Mike Schuttkowski, Clemens Steegborn (2012) A refined Mass spectrometry deacetylation assay reveals Sirt5 as Nicotinamide insensitive subfamily. *Manuscript submitted to ACS Chemical Biology*.

Mahadevan Lakshminarasimhan, Melanie Gertz, Giang Thi Tuyet Nguyen, Michael Weyand, Clemens Steegborn (2012) The molecular mechanism of Sirtuin inhibition by Ex-527. *Manuscript in preparation*.

Mahadevan Lakshminarasimhan, Melanie Gertz, Frank Fischer, David Rauh, Ute Curth, Mike Schuttkowski, Clemens Steegborn (2012) Resveratrol is a sequence-specific activator for Sirt1-dependent peptide and protein deacetylation. *Manuscript in preparation*.

David Rauh, Frank Fischer, Mahadevan Lakshminarasimhan, Melanie Gertz, Tim Bergbrede, Mike Schuttkowski, Clemens Steegborn (2012) Specificities and substrates of human Sirtuin isoforms revealed by profiling against an acetylome peptide array. *Manuscript in preparation*.

Conferences, courses and symposiums:

Oral and poster presentation at the Elite Network of Bavaria Structure Days symposium – Thurnau, Germany July’11, titled “Structural and biochemical characterization of Sirtuins.”

Poster presentation at the EMBO practical course on exploiting anomalous scattering in macromolecular structure determination, ESRF, Grenoble, France June’11m titled “Structural and biochemical characterization of mammalian Sirtuins”.

Oral presentation at the Max Planck Institute of Molecular Physiology – Dortmund, Germany, Sep’10, titled “Structural and biochemical characterization of mammalian Sirt1.”

Oral and poster presentation at the Elite Network of Bavaria Structure Days symposium – Thurnau, Germany July’10, titled “Structural and biochemical characterization of mammalian Sirt1.”

List of other publications and presentations**Publications:**

Mahadevan Lakshminarasimhan*, Peter Madzellan*, Ruth Nan, Nicole M. Milkovic, Mark A. Wilson (2010) Evolution of new enzymatic function by structural modulation of cysteine reactivity in *Pseudomonas fluorescens* isocyanide hydratase. *Journal of Biological chemistry*. 285: 29651-29661.

Jeff Blackinton*, Mahadevan Lakshminarasimhan*, Kelly J Thomas, Rili Ahmad, Ashraf S. Raza, Mark R. Cookson and Mark A. Wilson (2009) Formation of A Stabilized Cysteine Sulfinic Acid is Critical for the Mitochondrial Function of the Parkinsonism Protein Dj-1. *Journal of Biological chemistry*. 284: 6476–6485.

Featured on the Cover of the Journal of Biological chemistry, issue March 6, 2009.

Anna C. Witt, Mahadevan Lakshminarasimhan, Benjamin C. Remington, Sahar Hasim, Edwin Pozharski and Mark A. Wilson (2008) Cysteine pKa Depression by a Protonated Glutamic Acid in Human DJ-1. *Biochemistry*. 47: 7430-7440.

Mahadevan Lakshminarasimhan*, Marien Maldonado*, Wenbo Zhou, Anthony Fink and Mark A. Wilson (2008) The Impact of Three Parkinsonism-Associated Point Mutations on the Structure and Redox-Regulated Stability of DJ-1. *Biochemistry*. 47: 1381-1392.

Featured on the ACS Publications web site as a most-accessed article of the 1st quarter of 2008.*** = Equal contribution**

Mahadevan Lakshminarasimhan, Alajos Bérczi, Han Asard (2006) Substrate-dependent reduction of a recombinant chromaffin granule Cyt-b561 and its R72A mutant. *Acta Biol Szeged*. 50(1-2): 61-65.

Alajos Bérczi, Dan Su, Mahadevan Lakshminarasimhan, Amy Vargas and Han Asard (2005) Heterologous expression and site-directed mutagenesis of an ascorbate-reducible cytochrome b561. *Archives of Biochemistry and Biophysics*. 443: 82-92.

Presentations and posters:

Oral presentation at the Max Planck Institute of Molecular Physiology – Dortmund, Germany, Apr'09, titled “Molecular basis for the cytoprotective function of the Parkinsonism protein DJ-1.”

Poster presentation in American Crystallographic Association Annual meeting 2008 at Knoxville, Tennessee, USA, titled “Structural Impact of Three Parkinsonism-Associated Missense Mutations of Human DJ-1.”

Poster presentation in Redox Biology center-University of Nebraska-Lincoln, symposium titled “The structural determinants of regulatory cysteine oxidation in the Parkinsonism-associated protein DJ-1”

Poster presentation in Redox Biology center-University of Nebraska-Lincoln, symposium titled “Characterization and mutational studies on a mouse Cytochrome b561”

Abbreviations:

AATase	Aspartate aminotransferase 2
ACN	acetonitrile
ACS	acetyl-CoA synthetase
ADP	adenosine diphosphate
ADPr	ADP-ribose
AEC	anion exchange chromatography
AMC	7-amino-4-methylcoumarin
ANT	ADP/ATP carrier protein
AR	androgen receptor
AROS	active regulator of SIRT1
ART	adp-ribosyl transferase
ATP	adenosine triphosphate
AUC	analytical ultracentrifugation
BCL11A	B-cell CLL/lymphoma 11A (zinc finger protein)
BN-PAGE	blue-native polyacrylamide gel electrophoresis
BSA	bovine serum albumin
CADD	computer-aided drug design
CAPSO	<i>N</i> -cyclohexyl-3-aminopropanesulfonic acid
CD	circular dichroism
C/EBP α	CCAAT-enhancer-binding proteins) and E2F1
ChIP	chromatin immunoprecipitation
CPS1	carbamoyl phosphate synthetase 1

CK2	casein kinase 2
CR	calorie restriction or caloric restriction
CTIP2	COUP-TF interacting protein2 (also known as BCL11B)
CyclinB/Cdk1	cell cycle-dependent kinase B
Cyt. c	cytochrome c
DAC	deacetylase
DBC1	deleted in breast cancer 1
DMC	demalonylase
DMSO	diMethyl SulfOxide
DPF	Dortmund protein facility
DSC	desuccinylase
dsDNA	double stranded DNA
DTT	dithiothreitol
DYRK	dual specificity tyrosine phosphorylation Kinase
E2F1	E2F transcription factor 1
<i>E. coli</i>	<i>Escherichia coli</i>
EDTA	ethylenediaminetetraacetic acid
ELISA	enzyme-linked immunosorbent assay
EM	electron microscopy
eNOS	endothelial nitric oxide synthase
ERC	extrachromosomal rDNA circles
ETC	electron transport chain
FA	formic acid

FdL	<i>Fluor de Lys</i>
FITC	fluorescein isothiocyanate
FOXO	forkhead box protein O1
GDH	glutamate dehydrogenase
GK	glucokinase
GST	glutathione-S-transferase
HDAC's	histone deacetylases
HFBA	heptafluorobutyric acid
HIC1	hypermethylated In Cancer 1
His-tag	hexahistidine tag
HPLC	high performance liquid chromatography
HPSF	high purity salt free
HRP	horse radish peroxidase
HuR	hu antigen R
ICDH	isocitrate dehydrogenase
IDE	insulin-degrading enzyme
IGF-1	insulin-like growth factor-1
IPTG	isopropyl β -D-thiogalactopyranoside
IRS2	insulin receptor substrate 2
JNK1	c-Jun N-terminal kinase 1
LB	Luria-Bertani
LCAD	long-chain acyl Coenzyme A dehydrogenase
LXR	liver X receptor

MBP	maltose binding protein
MCF2	myocyte-specific enhancer factor2
MES	2-(<i>N</i> -Morpholino)EthaneSulfonic acid
MS	mass spectrometry
MyoD	myogenic differentiation
NAD ⁺	nicotinamide adenine dinucleotide oxidized
NAM	nicotinamide
NBS1	Nijmegen breakage syndrome 1
NCOR	nuclear receptor co-repressor
NF- κ B	nuclear factor- κ B
NO	nitric oxide
MPI	Max Planck Institute
OAADPr	2'-O-acetyl-ADP-ribose
OD ₆₀₀	optical density at 600 nm
PBS	phosphate buffered saline
PCR	polymerase chain reaction
PDACs	protein deacetylases
PDB	protein data bank
PDK1	Phosphoinositide-dependent kinase 1
PGC1- α	peroxisome proliferator-activated receptor-g co-activator 1 α
PMSF	phenylmethanesulfonyl fluoride
PreScission	human rhinovirus 3C protease
PTMs	post-translational modifications

PVDF	polyvinylidene fluoride
RB	retinoblastoma protein
rDNA	ribosomal DNA
ROS	reactive oxygen species
RPM	revolutions per minute
SDS-PAGE	sodium dodecyl sulfate-Polyacrylamide gel electrophoresis
Sir2Tm	<i>Thermotoga maritima</i> Sirtuin
SEC	size exclusion chromatography
SER	surface entropy reduction
Sir	silent information regulator
Sirtuins	Sir2-ins
SRT	Sirtris
SOB	super optimal broth
STACs	Sirtuin activating compounds
SUMO-1	Small ubiquitin-like modifier-1
SUV39H1	suppressor of variegation 3-9 homolog 1
TAE	Tris-acetate-EDTA
TAT	trans-activator of transcription
TAF ₁₆₈	TBF (TATA-box binding protein)-associated factor I 68
TB	transformation buffer
TBS	Tris buffer saline
TBST	TBS - Tween-20
TCA	tri carboxylic acid

TCEP	tris(2-carboxyethyl)phosphine
TEMED	tetramethylethylenediamine
TEV	tobacco etch virus
TFA	trifluoroacetic acid
Tfam	mitochondrial transcription factor A
TLE1	transducin-like enhancer of split 1
T _m	temperature of melting
TMB	3,3'-5,5'-tetramethylbenzidin
TORC2	transducer of regulated cAMP response element binding protein 2
UBF	upstream binding factor
UTR	untranslated Region
WAT	white adipose tissue
WRN	Werner syndrome protein
XDS	X-ray detector software

1. Introduction	1
1.1 Calorie restriction and lifespan extension	1
1.2 Molecular mechanism of lifespan extension by CR	1
1.3 Sirtuins, CR and aging	1
1.4 Mammalian Sirtuins – Function, classification and localization	2
1.4.1 Classification of mammalian Sirtuins	3
1.4.2 Localization of mammalian Sirtuins	4
1.5 Substrates, function, structure and enzymatic mechanism of Sirtuins	5
1.5.1 Substrates of Sirtuins	5
1.5.2 Role of Sirt1 in cellular functions and disease states	6
1.5.3 Structural features of Sirtuins	8
1.5.4 Catalytic mechanism of Sirtuins	9
1.6 Regulation of Sirt1	11
1.6.1 Proteins and PTMs involved in Sirt1 regulation	12
1.6.2 Regulation of Sirt1 by small molecules	14
1.6.2.1 Regulation by physiological metabolites	14
1.6.2.2 Regulation by pharmacological small molecules	14
1.6.3 Mechanism of Sirt1 modulation by small molecules	17
1.6.3.1 Mechanism of inhibition	17
1.6.3.2 Mechanism of activation	19
1.7 Objectives	20
2. Materials and Methods	21
2.1 Materials	21
2.1.1 Chemicals, Enzymes and Standards	21
2.1.2 Bacterial strains	21
2.1.3 Plasmids and cDNA constructs	21
2.1.4 Oligonucleotides	22
2.1.5 Miscellaneous materials	22
2.2 Microbiology methods	22
2.2.1 Sterilization	22

2.2.2	Culturing of <i>E. coli</i> cells	22
2.2.3	Competent cells.....	23
2.2.4	Transformation of competent cells	23
2.2.5	Heterologous overexpression of recombinant proteins.....	23
2.2.6	Cell lysis.....	26
2.3	Molecular biology methods	26
2.3.1	Agarose gel electrophoresis	26
2.3.2	Gene cloning	26
2.3.3	Site directed mutagenesis.....	28
2.3.4	DNA sequencing.....	28
2.4	Biochemical methods	28
2.4.1	Determination of protein concentration	28
2.4.2	SDS-Polyacrylamide gel electrophoresis (SDS-PAGE).....	29
2.4.3	Blue-native polyacrylamide gel electrophoresis (BN-PAGE).....	29
2.4.4	Purification of recombinant proteins	30
2.4.4.1	Affinity chromatography.....	30
2.4.4.2	Size exclusion chromatography	31
2.4.4.3	Ion exchange chromatography	31
2.4.5	Cleavage of affinity tags	32
2.4.6	Fluorescence based peptide deacetylation assay.....	35
2.4.7	Enzyme-linked immunosorbent assay (ELISA)	35
2.4.8	Continuous assay for deacetylation based on coupled enzymes.....	36
2.4.9	Limited proteolysis of proteins	36
2.4.10	Thermal denaturation shift assay	37
2.4.11	Microscale thermophoresis	37
2.4.12	Analytical ultracentrifugation	38
2.5	Mass spectrometry	38
2.5.1	Mass spectrometry based deacetylation assay	38
2.5.2	Analysis of protein samples from polyacrylamide gels using tryptic digest	39
2.6	Crystallography and structure determination	39

2.6.1 Crystallization trials of human Sirt1	39
2.6.2 Crystallization of <i>Thermotoga maritima</i> Sirtuin (Sir2Tm).....	40
2.6.3 Collection and analysis of X-ray diffraction data of Sir2Tm crystals	40
2.6.4 Molecular replacement of Sir2Tm crystal structures.....	40
2.6.5 Refinement, model building and structure validation of Sir2Tm complex structures	40
2.6.6 Homology modeling of human Sirt1	41
3. Results	42
3.1 Studies on Sirt1	42
3.1.1 Recombinant expression and purification of Sirt1.....	42
3.1.2 Investigating the role of termini in the oligomerization of Sirt1	47
3.1.3 The catalytic domain of Sirt1 is sufficient for activation by polyphenols.....	50
3.1.4 Identification of novel peptide substrates for Sirt1	53
3.1.5 Sirt1 modulation by resveratrol is sequence specific.....	55
3.1.6 Effect of polyphenol unrelated small molecules on Sirt1	56
3.1.7 Resveratrol can directly bind to Sirt1	59
3.1.8 Crystallization trials of Sirt1	59
3.1.9 Studies on AROS	61
3.2 Studies on the role of Zinc in Sirt3	64
3.3 Studies on Sirt5.....	66
3.3.1 Influence of NAD ⁺ on the activity of Sirt5	66
3.3.2 Sirt5 appears to be insensitive to Nicotinamide inhibition	67
3.4 Studies on Sirt7.....	70
3.4.1 Expression and purification of Sirt7	70
3.4.2 Effect of various buffers and salts on the stability of Sirt7.....	71
3.4.3 Identification of new Sirt7 constructs for crystallization.....	71
3.4.4 Crystallization trials of Sirt7	73
3.4.5 PTMs influence the activity of Sirt7	73
3.4.6 Investigating the modulation of Sirt7 by resveratrol and nicotinamide.....	75
3.5 Studies on Sir2Tm	76

3.5.1 Investigating the oligomerization behavior of Sir2Tm	76
3.5.2 Identification of substrate-modulator pairs for Sir2Tm	77
3.5.3 Ex-527 is a potent inhibitor of Sir2Tm	79
3.5.4 Ex-527 appears to require both the substrates to bind Sir2Tm	80
3.5.5 Sir2Tm - Crystallization and cryoprotection	81
3.5.6 Data collection	83
3.5.7 Structure solution, refinement and modeling	84
3.5.8 Analysis of crystal structures of Sir2Tm	86
3.5.9 EX-527 appears to bind to the “C-pocket” of Sir2Tm	91
4. Discussion	93
4.1 Purification and domain architecture of Sirt1	93
4.2 Sirt1 modulation by resveratrol	94
4.3 Crystallization of Sirt1	96
4.4 Zinc is essential for the structural stability and activity of Sirtuins	97
4.5 Sirt5 requires unusually high amount of NAD ⁺ for its deacetylase activity	97
4.6 Sirt5 is a NAM insensitive deacetylase among the Sirtuin family	98
4.7 Expression, purification and crystallization of Sirt7	99
4.8 Sirt7 Phosphorylation at Thr224 increases its activity	100
4.9 Sir2Tm as a model system for studying mammalian Sirt1	100
4.10 Mechanism of Sirtuin inhibition by Ex-527	101
4.11 Selectivity of Ex-527 towards Sirtuins	102
4.12 Insights for drug development	104
4.13 Outlook	105
5. Abstract	107
6. Zusammenfassung	108
7. References	110
8. Appendix	118
9. Erklärung	130

1. Introduction

1.1 Calorie restriction and lifespan extension

Calorie restriction or caloric restriction (CR) is a dietary regimen wherein the amount of calories consumed is reduced up to 20-40% from the amount consumed ad libitum. Lifespan extension by CR was first reported by McCay et. al (McCay et al., 1989) in 1930's. Calorie restricted male rats lived nearly twice as long as their counterparts that were fed with an ad libitum diet. This surprising and interesting phenomenon has since been researched extensively in various species ranging from the unicellular yeast to worms, flies, fish, mice etc. and confirmed that up to 50% increase in lifespan can be achieved by CR (Bordone and Guarente, 2005). CR has been linked not only to lifespan extension but also to an overall well being of the organism by reducing the incidences of age related ailments such as cancer, diabetes and cardiovascular diseases, indicating that maintenance of a disease free state due to CR may in turn lead to lifespan extension (Hursting et al., 2001; Lane et al., 1999).

1.2 Molecular mechanism of lifespan extension by CR

Although CR has been linked to lifespan extension for a long time, the molecular mechanisms behind the phenomenon are still intensely studied and various theories have been proposed. Initial studies on CR aimed at explaining the effect based on a slowing of metabolism. These events are coordinated by signaling molecules such as TOR (target of rapamycin), AMPK (5' adenosine monophosphate-activated protein kinase) and Sirtuins. The mechanisms proposed to contribute to CR mediated lifespan extension are reduction of oxidative damage, improvement of mitochondrial bioenergetics, hormesis, hormonal regulation and fatty acid metabolism (Bordone and Guarente, 2005; Koubova and Guarente, 2003).

1.3 Sirtuins, CR and aging

Aging in baker's yeast *Saccharomyces cerevisiae* was initially linked to a set of genes called Sir1-4 (Sir stands for silent information regulator), which are involved in the silencing of chromatin near telomeres. Later, Gottlieb and Esposito (Gottlieb and Esposito, 1989) demonstrated that Sir2 is the only gene among the set required for silencing of genes near telomeres and also responsible for the silencing of rDNA (ribosomal DNA). It was also shown that the regions near the telomeres that underwent silencing by Sir2 contained histones, hypoacetylated at the ϵ -amino group of their lysine side chains, predominantly at the at N-

terminus (Michan and Sinclair, 2007) and Sir2 was the only gene among the set found to be responsible for this observation. When a budding yeast mother cell's division was followed, several characteristic changes were observed including the accumulation of ERC (extrachromosomal rDNA circles), which was inversely correlated to lifespan (Sinclair and Guarente, 1997). Lin et al. showed that when yeast were grown on CR media, Sir2 mediated reduction in number of ERC was observed and was correlated with lifespan extension, thus connecting Sir2 and CR mediated lifespan extension (Lin et al., 2002). They also showed that CR enhances the activity of Sir2, most likely by increasing the availability of its co-substrate NAD^+ (nicotinamide adenine dinucleotide oxidized form) (see below) due to slowing down of glycolysis and increase in respiration via the TCA (tri carboxylic acid) cycle. Although CR mediated lifespan extension in yeast can also occur independent of Sir2 (Kaeberlein et al., 2005b) and a silencing independent mechanism can exist for suppressing ERC (Riesen and Morgan, 2009), Sir2 and their homologs called Sirtuins (Sir2-ins) in higher organisms appear, to contribute to CR mediated lifespan extension.

Sir2 homologs are present in all kingdoms of life ranging from bacteria to mammals and share a conserved catalytic domain and might be involved in more than gene silencing, for example in cell cycle progression (Brachmann et al., 1995). Roy Frye (Frye, 1999, 2000) later showed that there are seven Sir2 homologs in mammals (Sirt1-7) and grouped them into different classes (see below) and also showed that some Sirtuins (such as CobB from *E. coli* (*Escherichia coli*) and human Sirt2) function as weak NAD^+ dependent mono-ADP-ribosyl transferases. This activity was also found for yeast Sir2 and is essential for its gene silencing role in the chromatin (Tanny et al., 1999). However, several independent groups reported that Sir2 and its mammalian homologs (mouse Sirt1 and human Sirt1) have much higher NAD^+ dependent deacetylase activity and can deacetylate both histones and other proteins such as the transcription factor p53 (Imai et al., 2000; Landry et al., 2000; Vaziri et al., 2001). The hallmark of Sirtuins that distinguishes them from other HDAC's (histone deacetylases) is the absolute requirement of NAD^+ for their activity. Since Sirtuins can deacetylate proteins other than histones, a new protein terminology called PDACs (Lakshminarasimhan and Steegborn, 2011) has been coined to describe them.

1.4 Mammalian Sirtuins – Function, classification and localization

Regulation of cellular functions by amino acid PTMs (post-translational modifications) is an efficient and elegant process. In particular lysine, the most frequently modified amino acid is involved in several processes ranging from transcription, signaling,

protein turnover to disease states (Zhang et al., 2011). Several lysine modifications are known till date and more are still being discovered (Du et al., 2011; Zhang et al., 2011). Examples of lysine modifications include; acetylation, methylation, biotinylation, ubiquitination, sumoylation, propionylation, butyrylation, succinylation, malonylation. Lysine acetylation one of the most abundant PTM (next only to phosphorylation) (Khoury et al., 2011), expanded our understanding of how protein modifications play a dynamic role in all types of cellular functions.

Even though Sirtuins were initially thought to function as mono-ADP-ribosyl transferases, it is widely accepted that their primary function is lysine deacetylation. Because of their unique NAD^+ dependence, they have been grouped in a class of their own, HDAC Class III. Recent research (Du et al., 2011) has also shown that some isoforms can in fact desuccinylate and demalonylate lysine residues in proteins, opening up new exciting avenues in this field. Since Sirtuins NAD^+ is metabolized during the reaction, it is a co-substrate and not a co-factor. The presence of two substrates makes the enzyme very challenging to study in terms of understanding its mechanism and regulation, and the requirement for NAD^+ also makes it a metabolic sensor.

1.4.1 Classification of mammalian Sirtuins

There seven mammalian Sirtuins have different substrate preferences and localization. Sirtuins carry a conserved catalytic domain consisting of about 275 residues. This catalytic domain is the most conserved part among all the Sirtuins. Based on phylogenetic analysis mammalian Sirtuins are grouped into four different classes (I-IV) (Figure 1.1) (Frye, 2000; Michan and Sinclair, 2007). Sirt1, 2 and 3 are placed under Class I along with most eukaryotic Sirtuins such as the founding member yeast Sir2, HST 1 and 2 from yeast and Sir2.1 from *Drosophila melanogaster*. The Class I is further divided into Ia (Sirt1) and Ib (Sirt2 and 3). Sirt4 belongs to Class II along with Sirtuins from bacteria, nematodes, fungus and protozoans. Sirt5 is placed in a class of its own (Class III), along with Sirtuins from achea and protozoa, implying an early evolution. Sirt6 and 7 belong to class IV, which is further subdivided into IVa and IVb, respectively. Other representative members from this family include Sirtuins from metazoans and plants. Sirtuins from gram positive bacteria such as *Thermotoga maritima* fall into a unique undetermined class (Class U) and seem to have appeared very early in evolution.

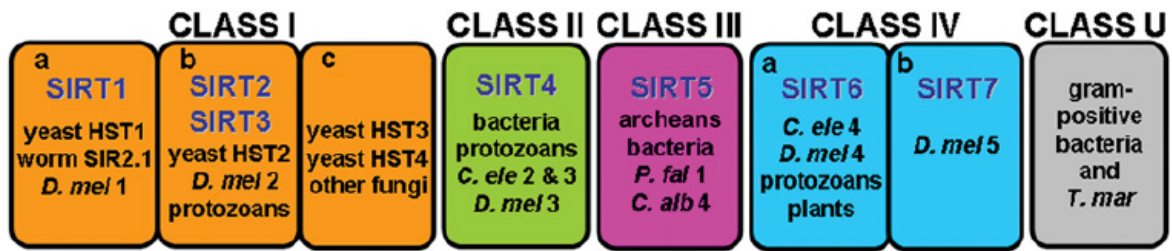


Figure 1.1: Classification of mammalian Sirtuins. A figure depicting different classes of mammalian Sirtuins is shown along with representative members from other kingdoms. *C. alb*, *Candida albicans*; *C. ele*, *Caenorhabditis elegans*; *D. mel*, *Drosophila melanogaster*; *P. fal*, *Plasmodium falciparum*; *T. mar*, *Thermotoga maritima*. Figure adapted from Michan and Sinclair Biochem. J. 2007 (Michan and Sinclair, 2007).

1.4.2 Localization of mammalian Sirtuins

Mammalian Sirtuins are localized in different compartment of the cells and seem to have different substrate specificity. Sirt1 is predominantly in the nucleus, although it has been reported to be present in the cytoplasm and also in mitochondria (Aquilano et al., 2010; Michan and Sinclair, 2007). Sirt2 is predominantly cytoplasmic (Frye, 1999) (North et al., 2003). Sirt3, 4 and 5 are mitochondrial and are localized in different compartments of the mitochondria (Gertz and Steegborn, 2010). Sirt3 and 4 are present in the mitochondrial matrix and Sirt5 can be translocated either to the intermembrane space (IMS) or to the matrix (Schlicker et al., 2008). Sirt6 is present in the heterochromatin of the nucleus (Tennen et al., 2010) and Sirt7 is present in the nucleolus (Figure 1.2).

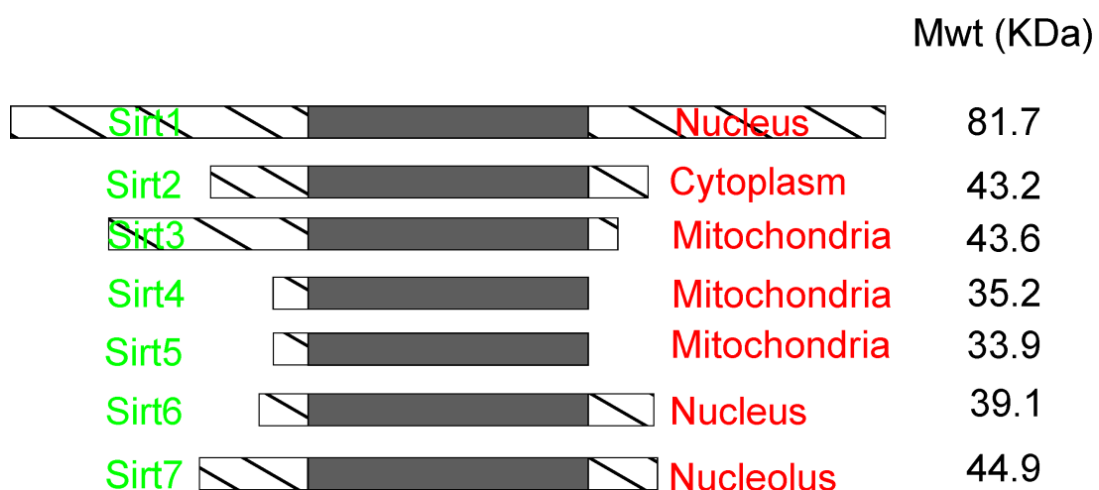


Figure 1.2: Schematic architecture of seven mammalian Sirtuins. The seven mammalian Sirtuins, which fall under different classes contain a conserved catalytic core (shaded regions). The N and the C-termini (hatched regions) are more unique for each Sirtuin.

1.5 Substrates, function, structure and enzymatic mechanism of Sirtuins

1.5.1 Substrates of Sirtuins

To date there are over 6800 acetylation sites known in mammalian proteins indicating the importance of this modification (Choudhary et al., 2009; Kim et al., 2006). Several of these acetylation sites are relatively uncharacterized and Sirtuins might serve as a deacetylase for several of them. Sirt1, the most studied and the largest member of the family, has more than two dozen physiologically relevant substrates identified (Lavu et al., 2008), which ranges from histones (H1, H4 etc.), transcription factors (p53, FOXO etc.), eNOS, (endothelial nitric oxide synthase), pGC1- α (peroxisome proliferator-activated receptor-g co-activator 1 α). Different Sirtuins can also act on same substrates either at the same lysine residue (Sirt1 and Sirt7 can deacetylate Lys382 of p53 (Vakhrusheva et al., 2008)) or at different lysine residue in the same protein (Sirt1 can deacetylate Lys1020, 1024 and Sirt2 can deacetylate Lys1542 and 1707 respectively in p300 (Black et al., 2008)). These common substrates might be either deacetylated in different tissues or cellular compartments or at a different time point in the cell cycle.

The mitochondrial Sirtuins Sirt3, 4 and 5 modify proteins mainly involved in metabolism and ETC (electron transport chain). Mice lacking Sirt3 exhibit hyperacetylation of many mitochondrial proteins, and confirmed substrates are a growing list of metabolic enzymes including GDH (glutamate dehydrogenase), ICDH (isocitrate dehydrogenase) and LCAD (long-chain acyl Coenzyme A dehydrogenase) (Hirschey et al., 2010; Schlicker et al., 2008) and proteins involved in the ETC such as Complex I (Ahn et al., 2008) and Complex II, V (Finley et al., 2011). Sirt4 has very few substrates identified so far. Initial studies showed that Sirt4 can ADP-ribosylate and inhibit GDH activity (Haigis et al., 2006; Lakshminarasimhan and Steegborn, 2011), but results from our lab show Sirt4 is also a substrate specific deacetylase (unpublished).

Sirt6 and Sirt7 are localized in the nucleus and nucleolus, respectively, and very little is known about their substrate preferences. Sirt6 was initially shown to auto-ADP-ribosylate itself (Liszt et al., 2005), but Pan et al. (Pan et al., 2011b) showed Sirt6 possesses weak deacetylase activity. Sirt7 interacts with RNAPolymerase I and positively regulates its transcription (Ford et al., 2006). Sirt7 can deacetylate FdL-1 peptide substrate and mice deficient in Sirt7 gene show increased acetylation levels of p53 at Lys382 and develop inflammatory cardiomyopathy (Vakhrusheva et al., 2008) indicating a role for Sirt7 in cardiac

function via p53 regulation. Sirt1 has been shown to undergo PTMs leading to increase in activity (see below), similarly PTMs could also influence activity of the weak deacetylase Sirt4, 5, 6 and 7.

A list of different mammalian Sirtuins and their substrates/interacting partners are listed in Table 1.1.

Protein	Function	Substrates	Interactors
Sirt1	DAC	P53, FOXO1, FOXO4, PGC1 α , Ku70, CTIP2, MEF2, TLE1, IRS2, LXR, SUV39H1, TORC2, 14-3-3, H1, H4, p300, Tat, ACS1, eNOS, WRN, E2F1, AR, p73, SMAD7, BCL11A, NF- κ B, NCOR, NBS1, RB, IRS2, MyoD ^a	DBC1, AROS, SET 7/9 ^b
Sirt2	DAC/ART	α -tubulin, H4, p300 ^c , FOXO3a, 14-3-3 ^d	HOXA10 ^d , HDAC6 ^d , 14-3-3 ^e
Sirt3	DAC	GDH ^f , ICDH ^f , Complex I ^g , II ^h , ACS2, LCAD ⁱ	Complex I ^g , II ^h , V ^h , FOXO3a ⁱ
Sirt4	DAC/ART	GDH	IDE, ANT2
Sirt5	DAC/DSC/DMC	Cyt c ^f , CPS1 ^j	Unknown
Sirt6	DAC	Sirt6, H3	RELA ^k
Sirt7	DAC	RNA Pol I, p53	RNA Pol I, H2, UBF ^l

Table 1.1: A list of mammalian Sirtuins, their function, substrates and interactors. Text modified from Lavu et. al (Lavu et al., 2008) with inputs from the following: a (Ford et al., 2006), b (Liu et al., 2011), c (Black et al., 2008), d (Smith et al., 2008) e (Jin et al., 2008), f (Schlicker et al., 2008), g (Ahn et al., 2008), h (Finley et al., 2011), i (Hirschey et al., 2010), j (Nakagawa et al., 2009), k (Kawahara et al., 2009), l (Grob et al., 2009). ACS, acetyl-CoA synthetase; ANT, ADP/ATP carrier protein; AR, androgen receptor; AROS, active regulator of SIRT1; ART, adp-ribosyl transferase; BCL11A, B-cell CLL/lymphoma 11A (zinc finger protein); CPS1, caobamoyl phosphate synthetase 1; CTIP2, COUP-TF interacting protein2 (also known as BCL11B); DAC, deacetylase; DMC, demalonylase; DSC, desuccinylase; DBC1, deleted in breast cancer 1; E2F1, E2F transcription factor 1; FOXO, forkhead box protein O1; IDE, insulin-degrading enzyme; IRS2, insulin receptor substrate 2; LXR, liver X receptor; MCF2, myocyte-specific enhancer factor2; MyoD, myogenic differentiation 1; NBS1, Nijmegen breakage syndrome 1; NCOR, nuclear receptor co-repressor; NF- κ B, nuclear factor- κ B; RB, retinoblastoma protein; SUV39H1, suppressor of variegation 3-9 homolog 1; TAT, trans-activator of transcription; TLE1, transducin-like enhancer of split 1; TORC2, transducer of regulated cAMP response element binding protein 2; UBF, upstream binding factor; WRN, Werner syndrome protein.

1.5.2 Role of Sirt1 in cellular functions and disease states

Among all the mammalian Sirtuins, human Sirt1 is the best characterized isoform with respect to its function. Sirt1 was initially implicated in CR mediated lifespan extension and chromatin silencing, but recent data validate its involvement in several processes ranging

from cell proliferation, metabolism, mitochondrial biogenesis, fat mobilization, apoptosis, cancer, diabetes, neuronal diseases, cell senescence, apoptosis etc. (Figure 1.3).

After the discovery of Sirt1's deacetylase activity and its first non-histone substrate p53, several labs reported various substrates of Sirt1 which ranges from transcription factors to enzymes involved in metabolism (Table 1.1 and Figure 1.3). By deacetylating transcription factors such as the FOXO family, NF- κ B, p53, PGC-1 α , PPAR γ , Sirt1 contributes towards fatty acid oxidation, gluconeogenesis, insulin secretion, lipogenesis and several other processes. Sirt1 mediated deacetylation of a single substrate can lead to various outcomes depending on the cell/tissue type and external stimuli (such as CR or carcinogens). For example, deacetylation of PGC-1 α by Sirt1 can lead to its upregulation and induce mitochondrial biogenesis in hepatocytes, at the same time in skeletal muscles it can induce a shift in energy production (by conserving glucose and increasing fatty acid oxidation) (Haigis and Sinclair, 2010). The role of Sirt1 in disease of aging such as cancer, diabetes and neurological disorders is also an intense field of research, with new studies suggesting its role even in anxiety and depression (Libert et al., 2011). Sirt1's role in cancer is hotly debated with several studies claiming it to an oncogene, whereas others show it is a tumor suppressor and much of this has been linked to its ability to deacetylate p53 at Lys382 and repress its transactivation potential (Haigis and Sinclair, 2010).

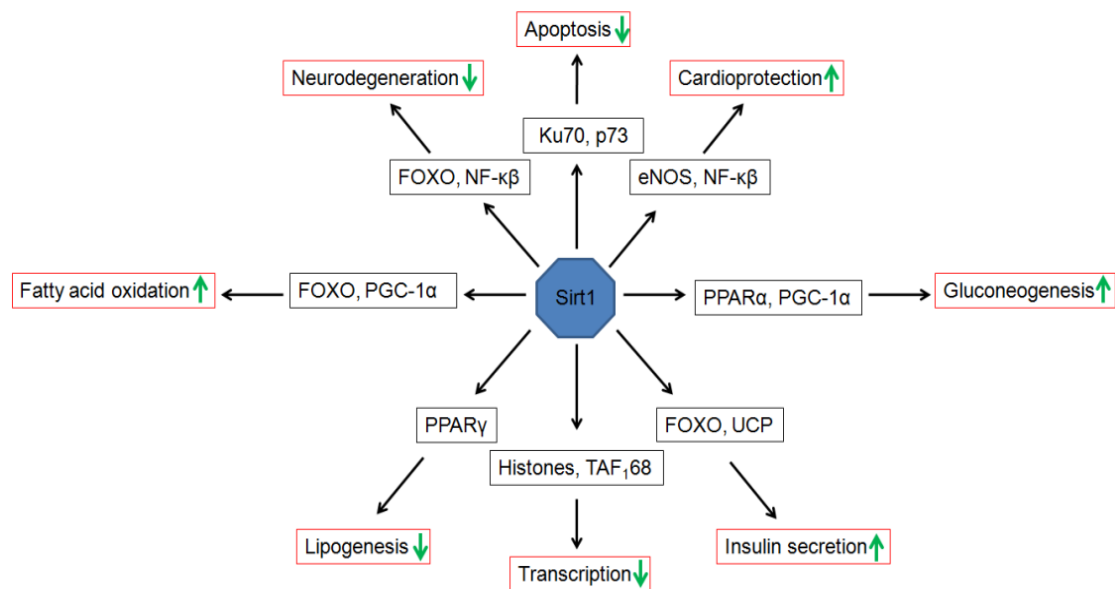


Figure 1.3: Sirt1 affects various cellular events. Sirt1 can deacetylate several proteins in the cell and thereby influence various cellular processes ranging from cell proliferation, metabolism to diseases. UCP, uncoupling protein; TAF₁₆₈, TBF (TATA-box binding protein)-associated factor I 68.

1.5.3 Structural features of Sirtuins

The conserved core of all Sirtuins contains similar structural features. As a representative, the three dimensional crystal structure of Sir2Tm is shown in Figure 1.4 (Hoff et al., 2006). The structure of Sirtuins can be divided into two domains (the large and small domain respectively) and a cleft region. The large domain contains the classical Rossmann fold (α/β fold), which contributes to the binding of pyridine dinucleotides such as NAD^+/NADH and $\text{NADP}^+/\text{NADPH}$. The small domain, which is more unique to each Sirtuin, contains a Zinc atom coordinated by four conserved Cysteins. The Zinc atom does not play any role in the catalysis as in the case of the classical HDACs, but seems to be required for structural stability. The two domains are connected by four loops that arise from the Rossmann fold and include a flexible loop called the co-substrate binding loop. Both the connection and the position of the small domain with respect to the large domain varies among different Sirtuins and is often influenced by the presence of ligands and other small molecules which can affect the co-substrate loop. The most interesting and unique feature of the Sirtuin structure is present in the cleft between the large and the small domain. The substrate and the co-substrate (NAD^+) have to bind in the cleft region in a particular orientation for catalysis to take place.

The binding of acetylated peptides to Sirtuins involve β -sheet interactions and structural studies suggest that the protein substrate might contain no repetitive secondary structure in that region (Sauve et al., 2006). The peptide orientation and backbone interactions observed in several crystal structures of Sirtuins augment biochemical data which suggests that Sirtuins discriminate between different substrates and on the protein level there might be other interactions between Sirtuins (especially the N and C-terminal domains) and its substrates that can lead to a substrate specificity.

The co-substrate NAD^+ enters the opposite side of the acetyllysine binding cleft and encounters the acetyllysine in between the large and the small domains. The contacts between the adenine ring, the ribose ring adjacent to adenine and the Rossmann fold of the Sirtuin are well defined and similar to a typical NAD^+ -protein interaction, but the second ribose moiety, the phosphate and the NAM attached to it are free to adopt several conformations and play an important role in catalysis mediated by Sirtuins. The presence of acetyllysine in the cleft imposes a constrain on the nicotinamide ring of NAD^+ and orients it to a particular pocket of the Sirtuin called the “C pocket” so that the enzyme mediated catalysis can take place (see below) (Sauve et al., 2006).

The co-substrate binding loop, which is often times disordered in Sirtuin structures, is one of the most conserved regions among Sirtuins (Avalos et al., 2005) and has been shown to play an important role in catalysis. The nicotinamide ring of NAD^+ while bound in the strained conformation makes contacts with the co-substrate binding loop and mutating residues in this loop lead to a decrease in the deacetylation activity of the Sirtuin, highlighting its importance (Hawse et al., 2008). When there is no NAD^+ present, the co-substrate loop adopts a relaxed state (open), but switches to an ordered state (closed) when the acetyllysine and NAD^+ are present in the cleft.

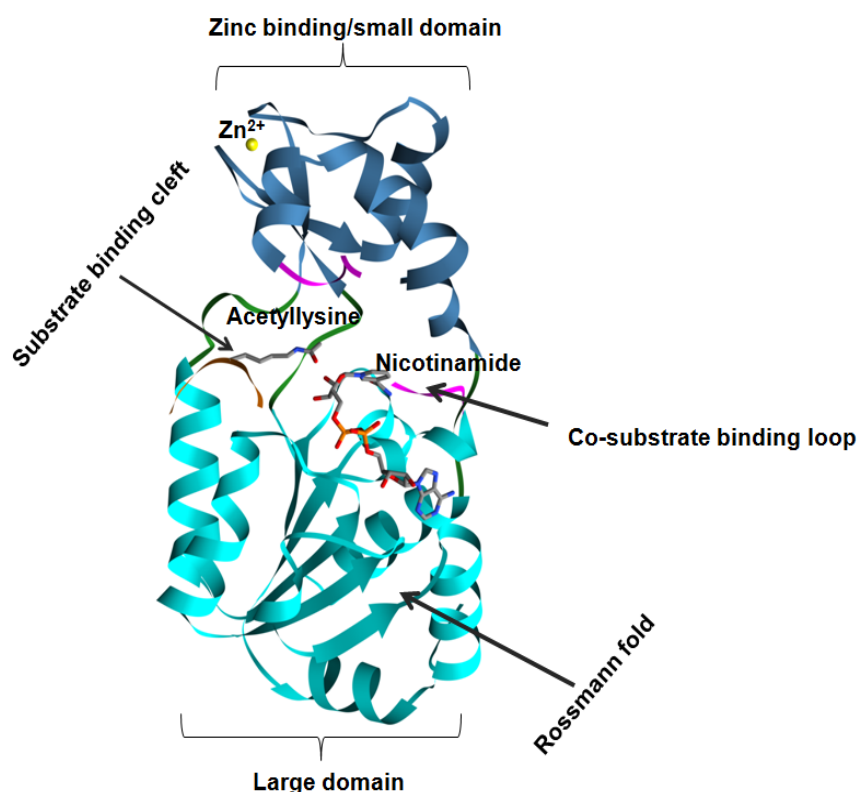


Figure 1.4: Crystal structure of Sirtuins. The catalytic core domain of Sirtuins present similar structural features. As a representative, the ribbon diagram of Sir2Tm is shown (PDB (protein data bank) id: 2H4F). The small domain also called the Zinc binding domain which contains a Zn^{2+} ion (yellow) is represented as blue ribbon. The large domain which harbors the Rossmann fold is colored in cyan. The loops that connect the large and small domains are indicated in green. The co-substrate binding loop is shown in magenta. The substrate binding cleft is shown bound to a peptide substrate. The NAD^+ is bound opposite to the peptide substrate in a productive conformation with the nicotinamide ring pointed at the C pocket.

1.5.4 Catalytic mechanism of Sirtuins

Sirtuins have been shown to possess both deacetylase (depropionylase/debutyrylase/desuccinylase/demalonylase etc.) and ADP-ribosyl transferase activity. The involvement of two substrates and release of three products makes the Sirtuin

mechanism both complicated and interesting at the same time. Several biochemical and structural data suggest multiple enzyme/intermediate and enzyme/transition state complexes (Hoff et al., 2006; Sanders et al., 2010). The deacetylation is considered as the main function of the Sirtuins and the ADP-ribosyl transferase activity (although initially assigned to Sirtuins) is often considered as a side reaction or a secondary reaction and the ADP-ribosyl transferase mechanism is subject to debate (Sauve, 2010).

The deacetylation reaction of Sirtuins involves binding of the substrates acetyllysine followed by the NAD^+ in the cleft region, yielding the deacetylated lysine, OAADPr (2'-O-acetyl-ADP-ribose) and NAM (nicotinamide). The NAM is released first but the release of OAADPr or lysine does not follow a particular order (Hoff et al., 2006). The acetyl group attached to the ADPr (ADP-ribose) can exist in equilibrium between the isomers either as 2' OAADPr or 3' OAADPr (Jackson and Denu, 2002; Sauve et al., 2001).

Step 1 of the Sirtuin catalyzed deacetylation starts after NAD^+ binds in the productive conformation following the binding of the acetyllysine (Figure 1.5). In this productive conformation, the NAD^+ is both destabilized from its ground state and α face of the N-ribose is exposed to the carbonyl moiety of the acetyllysine. As the NAM part of the NAD^+ is dissociated, the carbonyl group of the acetyllysine is drawn towards to the C1' of the ribose ring and attacks it to reversibly form a peptidylimidate intermediate. The exact mechanism behind the breakage of the glycosidic bond and the release of NAM is still debatable, with several studies suggesting an $\text{S}_{\text{N}}1$ type of mechanism and others proposing an $\text{S}_{\text{N}}2$ type mechanism. At this stage the peptidylimidate intermediate (transitions state) is still vulnerable to attack by the released NAM or excess NAM present in the solution via a base-exchange reaction and needs to be shielded by the enzyme. This effect occurs at physiological NAM concentration making it a physiologically relevant inhibitor of Sirtuins. The presence of neighboring residues (step 2) (for example Phe33 in the case of Sir2Tm) in the co-substrate binding loop has been shown to play an important role in shielding the positive charge developed on the intermediate from water molecules and the NAM (Hoff et al., 2006). In step 3 of the reaction, the catalytic Histidine acts as a base (His116 in the case of Sir2Tm) and abstracts an H^+ from either the 2' or 3' OH of the ribose and in turn activates the 2' OH to attack the carbonyl of the acetyllysine to form the bicyclic intermediate (step 4). The same Histidine then acts as an acid and protonates the imidate intermediate, leading to the formation of a cyclic acyl-oxonium ion due to the cleavage of the amide bond (step 5). In the next series of steps (steps 6 to 8) an active site water mediated attack can occur on the acyl-

oxonium ion leading to the release of the deacetylated lysine (Sauve et al., 2001; Smith and Denu, 2006), followed by the abstraction of H^+ from this intermediate probably by the leaving NH_2 group of the lysine side chain and resolving of the cyclic intermediate by the 1' oxygen to yield the final substrate 2'OAADPr.

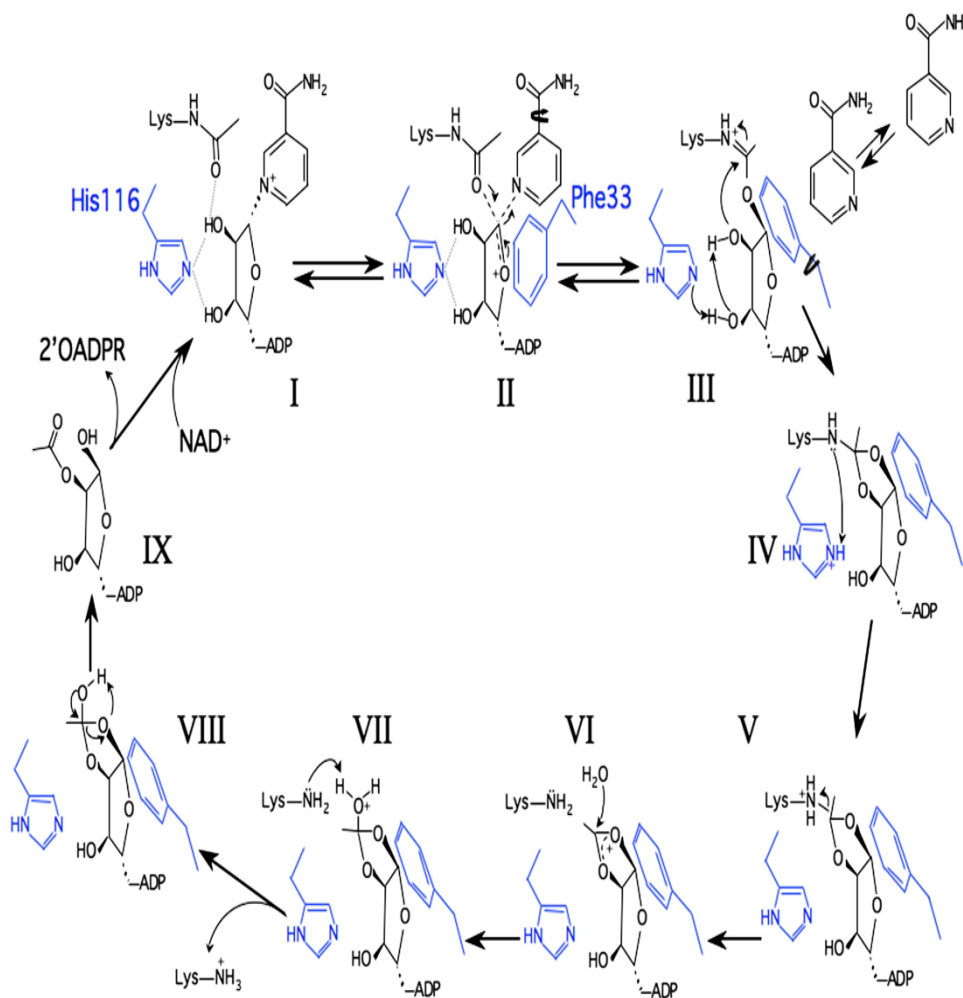


Figure 1.5: Mechanism of Sirtuin catalyzed deacetylation. A schematic representation of the steps involved in Sirtuin mediated deacetylation. Figure reproduced with permission from Elsevier Ltd. (Hoff et al., 2006). See above text for explanation.

1.6 Regulation of Sirt1

The role Sirt1 plays in various types of cellular process by acting as a regulator makes its physiological and pharmacological regulation very interesting. At the physiological level, Sirt1 regulation can occur through processes such as; transcription/translation, shuttling between nucleus and cytoplasm, interacting partner proteins, PTMs and cellular metabolites ($NAD^+/NADH$, NAM). The idea behind modulating the activity of Sirt1 at the pharmacological level started as soon as their involvement in lifespan extension was discovered, leading to a search for small molecules that can modulate Sirt1.

1.6.1 Proteins and PTMs involved in Sirt1 regulation

In spite of more than a decade of research on Sirt1, less information is available about Sirt1's regulation compared to its function. To date only three interacting partners (Table 1.1) and a handful of PTMs (Table 1.2) are known for Sirt1. Recently, two research groups claimed that the N and C-terminal regions of Sirt1 (a feature that distinguishes Sirt1 from its isoforms) play a role in regulating its activity, similar to the regulation of Sirt3 (shown in our laboratory (Schlicker et al., 2008)) and Sirt6 (Tennen et al., 2010). But the results of Sirt1 experiments from these groups contradict each other, indicating that a more careful and conclusive study is required to understand the protein's regulation (Kang et al., 2011; Pan et al., 2011a).

At the transcription level, Sirt1 is regulated by at least four transcription factors; p53, HIC1 (hypermethylated in cancer 1), C/EBP α (CCAAT-enhancer-binding proteins) and E2F1 (Satoh et al., 2011). P53 and HIC1 are involved in transcriptional repression of Sirt1 under basal conditions, whereas C/EBP α and E2F1 can enhance Sirt1 transcription. Sirt1 translation can be regulated by at least one protein (HuR (Hu antigen R) and three microRNAs (miR-34a, miR-132, miR-217) by binding to the 3' UTR (untranslated region) of Sirt1's mRNA. HuR is an mRNA binding protein, which binds to the mRNA of Sirt1 and increases its half-life (Abdelmohsen et al., 2007). All three microRNAs were shown to decrease the expression level of Sirt1 (Satoh et al., 2011).

At the protein level, Sirt1 is regulated by at least three proteins; AROS, DBC1 and SET7/9 (Table 1.1). AROS, a nuclear protein, can bind to the N-terminus of Sirt1 (114-217) and enhance its p53-mediated activity (Kim et al., 2007). DBC1 on the other hand binds to the catalytic domain of Sirt1 and inhibits its activity (Kim et al., 2008; Zhao et al., 2008) leading to up-regulation of p53 and FOXO3a mediated apoptosis. A recent study showed that the methyltransferase SET7/9 also directly interacts with Sirt1 at its N-terminal region (121-295) leading to increased acetylation levels of p53, indicating an inhibitory role (Liu et al., 2011).

Sirt1 PTMs known to date include; sumoylation, phosphorylation and methylation (Table 1.2). Sumoylation of Lys734 by SUMO-1 (small ubiquitin-like modifier-1) has been shown to activate Sirt1 (Yang et al., 2007b). Studies in our laboratory (see results section) and by others (Nasrin et al., 2009) has shown that phosphorylation of Sirt1 also increases its activity in a substrate dependent manner, indicating a major role for PTMs in Sirt1's regulation. The kinases responsible for phosphorylation of Sirt1 include; JNK1 (c-Jun N-

terminal kinase 1), DYRK1A, DYRK3 (dual specificity tyrosine phosphorylation kinase), CK2 (casein kinase 2), cyclinB/Cdk1 (cell cycle-dependent kinase B) (Ford et al., 2008; Guo et al., 2010; Kang et al., 2009; Nasrin et al., 2009; Sasaki et al., 2008; Zschoernig and Mahlknecht, 2009). Sirt1 was shown to be methylated in vitro by SET7/9 at Lys 233, 235, 236 and 238 and was found to have no influence on its activity (Liu et al., 2011), but this type of in vitro methylation might have aroused from non-specific activity of SET7/9 and may not reflect the true status in the cell.

Residue number	Modification	Modifying enzyme	References
S14	Phosphorylation	Unknown	(Gauci et al., 2009; Sasaki et al., 2008)
S16	Phosphorylation	Unknown	(Gauci et al., 2009)
S26	Phosphorylation	Unknown	(Beausoleil et al., 2006)
S27	Phosphorylation	JNK1	(Beausoleil et al., 2004; Ford et al., 2008; Nasrin et al., 2009; Sasaki et al., 2008)
S47	Phosphorylation	CK2, NEK6, JNK1	(Beausoleil et al., 2006; Nasrin et al., 2009)
S162	Phosphorylation	CK2	(Kang et al., 2009; Sasaki et al., 2008)
S173	Phosphorylation	Unknown	(Sasaki et al., 2008)
K233	Methylation	SET7/9	(Liu et al., 2011)
K235	Methylation	SET7/9	(Liu et al., 2011)
K236	Methylation	SET7/9	(Liu et al., 2011)
K238	Methylation	SET7/9	(Liu et al., 2011)
S434	Phosphorylation	cAMP/PKA	(Gerhart-Hines et al., 2011)
T530	Phosphorylation	JNK1, CyclinB/CDK, DYRK1A and DYRK3	(Guo et al., 2010; Nasrin et al., 2009; Sasaki et al., 2008)
S535	Phosphorylation	ERK; NEK6	(Mayya et al., 2009)
S538	Phosphorylation	Unknown	(Mayya et al., 2009)
S539	Phosphorylation	Unknown	(Mayya et al., 2009)
T540	Phosphorylation	GSK3; NEK6, CyclinB/CDK	(Sasaki et al., 2008)
T554	Phosphorylation	Unknown	(Olsen et al., 2010)
S569	Phosphorylation	Unknown	(Dephoure et al., 2008)
S659	Phosphorylation	CK2	(Kang et al., 2009; Zschoernig and Mahlknecht, 2009)
S661	Phosphorylation	CK2	(Kang et al., 2009; Zschoernig and Mahlknecht, 2009)
S693	Phosphorylation	CK2	(Kang et al., 2009)
T719	Phosphorylation	Unknown	(Gauci et al., 2009; Mayya et al., 2009; Sasaki et al., 2008)
K734	Sumoylation	SUMO-1	(Yang et al., 2007b)
S747	Phosphorylation	Unknown	(Sasaki et al., 2008)

Table 1.2: PTMs of Sirt1 and their modifying enzymes. S14, S16, S26, S27, S47, S173, S535, S538, S539, T554, S569, T719 and S747 were found to be phosphorylated from proteomic studies (Beausoleil et al., 2004; Beausoleil et al., 2006; Dephoure et al., 2008; Gauci et al., 2009; Gerhart-Hines et al., 2011; Mayya et al., 2009; Olsen et al., 2010).

1.6.2 Regulation of Sirt1 by small molecules

1.6.2.1 Regulation by physiological metabolites

The two physiologically relevant small molecular regulators of Sirt1 are NAD^+ and NAM, because of the former's absolute requirement for Sirt1's activity and the latter's ability to inhibit the enzyme. The requirement for NAD^+ cannot be replaced by NADH or $\text{NADP}^+/\text{NADPH}$. Although the total level of NAD^+/NADH in the cell is in the millimolar range, the free NAD^+ level in the cell is $\sim 300 - 400 \mu\text{M}$ (Yang et al., 2007a), because the majority of NAD^+ in the cell is sequestered by proteins involved in metabolic processes such as glycolysis and TCA cycle in order to carry out their function. Sirt1's affinity towards NAD^+ being rather low ($\sim 150\text{-}170 \mu\text{M}$, (Smith et al., 2009)) makes NAD^+ an important regulator of Sirt1 and the enzyme a metabolic sensor/signaling agent, and the availability of NAD^+ can influence several cellular events by increasing the activity of Sirt1. For example, the availability of NAD^+ can help decide the cellular machinery if it is necessary to carry out metabolic activities or regulate gene transcription (such as activating Sirt1). NADH has been shown to inhibit the activity of Sirtuins but only in the high millimolar range (Schmidt et al., 2004) which is beyond physiological levels. In spite of this, it is still a matter of debate if it is the production of NAD^+ (the genes involved in NAD^+ biosynthesis) or the ratio of NAD^+/NADH that regulates the activity of Sirt1 in events such as CR.

The discovery of NAM as an inhibitor of Sirt1 generated a lot of interest in finding small regulators of Sirt1 that mimic NAM (Bitterman et al., 2002). NAM is physiologically relevant inhibitor, because it inhibits Sirt1 with an IC_{50} of $<50 \mu\text{M}$ and the cellular levels of NAD range from $11\text{-}400 \mu\text{M}$. Several structural and biochemical studies have elucidated the mechanism behind NAM inhibition (Avalos et al., 2005; Sauve and Schramm, 2003). NAM inhibits Sirt1 in a non-competitive manner by binding in the conserved C pocket after formation of the alkylimidate, leading to a base exchange reaction reversing intermediate formation.

1.6.2.2 Regulation by pharmacological small molecules

Since Sirtuins were linked to CR and lifespan extension, extensive research was carried out to find small molecules that can regulate them. Howitz et al. screened a library of NAD^+ analogs and plant polyphenols to identify small molecules that can modulate the activity of Sirt1 and its homologs. Several inhibitors were identified, but most notably several plant derived polyphenols seemed to activate Sirt1 (Howitz et al., 2003). These Sirtuin

activating compounds are collectively called STACs (Sirtuin activators). Among polyphenols, the most potent activator was resveratrol (Figure 1.6), a flavonoid that is synthesized by several plant species including grapes (high amounts can be found in red wine). Resveratrol's structure consists of a stilbene moiety with OH groups on both of the benzyl rings, the most stable isomer being trans-resveratrol. Even before the identification of resveratrol's ability to activate Sirt1, it was shown to confer cardiac and neuro-protection through its antioxidative properties (Pervaiz and Holme, 2009). Yeast grown in media supplemented with resveratrol showed lifespan extension similar to CR and this effect was directly dependent on resveratrol's ability to activate yeast Sir2 (Howitz et al., 2003). Resveratrol has also been shown to mimic anti-aging effects in lower organisms such as *Caenorhabditis elegans* and *Drosophila melanogaster* in a Sirtuin dependent manner (Wood et al., 2004). Furthermore, mice fed with resveratrol show higher mitochondrial content, protection against metabolic diseases (Lagouge et al., 2006) and increased survival in a Sirt1 dependent manner (Baur et al., 2006). In another screen, several small molecules that do not share any structural similarity to polyphenols were also identified, and were shown to be up to 1000 fold more potent in activating Sirt1 compared to resveratrol (SRTs (Sirtris) Figure 1.6) (Milne et al., 2007). In diet induced and genetically obese mice, these compounds were claimed to increase insulin sensitivity and lower blood glucose levels, and are currently under preclinical trials to treat type 2 diabetes.

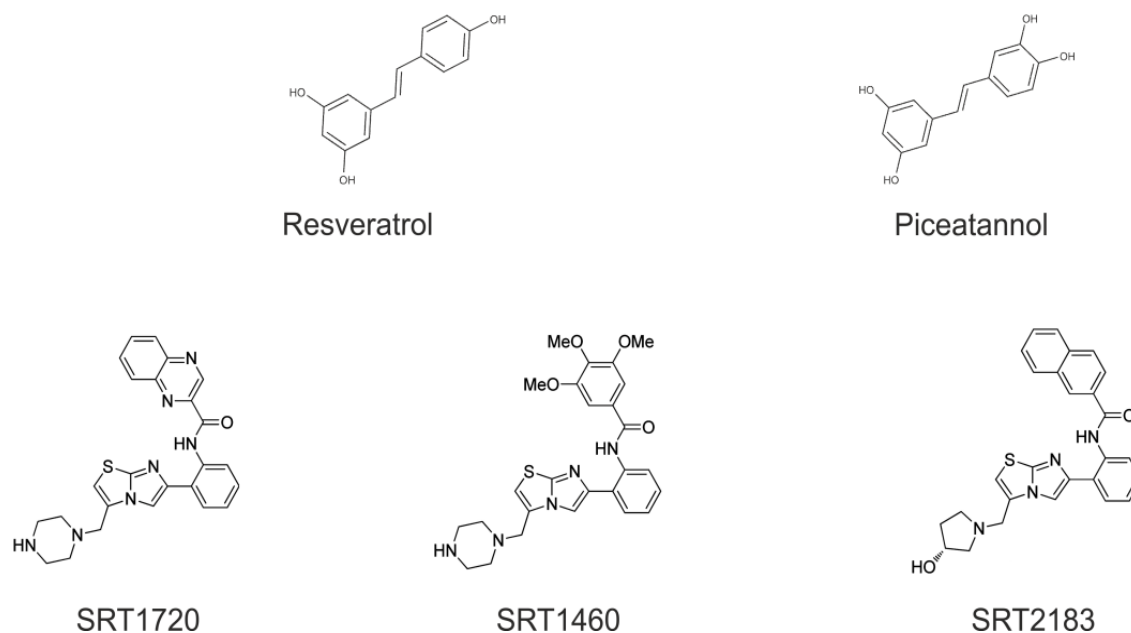


Figure 1.6: Representative small molecule activators of Sirt1 (STACs). Figures were either created using MarvinSketch or adapted with permission from Blum et al. (Blum et al., 2011) Copyright 2011 American Chemical Society.

Several small molecule inhibitors of Sirt1 have been identified and characterized over the past several years (reviewed by Blum et al (Blum et al., 2011)), the majority of them are based on peptide mimics and NAD⁺/NAM analogs (Figure 1.7). Some of these inhibitors such as Ex-527 (IC₅₀ 0.098 μM) and Suramin (IC₅₀ 0.3 μM) inhibit Sirt1 in the nanomolar range, whereas others such as Sirtinol, Tenovin and Cambinol and their derivatives inhibit in the micromolar range. Several of these so called lead compounds were used as analogs to develop more potent and bioavailable compounds, but rarely show specificity towards Sirt1. For example, Salermide was developed based on the scaffold of Sirtinol and was shown to be more potent than its parent compound (IC₅₀ of 43 μM vs 123 μM respectively) (Pasco et al., 2009). Salermide was well tolerated by mice up to 100 μM and caused tumor specific cell death in various tissues (Lara et al., 2009), but was also shown to equally inhibit Sirt2 (IC₅₀ 25 μM). Similarly, Tenovin based derivatives were also developed with Tenovin-6 showing the best water solubility and potency (IC₅₀ 21 μM for Sirt1) and decreased tumor growth by increasing the acetylation levels of p53-Lys382. Kinetic studies indicated that Tenovin-6 inhibits Sirt1 in a non-competitive manner, but it was also shown to inhibit Sirt2 in the micromolar range (IC₅₀ 10 μM), again leading to lack of selectivity (Lain et al., 2008). Cambinol also inhibits Sirt1 and Sirt2 equally and was shown to possess antitumor activity in preclinical models, but its analog containing a Bromide in the para position of the phenyl ring improved its potency and specificity towards Sirt1 (IC₅₀ of 13 μM vs. >90 μM respectively) indicating that subtle changes in the small molecules can lead to isoform specificity (Medda et al., 2009). A high throughput screen using 50,000 compounds identified four scaffolds with Sirtuin inhibitory activity, out of which one had moderate selectivity for Sirt1 with IC₅₀ ~ 6 μM (Sanders et al., 2009).

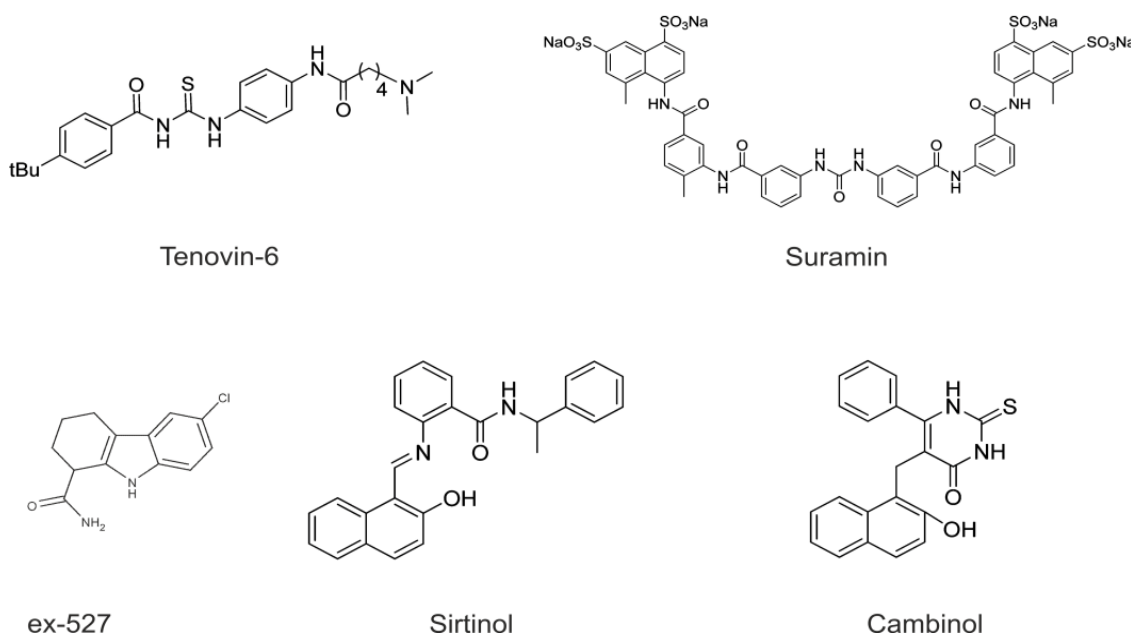


Figure 1.7: Representative small molecule inhibitors of Sirt1. Figures were either created using MarvinSketch or adapted with permission from Blum et. al.(Blum et al., 2011). Copyright 2011 American Chemical Society.

1.6.3 Mechanism of Sirt1 modulation by small molecules

1.6.3.1 Mechanism of inhibition

The lack of structural information for Sirt1 has hampered mechanism based/structure aided drug development, but several biochemical and CADD (computer-aided drug design) studies have been performed to develop novel compounds to inhibit Sirt1. Most Sirt1 inhibitors likely either bind to the acetyllysine binding site (peptide mimics) or to the NAD^+ /NAM binding site to inhibit the enzyme. In the case of peptide based inhibitors, competitive inhibitors can easily be made specific based on the Sirtuin's substrate preference, but such inhibitors are difficult to develop into suitable drugs. Even a single amino acid analog of acetyllysine containing a thioacetyllysine (and aniline and benzyloxycarbonyl groups attached to the carbonyl and amino groups of the thioacetyllysine) was shown to have an inhibitory effect against Sirt1 with an IC_{50} of 2.7 μM which had 8.5-37 fold selectivity over Sirt2 and Sirt3 (Suzuki et al., 2009). The formation of a stable thio-acetyl-ADP-ribose conjugate (attack of the thioacetyllysine on the ribose ring of NAD^+ which carries the NAM) was confirmed by mass spectrometric analysis. The most likely mechanism for such a type of inhibition, is the slow substrate turnover due to the formation of a stable thioimide intermediate which blocks the acetyllysine binding cleft and renders the enzyme inactive (Smith and Denu, 2007). The mechanism behind NAD^+ /NAM based inhibition arises either from competition between the inhibitor and NAD^+ or a mixed type inhibition. Napper et. al

synthesized several indole based derivatives which have some similarity to NAM and showed that some of these compounds inhibited Sirt1 with a very high potency and specificity compared to Sirt2, 3 and 5 (Napper et al., 2005). Based on kinetic analysis they proposed a mixed type inhibition and suggested that the inhibitor binds to the C-site after the release of NAM and prevents further release of the products; 2OAADPr and deacetylated lysine. However, binding site and the inhibition mechanism remain uncertain.

Till date the only mechanistically understood Sirtuin inhibitor is suramin, because of the availability of its crystal structure in complex with Sirt5 (Schuetz et al., 2007). The symmetry of suramin allows it to bind two molecules of Sirt5 at the same time, creating a link between them, which in turn leads to dimerization. Suramin makes contacts with several residues of the co-substrate binding loop leading to its stabilization. The sulfonyl groups of suramin binds to the catalytic core of Sirt5 and mediates majority of the interaction. The sulfonyl groups mimic NAM and occupies the C-pocket, thus preventing NAD^+ from binding. Comparison of Sir2Tm complexed with p53 peptide and NAM (pdb id: 1YC5) and the Sirt5 structure complexed with suramin, indicates that Ssuramin also occupies the acetyllysine binding site and extends up to two residues further to the C-terminus of the peptide substrate, thus preventing its binding. Furthermore, the sulfonyl groups also occupy the ribose part of NAD^+ which is attached to NAM. Taken together, this shows that suramin inhibits Sirt5 by preventing the binding of both the substrate and co-substrate at the same time. Due to these reasons, suramin by itself may lack isoform specificity, because the substrate binding cleft and NAD^+ binding pocket are very similar among the Sirtuins. Nevertheless, several new compounds were synthesized and characterized using the scaffold of suramin and were found to be isoform specific based on the small modifications on the sulfonyl rings. For example, introduction of aminoanthralic derivatives or small urea like groups in the sulfonyl head of suramin lead to Sirt1 specific inhibition with IC_{50} as low as 93 nM (Trapp et al., 2007), indicating that subtle differences existing in the catalytic core of Sirtuins can be exploited to discover isoform specific drug targets.

Kinetic studies using inhibitors identified from high throughput screen suggested non-competitive or mixed type inhibition relative to both substrate and co-substrate, implying that the inhibitor binds in the conserved catalytic domain (Sanders et al., 2009) and therefore may not show isoform specificity. In order to develop Sirt1 specific inhibitors, future efforts could focus on the termini of Sirt1, because of its uniqueness among the isoforms.

1.6.3.2 Mechanism of activation

The mechanism of Sirtuin activation by polyphenols and STACs is perhaps the most intensely debated topic among the Sirtuin research community. Protein/enzyme activation by a small molecule is less prevalent compared to inhibition. Examples of small molecules activating proteins include; Sirt1, GK (glucokinase), PDK1 (phosphoinositide-dependent kinase 1) and p300 (Zorn and Wells, 2010). Since Sirt1 is involved in various cellular events it would be beneficial to identify both inhibitors and activators of Sirt1, especially small molecules that specifically modulate Sirt1 (among its mammalian isoforms) on a substrate specific manner in order to target a particular disease pathway.

Initial high-throughput screening assays employed fluorescence based peptides as substrates to identify potential Sirtuin modulators, which were then used in other screens as well (Howitz et al., 2003; Milne et al., 2007). Based on kinetic studies an activation mechanism was proposed where resveratrol and STACs increased substrate affinity (by decreasing the K_m of the fluorescent peptide) but had no effect on the V_{max} . Later, it was found that resveratrol activation was dependent on the fluorophore (AMC (7-amino-4-methylcoumarin)) present on the substrate peptide and when unmodified peptides (in vitro) or full length proteins (in vivo) were used as substrates there was no resveratrol dependent activation of Sirt1 (Beher et al., 2009; Borra et al., 2005; Kaeberlein et al., 2005a). A resveratrol dependent activation mechanism was proposed where the polyphenol binds to and induces a conformational change in Sirt1 near the binding area of the coumarin group of the fluorophore, leading to better accommodation of the fluorescent peptide by the enzyme. Pacholec et al. (Pacholec et al., 2010) showed that the SRT series of compounds (SRT1720, SRT2183 and SRT1460) also do not activate Sirt1 when unmodified peptides or full length proteins were used as substrates and concluded that these compounds directly interact with the fluorophore and formation of a complex between the fluorophore and the compound may lead to Sirt1 activation in an “indirect” manner. But in a recent report Dai et al. (Dai et al., 2010) showed that the activation of Sirt1 by STACs depend on the structural features of the peptide substrate and proposed an allosteric mechanism for activation of Sirt1 by STACs, where the specific features of the substrate peptide plays a role in the activation process and the activator may bind to the enzyme-substrate complex. Indeed we find in this thesis that resveratrol can directly bind to Sirt1 and that the sequence of deacetylation site decides whether resveratrol modulates Sirt1 (activation or inhibition) explaining the previous contradictory reports.

1.7 Objectives

Sirtuins are a conserved family of proteins found in all domains of life. Sirtuins are classified as class III Histone deacetylases and contain a special feature; wherein they metabolize NAD^+ to deacetylate and or ADP-ribosylate protein residues, thereby acting as metabolic sensors. The mammalian Sirtuin (Sirt) family encompasses seven isoforms (Sirt 1-7), each with a conserved catalytic core consisting of ~275 residues. The N and C-terminal extensions and localization in different cellular compartments, differentiate mammalian Sirtuins among each other.

The human Sirt1 is the largest isoform among all the mammalian Sirtuins and is involved in several cellular processes and disease states. Sirt1 also participates in CR mediated lifespan extension in lower organisms and several small molecules can modulate its activity. The molecular mechanism of Sirt1 modulation by small molecules is still not fully understood, primarily due to the unavailability of structural information. Understanding this mechanism would allow isoform specific and substrate specific modulation of Sirt1 leading to better therapeutic agents for age related diseases. The major focus of this study is structural and biochemical characterization of Sirt1, to gain insights into the mechanism of modulation by small molecules. In order to achieve this, full length and various constructs of human Sirt1 were to be cloned, expressed and purified to homogeneity. Crystallization trials should be pursued on these pure proteins and their substrate/modulator complexes to understand the mechanism of modulation from a structural perspective. Biophysical and biochemical studies were to be carried out to analyze the role of N and C-terminal domains of Sirt1 towards its activity and modulation by small molecules. Other isoforms of Sirt1 (Sirt2, Sirt3, Sirt5 and Sirt7) and the bacterial homolog of Sirt1 from Sir2Tm were to be used as a models systems to understand and compare the structure, function and modulation mechanisms of Sirtuins.

2. Materials and Methods

2.1 Materials

2.1.1 Chemicals, Enzymes and Standards

All chemicals were purchased from Sigma, Applichem, Serva, Roth or J.T. Baker unless stated differently. Peptides were synthesized by GL Biochem, Shanghai, China. Supplemental table S4 lists all the peptides used in this study. DNA modifying enzymes, DNA and protein standards were purchased from Serva, Agilent Technologies, Promega, New England Biolabs, Bio-Rad and Fermentas. Trypsin, Chymotrypsin, Cyt. c (cytochrome c), Glutamate dehydrogenase were purchased from Sigma.

2.1.2 Bacterial strains

All bacterial strains used in this study were derived from *E. coli* (*Escherichia coli*) K-12. The *E. coli* strains XL-1 Blue (Stratagene, USA) was used for cloning, plasmid propagation and site-directed mutagenesis. The *E. coli* strain BL21 Star (DE3) (Invitrogen, USA) and Rosetta (DE3) (Merck, Germany) were mostly used for overexpression of recombinant proteins.

The strains have the following genotypes:

XL1-Blue: *recA1 endA1 gyrA96 thi-1 hsdR17 supE44 relA1 lac* [F' *proAB lacI^fZΔM15 Tn10* (Tet^r)].

BL21 Star (DE3): F- *ompT hsdSB* (*r_B-m_B-*) *gal dcm rne131* (DE3)

BL21(DE3) pLysS: F – *ompT hsdSB*(*r_B- m_B-*) *gal dcm* (DE3)pLysS (Cam^R)

Rosetta (DE3): F⁻ *ompT hsdSB*(*r_B⁻ m_B⁻*) *gal dcm lacY1*(DE3) pRARE (Cam^R)

C43 (DE3): F⁻ *ompT hsdS_B* (*r_B⁻ m_B⁻*) *gal dcm* (DE3) (Kan^r), transformed with the F-ATPase subunit gene and cured and contains at least one uncharacterized mutation.

BL21 (DE3) codonPlus RIL: *argU* (AGA, AGG), *ileY* (AUA), *leuW* (CUA) (Cam^R).

2.1.3 Plasmids and cDNA constructs

Overexpression of recombinant protein in *E. coli* cells was performed by cloning the genes of interest in pET11a, pET15b, pET21a(+) (Merck, Germany), pASK-IBA17 (BioTAGnology, Germany), pGEX-6P3 (GE Healthcare, USA), pET151/D-TOPO (Life

Technologies, USA) and modified pOPIN vectors (Oxford University, UK). Mouse Sirt1 was cloned using the mouse cDNA library obtained from DB Biosciences, USA. Full length human Sirt1 in pCDNA3.1 vector was a kind gift from Dr. Tony Kouzarides, The Gurdon Institute, Cambridge, UK. Human AROS in pCMV-SPORT6 vector was purchased from Source BioScience, Germany. All the genes of interest are under the control of T7 promoter.

2.1.4 Oligonucleotides

All oligonucleotides used for cloning and site-directed mutagenesis were purchased either from Sigma, USA or Eurofins MWG Operon, Germany. The oligonucleotides were HPLC (high performance liquid chromatography) or HPSF (high purity salt free) purified. A complete list of oligonucleotides used in this work is listed in supplemental table S1.

2.1.5 Miscellaneous materials

Other materials were purchased from Eppendorf, Hampton Research, Molecular Dimensions, Jena Biosciences, Qiagen, Millipore, Star Labs if not stated explicitly.

2.2 Microbiology methods

2.2.1 Sterilization

Solutions and materials required for sterile bacterial culture were prepared by either autoclaving at 121 °C for 20 minutes in a Systec DX-150 autoclave (Systec GmbH, Germany) or sterile filtered using a 0.22 µm membrane filter (Millipore, USA).

2.2.2 Culturing of *E. coli* cells

General procedure

E. coli cells were grown either in LB (Luria-Bertani) media which consists of 1% (w/v) Tryptone, 0.5% (w/v) Yeast and 1% (w/v) NaCl or in autoinduction media consisting of 1.2% (w/v) Tryptone, 2.4% (w/v) Yeast extract and 0.5% (v/v) Glycerol autoclaved and supplemented with 0.17 M KH₂PO₄, 0.72 M K₂PO₄, 0.05% (w/v) glucose and 0.2% (w/v) alpha-lactose. LB plates used for plating bacteria also contained 1.5% (w/v) Agarose. Before addition of *E. coli* to the media, appropriate amount of antibiotics were added. The cultures were initially grown at 37 °C by shaking at a speed of 120 RPM (revolutions per minute) and then shifted to 22 °C before induction of the protein of interest.

2.2.3 Competent cells

Chemically competent *E. coli* cells were prepared by starting an overnight culture of the strain of interest with appropriate antibiotics in sterile SOB (super optimal broth) media (For 1 liter: 2 % (w/v) Tryptone, 0.5 % (w/v) Yeast extract, 0.05 % NaCl; autoclave, cool and then add filter sterilized: 250 mM KCl, 10 mM MgSO₄ and 0.5 mM NaOH). The overnight grown cells were transferred to 100 ml SOB media and grown at 37 °C by shaking at 180 RPM until the OD₆₀₀ (optical density at 600 m) reached 0.5 and then placed on ice for 10 minutes. The cells were centrifuged at 2500 X g for 10 minutes at 4 °C. The supernatant was removed and cell pellets were re-suspended in 30 ml of ice cold TB (transformation buffer) (10 mM PIPES, 15 mM CaCl₂, 250 mM KCl, pH to 6.7 using KOH, then MnCl₂ was added to a final concentration of 55 mM) and incubated on ice for 10 minutes. The cells were centrifuged for 10 minutes at 1000 X g at 4 °C and supernatant discarded. The cell pellet was re-suspended in 8 ml TB followed by addition of 7 % (v/v) DMSO (DiMethyl SulFOxide) and required antibiotics and incubated on ice for 10 minutes. The cells were aliquoted into 50 µl, snap frozen in liquid Nitrogen and stored at -80 °C until required. Competent cells transformed using the electroporation method were grown in the same way as described above, but after initial centrifugation, the cells were re-suspended in deionized water and centrifuged again at 1000 X g for 10 minutes at 4 °C followed by re-suspension in 10 % (v/v) glycerol and split into 50 µl aliquots and snap frozen in liquid Nitrogen before storing them at -80 °C.

2.2.4 Transformation of competent cells

10-50 ng of plasmid DNA was added to 50 µl of competent cells and placed on ice for 30 minutes. For chemically competent cells, the cells were incubated at 42 °C for 45 seconds (heat shock), followed by 2 minutes on ice, whereas for the electroporation method, the cells were placed on a 1 millimeter electroporation cuvette (Serva, Germany) and pulsed with a voltage of 2.5 KV using the Bio-Rad Gene Pulser electroporation system (Bio-Rad, USA). 500 µl of LB media was added to the cells and recovered for 1 hr at 37 °C followed by either plating on LB-Agar plates or transferred to LB media for overnight growth with appropriate antibiotics.

2.2.5 Heterologous overexpression of recombinant proteins

Recombinant protein was overexpressed in Rosetta (DE3) *E. coli* grown in LB media

supplemented with the appropriate antibiotics. Initially the cultures were incubated at 37 °C by shaking (Infors HT, Switzerland), once the OD₆₀₀ reached 0.5 – 0.7, the temperature was decreased to 22 °C. Protein overexpression was induced by the addition of IPTG (isopropyl β-D-thiogalactopyranoside) when the OD₆₀₀ of the cells reach 0.8 – 1.0. The cells were grown at 22 °C overnight and harvested by centrifuging at 5,000 RPM for 20 minutes at 4 °C and stored at -80 °C until required.

Procedures deviating from the above protocol are:

Sirt3

The human Sirt3 construct used in this study comprises amino acids 114-399 and was cloned in pET151/D-TOPO vector harboring a His-tag (hexahistidine tag) affinity tag and a TEV (tobacco etch virus) protease cleavage site. Sirt3 protein was overexpressed in Rosetta 2 (DE3) *E. coli* cells grown in LB media (containing 100 µg/ml Ampicillin and 34 µg/ml Chloramphenicol) by the addition of 0.5 mM IPTG at mid log phase followed by overnight incubation at 20 °C/150 RPM in a shaker (Infors HT, Switzerland). After overnight protein expression, the cells were centrifuged at 5,000 RPM at 4 °C for 20 minutes; cell pellets were collected and stored at – 80 °C until required.

Sirt5

The human Sirt5 construct used in this study (provided by Prof. Dr. Clemens Steegborn) comprises amino acids 34-302 cloned in pET151/D-TOPO vector harboring a His-tag tag and a TEV protease cleavage site. Sirt5 protein was overexpressed in Rosetta 2 (DE3) *E. coli* cells grown in LB media (containing 100 µg/ml Ampicillin and 34 µg/ml Chloramphenicol) by the addition of 0.5 mM IPTG at mid log phase followed by overnight incubation at 20 °C/140 RPM in a shaker (Infors HT, Switzerland). After overnight protein expression, the cells were centrifuged at 5,000 RPM at 4 °C for 20 minutes, cell pellets were resuspended in lysis buffer containing 50 mM Tris, pH 7.8, 200 mM NaCl, 1:200 PMSF (phenylmethanesulfonyl fluoride) and stored at – 80 °C until required.

Sirt7

The human Sirt7 constructs used in this study were cloned, expressed and purified (initial steps) at the DPF (Dortmund protein facility), MPI (Max Planck Institute) Dortmund, Germany, by Dr. Tim Bergbrede and colleagues. All Sirt7 protein constructs (except the insect cell expressed full length Sirt7) were overexpressed in BL21 (DE3) codonPlus RIL *E.*

coli cells grown in Autoinduction media supplemented with 100 µg/ml Ampicillin, initially at 37 °C/180 RPM for 4 hours, followed by 20-24 hour incubation at 25°C/180 RPM in a shaker. After overnight protein expression, the cells were centrifuged at 6,000 RPM at 4 °C for 20 minutes, cell pellets were collected and resuspended in ice cold PBS (phosphate buffered saline) buffer followed by an additional spin at 4,500 RPM at 4 °C for 15 minutes. Cell pellets were collected and stored at – 80 °C until required.

Sir2Tm

The pET11a plasmid encoding full length Sir2Tm gene was obtained from Addgene, USA (Addgene plasmid 25815) and transformed into the *E. coli* strain BL21 (DE3) pLysS. Protein expression was performed as described by Smith et. al. (Smith et al., 2002). *E. coli* cells transformed with pET11a plasmid was grown in glucose enriched M9ZB minimal media (containing 34 µg/ml Chloramphenicol) at 37 °C by shaking in an incubator at 150 PRM until the OD₆₀₀ reached 0.5-0.6, at which point the protein overexpression was induced by the addition of 1 mM IPTG and growing the cells for an additional 4-5 hrs. The cells were then centrifuged at 5,000 RPM at 4 °C for 20 minutes; cell pellets were collected and stored at – 80 °C until required.

AROS

AROS gene was cloned into three different types of plasmids: pET15a (containing thrombin cleavable His-tag at N-terminus), pGEX-6P-3 (containing Rhino virus 3C cleavable GST (glutathione-S-transferase) tag at N-terminus) and a modified vector (obtained from the lab of Prof. John Denu at University of Wisconsin, Madison, USA, containing nicotinamidase gene, which was removed and AROS was inserted resulting in hexa-histidin-MBP (maltose-binding protein)-tag at N-terminus of AROS). Plasmids encoding AROS gene were transformed into the *E. coli* strain Rosetta 2 (DE3). AROS protein was overexpressed in Rosetta 2 (DE3) *E. coli* cells grown in LB media (containing 100 µg/ml Ampicillin and 34 µg/ml Chloramphenicol) by the addition of IPTG (0.1 mM for pET15b vector and 1 mM for pGEX-6P-3 and modified vector) at mid log phase followed by overnight incubation at 12 °C/120 RPM in a shaker (Infors HT, Switzerland). After overnight protein expression, the cells were centrifuged at 5,000 RPM at 4 °C for 20 minutes; cell pellets were collected and stored at – 80 °C until required.

2.2.6 Cell lysis

Frozen cells were thawed and resuspended in respective lysis buffer and homogenized using a pottering devise and passed over a Microfluidizer (Microfluidics, USA) maintained at 4° C, in order to lyse the cells. The lysed cells were centrifuged at 18,000 RPM for 45 minutes in a refrigerated Beckman Coulter Avanti J-26XP centrifuge fitted with a JA-30.50 Ti rotor (Beckman Coulter, USA) to remove cell debris.

2.3 Molecular biology methods

2.3.1 Agarose gel electrophoresis

Nucleic acid electrophoreses were performed in a Bio-Rad Sub-cell horizontal gel electrophoresis system (Bio-Rad, USA) using 1x TAE (Tris-acetate-EDTA (ethylenediaminetetraacetic acid)) as running buffer. Samples and DNA ladder (New England Biolabs, USA) mixed with loading buffer (6 mM EDTA, 6 % glycerol and 0.015 % bromophenol blue) were electrophorezed on a 1 % (w/v) agarose matrix (made in 1x TAE buffer) containing 1 µg/ml ethidium bromide. After electrophoresis, the gel was placed under UV light for visualization of nucleic acids.

2.3.2 Gene cloning

In order to clone a gene of interest, primers were synthesized that amplify the gene from a template using the (polymerase chain reaction) technique (Mullis et al., 1986). A typical PCR reaction consisted of the following in a 50 µl reaction volume: template DNA (10-50 ng), forward and reverse primers (0.5 µM each), deoxynucleotide mix (0.2 µM of each dATP, dCTP, dGTP and dTTP), 4 % (v/v) DMSO, 2 Units of Phusion DNA polymerase (Thermo Scientific, USA), 1x Phusion HF buffer (containing a final concentration of 1.5 mM MgCl₂). The conditions used for PCR were: 1) initial denaturation at 98 °C for 30 seconds; 2) denaturation at 98 °C for 10 seconds, annealing at 62 °C for 30 seconds, extension at 72 °C for 30 seconds; 3) final elongation at 72 °C for 10 minutes. Step 2 was repeated 25 times to amplify the DNA. The amplified DNA was purified using the Nucleospin Gel and PCR clean-up kit (Macherey-Nagel, Germany) and visualized by agarose gel electrophoresis.

The amplified gene/insert and the plasmid/vector in which the gene of interest is to be cloned were treated with appropriate restriction enzymes encoded in the primers (of the gene of interest) and present in the vector and digested according to the manufacturer's recommendations (typically Fermentas FastDigest Restriction enzymes NdeI and XhoI was

used) (Thermo Scientific, USA) followed by agarose gel electrophoresis to visualize and purify the restriction enzyme digested insert and vector.

The insert was ligated into the vector using a molar ratio of 3:1 (insert : vector) followed by addition of T4 DNA ligase (New England Biolabs, USA) and incubation at 16 °C overnight. 3-5 µl of the ligated product was used for the transformation of the plasmid into 50 µl of XL-1 blue competent cells.

An alternative to the cloning procedure described above called ligation independent cloning was also used (adapted from (Chen et al., 2000)). In this technique the primers were designed in such a way that, one part binds to the gene to be amplified and the other part binds to the plasmid into which the gene will be inserted. Two rounds of PCR were performed during the cloning procedure; the first PCR was same as the one mentioned above, following which the gene was purified by electrophoresis. For the second PCR, the gel purified PCR product from the first PCR served as the primer (~100-200 ng) and the vector (~100 ng) served as the template. The reaction also contained deoxynucleotide mix (0.2 µM of each dATP, dCTP, dGTP and dTTP), 4 % (v/v) DMSO, 1.25 Units of *Pfu Turbo* DNA polymerase (Agilent Technologies, USA), 1x Cloned *Pfu* DNA polymerase reaction buffer (20 mM Tris-HCl (pH 8.8), 2 mM MgSO₄, 10 mM KCl, 10 mM (NH₄)₂SO₄, 0.1% Triton X-100, 0.1 mg/ml nuclease-free BSA). The final volume of the second PCR reaction was 25 µl. The conditions used for PCR were: 1) initial denaturation at 95 °C for 30 seconds; 2) denaturation at 95 °C for 30 seconds, annealing at 55 °C for 1 minute, extension at 68 °C for 10 minutes; 3) final elongation at 72 °C for 10 minutes. Step 2 was repeated 18 times to amplify the DNA. The PCR product was then treated with 5 Units of DpnI restriction enzyme for 1 hr at 37 °C to digest the template vector and 1 µl of the reaction mixture was transformed into 50 µl of XL-1 blue competent cells.

Colonies obtained after transformation of the ligation/PCR product were screened for positive clones using a colony screening PCR (conditions similar to the first PCR described above) and the colonies containing the insert were cultured overnight for plasmid isolation, followed by a restriction digest analysis to verify the presence of the gene of interest in the plasmid.

Plasmid isolation from overnight grown *E. coli* cells was performed using the GeneJET plasmid miniprep kit (Thermo Scientific, USA).

2.3.3 Site directed mutagenesis

Site directed mutagenesis were performed by following the Quick-change mutagenesis protocol (Agilent Technologies, USA). The PCR contained the following in a 25 µl reaction volume: ~ 50 ng of template DNA, 240 µM each forward and reverse primers, 0.2 µM deoxynucleotide mix (equimolar mixture of dATP, dCTP, dGTP and dTTP), 1.25 Units of *Pfu Turbo* DNA polymerase (Agilent Technologies, USA), 1x Cloned *Pfu* DNA polymerase reaction buffer (20 mM Tris-HCl (pH 8.8), 2 mM MgSO₄, 10 mM KCl, 10 mM (NH₄)₂SO₄, 0.1% Triton X-100, 0.1 mg/ml nuclease-free BSA). The conditions used for PCR were: 1) initial denaturation at 95 °C for 30 seconds; 2) denaturation at 95 °C for 30 seconds, annealing at 55 °C for 1 minute, extension at 68 °C for 10 minutes; 3) final elongation at 72 °C for 10 minutes. Step 2 was repeated 18 times to amplify the DNA. The PCR product was then treated with 5 Units of DpnI restriction enzyme for 1 hr at 37 °C to digest the template vector and 1 µl of the reaction mixture was transformed into 50 µl of XL-1 blue competent cells.

2.3.4 DNA sequencing

All the cloned genes and point mutants were sequenced in order to verify that no undesirable mutations happened using either LGC Genomics, Germany, Eurofins MWG Operon, Germany or DNA sequencing facility at the Ruhr University, Bochum, Germany.

2.4 Biochemical methods

2.4.1 Determination of protein concentration

Protein concentration was determined using two spectrophotometric methods. In the first method, the Bradford dye (Bio-Rad, USA) was used to determine the concentration of the protein using a calorimetric assay. 1-10 µl of protein was added to 200 µl of the dye, made up to 1000 µl and incubated for two minutes before measuring the absorbance at 595 nm on a Cary 50 UV-Vis spectrophotometer (Agilent Technologies, USA) that was already blanked with the dye alone. The concentration was then calculated using the following equation:

$$\text{Protein concentration (mg/ml)} = ((37.4 * A_{595}) - 0.74) * \text{total volume } (\mu\text{l}) / (\text{sample volume } (\mu\text{l}) * 1000).$$

The value obtained using the above equation is multiplied by a correction factor (0.6 for full length human Sirt1) to yield the actual concentration of the protein.

In the second spectrophotometric method, a UV scan from 350 – 200 nm was performed on the protein sample using a Cary 50 UV-Vis spectrophotometer (Agilent Technologies, USA) after performing a blank with the buffer and the A_{280} was used to calculate the concentration of protein according to the Beer-Lambert law as follows:

$$\text{Protein concentration (mg/ml)} = (A_{280}/(\epsilon_{280} \cdot \text{path length})) \cdot \text{dilution factor}$$

The path length is 1 cm and the theoretical extinction coefficient (ϵ_{280}) value at 1 mg/ml for a particular protein is obtained from the ExPASy's protparam server (<http://web.expasy.org/protparam/>). For full length human Sirt1 with N-terminal 6x His-tag the ϵ_{280} at 1 mg/ml is 0.547 (45840 M⁻¹ cm⁻¹).

2.4.2 SDS-Polyacrylamide gel electrophoresis (SDS-PAGE)

The purity and size of protein samples were accessed using SDS-PAGE containing the Tris-glycine discontinuous buffer system adapted from Laemmli (Laemmli, 1970). The percentage of acrylamide in separating gel ranged from 12 – 15 %. The stacking gel, running gel, running buffer and SDS loading buffer were prepared according to Sambrook, J., and Russell, D. W., (Molecular cloning: A Laboratory manual, third edition). Protein samples were denatured by boiling for 5 minutes at 95 °C before loading on the gel. The SDS loading buffer contained β -mercapto ethanol to ensure a reducing atmosphere. The Mini-PROTEAN Tetra Cell vertical electrophoresis system (Bio-Rad, USA) was used for electrophoresis, at a constant voltage of 150 volts. After electrophoresis, the gel was rinsed in water, followed by few seconds of soaking in hot Coomassie blue solution (0.025 % (w/v) Coomassie-Briliant Blue R-250 (Applichem, Germany), 50 % (v/v) methanol, 10 % (v/v) acetic acid). The gel was then transferred to a destaining solution containing 20 % (v/v) methanol and 12 % (v/v) acetic acid.

2.4.3 Blue-native polyacrylamide gel electrophoresis (BN-PAGE)

To analyze the oligomeric state of Sirtuins, BN-PAGE (blue-native polyacrylamide gel electrophoresis) was performed according to the protocol of Schaeffer (Schaeffer, 1991). BN-PAGE was performed using a *Hoefler Mighty Small* apparatus (GE Healthcare, USA) at a constant voltage of 150 V for the first 15 minutes and then at 250 V until the end. The samples were prepared by mixing them with 10 % (v/v) glycerol followed by centrifugation for 10 minutes at 13,200 RPM in a refrigerated Eppendorf microfuge (Eppendorf, Germany). Molecular weight markers were purchased from Serva, Germany. The gel consisted of three

layers with different percentage of acrylamide in each of them. The composition of the gels and the buffers are as follows:

Top layer: 50 mM Bis-Tris/HCl, pH 7.0, 200 mM ϵ -aminocaproic acid, 0.1 % (v/v) TEMED, 1 % (w/v) ammonium persulfate, 5 % acrylamide/bisacrylamide (37.5:1).

Middle layer: 50 mM Bis-Tris/HCl, pH 7.0, 200 mM ϵ -aminocaproic acid, 10 % (v/v) glycerol, 0.5 % (v/v) TEMED, 0.5 % (w/v) ammonium persulfate, 10 % acrylamide/bisacrylamide (37.5:1).

Bottom layer: 50 mM Bis-Tris/HCl, pH 7.0, 200 mM ϵ -aminocaproic acid, 20 % (v/v) glycerol, 0.25 % (v/v) TEMED, 0.25 % (w/v) ammonium persulfate, 14 % acrylamide/bisacrylamide (37.5:1).

Anode buffer: 50 mM Bis-Tris/HCl, pH 7.0, 50 mM Tricine, 0.02 % (w/v) Coomassie BrilliantBlue G-250 (Serva, Germany).

Cathode buffer: 50 mM Bis-Tris/HCl, pH 7.0,

2.4.4 Purification of recombinant proteins

2.4.4.1 Affinity chromatography

Purification of recombinant proteins containing His-tag was performed using TALON resin (Clontech, USA). The His-tag was used on majority of the proteins including Sirt1, Sirt2, Sirt3, Sirt5, Sirt7 and AROS. AROS with GST tag was purified using Glutathione sepharose resin (GE Healthcare, USA). Proteins with His-MBP fusion tag were purified using TALON or Ni-NTA resin. Full length Sirt1 (wild-type and H363A mutant) containing Strep tag were purified using the Strep-Tactin sepharose resin (IBA, Germany). For every liter of *E. coli* culture, 1 ml bed volume of resin was used. Prior to usage, the resin was washed twice with water, followed by equilibration in lysis buffer. The cleared *E. coli* supernatant containing the recombinant protein in lysis buffer was incubated with the resin at 4 °C for 1 hr by stirring for efficient binding of the protein to the resin. After the incubation, the flow-through was collected by gravity flow using a glass column (Bio-Rad, USA) and the resin was incubated for 30 minutes at 4 °C with 20 μ g/ml (bed volume) of bovine RNase A and 10 μ g/ml of bovine DNase in 25 mM Tris, pH 7.5, 20 mM NaCl, 5 mM MgCl₂, 0.2 mM PMSF to remove nucleic acids binding to the protein of interest. After incubation, the flow-through was collected and the column washed with 20 bed volumes of wash buffer and then eluted

with elution buffer (buffer compositions see below). The samples were run on SDS-PAGE to access the size and purity before performing additional purification steps.

TALON resin:

Lysis buffer: 50 mM Tris, pH 7.5, 300 mM NaCl, 0.2 mM PMSF (for AROS and Sirt1 229to516 10 mM Imidazole was added in the lysis buffer).

Wash buffer: 50 mM Tris, pH 7.5, 300 mM NaCl, 0.2 mM PMSF, 10 mM Imidazole (for AROS and Sirt1 229to516 15 mM Imidazole was added).

Elution buffer: 50 mM Tris, pH 7.5, 300 mM NaCl, 0.2 mM PMSF, 150 mM Imidazole

GST resin:

Lysis and wash buffer: 50 mM Tris, pH 7.5, 300 mM NaCl, 0.2 mM PMSF.

Elution buffer: 50 mM Tris, pH 7.5, 300 mM NaCl, 0.2 mM PMSF, 10 mM Glutathione.

Strep-Tactin resin:

Lysis and wash buffers: 100 mM Tris·Cl, 150 mM NaCl, 1 mM EDTA, pH 8, 0.2 mM PMSF.

Elution buffer: 100 mM Tris·Cl, 150 mM NaCl, 1 mM EDTA, 2.5 mM desthiobiotin, pH 8, 0.2 mM PMSF.

2.4.4.2 Size exclusion chromatography

Elution samples from the affinity chromatography were pooled, concentrated using an Amicon centrifugal concentrator (Millipore, USA) to 5 ml and applied on to a preequilibrated Superdex200 16/60 size exclusion column (GE Healthcare, USA) and eluted with 25 mM HEPES, pH 7.5, 100 mM KCl, 2 mM DTT (dithiothreitol), 0.1 mM PMSF, 0.5 mM EDTA. For analytical purposes a Superose12 GL300 column was also used with the same buffer as mentioned above but without PMSF and EDTA. Following chromatography, the samples were run on SDS-PAGE to access their purity; appropriate fractions were pooled and concentrated.

2.4.4.3 Ion exchange chromatography

Ion exchange chromatography was performed using the 1 ml HiTrap Q HP anion exchange column (GE Healthcare, USA) that was preequilibrated with buffer A (25 mM HEPES, pH 7.5, 100 mM KCl, 2 mM DTT, 0.1 mM PMSF, 0.5 mM EDTA). The samples

from SEC (size exclusion chromatography) were concentrated to 5 ml and applied on the ion exchange column at a very low flow rate of 0.05 ml/minute. The column was washed with 2 column volumes of buffer A followed by elution of the bound protein using a linear gradient against buffer B (buffer A containing total 500 mM KCl). Appropriate fractions were pooled after accessing their purity using SDS-PAGE, desalted in storage buffer (25 mM HEPES, pH 7.5, 100 mM KCl, 2 mM DTT), concentrated, flash frozen in liquid Nitrogen and stored at -80 °C until required.

2.4.5 Cleavage of affinity tags

Affinity tags or fusion proteins were cleaved using proteases that recognize sequences present between the tags and the protein of interest. The affinity purified proteins were dialyzed in 25 mM HEPES, pH 7.5, 100 mM KCl, 2 mM DTT at 4 °C and concentration determined before adding proteases. Thrombin protease (GE Healthcare, USA) was added at 1 Unit/mg of recombinant protein and incubated overnight at 4 °C. TEV (tobacco etch virus) protease and PreScission (human rhinovirus 3C protease) were added at a ratio of 1:20 mg of recombinant protein and incubated overnight at 4 °C. Following overnight incubation with the required proteases, the samples were passed over the same affinity columns over which they were initially purified in order to remove the uncleaved protein and the protease (TEV and PreScission contain His-tag and GST tag respectively). Thrombin protease was separated from the protein of interest by passing it over benzamidine sepharose resin.

Procedures deviating from the above protocol are:

Sirt3

The cells containing overexpressed Sirt3 were resuspended in 50 mM HEPES, pH 7.5, 300 mM NaCl, 10 mM Imidazole, 1 mM TCEP (tris(2-carboxyethyl)phosphine), lysed and affinity purified using TALON resin as mentioned above (except for the addition of nucleases). The purified protein was dialyzed in 25 mM HEPES, pH 7.5, 100 mM KCl, 2 mM DTT for 3 hours (except for the addition of nucleases) at 4 °C followed by addition of TEV protease (1 mg of TEV protease per 20 mg of affinity purified Sirt3) and stored at 4 °C overnight for cleavage of the affinity tag. The following day, the sample was passed through His-Select Nickel affinity resin (Sigma, USA) to remove uncleaved protein and the TEV protease (contains His-tag at the C-terminus), concentrated to 1 ml and applied on a Superose12 size exclusion column (GE Healthcare, USA) equilibrated in dialysis buffer, to

separate Sirt3 from aggregates and other contaminants. Sirt3 containing samples were pooled, concentrated, snap frozen in liquid N₂ and stored at -80 °C until needed.

Sirt5

The cells containing overexpressed Sirt5 were thawed, lysed and affinity purified using TALON resin as mentioned above (except for the addition of nucleases) with the following wash and elution buffers: wash buffer = 50 mM Tris, pH 7.8, 200 mM NaCl, 20 mM Imidazole and elution buffer = 50 mM Tris, pH 7.8, 200 mM NaCl, 150 mM Imidazole. The purified protein was concentrated and desalted in 20 mM Tris, pH 7.8, 200 mM NaCl, 1 mM DTT using a NAP column (GE Healthcare, USA) followed by addition of TEV protease (1 mg of TEV protease per 20 mg of affinity purified Sirt5) and stored at 4 °C overnight for cleavage of the affinity tag. The following day, the sample was passed through Nickel affinity resin (Qiagen, USA) to remove uncleaved protein and the TEV protease (contains His-tag at the C-terminus), concentrated to 1 ml and applied on a Superose12 size exclusion column (GE Healthcare, USA) equilibrated in desalting buffer, to separate Sirt5 from aggregates and other contaminants. Sirt5 containing samples were pooled, concentrated, snap frozen in liquid N₂ and stored at -80 °C until needed.

Sirt7

The cells containing overexpressed Sirt7 were resuspended in lysis buffer (50 mM HEPES, pH 8.0, 300 mM NaCl, 20 mM Imidazole, 1 mM TCEP), lysed and applied on to a 5 ml HisTrap FF resin (GE Healthcare, USA) connected to an AKTAXPress HPLC (Hi-Performance Liquid Chromatography) system (GE Healthcare, USA). After washing the column with 20 column volumes of wash buffer (lysis buffer containing 30 mM Imidazole), the column was equilibrated with 5 column volumes of cleavage buffer (50 mM HEPES, pH 8.0, 150 mM NaCl, 1 mM TCEP), followed by addition of 0.7 column volumes of respective protease and incubation for 5 hours. The tag-less protein was then washed out of the column using wash buffer. The largest peak (based on area) was collected (maximum 13 ml) and passed over 26/60 Superdex size exclusion column (GE Healthcare, USA) equilibrated in 25 mM HEPES, pH 7.5, 40 mM NaCl, 1 mM TCEP, to separate Sirt7 from aggregates and other contaminants. Sirt7 containing samples were pooled, concentrated, snap frozen in liquid N₂ and stored at -80 °C until needed.

Sir2Tm

Purification of Sir2Tm was performed as described by Smith et. al. (Smith et al., 2002) with few modifications. The *E. coli* containing overexpressed Sir2Tm were lysed (as mentioned above) in 50 mM Tris pH 7.5, 100 mM NaCl, 1 mM EDTA, 5 mM DTT and the inclusion bodies containing overexpressed Sir2Tm were isolated by multiple centrifugation and washing steps as described by Smith et. al. and solubilized in 50 mM Tris, pH 8.0, 4M Urea, 100 mM NaCl, 5 mM DTT, 25 μ M ZnCl₂ by rocking over night at 4 °C. The solubilized protein was diluted to 1 mg/ml and dialyzed for 3 hours at 4 °C in 50 mM Tris, pH 8.0, 100 mM NaCl, 5 mM DTT, 25 μ M ZnCl₂ in order to refold it followed by another 3 hour dialysis in Buffer A (40 mM Tris, pH 8.0, 5 mM DTT, 25 μ M ZnCl₂). The protein was bound to HiTrapQ HP anion exchange column (GE Healthcare, USA) in Buffer A and eluted in a gradient to buffer A supplemented with 1M NaCl at a flow rate of 0.3 ml/min. The eluted fractions were analyzed by SDS-PAGE and fractions containing Sir2Tm were pooled (~28.7 % B), concentrated to 1 ml and applied to a Superose12 size exclusion column (GE Healthcare, USA) equilibrated in 20 mM HEPES, pH 8.0, 150 mM NaCl, 5 mM DTT in order to remove further contaminations and aggregated proteins. Sir2Tm containing samples were pooled, concentrated to 10 mg/ml, snap frozen in liquid N₂ and stored at -80 °C until needed.

AROS

AROS containing His-tag and His-MBP-tag was purified similar to Sirt1. AROS containing GST-tag was affinity purified using Glutathione resin similar to other AROS constructs with the following lysis, wash and elution buffers: lysis buffer = 50 mM Tris, pH 7.5, 150 mM NaCl, 0.2 mM PMSF, wash buffer = 50 mM Tris, pH 7.5, 150 mM NaCl, 5 mM DTT and elution buffer = 50 mM Tris, pH 8.0, 1500 mM NaCl, 5 mM DTT, 20 mM reduced L-Glutathione.

Solubilization and purification of AROS from *E. coli* pellets were performed as follows: the lysates resulting from sonication were centrifuged at 18,000 RPM for 45 minutes at 4 °C. The resulting pellet was solubilized in 50 mM Tris, pH 7.5, 300 mM NaCl, 10 mM Imidazole and 6M Guanidin hydrochloride by stirring at room temperature for ~ 30 minutes. The sample was then centrifuged at 18,000 RPM for 45 minutes at 20 °C; supernatant was removed and incubated with TALON resin for 1 hour at room temperature. The mixture was then applied to a column and the flow through was collected. The protein was refolded in a stepwise manner by washing with 5 column volumes each of buffer1 (50 mM Tris, pH 7.5, 300 mM NaCl, 20

mM Imidazole, 8 M Urea), buffer2 (buffer1 containing 4 M Urea), buffer3 (buffer1 containing 2 M Urea), buffer4 (buffer1 containing 1 M Urea) and finally with buffer5 (buffer1 without Urea). This was followed by elution buffer (50 mM Tris, pH 7.5, 300 mM NaCl, 150 mM Imidazole). The eluted protein was concentrated to 1 ml and applied on to a Superose12 column which was equilibrated in 25 mM HEPES, pH 7.5, 100 mM KCl, 2 mM DTT and fractions corresponding to AROS were collected.

2.4.6 Fluorescence based peptide deacetylation assay

A fluorescently labeled peptide called *Fluor de Lys1* (FdL-1) based on the sequence of p53 with acetylation at Lys382 (RHKK[ac]-coumarin) (Enzo Life Sciences, USA) was used as a substrate in deacetylation assays. The principle behind the assay is the ability of the Sirtuin to deacetylate the fluorescent peptide in the presence of the co-substrate NAD^+ , following which the addition of Trypsin cleaves the fluorescent tag (coumarin) leading to an increase in the fluorescence. The assay was performed by addition of 1 μg of Sirtuin, 100 μM FdL-1, 1 mM NAD^+ in the assay buffer (50 mM Tris, pH 8.0, 137 mM NaCl, 2.7 mM KCl, 1 mM MgCl_2 , 1 mg/ml BSA (bovine serum albumin) followed by incubation for 30 minutes at 37 °C. After the incubation, a developer mixture containing 2 mM NAM, 10 mg/ml Trypsin was added to the reaction mixture and incubated for 45 minutes at room temperature, after which the fluorescence was measured on a FluoDiaT70 microplate reader (Photal Otsuka Electronics, Japan) using an excitation wavelength of 360 nm and an emission wavelength of 460 nm. A reaction mixture containing all the components of the assay sans the enzyme was used as a blank and subtracted from the samples containing the enzyme. While testing for potential Sirtuin activators, the concentration of the substrate (FdL-1) and the co-substrate (NAD^+) was kept at 25 μM and 25/50 μM respectively.

For Sirt3, the substrate used was *Fluor de Lys2* (FdL-2) which is based on the sequence of p53 peptide 317-320 (QPKK[ac]-coumarin) (Enzo Life Sciences, USA), because the deacetylation efficiency was higher when compared to the FdL-1 peptide substrate.

2.4.7 Enzyme-linked immunosorbent assay (ELISA)

Deacetylation of Glutamate dehydrogenase (GDH) by Sirt3 and Cyt. c by Sirt5 was carried out using ELISA as described in Schlicker et. al., (Schlicker et al., 2008). 10 μg of Cyt. c or mitochondrial GDH (both from Sigma, USA) was dissolved in 100 μl of TBS (Tris buffered saline; 50 mM Tris, pH 7.4, 150 mM NaCl) and incubated at 4 °C overnight in a 96 well microtiter plate (Beckton and Dickenson, USA). The plates were washed with TBST

(TBS buffer containing 0.1 % Tween-20) and incubated with blocking buffer (TBST containing 3 % skimmed milk) for 2 hrs at room temperature. The plates were again washed with TBST, followed by TBS. 10 μg of Sirt5 or Sirt3 was added to the plates with varying concentrations of NAD^+ and incubated at 37 °C for 30 minutes followed by washing with TBST and TBS. Anti acetyl lysine antibody (Stressgen, USA) at a ratio of 1:1000 were then added to the plates and incubated for 2 hrs at room temperature and washed with TBST. A secondary antibody (Sigma, USA) raised against rabbit IgG conjugated with horse radish peroxidase was added at a dilution of 1:2000 and incubated for 2 hrs at room temperature and washed thoroughly with TBST. The peroxidase substrate TMB (3,3',5,5'-tetramethylbenzidin) (Sigma, USA) was added at a concentration of 1.5 mg/ml to the plates and incubated for 3 minutes before stopping the reaction with 1M H_2SO_4 . The reaction was quantified calorimetrically at a wavelength of 450 nm using an EL800 Microplate reader (BioTek, USA).

2.4.8 Continuous assay for deacetylation based on coupled enzymes

A continuous deacetylation assay for Sirtuins recently described by Smith et. al., (Smith et al., 2009) based on the principle of a coupled assay was also used to monitor the deacetylation activity of Sirtuins. In this assay, one of the reaction product NAM, serves as a substrate for a downstream enzyme Nicotinamidase, which converts it to NH_3 , which in turn is used by GDH in the presence of NADPH and α -ketoglutarate to produce L-glutamate and NADP^+ . The decrease in absorbance at 340 nm due to the consumption of NADPH ($\epsilon_{340} = 6.22 \text{ mM}^{-1} \text{ cm}^{-1}$) is monitored continuously over time using a spectrophotometer (Cary 50, Agilent technologies, USA). A typical reaction mixture consisted of 1 μM Sirutin, 1 mM peptide substrate, 1 mM NAD^+ , 1 mM DTT, 3.3 mM α -ketoglutarate, 2 μM tag cleaved Nicotinamidase (*Salmonella enterica*), 2 units of bovine GDH or 0.3 units of proteus GDH and 0.2 mM NADPH in 20 mM Na- PO_4 , pH 7.5 in a total volume of 100 μl . The reaction was performed at 25 °C using a Peltier temperature controller device. All components but for the Sirtuin was added initially and the reaction was monitored for 5 minutes after blanking to establish a base line followed by the addition of Sirtuin.

2.4.9 Limited proteolysis of proteins

In order to identify potential stable constructs of Sirt1 for crystallization, a limited proteolysis approach was performed. Roughly 10 μg of protein was incubated with 0.1 μg of protease (Trypsin, Chymotrypsin or Subtilisin) for 30 minutes at 4 °C or at room temperature,

followed by quenching with hot SDS loading buffer (maintained at 80 °C) and run on SDS-PAGE. The Coomassie stained and de-stained gel was transferred to a PVDF (polyvinylidene fluoride) membrane, the most prominent band was cut and sent for N-terminal sequencing. (Toplab, Germany).

2.4.10 Thermal denaturation shift assay

Protein thermal denaturation was followed by exploiting the change in the fluorescence of the dye SYPRO Orange (Life Technologies, USA), which upon binding to hydrophobic (unfolded) parts of the protein increases its intrinsic fluorescence. 3 µg of total protein was taken in a 96 well microtiter plate (Bio-Rad, USA), 1 µl of 1 to 10 diluted SYPRO dye was added to it and made up to 50 µl using different buffers followed by 15 µl of mineral oil. The buffers used were 50 mM each of sodium citrate (pH 4.0 and 5.0), MES (2-(*N*-Morpholino)EthaneSulfonic acid) (pH 6.0), HEPES (pH 7.0), Tris (pH 8.0) and CAPSO (*N*-cyclohexyl-3-aminopropanesulfonic acid) (pH 9.0) and the salt concentrations were 0, 50, 200 and 500 mM KCl. The temperature was gradually increased from 25 °C to 73 °C in 2 °C intervals. The change in fluorescence was followed using a FluoDIA70 microplate reader (Photal Otsuka Electronics, Japan) using an excitation wavelength of 465 nm and an emission wavelength of 580 nm.

2.4.11 Microscale thermophoresis

Binding measurements were performed using the principle of microscale thermophoresis on a NanoTemper Monolith NT.115 instrument (NanoTemper Technologies GmbH, Germany). 20 µM protein was dialyzed against 100 mM ammonium carbonate ((NH₄)₂CO₃), pH 8.3 for 3 hours at 4 °C and mixed with NT-647 fluorescent dye at a ratio of 1:1 in a total volume of 250 µl and incubated at room temperature for 30 minutes in the dark. The unreacted dye was removed from the protein by applying the sample on a gel filtration column (NAP column, GE Healthcare, USA) that was pre-equilibrated in 25 mM HEPES, pH 7.5, 100 mM KCl, 2 mM DTT. The labeling efficiency was monitored spectrophotometrically by calculating the concentration of protein and dye using their respective extinction coefficients (the extinction coefficient of NT-647 dye is 250000 M⁻¹ cm⁻¹ at 650 nm and the extinction coefficient of human Sirt1 at 280 nm is 45840 M⁻¹ cm⁻¹). An alternative label called FITC (fluorescein isothiocyanate) was also used with the same procedure, except for changes in the pH of the buffer (100 mM (Na)₂CO₃, pH 9.3), the ratio of protein to dye (1:2) and incubation time (1 hr at room temperature in the dark). The extinction coefficient of FITC

dye is $73,000 \text{ M}^{-1} \text{ cm}^{-1}$ at 495 nm in pH 9.3 buffer and the extension coefficient of Sir2Tm is $13410 \text{ M}^{-1} \text{ cm}^{-1}$ at 280 nm. The elution buffer for Sir2Tm was 20 mM HEPES, pH 7.5, 150 mM NaCl. Typical ratios between protein and dye were $\sim 1:1$ (NT-647) and $\sim 1:1.66$ (FITC). 200 nM of the labeled protein or 1 μM of the label free protein were mixed with different concentrations of the ligands to be titrated and loaded on thin glass capillaries for analysis. Microscale thermophoresis of the protein sample was followed after applying a definite amount of heat on the sample using an infrared laser and following the fluorescence simultaneously, since it is coupled to the laser path using an infrared dichroic mirror and focused on the sample through the same objective. Analysis of the results were performed using GraFit (Erithacus Software Limited, UK).

2.4.12 Analytical ultracentrifugation

AUC (analytical ultracentrifugation) experiments were performed at Hannover medical school with the help of Dr. Ute Curth. Briefly, different concentration of Sirt1 samples were prepared in 25 mM HEPES, pH 7.5, 100 mM KCl, 0.5 mM DTT buffer and centrifuged at 40,000 RPM on a Beckman Optima XL-A ultracentrifuge fitted with An-50 Ti rotors that was maintained at 20 °C. Concentration profiles were measured with the UV-absorption scanning optics at a wavelength of 280 nm. The measured concentration profiles were evaluated using the program SEDFIT (Peter, 2000) which transformed them into diffusion corrected sedimentation coefficient $c(s)$ distributions.

2.5 Mass spectrometry

2.5.1 Mass spectrometry based deacetylation assay

A novel MS (mass spectrometry) based assay was developed to assay Sirtuins. 100 to 250 nM Sirtuin was incubated with 5 to 50 μM substrate peptide and 50 μM NAD^+ in 25 mM HEPES, pH 7.5, at 37 °C. After the required time was reached, an aliquot was withdrawn and quenched with equal volume of 0.1 % (v/v) FA (formic acid), centrifuged using a 10 kDa cut off centrifugal concentrator (Pall Life Sciences, USA) and 5 to 10 μl of the filtrate applied to a LC-ESI-MS (LTQ XL mass spectrometer, Thermo Scientific, USA) coupled to an HPLC (Shimadzu, USA). The samples were loaded over a Kromasil 100 C18 5 μm pre-column (Higgins Analytical, USA) followed by a reverse phase C18 column at a flow rate of 300 nl/min. The acetylated and deacetylated peptides were separated using a linear gradient from 0 % to 45 % buffer B within 30 min (buffer A: 0.1 % TFA (trifluoroacetic acid), 0.02 % HFBA (heptafluorobutyric acid); buffer B: 70 % ACN (acetonitrile), 0.1 % TFA, 0.02 %

HFBA. The results were analyzed using Xcalibur software package (Thermo Scientific, USA).

2.5.2 Analysis of protein samples from polyacrylamide gels using tryptic digest

A mass spectrometry based tryptic digest approach was followed to identify a protein of interest from a mixture. Protein samples were resolved on SDS-PAGE and the protein band to be analyzed was cut from the gel and destained by first adding 100 μ l of 50 % (v/v) methanol for few seconds followed by 100 μ l of 12.5 mM NH_4HCO_3 -50 % (v/v) ACN) mixture and incubation at 37 °C for 20 minutes on an Eppendorf shaker (Eppendorf, Germany) at a speed of 300 RPM. The gel pieces were dried on a speed-vac (Vacuum Concentrator, BA-VC-300H, Helmut Saru Laborbedarf, Germany) at 55 °C until the samples were completely dry. 10 μ l Trypsin (12.5 ng/ μ l in 25 mM NH_4HCO_3 , pH 8.0) was added to the samples and incubated at room temperature for 10 minutes followed by the addition of 10 μ l NH_4HCO_3 , pH 8. The samples were incubated at 37 °C overnight for complete digestion of the protein into peptides. Following incubation the supernatant was saved and 10 μ l of 50 % (v/v) ACN-0.5 % (v/v) TFA mixture was added to the gel pieces and sonicated for 20 minutes on a sonifying bath after which the supernatant was pooled with the supernatant from overnight incubation. The samples were again subjected to speed-vac at 55 °C and the peptides were resolved in 20 μ l of 0.1 % FA. The peptides were then applied over a Kromasil 100 C18 5 μ m pre-column (Higgins Analytical, USA) followed by a reverse phase C18 column at a flow rate of 300 nl/min. The acetylated and deacetylated peptides were separated using a linear gradient from 0 % to 45 % buffer B within 30 min (buffer A: 0.1 % FA, buffer B: 70 % ACN, 0.1 % FA). The results were analyzed using Xcalibur software package (Thermo Scientific, USA).

2.6 Crystallography and structure determination

2.6.1 Crystallization trials of human Sirt1

Crystallization trials were performed either manually or using a Phoenix robot (Art Robbins, USA). Manual crystallization trials were setup by mixing equal volumes of protein and reservoir solutions (typically 1 μ l + 1 μ l) on a 96 well sitting drop corning plates and incubation at 18 °C. While using the robot 0.1 μ l protein mixture and 0.1 μ l reservoir solution was mixed on a 96 well sitting drop plate (Corning, Intelli, Greiner etc. plates) and incubated at 18 °C in a formulatrix imager (Formulatrix Inc., USA).

2.6.2 Crystallization of *Thermotoga maritima* Sir2Tm (Sir2Tm)

Initial crystallization screens for Sir2Tm were performed using the sitting drop vapor diffusion method using a Phoenix robot (Art Robbins, USA). The crystallization plates used were 96 well/3 drop from either MRC or Greiner (Jena Biosciences, Germany). Each drop contained 0.15 μ l protein sample and 0.15 μ l reservoir. Drop A contained 9.71 mg/ml Sir2Tm and 1.5 mM Ex-527, Drop B contained ~9.71 mg/ml Sir2Tm, 1.5 mM Ex-527 and 1 mM p53 acetylated peptide, Drop C contained 9.71 mg/ml, 1.5 mM Ex-527, 1 mM p53 acetylated peptide and 1mM ADPr. The reservoir contained 75 μ l of solution from the Qiagen JCSG Core suite I-IV (Qiagen, USA). The trays were stored in a Formulatrix imaging system (Formulatrix, USA) at 20 °C and imaged at regular intervals.

2.6.3 Collection and analysis of X-ray diffraction data of Sir2Tm crystals

X-ray diffraction data were collected at 100° K at BESSY beamline 14.1 (Helmholtz Centre, Berlin, Germany) using an MX-225 CCD detector (Rayonix, USA) at a wavelength of 0.92 Å. Diffraction data were integrated, scaled and merged using XDS (X-ray detector software) (Kabsch, 2010).

2.6.4 Molecular replacement of Sir2Tm crystal structures

The structure of Sir2Tm in complex with the ligand mix and modulator was solved through Patterson searches with PHASER (McCoy et al., 2007), using a Sir2Tm/peptide/nicotinamide complex (PDB ID 1YC5) as a search model after removing all the water molecules, p53 peptide and NAM.

2.6.5 Refinement, model building and structure validation of Sir2Tm complex structures

The structure of the protein complex was refined using REFMAC's restrained refinement feature (Murshudov et al., 1997) and PHENIX's phenix.refine refinement feature (Adams et al., 2010) and models manually rebuilt in COOT (Emsley et al., 2010), with 5% of the reflections excluded from refinement for R_{free} calculation (Brunger, 1992). Individual isotropic Debye-Waller factors were refined, and solvent molecules were added at a later stage of model refinement. Parameter files for Ex-527/Ex-243 (modulator) and the reaction intermediate were created using MarvinSketch (Version number: 5.6, ChemAxon (<http://www.chemaxon.com>)) and ProDrg (Schuttelkopf and van Aalten, 2004) software. Final model quality was assessed using MolProbity (Chen et al., 2010b) and validation tools

in COOT. Figures were generated using CCP4mg molecular-graphics software (McNicholas et al., 2011).

2.6.6 Homology modeling of human Sirt1

A homology model for the catalytic domain of human Sirt1 (residues 214-497) was generated using the crystal structure of Sirt2 (residues 34-356, PDB code 1J8F) as template. The amino acid sequences of Sirt1 and Sirt2 were aligned using ClustalW2 software (Larkin et al., 2007), edited manually and Sirt1 structure was modeled using Modeller version 9.8 using standard parameters (Eswar et al., 2006) (<http://salilab.org/modeller/>).

3. Results

3.1 Studies on Sirt1

3.1.1 Recombinant expression and purification of Sirt1

Human Sirt1 (Sirt1) is the largest member among the mammalian Sirtuins with extensions at both N and C-terminus (Figure 3.1). Sirt1 was one of the first mammalian isoform to be studied extensively, yet the roles of residues at the termini are unclear and a crystal structure of Sirt1 is not yet available. To gain further insights into the domain architecture of Sirt1 and solve the crystal structure of Sirt1 several constructs of human Sirt1 and its mouse homolog (mSirt1) were generated and tested for expression, purification, and biochemical and crystallization trials. Table 3.1 lists Sirt1 constructs with different affinity tags and proteases required for tag cleavage. Protein expression was observed in all the constructs but protein solubility was affected when the catalytic domain alone was expressed. For example mSirt1 catalytic core constructs 222-483 (human equivalent 230-491) and 206-508 (human equivalent 214-516) were expressed in high amounts but with poor solubility. Several attempts to increase protein solubility during overexpression by altering growth conditions such as temperature, media, concentration of IPTG and various refolding/solubilization strategies such as in-column refolding, re-folding by step wise dialysis and in the presence of Zinc, co-substrate (NAD⁺) resulted in no soluble protein. It is interesting to note that when similar constructs were cloned from human Sirt1 (225-527 and 245-510) soluble proteins are obtained, but they were impure and unstable leading to degradation after affinity purification. Possible reasons for this behavior could be due to slight variations in amino acid composition between the mouse and human which may contribute to proper protein folding and solubility. In order to avoid solubility issues, latter constructs were cloned with MBP at the N-terminus, as MBP has been shown to increase protein overexpression and solubility in *E. coli*.

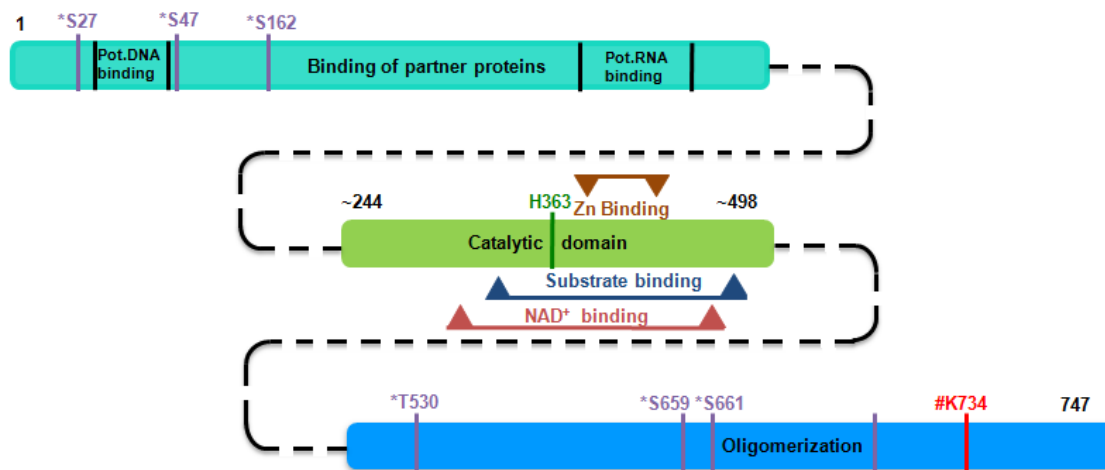


Figure 3.1: Domain architecture of human Sirt1. Cartoon representation of Sirt1 showing various binding sites and residues involved in post-translational modifications. Pot. RNA binding = potential/predicted RNA binding motif, Pot. DNA binding = potential/predicted DNA binding motif, # = sumoylation, H363 = catalytic residue, * = phosphorylation. The dotted black lines just connect the domains and are not part of the protein.

Construct	Vector	Tag	Protease cleavage site
hSirt1 FL	pASKIBA17plus	N-terminal Strep	TEV
hSirt1 FL	pET15b	N-terminal Hexa-Histidine	Thrombin
hSirt1 FL	modified pET15b	N-terminal Hexa-Histidine	TEV
hSirt1 FL H363A	pASKIBA17plus	N-terminal Strep	TEV
hSirt1 FL T530D	pET15b	N-terminal Hexa-Histidine	Thrombin
hSirt1 MAD+82-747+LRSGC at end	pET21a(+)	C-terminal Hexa-Histidine	None
hSirt1 1-664	pET15b	N-terminal Hexa-Histidine	Thrombin
hSirt1 129-747	pET15b	N-terminal Hexa-Histidine	Thrombin
hSirt1 181-747	pET15b	N-terminal Hexa-Histidine	Thrombin
hSirt1 214-747	pET21a(+)	C-terminal Hexa-Histidine	None
hSirt1 214-747	pET15b	N-terminal Hexa-Histidine	Thrombin
hSirt1 217-747	pET15b	N-terminal Hexa-Histidine	Thrombin
hSirt1 214-747 A313V	pET21a(+)	C-terminal Hexa-Histidine	None
hSirt1 MAD+82-664	pET15b	N-terminal Hexa-Histidine	Thrombin
hSirt1 183-664	pET15b	N-terminal Hexa-Histidine	Thrombin
hSirt1 183-664	pET21a(+)	C-terminal Hexa-Histidine	None
hSirt1 183-664 T530D	pET15b	N-terminal Hexa-Histidine	Thrombin
hSirt1 183-516	modified pOPIN	N-terminal Hexa-Histidine-MBP	TEV
hSirt1 214-664	pET21a(+)	C-terminal Hexa-Histidine	None
hSirt1 214-664	pET15b	N-terminal Hexa-Histidine	Thrombin
hSirt1 214-664 EEK-AAA 576-578	pET15b	N-terminal Hexa-Histidine	Thrombin
hSirt1 225-747	pET15b	N-terminal Hexa-Histidine	Thrombin
hSirt1 225-664	pET21a(+)	C-terminal Hexa-Histidine	None
hSirt1 225-664	pET15b	N-terminal Hexa-Histidine	Thrombin
hSirt1 225-664 T530D	pET15b	N-terminal Hexa-Histidine	Thrombin
hSirt1 225-664 A313V	pET21a(+)	C-terminal Hexa-Histidine	None

hSirt1 225-664 H363A	pET15b	N-terminal Hexa-Histidine	Thrombin
hSirt1 225-664 EEK-AAA 576-578	pET15b	N-terminal Hexa-Histidine	Thrombin
hSirt1 225-527	pET15b	N-terminal Hexa-Histidine	Thrombin
hSirt1 229-516	modified pOPIN	N-terminal Hexa-Histidine-MBP	TEV
hSirt1 245-510	pET15b	N-terminal Hexa-Histidine	Thrombin
mSirt1 206-737	pET15b	N-terminal Hexa-Histidine	Thrombin
mSirt1 206-737	pET21a(+)	C-terminal Hexa-Histidine	None
mSirt1 206-508	pET15b	N-terminal Hexa-Histidine	Thrombin
mSirt1 206-508	pET21a(+)	C-terminal Hexa-Histidine	None
mSirt1 222-483	pET15b	N-terminal Hexa-Histidine	Thrombin
mSirt1 222-483	pET21a(+)	C-terminal Hexa-Histidine	None

Table 3.1: A list of constructs (with their affinity tag and proteases for tag cleavage) used in the expression and purification of different Sirt1 variants. hSirt1 and mSirt1 stand for human and mouse, Sirt1 respectively and FL stands for full length.

Expression and purification of Sirt1 constructs were performed as mentioned in the methods section. Several purification strategies were tested in order to optimize the purification process, because the purity of Sirt1 after the affinity step is at best ~70 % as judged by SDS-PAGE (Figure 3.2a). Addition of detergents such as Tween-20 and Triton, NAD⁺ (co-substrate) and stabilizers (glycerol, ethylene glycol) did not result in an increase in purity. Initially, affinity purified Sirt1 was loaded on an anion exchange column (calculated pI of Sirt1 = 4.55) to separate the contaminants, but a major part of Sirt1 was not bound and was found in the flow through fractions along with *E. coli* proteins. SEC profiles of ion exchange purified Sirt1 indicated an aggregated state (elution in void volume) with reduced activity. To overcome this problem, affinity purified Sirt1 was purified over a gel filtration column followed by a very slow AEC (anion exchange chromatography) step. Since several *E. coli* contaminants are still present with Sirt1, all the buffers contained protease inhibitors to avoid degradation. The ion exchange purified Sirt1 was analyzed by SDS-PAGE and found to be \geq 90 % pure (Figure 3.2a). To confirm that purified Sirt1 is folded properly, a CD (circular dichroism) spectrum of the protein was recorded, which shows secondary structural features (Figure 3.2b). Estimation of secondary structure content using a theoretically derived spectra from the K2D3 program (<http://www.ogic.ca/projects/k2d3/>) (Louis-Jeune et al., 2012) indicates Sirt1 may be composed of ~10.5 % α helical content, ~ 22.5 % of β strand content, and the rest formed of coil/turn/other.

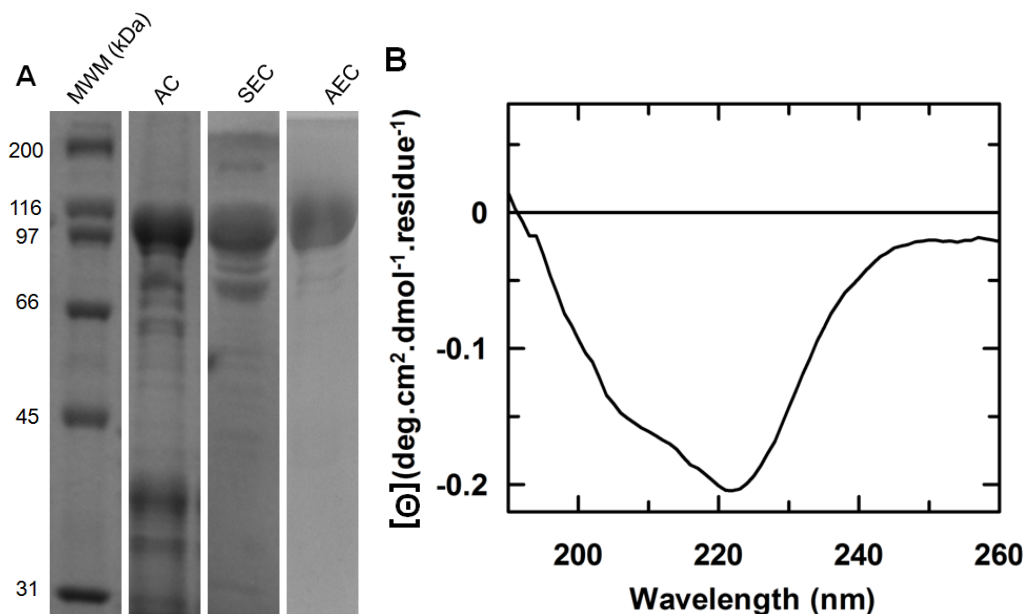


Figure 3.2: Purification and secondary structure analysis of Sirt1. A) 10 % (w/v) SDS polyacrylamide gel showing the purity of full length Sirt1 after AC (Affinity Chromatography), SEC (Size Exclusion Chromatography) and AEC (Anion Exchange Chromatography). Although Sirt1's molecular weight is ~82 kDa, it runs at ~ 110 kDa in SDS-PAGE, due to the high amount of positive charge. B) CD spectra of 9.5 μ M full length Sirt1 collected at 15 $^{\circ}$ C, pH = 7.5. Mean residue molar ellipticity $[\Theta]$ is plotted against wavelength in nm. Sirt1 has proper secondary structure with ~ 10.5 % α -helix and ~ 22.5 % β -strand content as determined using the K2D3 program.

Spectrophotometric analysis of affinity purified Sirt1 revealed an unusually high absorbance at 260 nm compared to 280 nm (high A_{260}/A_{280} ratio) (Figure 3.3a), an indication for nucleic acid contamination, because SEC and AEC purified Sirt1 behaves as expected. Further analysis of the fractions using agarose gel electrophoresis revealed high amounts of nucleic acids in the elute fractions (Figure 3.3b). Incubation of these fractions with DNase lead to a moderate decrease in the amount of nucleic acids, whereas incubation with RNase lead to almost complete loss of nucleic acids. These results indicate that Sirt1 co-purifies with nucleic acids, in particular RNA (Figure 3.3b). Inclusion of either DNase or RNase or both during the purification process resulted a decrease in absorbance at 260 nm only when RNase was present (Figure 3.3a). To avoid nucleotide contamination, further Sirt1 affinity purification steps included DNase and RNase treatment.

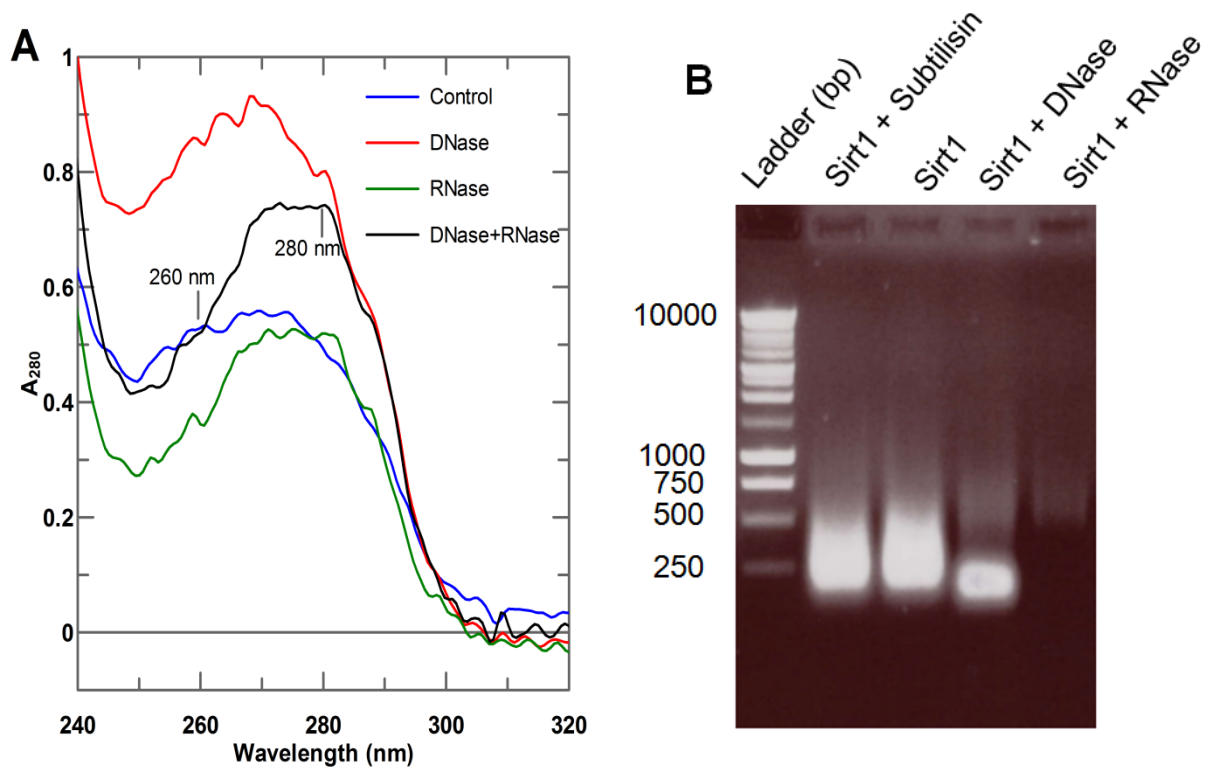


Figure 3.3: Sirt1 appears to co-purify with nucleotides. A) Spectroscopic analysis of different fractions of affinity purified Sirt1 indicates high A_{260}/A_{280} ratio for control sample, whereas samples treated with nucleases shows a decrease in the ratio. (A_{260}/A_{280} ratios are control: ~ 1.08 , with DNase: ~ 1.06 , with RNase: ~ 0.68 , with DNase+RNase: ~ 0.70). B) 1 % (w/v) agarose gel electrophoresis of Sirt1 in the presence of nucleases indicates a decrease in nucleic acid content when Sirt1 was incubated with bovine DNase (moderate decrease) or bovine RNase A (complete loss). Sirt1 was incubated with Subtilisin to investigate if loss of Sirt1 leads to a shift in the migration of nucleic acids. $\sim 6.25 \mu\text{g}$ Sirt1 was incubated with 0.625 ng Subtilisin (10000 fold less), $0.25 \mu\text{g}$ DNase or $0.5 \mu\text{g}$ RNase for 15 minutes at 37°C and loaded on the gel.

To further investigate if Sirt1 binds to nucleotides, the protein was incubated with either DNA or RNA and resolved on an agarose gel. Figure 3.4a shows a representative gel where the mobility of dsDNA (double stranded DNA) was not affected by the presence of Sirt1, possibly indicating a lack of direct interaction between the two. Similar experiments to identify interactions between Sirt1 and RNA proved unsuccessful. We also tested the influence of nucleic acids on the activity of Sirt1, by performing activity assays in the presence and absence of nucleic acids (Figure 3.4b). The assays revealed that Sirt1's activity is not influenced in the presence of either DNA or RNA. It remains to be clarified why Sirt1 seems to strongly associate with RNA when expressed in *E. coli*.

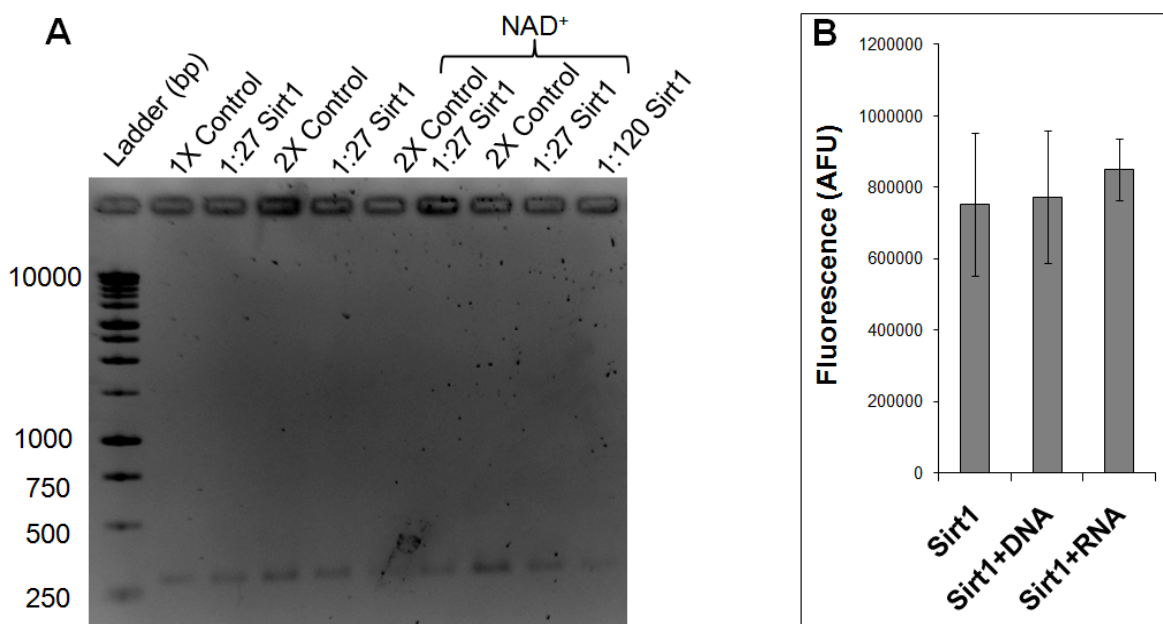


Figure 3.4: Nucleotides neither interact with Sirt1 nor influence its activity. A) Mobility shift assay performed on 1 % (w/v) agarose gel shows no shift of dsDNA (296 base pairs) in the presence of Sirt1. 1X control = 45 ng DNA. The ratio indicates the amount of excess Sirt1 added over DNA. 1 mM NAD^+ was added separately to assess its influence on Sirt1. The lack of shift in the migration of dsDNA indicates no binding with Sirt1. B) The activity of 1 μg Sirt1 with 100 μM FdL-1 peptide and 1 mM NAD^+ was measured with PCR amplified dsDNA (1467 base pairs, 1:0.3 ratio of Sirt1:DNA) or tRNA from *E. coli* (~ 75 base pairs, 1:10 ratio of Sirt1:RNA).

3.1.2 Investigating the role of termini in the oligomerization of Sirt1

Mammalian Sirtuins (Sirt2-Sirt7) and other Sirtuins have so far been reported as monomers (Finnin et al., 2001; Schlicker et al., 2011; Schlicker et al., 2008; Schuetz et al., 2007) except for the yeast homolog Hst2, which was reported as trimer in both solution and crystal structure and the N-terminus was shown to be involved in trimer formation (Zhao et al., 2003). SEC profile of flag-tagged Sirt1 overexpressed and purified from HeLa cells suggested trimerization with an apparent molecular weight of ~ 350 kDa (Vaquero et al., 2004). We performed gel filtration analysis on the full length and deletion constructs of Sirt1 to analyze which domain(s) might be responsible for oligomerization. SEC profiles of full length, N-terminal and C-terminal deletion constructs indicated a higher order oligomer like behavior (similar to HeLa cells purified Sirt1), whereas constructs lacking both termini behaved as lower order oligomers (Figure 3.5). The apparent sizes seen on SEC could be a result of oligomerization or an extended shape of full length Sirt1 and its constructs. BN-PAGE on various Sirt1 constructs showed results similar to size exclusion profiles for full length and 214to747 constructs but the 1to664 and 214to664 constructs were seen as a smear on the gel despite repeated attempts, leading to a lack of clear understanding on the nature of

oligomerization (Figure 3.6). If full length Sirt1 indeed is a trimer or higher order oligomer, it should have a molecular weight of at least ~ 240 kDa or above and therefore might be a good candidate for EM (Electron Microscopy) studies. Cryo EM studies on full length Sirt1 (Figure 3.7a) indicates it to be a monomer, however this could have also resulted due to dilution during sample preparation. We therefore used AUC to analyze the oligomerization of Sirt1, because AUC is insensitive to molecular shape. Figure 3.7b shows the results of sedimentation velocity AUC runs performed on different Sirt1 constructs. Under the conditions tested, all Sirt1 samples seem to behave as monomers in AUC experiments.

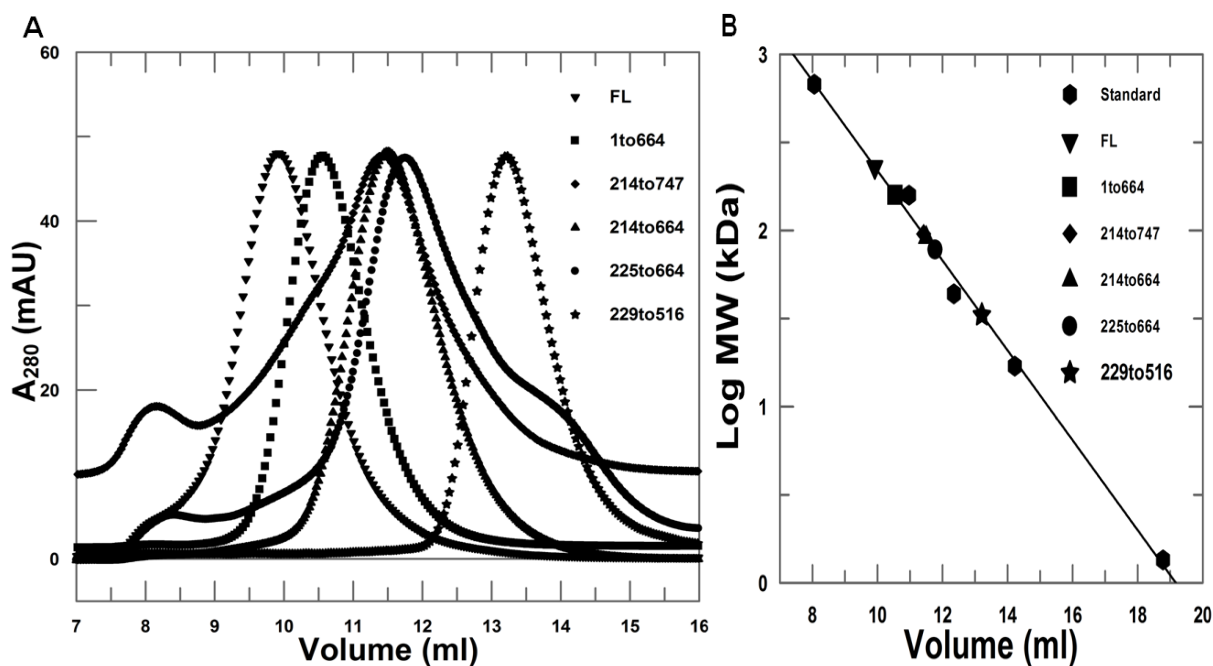


Figure 3.5: SEC indicates oligomerization of Sirt1. A) SEC elution profiles of different Sirt1 constructs: normalized absorbance (at 280 nm) is plotted against elution volume. B) A plot of Logarithm of SEC standards against elution volume. Comparing the elution volume of Sirt1 constructs to that of the standards indicate oligomeric behavior for all Sirt1 except for the catalytic core construct. FL = full length. Apparent molecular weights based on SEC standards: FL – 230 kDa (trimer), 1to664 – 158.7 kDa (dimer), 214to747 – 95.3 kDa, 214to664 – 90.9 kDa, 225to664 – 77.2 kDa (the molecular weights of the later three constructs corresponds in between monomer and dimer) and 229to516 – 33.4 kDa (monomer).

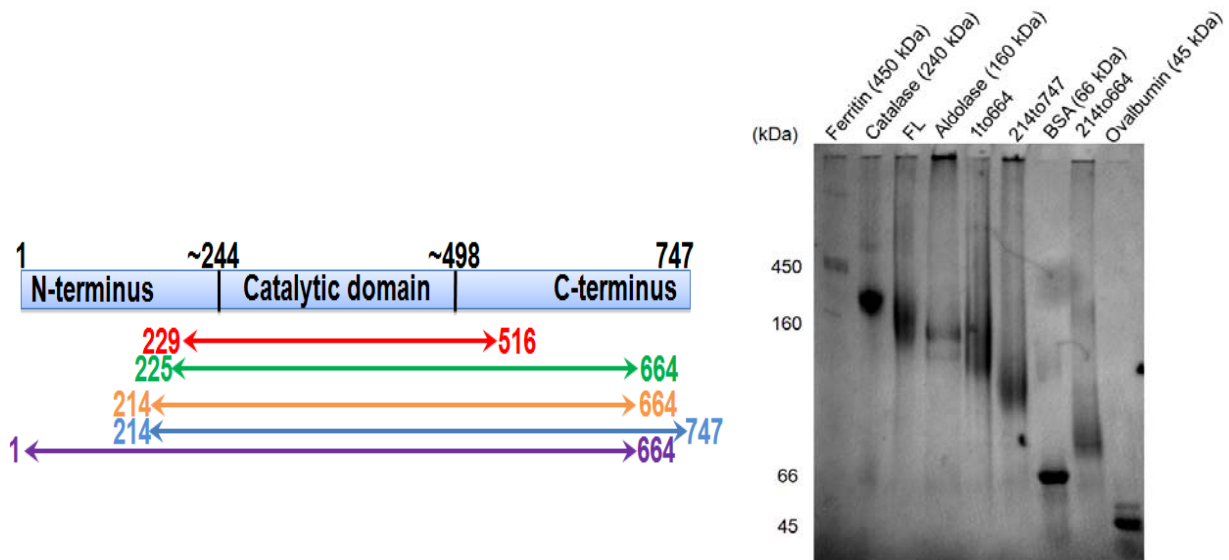


Figure 3.6: BN-PAGE Analysis of Sirt1 indicates oligomerization. Left panel: A cartoon representation of Sirt1 constructs used in probing the domain involvement in oligomerization of Sirt1. Right panel: BN-PAGE analysis of different Sirt1 constructs along with protein markers indicate an oligomerization profile for Sirt1 constructs similar to SEC. 10 μ g of each marker proteins were loaded in the gel along with 27 μ g FL (full length), 30 μ g 1to664, 27 μ g 214to747, 32 μ g 214to664 Sirt1 constructs respectively

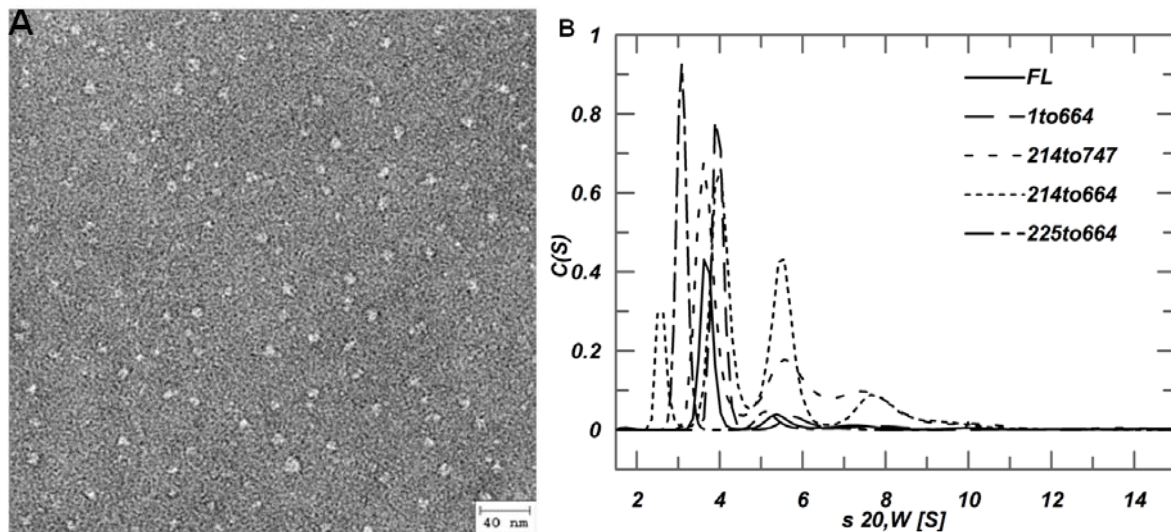


Figure 3.7: EM and AUC analysis indicates Sirt1 to be monomeric. A) Sirt1 at a concentration of ~ 10 μ g/ml was negatively stained with Uranyl formate, adsorbed on grids and observed under a JOEL-1400 electron microscope at a magnification of 50,000. Full length Sirt1 can be visualized as small tiny particles which are globular and homogenous indicating monomeric behavior. EM image analysis was performed at MPI-Dortmund in the lab of Dr. Stefan Raunser. B) A representative plot of continuous c(s) distribution against sedimentation coefficient (corrected for water at 20 $^{\circ}$ C) from sedimentation velocity AUC runs of Sirt1 constructs indicate a clustering at around sedimentation coefficient value of ~ 3.1 - 3.9 S implying a monomeric behavior for all the constructs. All runs were performed at 20 $^{\circ}$ C and 40,000 RPM and the protein concentration was monitored at 280 nm.

3.1.3 The catalytic domain of Sirt1 is sufficient for activation by polyphenols

Resveratrol was one of the first small molecules identified that can activate Sirt1. The unique N-terminus of Sirt1 was reported to be essential for the activating effect of resveratrol (Milne et al., 2007), but other studies have shown that resveratrol can also activate yeast Sir2, whose N-terminal domain is unrelated to its human counterpart (Howitz et al., 2003). To further investigate the regions responsible for Sirt1 activation by resveratrol, we assessed the activity of full length Sirt1 and the deletion constructs in the presence and absence of resveratrol using the fluorogenic substrate peptide FdL-1 employing both the fluorescence as well as MS based assays (Figure 3.8). The assay revealed various basal activities for different constructs (Figure 3.9), but stimulation by resveratrol was observed in each construct including the shortest one comprised of just the catalytic domain. To verify if this activation can also be achieved by piceatannol (another naturally occurring polyphenol very similar to resveratrol in structure) we performed the same assay in the presence of piceatannol. Indeed as expected activation by piceatannol also required only the catalytic domain (Figure 3.10). Comparison of activation relative to basal level in both resveratrol and piceatannol indicates that all constructs can be stimulated in a similar manner, even though their basal activity differs. To test if the difference in basal activity is in part due to the stability of the constructs, we performed thermal shift denaturation assays. In a thermal shift assay, the protein is diluted in a variety of buffer and salt conditions and a fluorescent dye is added to it. Protein unfolding is monitored by recording the increase in fluorescence (the dye binds to hydrophobic parts of the protein) with gradual raise in temperature, which is then fitted to an equation, to obtain the half-transition point, T_m (Temperature of Melting). Figure 3.11 shows representative thermal shift curves of different Sirt1 constructs. With the exception of full length Sirt1, melting curves with more than one transition were obtained, so that no T_m values could be obtained with the standard two-state model, However, it appears that all the constructs have similar stability, suggesting a role for the termini in modulating the activity of Sirt1 (see discussion section).

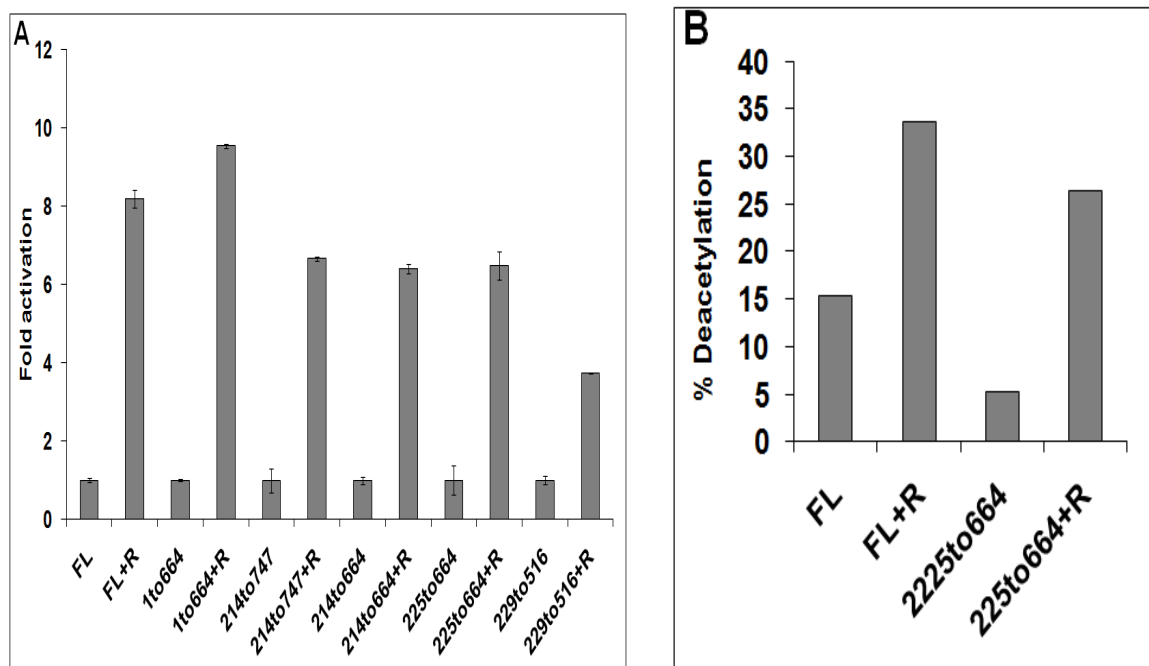


Figure 3.8: Catalytic domain is sufficient for activation by resveratrol. A) Full length (FL) Sirt1 along with different truncation constructs were used in the fluorescence assay containing FdL-1 peptide substrate, NAD^+ and 100 μM Resveratrol (R). B) The same assay was performed with FL (full length) and the catalytic construct 225to664 and analyzed by MS. In both the cases activation by resveratrol can be observed even for the shortest construct which contains only the catalytic domain. Control samples contained 1% (v/v) DMSO and the assay was performed at 37 $^{\circ}\text{C}$.

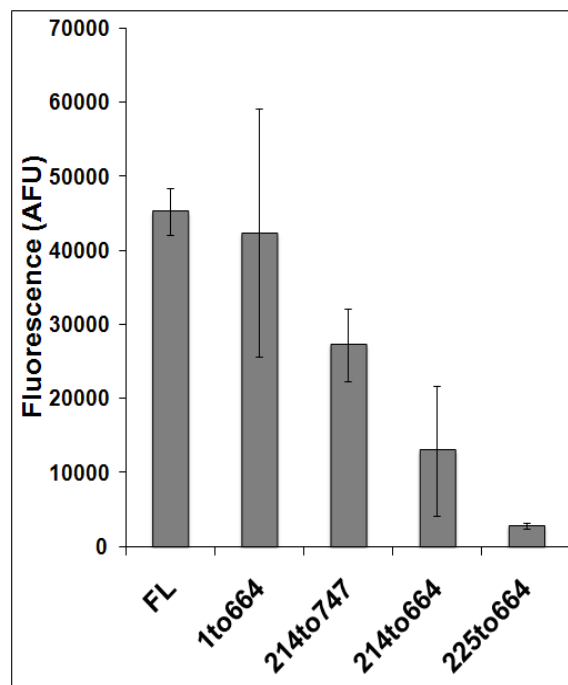


Figure 3.9: The activity of Sirt1 appears to be regulated by its termini. ~ 200 nM each Sirt1 construct was used in the FdL-1 substrate based fluorescence assay. The basal activity of Sirt1 appears to be dependent on the termini, as the construct containing only the catalytic core domain has lower activity compared to the full length protein (FL = full length).

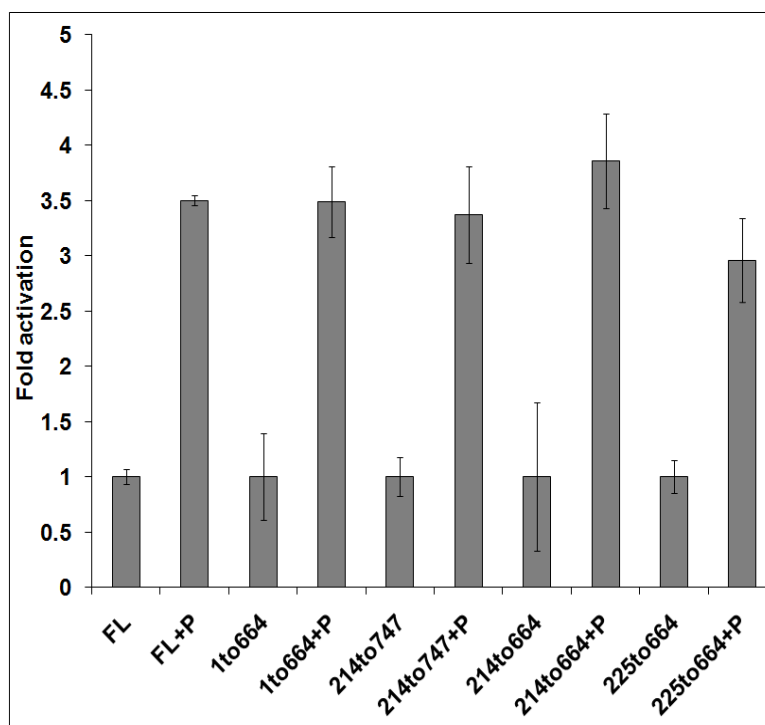


Figure 3.10: Piceatannol can also activate the catalytic core of Sirt1. Similar to resveratrol 100 μ M Piceatannol (P) is also able to activate Sirt1 comprising only the catalytic domain. The FdL-1 substrate was used in the fluorescence based assay. (FL = full length).

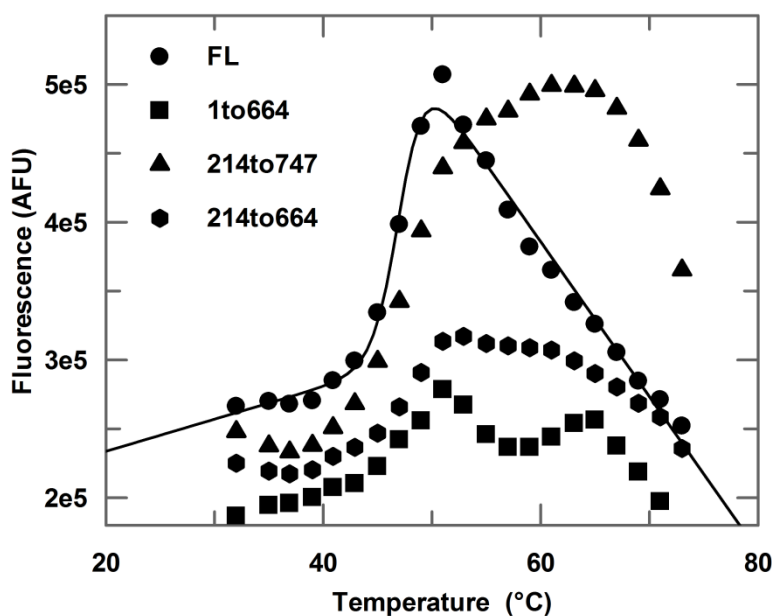


Figure 3.11: Thermal denaturation shift assay on different Sirt1 constructs. Representative thermal shift curves of four different Sirt1 constructs comprising either FL (full length), lacking N or C-terminus or both indicate an unusual transition state for the proteins. Nevertheless, all the protein samples appear to have similar stabilities. Fitting the curve for FL using a two state transition reveals a T_m close to ~ 47 °C.

3.1.4 Identification of novel peptide substrates for Sirt1

Over 6800 acetylation sites have been identified in mammalian proteome, presenting an excellent opportunity to perform substrate profiling on mammalian Sirtuins to identify novel isoform specific substrates as well as their substrate sequence preferences. In collaboration with Dr. Mike Schutkowski's laboratory at University of Halle, Germany, we established a chip-based array system that can be used to characterize isoform specific substrate preferences of different mammalian Sirtuins (Rauh et. al. manuscript in preparation). Roughly 6800 acetylated peptides comprising six residues N and C-terminal from the acetylation sites were synthesized and spotted on a chip to create an array (herein referred to as acetylome chip) similar to the one described by Schutkowski et. al. (Schutkowski et al., 2004). To identify novel substrate peptides for Sirt1, the protein was mixed with NAD^+ and incubated on the acetylome chip. As a control, we incubated a chip with only buffer and NAD^+ or Sirt1 catalytic mutant H363A and NAD^+ . The deacetylation efficiency of Sirt1 was analyzed by employing an ELISA type method as shown in figure 3.12. Several new potential substrates were identified for Sirt1 such as Lys12 of HMG-B1 (High Mobility Group B1), Lys628 of TFIID (Transcription initiation factor TFIID subunit 3) to name a few.

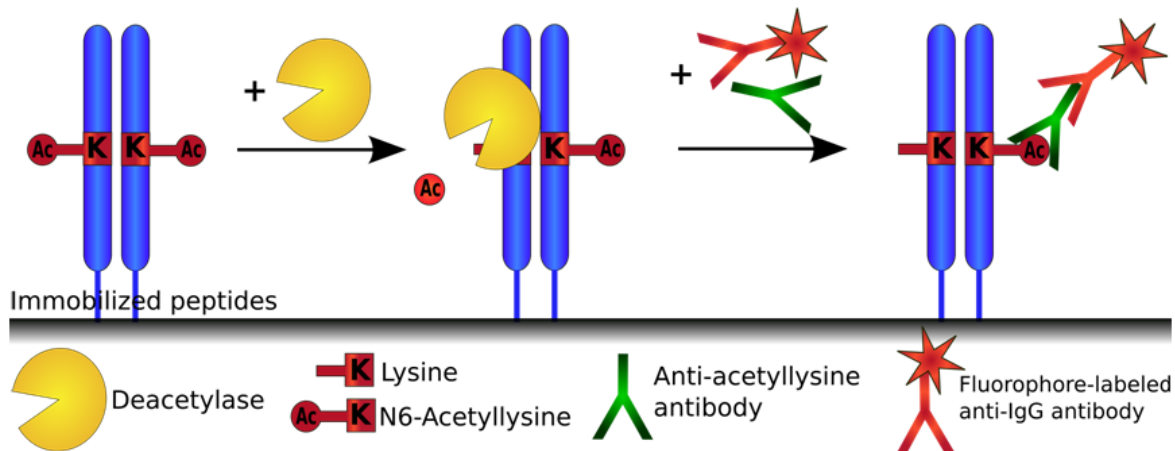


Figure 3.12. Schematic representation of the principle behind the acetylome-chip assay. The chip containing several acetylated peptides is first incubated with Sirt1, NAD^+ and modulators. This is followed by incubation with anti-acetyllysine antibody and a fluorophore labeled secondary antibody. Efficient deacetylation by Sirt1 will lead to a decrease in fluorescence, which is compared with a buffer control. Figure kindly provided by Dr. David Rauh, University of Halle, Germany.

To ensure that substrate peptides identified using the array are also efficiently deacetylated in solution, we tested several peptides using the continuous assay (Figure 3.13). As expected, peptides were deacetylated by Sirt1 in solution with varying degree. Kinetic characterization of H3-Lys116 using the continuous assay resulted in similar kinetic values

compared to p53-Lys382 peptide, a widely used substrate peptide of Sirt1 (Figure 3.14). If Lys116 and Lys12 of full length H3 and HMG-B1 proteins, respectively, are accessible to Sirt1 they will be deacetylated, indicating that deacetylated lysine residues from array experiments serve as excellent candidates to test if they serve as, physiological Sirt1 substrates.

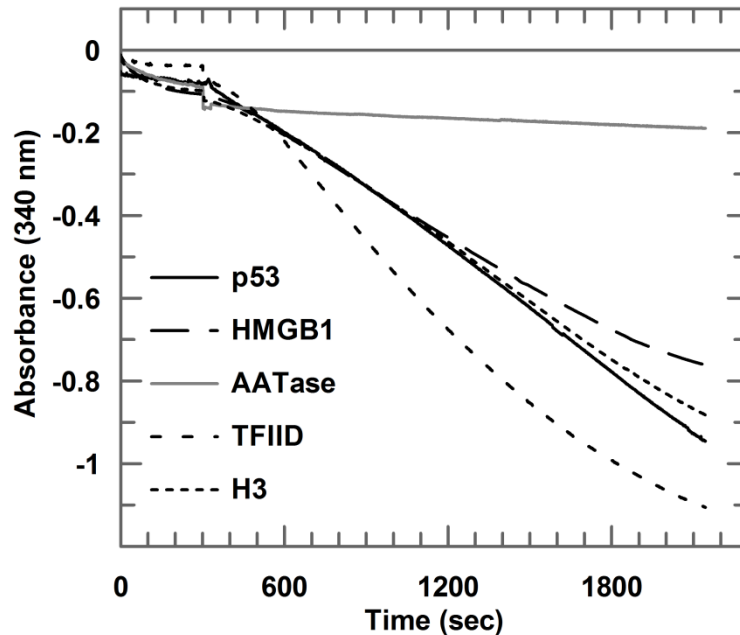


Figure 3.13. Novel substrates for human Sirt1. A continuous assay was performed using 1 μM Sirt1, 0.64 mM respective peptides and 1 mM NAD^+ . The decrease in absorbance at 340 nm was followed over time in a 96 well plate reader. The absorbance of a control (without peptide substrate) was subtracted from each peptide value and plotted over time. The known Sirt1 substrate site p53-K382 peptide was used as a positive control and AATase-K159 (Aspartate aminotransferase 2) which was not deacetylated on the array as a negative control.

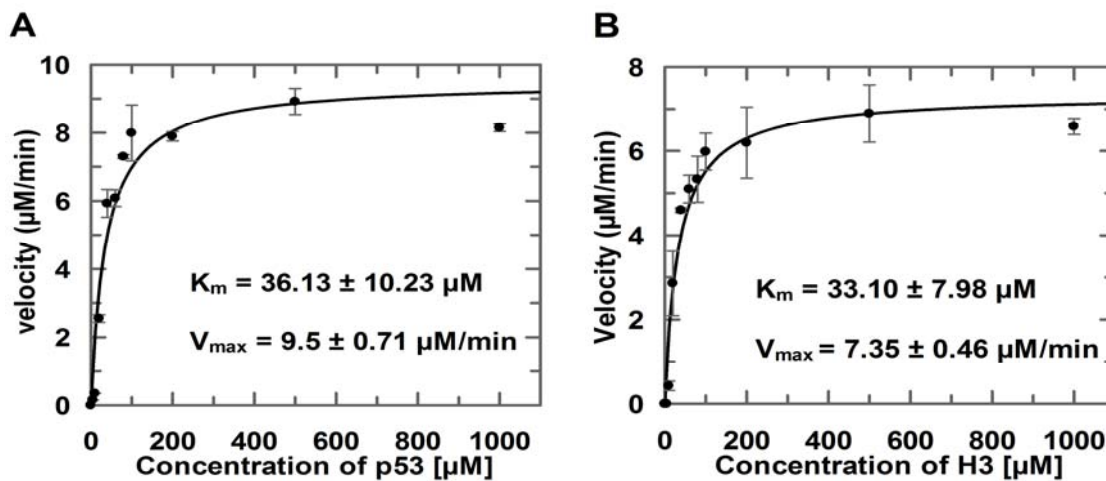


Figure 3.14: Michaelis-Menten plot of Sirt1 kinetics. A hyperbolic representation of the kinetics of catalysis of Sirt1 using p53-Lys382 peptide (A) and H3-Lys116 peptide (B) shows that the kinetic properties of H3 peptide identified from the acetylome-array is similar to the commonly used p53 peptide.

3.1.5 Sirt1 modulation by resveratrol is sequence specific

The mechanism of Sirt1 activation by resveratrol has been subjected to extensive debate (see section 1.6.3.2 above). Since different substrates were used in these assays leading to different outcomes, we wondered whether resveratrol activation depended on the sequence of the substrate. Our chip-based array serves as a perfect system to test this, as it contains a vast pool of substrates. The experiment was performed by incubating the chip with Sirt1, NAD⁺ and with or without resveratrol to identify peptides that showed differences in deacetylation efficiency in the presence of resveratrol. Figure 3.15 shows a general trend of the activity of Sirt1 in the presence of resveratrol. The polyphenol appears to modulate the activity of Sirt1 in a substrate dependent manner, as both activation and inhibition were observed, but a majority of the substrates were unaffected or only mildly affected. To validate the array results in solution, we tested representative candidates using MS based assay, as resveratrol interferes with spectrophotometric assays. As expected, resveratrol modulated the activity of Sirt1 depending on the sequence of the substrate peptide (Figure 3.16). For example, HMG-B1-Lys12 (KKPRGK[ac]MSSY) deacetylation showed no change in Sirt1 activity in the presence of resveratrol, whereas SF38-Lys23 (PQYLVEK[ac]IIRTRI) showed roughly four fold activation and H3-Lys116 (IHAK[ac]RVT) showed two fold inhibition. Although only few representative substrates were tested in solution, the array results which included several thousand peptides, indicates that Sirt1 modulation by resveratrol depends on the sequence of the substrate.

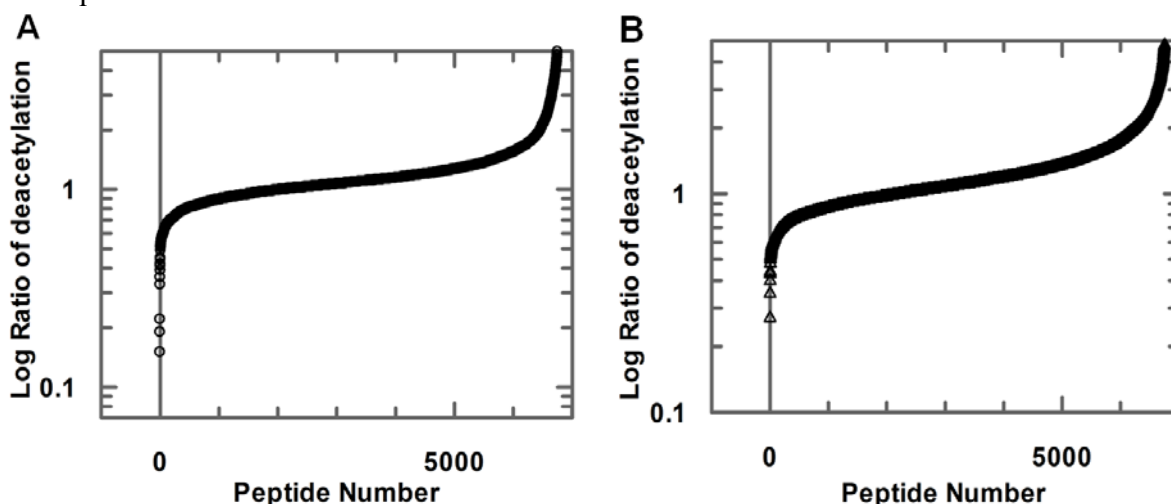


Figure 3.15: Acetylome-chip array reveals novel substrate-modulator pairs. A semi log plot showing the ratio of peptide deacetylation with respect to control (without the modulator) against the peptide number. Majority of the peptides show deacetylation similar to controls (ratio close to 1). Ratio below 1 represents activation whereas ratio above 1 represents inhibition. A) Assay performed in the presence of resveratrol. B) Assay performed in the presence of SRT1720.

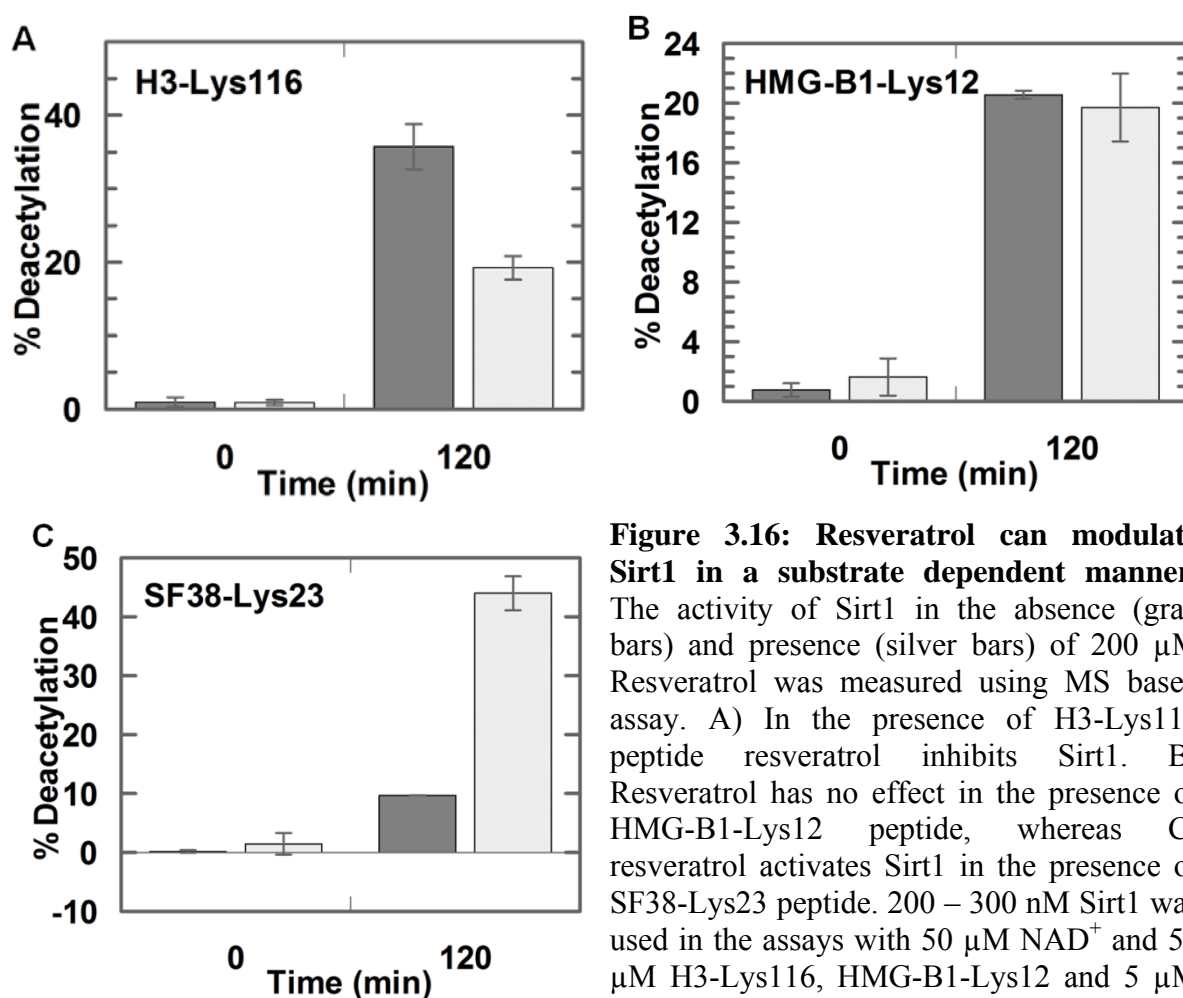


Figure 3.16: Resveratrol can modulate Sirt1 in a substrate dependent manner. The activity of Sirt1 in the absence (gray bars) and presence (silver bars) of 200 μ M Resveratrol was measured using MS based assay. A) In the presence of H3-Lys116 peptide resveratrol inhibits Sirt1. B) Resveratrol has no effect in the presence of HMG-B1-Lys12 peptide, whereas C) resveratrol activates Sirt1 in the presence of SF38-Lys23 peptide. 200 – 300 nM Sirt1 was used in the assays with 50 μ M NAD^+ and 50 μ M H3-Lys116, HMG-B1-Lys12 and 5 μ M SF38-Lys23 peptides respectively.

3.1.6 Effect of polyphenol unrelated small molecules on Sirt1

Sirt1 activation by small molecules other than polyphenols such as resveratrol, piceatannol etc. has been reported. Few examples include SRT series (SRT1720, SRT2383 etc.) (Milne et al., 2007) and thyroid hormones (Engel and Mahlkecht, 2008). SRT1720, which was shown to be 1,000 fold more potent than resveratrol in stimulating Sirt1 using a modified peptide, showed no strong effect, neither in the FdL-1 assay nor in the continuous assay using unmodified p53 as substrate (Figure 3.17), consistent with a previous study (Pacholec et al., 2010) (Pacholec et al., 2010). This discrepancy could again depend on the substrate-modulator pair similar to resveratrol, i.e. the modulatory effect of SRT1720 could also depend on the substrate used and therefore we tested SRT1720 also on the acetylome chip. Figure 3.15 shows that similar to resveratrol, SRT1720 also modulates Sirt1 in a substrate sequence dependent manner on the acetylome-chip array.

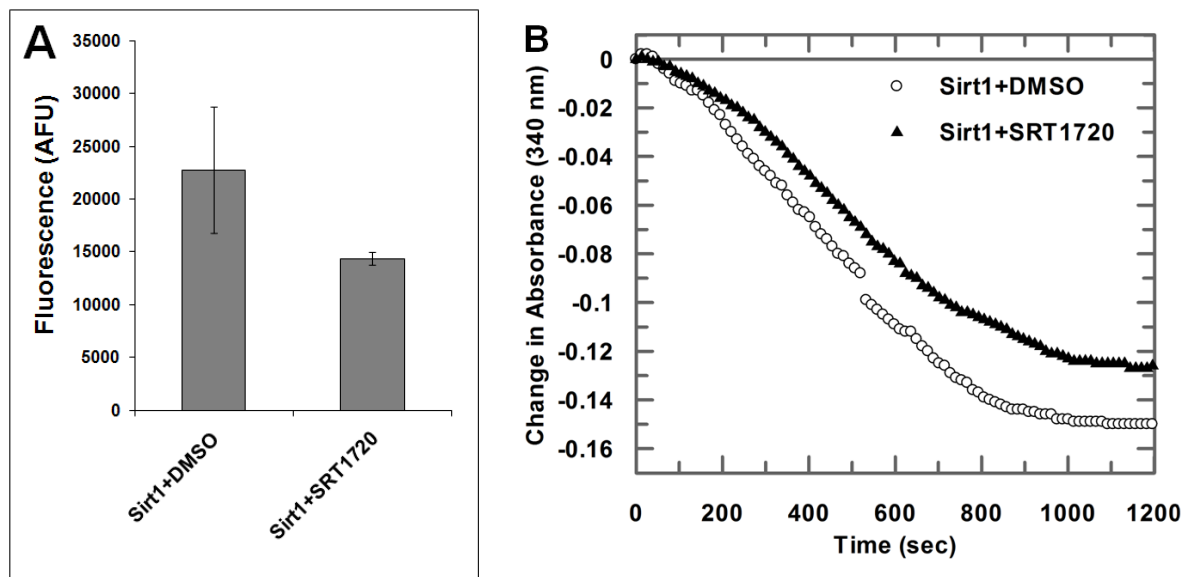
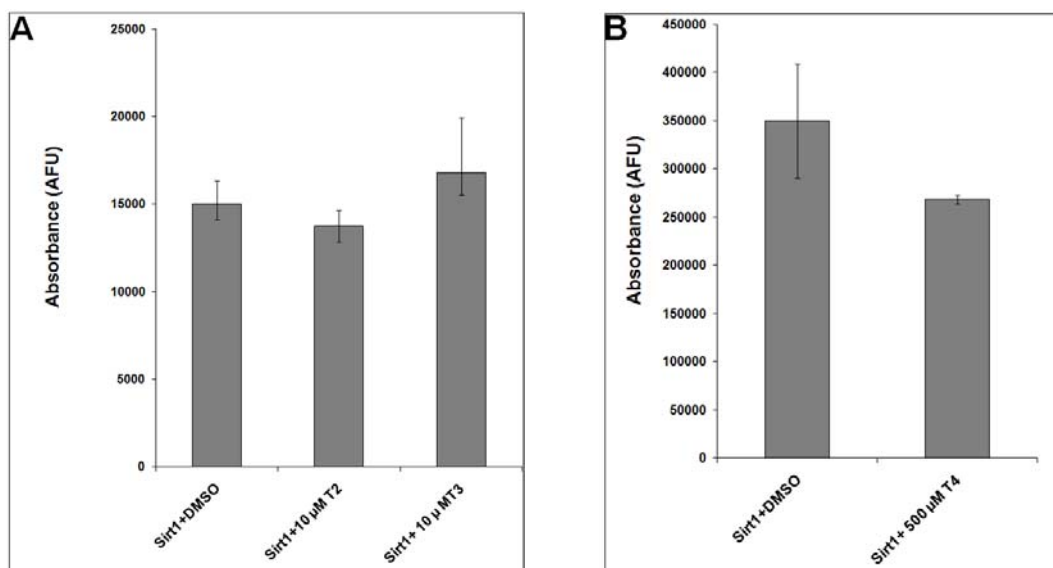


Figure 3.17: Effect of SRT1720 on Sirt1. A) A fluorescence assay in the presence of ~ 200 nM Sirt1, 25 μ M each FdL-1 peptide and 25 μ M NAD^+ indicates a weak inhibition in activity of Sirt1 in the presence of 1 μ M SRT1720. B) A continuous assay in the presence of 10 μ M Sirt1, 100 μ M p53-Lys382 peptide and 100 μ M NAD^+ also indicates no change in the activity of Sirt1 compared to DMSO control.

We also tested thyroid hormones T2 (3,5-diiodo-L-thyronine), T3 (3,3',5-triiodo-L-thyronine) and T4 (3,5,3',5'-tetraiodo-L-thyronine). However, they also had no effect on Sirt1 at physiologically relevant levels with FdL-1 substrate. Only at physiologically irrelevant high concentrations (0.5 – 1 mM), T3 showed an inhibitory effect (Figure 3.18).



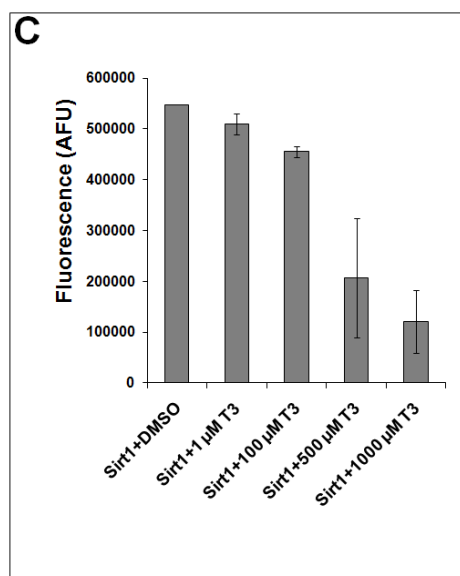


Figure 3.18: Influence of Thyroid hormones on the activity of Sirt1. A) A fluorescence based assay was performed by incubating ~ 100 nM Sirt1, 25 μM FdL-1 substrate, 25 μM NAD⁺ and 10 μM T2 or T3. B) ~ 200 nM Sirt1 was incubated with 100 μM FdL-1, 1000 μM NAD⁺ and 500 μM T4. C). ~ 200 nM Sirt1 was incubated with 100 μM FdL-1, 1000 μM NAD⁺ and various concentrations of T3. No change in the activity of Sirt1 was observed in the presence of T2, T3 (A) or T4 (B). Only at high concentration T3 inhibits Sirt1.

Recently, our lab identified Sirt2 specific inhibitors based on virtual docking of compound library on known mammalian Sirtuin structures (Schlicker et al., 2011). Two compounds from the screen namely; Compounds CSC8 and CSC13 showed micromolar potency for Sirt2 with an IC₅₀ of 4.8 ± 0.5 μM for compound CSC8 and 9.7 ± 1.5 μM for compound CSC13 respectively. In order to investigate the effect of these compounds on Sirt1, we assayed the activity of Sirt1 in the presence of 100 μM CSC8 and CSC13 respectively using the Fdl-1 substrate peptide (Figure 3.19). The compounds had only a weak inhibitory effect on Sirt1, indicating they are indeed specific for Sirt2 and could also serve as lead compounds for developing Sirt2 specific drugs.

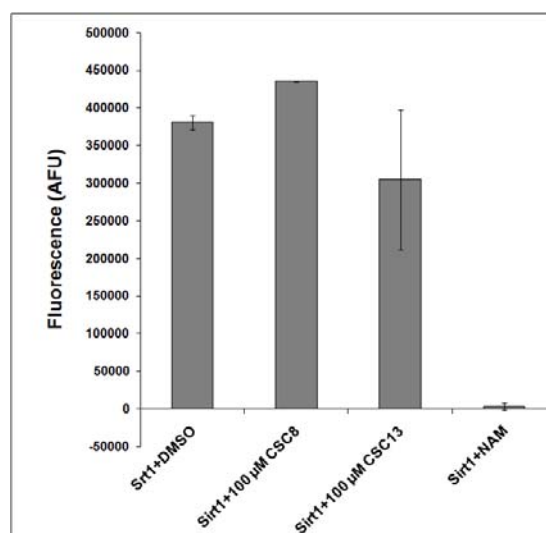


Figure 3.19: Effects of Sirt2 docking on the activity of Sirt1. Compounds that specifically inhibit Sirt2 were tested on Sirt1 and found to have weak or no inhibitory effect. FdL-1 assay was performed with 100 μM substrate, 500 μM NAD⁺, ~ 200 nM Sirt1 and 100 μM Compound CSC8 or CSC13 respectively. 2 mM NAM was used as a positive control to show inhibition.

3.1.7 Resveratrol can directly bind to Sirt1

Initial binding studies between small molecule modulators of Sirt1 and fluorogenic substrate peptides indicated direct interaction between the small molecule and the peptide fluorophore (Pacholec et al., 2010), implying Sirt1 activation to be an artifact of substrate modification. Later Dai et. al (Dai et al., 2010) reported that some small molecules can also interact directly with Sirt1 and the interaction between modified peptides and small molecules depend on the substrate-modulator pair. Along the same lines, we also tested if resveratrol can directly bind to Sirt1. Microscale thermophoresis studies indicate that resveratrol indeed binds to Sirt1 and the presence of unmodified peptides does not have an effect on this interaction (Figure 3.20). The poor solubility of resveratrol in aqueous buffer makes it difficult to quantify the binding. Nevertheless resveratrol appears to bind to Sirt1 with a K_d in the range of 100 μ M.

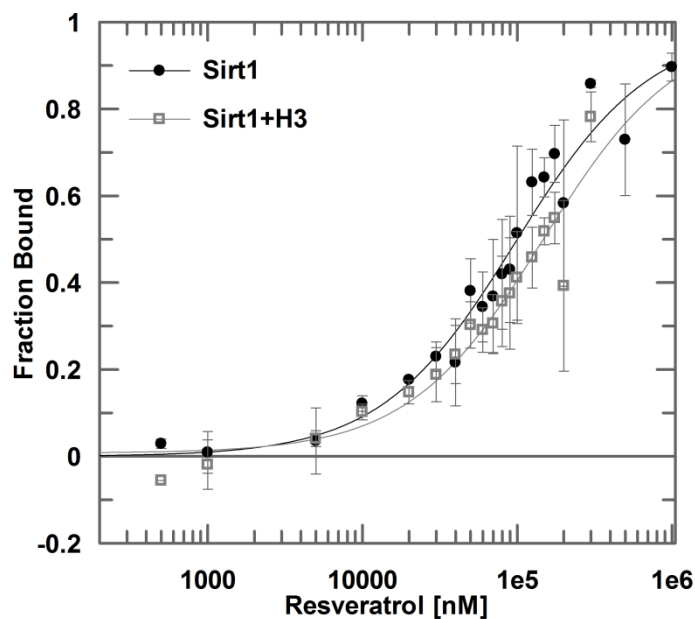


Figure 3.20: Resveratrol interacts directly with Sirt1. 200 nM NT-647 labeled Sirt1 was mixed with various compounds and titrated against resveratrol. The binding was analyzed using microscale thermophoresis. H3-Lys116 was used at a concentration of 500 μ M. The thermophoresis obtained with 40 % LASER power was used for analysis from all the measurements. Although a K_d cannot be determined since saturation is not reached, a clear binding can be observed between Sirt1 and resveratrol.

3.1.8 Crystallization trials of Sirt1

In addition to biochemical characterizations, structural studies were pursued to solve the crystal structure of Sirt1. Several Sirt1 constructs were purified followed by crystallization trials using various commercially available kits and at different protein concentration and

temperature, but no diffraction quality crystals were obtained. Supplemental table S2 lists the various constructs of Sirt1 used in the crystallization along with their concentration and crystallization conditions. The full length Sirt1 protein yielded precipitates in conditions with low pH, but did not result in crystals. Since crystallization prediction servers XtalPred (<http://ffas.burnham.org/XtalPred-cgi/xtal.pl>) (Slabinski et al., 2007) and PHYRE (Protein Homology/analogY Recognition Engine) (<http://www.sbg.bio.ic.ac.uk/~phyre/>) (Kelley and Sternberg, 2009) suggested full length Sirt1 may possess unstructured and extended conformation at its termini, we also tried crystallization of shorter constructs including only the catalytic domain. Several mutational studies were also pursued to enhance the crystallizability of Sirt1. One approach used was the mutation of residues that are likely to enhance the crystallizability of Sirt1 via generation of crystal contacts by SER (surface entropy reduction) as described by Derewenda (Derewenda, 2004). This idea is based on the targeted mutagenesis of surface patches that contain residues with large flexible side chains, where exchanging them for smaller side chain containing amino acids leads to an increase in probability of protein crystallization. Sirt1 construct 225to664 with SER mutation 576-578 EEK-AAA was used in crystallization trials. Several conditions yielded leads such as precipitation, potential showers of micro crystals, phase separation. When a protein crystal staining dye (Jena Bioscience, Germany) was used to test if the micro crystals were indeed from protein, the crystals imbibed the dye indicating genuine protein crystals (Figure 3.21). When optimization trials were setup based on this condition, the crystals were not reproducible.

PTMs in protein can often lead to changes in their conformation leading to their crystallization. Sirt1 has been shown to possess several modifications. In fact, Sirt1 phosphorylation has been shown to increase its activity (Section 1.6.1 and table 1.2). We mutated Thr530 of Sirt1 to Asp to mimic phosphorylation and overexpressed the protein in *E. coli* followed by purification to perform activity as well as crystallization studies. Similar to reported results (Nasrin et al., 2009), Sirt1 Thr530Asp mutant appears to be more active than the wildtype (Figure 3.22). Sirt1 constructs carrying the Thr530Asp mutation were used in crystallization trials with commercially available kits, alternative reservoir strategies (Newman, 2005), in the presence of modulators but resulted in no diffraction quality crystals. Crystallization trials using Trypsin and chymotrypsin (with various Sirt1 to protease ratio) were pursued in order to identify stable in situ protein constructs that are more amenable for crystallization, but resulted in no crystals.



Figure 3.21: Crystallization of Sirt1. A representative picture of potential Sirt1 crystals stained with a red dye. The concentration of dye in the crystal could indicate potential protein crystal. The crystallization conditions are: hSirt1 225-664 SER mutant at a concentration of 10 mg/ml, 300 mM citric acid and 40 % (v/v) MPD ((±)-2-Methyl-2,4-pentanediol).

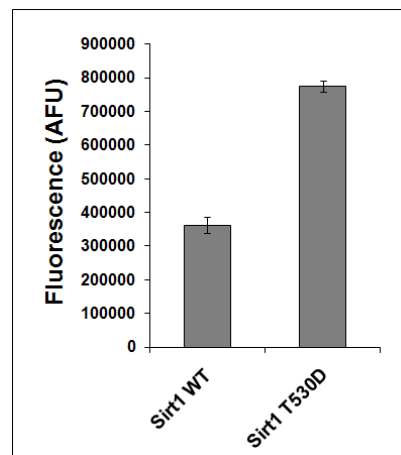


Figure 3.22: Phosphorylation mimic of Sirt1 may regulate its activity. ~ 200 nM full length WT (wildtype) and Thr530Asp Sirt1 were incubated with 100 μ M FdL-1 substrate and 1 mM NAD^+ . A twofold higher activity can be observed for the mutant compared to wildtype Sirt1.

3.1.9 Studies on AROS

Human AROS is a small nuclear protein (15.4 kDa), shown to activate human Sirt1 by interacting with its N-terminus (residues 114to217) (Kim et al., 2007). To date there are no biochemical or structural studies that characterize the Sirt1 interaction with AROS. In order to understand how AROS regulates Sirt1 function, we attempted overexpression and purification of AROS in *E. coli*. AROS containing an N-terminal hexa histidine tag was overexpressed in high yield, but was mostly insoluble (Figure 3.23A). Several attempts were made to increase the solubility of AROS, without success. Attempts to solubilize the protein from inclusion bodies using guanidine hydrochloride followed by on-column refolding and affinity purification were successful and yielded pure protein which elutes as a single peak in SEC

with an apparent molecular weight corresponding to that of a monomer (Figure 3.23 B) and a CD spectrum indicates that it possesses secondary structure (Figure 3.23C). When FdL-1 based fluorescence assay was performed using AROS and Sirt1 a very mild decrease in Sirt1 activity was observed (Figure 3.24A). To purify AROS in its native form, we created constructs harboring GST and MBP on the N-terminus of AROS respectively. Although GST-tagged AROS was more soluble than His-tagged AROS, purification was not possible as the GST tag did not bind to Glutathione resin. MBP-tagged AROS was soluble and easily purified with roughly 60 % purity (Figure 3.23A), but efforts to cleave the MBP tag or further purification of the protein resulted in almost complete precipitation of AROS. Nevertheless MBP-tagged AROS was used in FdL-1 assay to investigate the modulation of Sirt1. Although not statistically significant, the results show a mild inhibition of Sirt1 (Figure 3.24B).

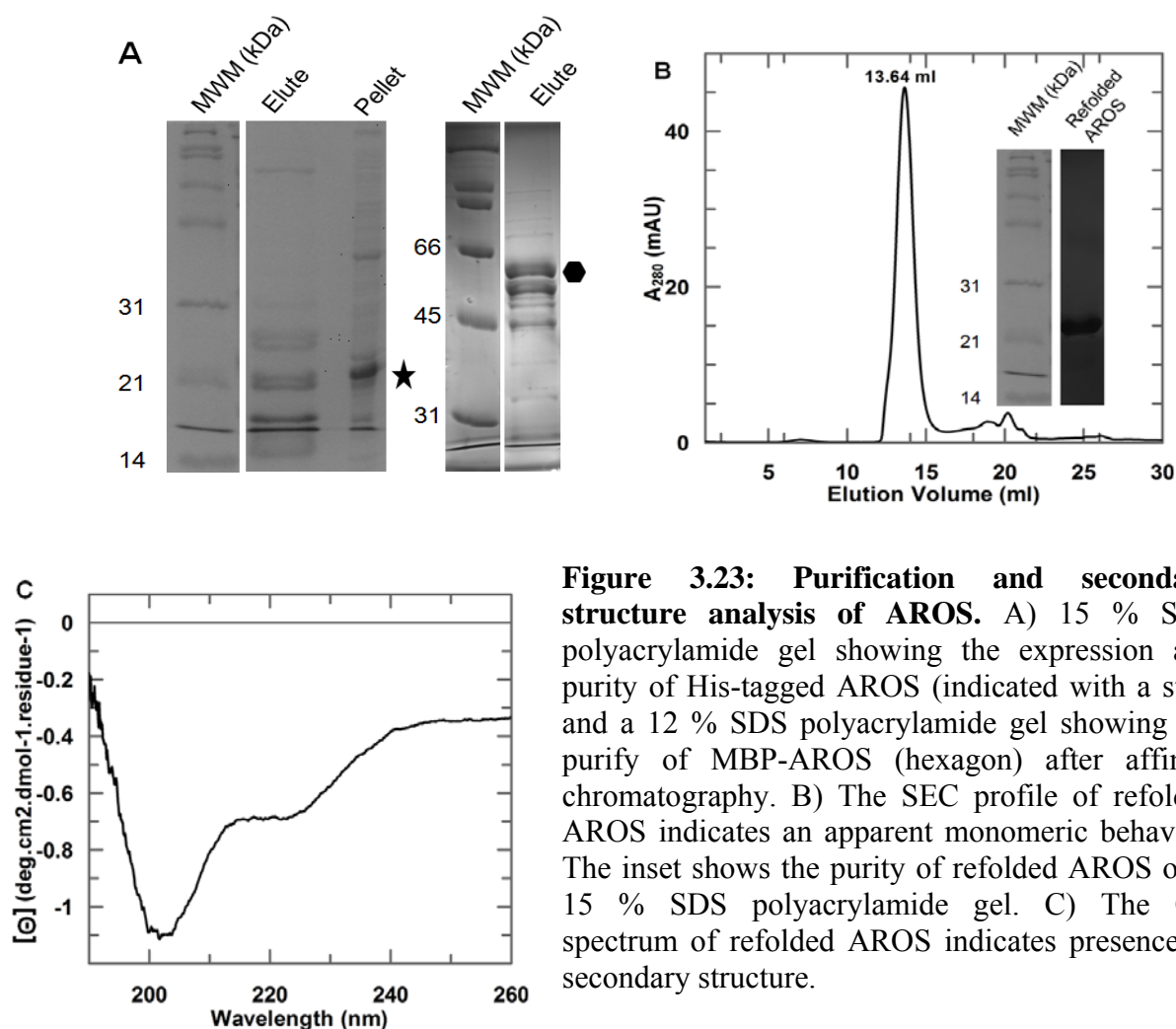


Figure 3.23: Purification and secondary structure analysis of AROS. A) 15 % SDS polyacrylamide gel showing the expression and purity of His-tagged AROS (indicated with a star) and a 12 % SDS polyacrylamide gel showing the purify of MBP-AROS (hexagon) after affinity chromatography. B) The SEC profile of refolded AROS indicates an apparent monomeric behavior. The inset shows the purity of refolded AROS on a 15 % SDS polyacrylamide gel. C) The CD spectrum of refolded AROS indicates presence of secondary structure.

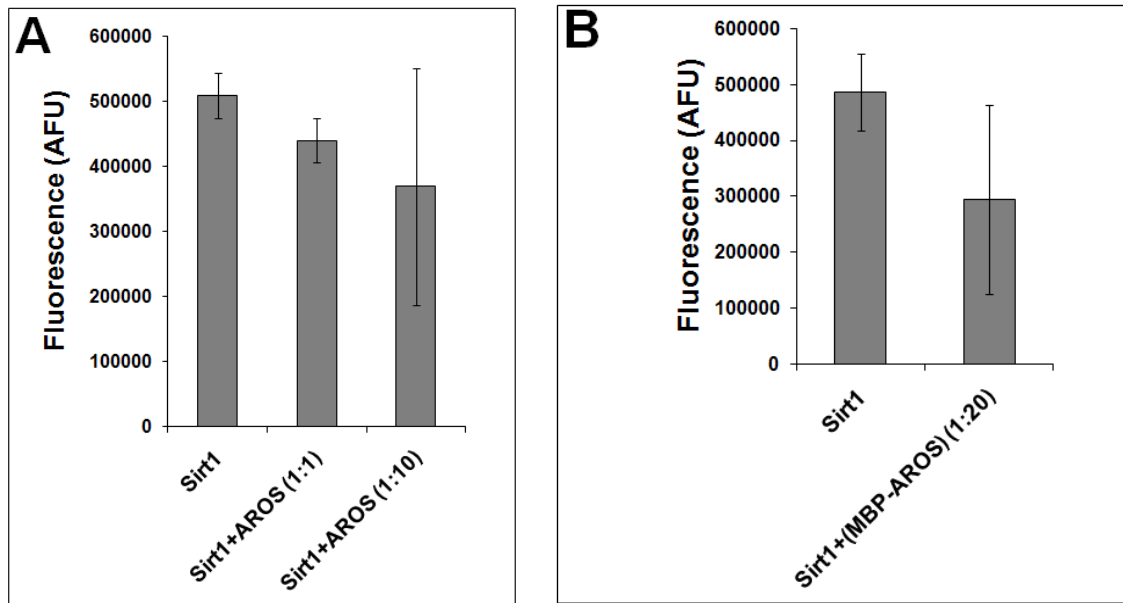


Figure 3.24: Influence of AROS on the activity of Sirt1. The influence of refolded AROS protein on the activity of ~ 200 nM Sirt1 was analyzed using $100 \mu\text{M}$ FdL-1 peptide, $1000 \mu\text{M}$ NAD^+ and 1:1 or 1:10 molar excess of AROS. B) The same assay performed in the presence of 20 fold molar excess of MBP tagged AROS with $50 \mu\text{M}$ FdL-1 substrate, $1000 \mu\text{M}$ NAD^+ and ~ 200 nM Sirt1. Under the conditions tested, AROS seems to weakly inhibit Sirt1, but further investigation is required to confirm this result.

3.2 Studies on the role of Zinc in Sirt3

The human Sirt3 protein cloning, expression and purification procedures were performed as mentioned in sections 2.2.5, 2.2.6 and 2.4.4 respectively. Slight modifications adopted for Sirt3 are detailed explicitly. The purity of the protein was $\geq 95\%$ and the yield was ~ 3 mg/liter of *E. coli* culture. Figure 3.25 shows the purity of Sirt3 visualized on an SDS-PAGE. The enzyme showed activity in assays (see below) indicating a well folded and active protein.

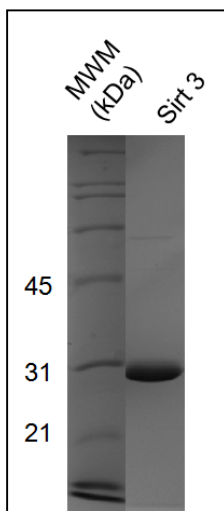


Figure 3.25: Purification of Sirt 3. 15 % (w/v) SDS polyacrylamide gel showing the purity of tag cleaved Sirt3 (114-399) after size exclusion chromatography.

To understand the role of Zinc in the structure and function of mammalian Sirtuins, Sirt3 was used as a model because of its ease of purification, activity, and availability of crystal structure. Sirt3, like all other mammalian Sirtuins studies so far contains four conserved Cysteines (256, 259, 280 and 283) (supplemental figure S2), which coordinate a Zinc ion. To probe the role of Zinc, site directed mutagenesis studies were pursued by mutating the Cysteines that coordinate the Zinc ion (C259A or C259/280A). The mutant proteins were overexpressed in *E. coli* Rosetta 2 (DE3) cells similar to the wildtype protein. Protein overexpression was observed, but attempts to purify either the single or the double mutant proved futile, because the proteins were found in the insoluble fraction (Figure 3.26). Inclusion of ZnCl_2 (10 μM) either in the purification buffer or while overexpressing the protein also did not yield soluble protein. These expression studies indicate that the mutant proteins appear not to fold properly or to be unstable.

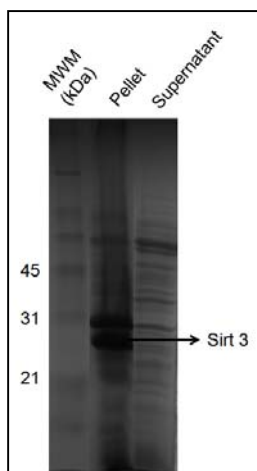


Figure 3.26: Purification of Sirt3 Cysteine mutants. A representative 12 % (w/v) SDS polyacrylamide gel showing the presence of Sirt 3 Cysteine mutant (C259A) in the pellet.

Since mutational studies proved unsuccessful in obtaining soluble protein, the wildtype protein was used to probe the role of Zinc. Sirt3 was incubated with EDTA at 4 °C for 30 minutes, followed by centrifugation for 5 minutes at 14,000 RPM at 4 °C and assayed using the commercially available fluorescence based assay kit as mentioned in section 2.4.6. As shown in Figure 3.27a, the treatment of EDTA did not affect the activity of Sirt3, indicating either a strong affinity between Zinc and Sirt3 or a lack of function for Zinc. On the other hand, incubation of Sirt3 with 200 μ M 1,10-phenanthroline immediately precipitated the protein leading to a complete loss of activity as shown in Figure 3.27b. Thus, Zinc is essential for stability of Sirt3.

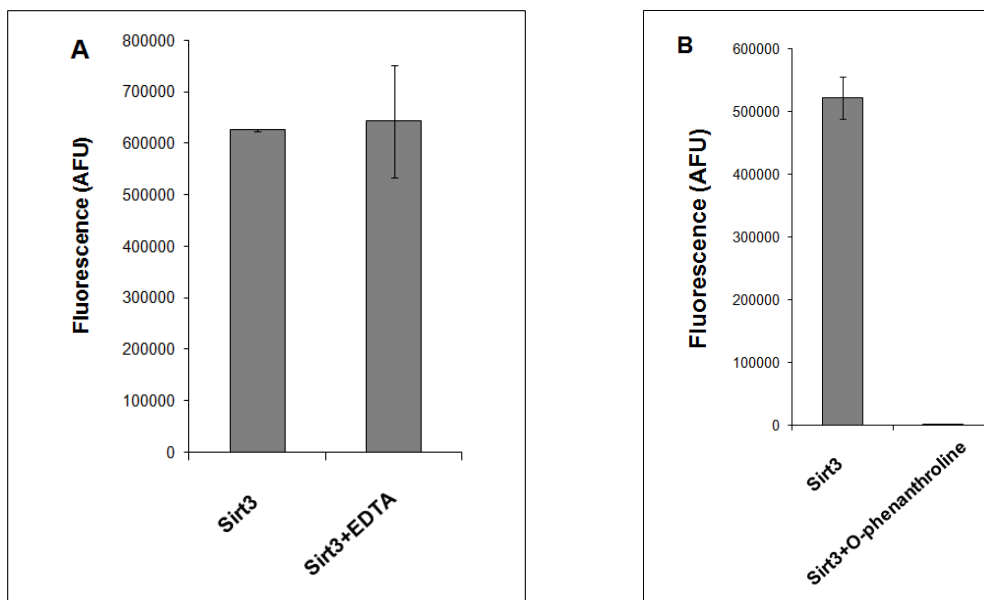


Figure 3.27: Zinc is essential for the stability and activity of Sirt3. The fluorescence assay was used to measure the activity of Sirt3, using 100 μ M FdL-2 peptide substrate (QPKK[ac]-coumarin) and 1 mM NAD⁺. A) 1 μ g of Sirt3 was incubated with either buffer or 2 mM EDTA for 30 minutes on ice and centrifuged before performing the assay. B) Sirt3 was incubated with buffer or with 200 μ M O-phenanthroline and centrifuged before performing the assay.

3.3 Studies on Sirt5

The human Sirt5 protein cloning, expression and purification procedures were performed as mentioned in sections 2.2.5, 2.2.6 and 2.4.4 respectively. Slight modifications adopted for Sirt5 are detailed explicitly. The purity of the protein was $\geq 95\%$ and the yield was ~ 15 mg/liter of *E. coli* culture. Figure 3.28 shows the purity of Sirt5 visualized on an SDS-PAGE. The enzyme showed activity in several assays (see below) indicating a well folded and active protein.

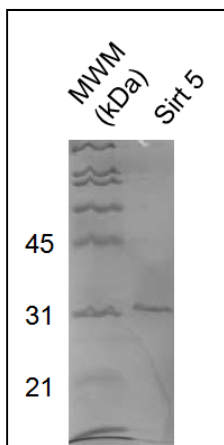


Figure 3.28: Purification of Sirt 5. 15 % (w/v) SDS polyacrylamide gel showing the purity of tag cleaved Sirt5 (34-302) after size exclusion chromatography.

3.3.1 Influence of NAD^+ on the activity of Sirt5

The human Sirt5, which is localized in the mitochondria, is poorly characterized in terms of substrates and regulators compared to its isoforms and to date only one in vivo substrate (CPS1) is known. Our lab had previously identified that Cyt c, can be deacetylated in vitro by Sirt5 in an ELISA (Schlicker et al., 2008). In general, Sirt5 seems to behave as a weak deacetylase compared to other Sirtuins when fluorogenic peptides or Cyt. c are used as substrates (Schlicker et al., 2008). In order to identify if Sirt5's activity is dependent on its co-substrate NAD^+ an ELISA was performed in the presence of increasing amounts of NAD^+ and 10 μg of Cyt c. As shown in Figure 3.29, the deacetylase activity of Sirt5 increased dramatically with increasing concentration of NAD^+ until 10 mM, leading to a $\sim 200\%$ increase in activity.

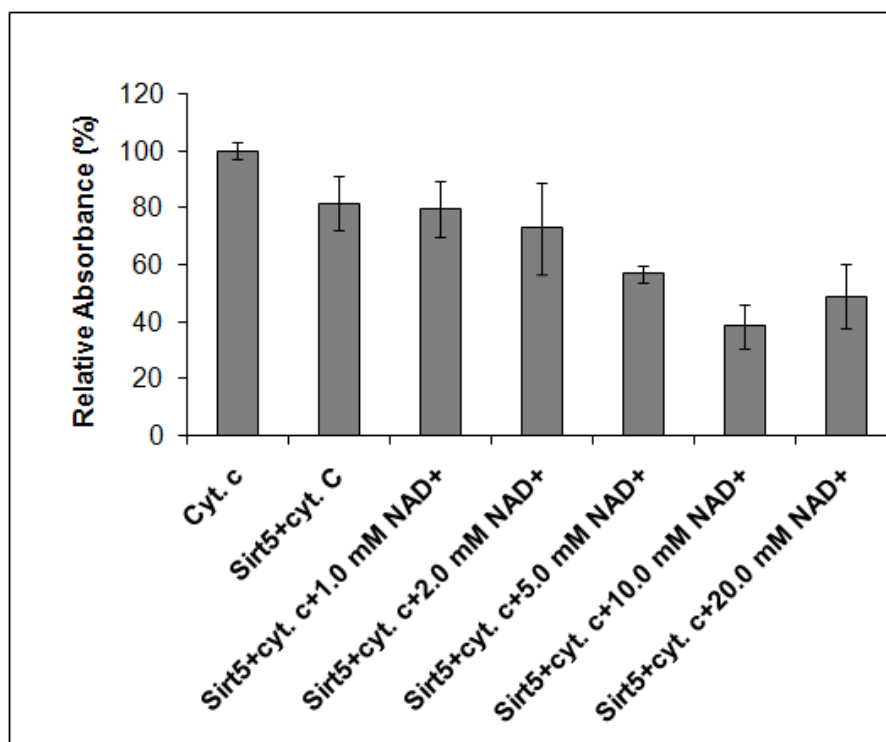


Figure 3.29: Sirt5 appears to require higher amounts of NAD⁺ for its deacetylase activity. An ELISA was performed with 10 μ g Cyt. c as substrate and 10 μ g Sirt5 and increasing amounts of NAD⁺. A decrease in absorbance indicates an increase in the ability of Sirt5 to deacetylate the substrate Cyt. c. The activity of Sirt5 increased linearly until 10 mM NAD⁺, beyond which no increase was seen.

3.3.2 Sirt5 appears to be insensitive to Nicotinamide inhibition

NAM, one of the products of Sirtuin catalyzed deacetylation is a potent physiological inhibitor (IC₅₀ in the micro molar range) of several Sirtuins including Sirt1 and Sirt3. In order to identify if NAM can also inhibit Sirt5 an ELISA was performed using 10 μ g Cyt. c and 5 mM NAD⁺ (Figure 3.30). Even in the presence of 10 mM NAM, the activity of Sirt5 was not affected, indicating that Sirt5 might possess unique features in the NAM binding pocket (“C pocket”) that renders it insensitive to inhibition by NAM (Avalos et al., 2005; Sauve and Schramm, 2003).

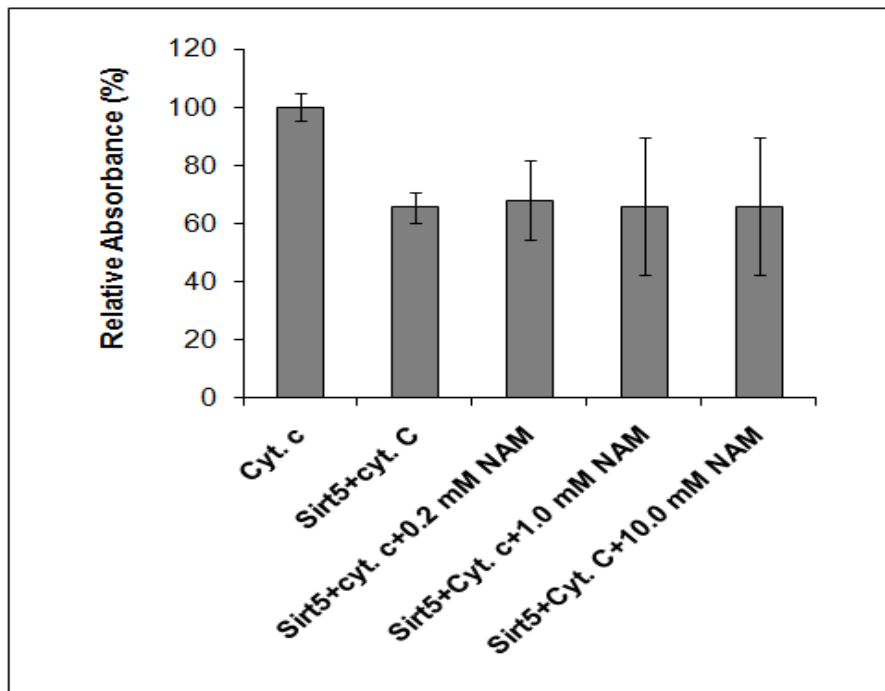


Figure 3.30: Sirt5 appears to be insensitive to NAM. An ELISA was performed with 10 μ g of Sirt5 and 10 μ g Cyt. c, 5 mM NAD^+ as substrates. Increasing amounts of NAM were added to test its ability to inhibit Sirt5. Even at 10 mM concentration, NAM did not inhibit Sirt5.

In order to identify the reason behind Sirt5's insensitivity towards NAM, a point mutant (Thr69Asp) was generated based on sequence alignment of Sirtuin homologs (supplemental figure S2). All mammalian Sirtuins except Sirt5 contain Asp in the flexible co-substrate binding loop, which takes part in NAM binding (Avalos et al., 2005). The Thr69Asp mutant protein showed less activity compared to the wildtype and did not sensitize Sirt5 to NAM (Figure 3.31), indicating that other molecular differences should be responsible for the unique NAM insensitivity of human Sirt5.

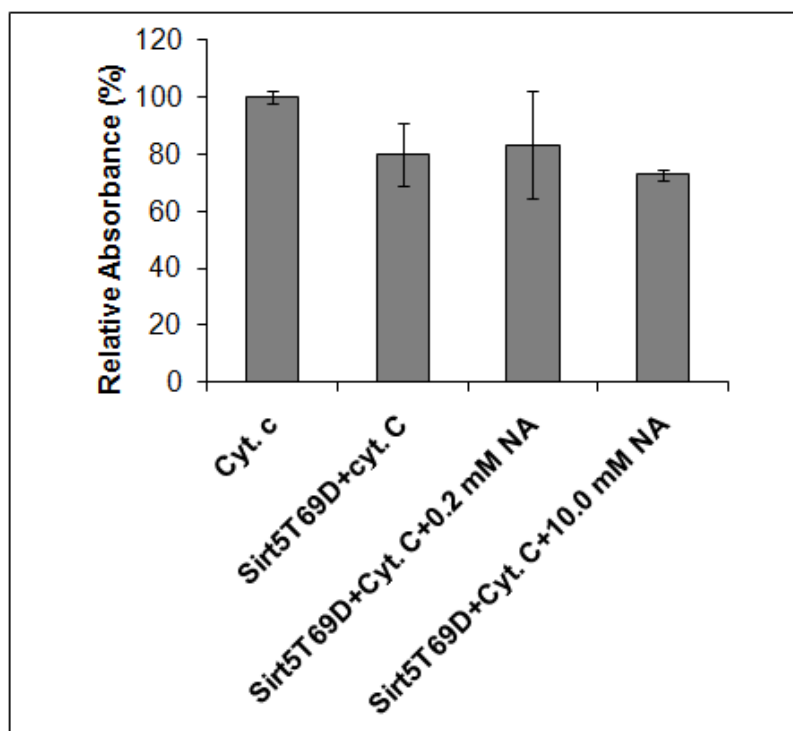


Figure 3.31: Thr69Asp mutation impairs the activity of Sirt5. An ELISA was performed with 10 μg of Sirt5T69D and 10 μg Cyt. c, 5 mM NAD^+ as substrates. The activity of the mutant enzyme was impaired when compared to the wild type (Figure 3.30) and addition of NAM had no effect on its activity.

3.4 Studies on Sirt7

3.4.1 Expression and purification of Sirt7

Cloning, expression and purification procedures of human Sirt7 constructs (Table 3.2) were performed as mentioned in sections 2.2.5, 2.2.6 and 2.4.4 respectively. Slight modifications adopted for Sirt7 are detailed explicitly. The different proteases used to cleave affinity tags are listed in table 3.2. The purity of the eluted samples were $\geq 90\%$ as judged by capillary electrophoresis (Caliper Life Sciences, USA) or SDS-PAGE. A representative gel showing different constructs of Sirt7 is shown in Figure 3.32. Typical yields of Sirt7 constructs overexpressed in *E. coli* were $\sim 1-3$ mg/liter media.

Construct	Vector	Antibiotic	Tag	Protease	Expression system
Full length	pOPIN-MBP	Ampicillin	MBP	Rhino virus 3C	High Five
Full length	pOPIN-MBP	Ampicillin	MBP	Rhino virus 3C	<i>E. coli</i>
14-367	pOPIN-SUMO	Ampicillin	SUMO	SUMO	<i>E. coli</i>
25-356	pOPIN-NHis	Ampicillin	NHis	-	<i>E. coli</i>
59-356	pOPIN-NHis	Ampicillin	NHis	-	<i>E. coli</i>
81-356	pOPIN-NHis	Ampicillin	NHis	-	<i>E. coli</i>

Table 3.2: Table representing the constructs of Sirt7 used in this study. The cloning, expression and initial purification steps were performed at the DPF.

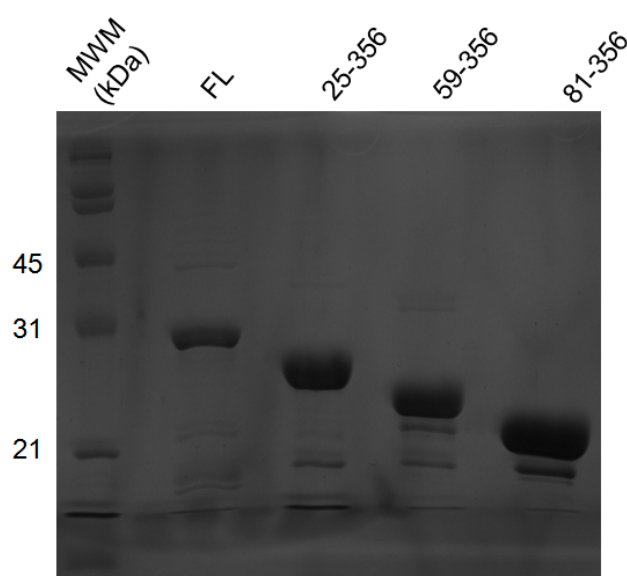


Figure 3.32: Purification of Sir7. 12 % (w/v) SDS polyacrylamide gel showing the purity of various constructs of Sirt7 (indicated on top) after size exclusion chromatography.

3.4.2 Effect of various buffers and salts on the stability of Sirt7

Sirt7 construct 81-356 was used to perform thermal denaturation shift assay in order to identify optimal buffer and salt conditions for crystallization trials. Sirt7 seems to be more stable in basic pH and presence of at least 50 mM salt enhances its stability. Figure 3.33 shows a representative buffer (pH 8.0) and salt range for Sirt7. Starting from pH 7 until pH 9, almost all the buffers stabilized the protein in the presence of increasing amounts of salt (up to 500 mM KCl). The T_m ranged between ~ 40 to 42 °C. Even though the highest T_m (~ 42 °C) was observed when 500 mM salt was used, the buffer condition chose for subsequent experiments was 25 mM HEPES, pH 8.0 and 150 mM KCl, because high amount of salts can interfere with the crystallization process.

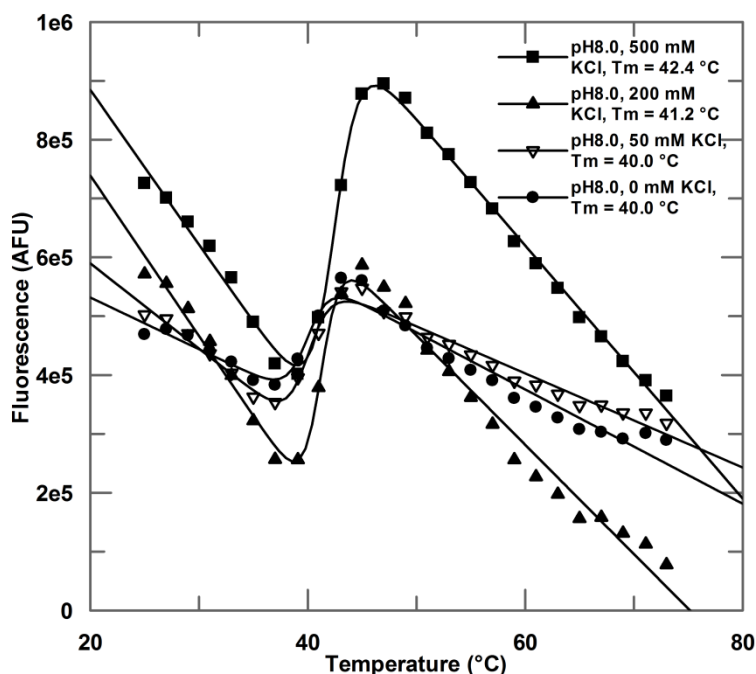


Figure 3.33: Optimization of buffer conditions for Sirt7 81-356. Representative thermal denaturation shift assay of Sirt7 81-356. The increase in the fluorescence of the dye (AFU) is plotted against the temperature (°C). The buffer used was 50 mM HEPES, pH 8.0, with 0, 50, 200 and 500 mM KCl. The fitting of the curve to a two state transition yielded T_m in the range of 40 to 42 °C as indicated.

3.4.3 Identification of new Sirt7 constructs for crystallization

For crystallization trials, an additional purification step was performed for the 81-356 Sirt7 construct. The protein (calculated $pI = 8.89$) was bound to HiTrapSP cation exchange column (GE Healthcare, USA) in Buffer A (25 mM HEPES, pH 8.0, 100 mM KCl, 2 mM DTT) and eluted in a gradient to buffer A supplemented with 400 mM KCl (buffer B). A very low flow rate of 0.05 ml/min was used to ensure better purity of Sirt7. While analyzing the

eluted fractions by SDS-PAGE an additional protein band was observed below the expected Sirt7 81-356 construct. The majority of the desired protein eluted at 45.4 % B, and the majority of the 2nd specie at 39.2 % B (Figures 3.34 a and b). It is possible that the protein was degraded during the slow ion exchange process leading to a more stable fragment. In order to identify the new specie, one of the bands was extracted from the gel and tryptic digest followed by MS analysis (Figure 3.35) was performed to identify peptides covered by the new specie. Since this method does not ensure the exact N and C-terminus, another gel band was transferred to a PVDF membrane and sent for N-terminal sequencing analysis (section 2.4.9). The N-terminal sequencing and the tryptic digest results identified that the new fragment started at Thr127 and continued at least until Arg348 (Figure 3.35).

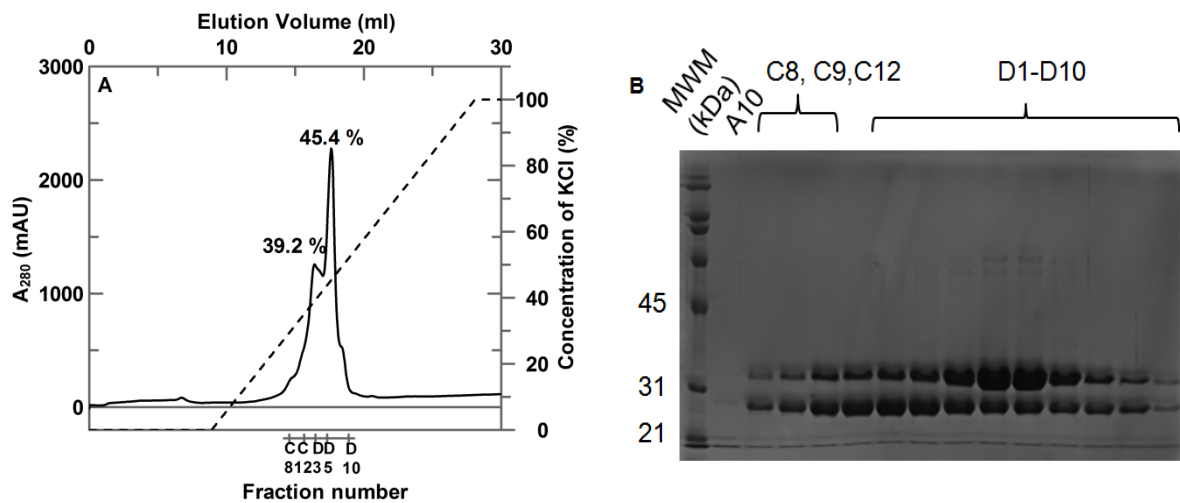


Figure 3.34: Cation exchange chromatography of Sirt7 81-356. A) Chromatography elution profile showing two prominent peaks at 39.2 % and 45.2 % of Buffer B respectively. Representative fractions C8, C12, D3, D5 and D10 are indicated below the peaks. B) Analysis of elution fractions by SDS-PAGE indicates that the peak eluting at 39.2 % B contains the majority of the low molecular weight protein (degradation product). Fraction numbers are indicated on top of the gel.

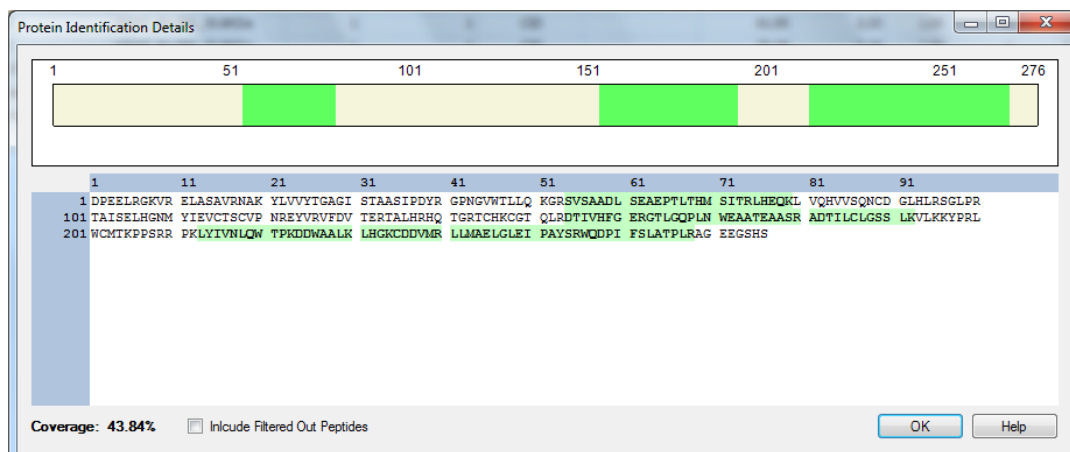


Figure 3.35: Identification of Sirt7 degradation product using MS. Screen shot of the Tryptic digest of the lower band from SDS PAGE followed by MS (43.84 % sequence coverage) showing the identified peptides in green. The proteolyzed Sirt7 contains at least Arg348 at the C terminus.

3.4.4 Crystallization trials of Sirt7

Several crystallization trials were pursued to solve the structure of Sirt7. Supplemental table S3 lists the constructs of Sirt7, crystallization screens and conditions that were used in the trials. Crystallization trials were also set up using the in situ proteolysis method containing different proteases along with Sirt7 in order to identify stable protein parts that are more amenable to form crystals. A number of conditions yielded precipitate or phase separations that were quite promising and revealed a tendency for the protein to precipitate at acidic pH, nevertheless no diffraction quality crystals were obtained.

3.4.5 PTMs influence the activity of Sirt7

Initial activity studies on Sirt7 constructs overexpressed in *E. coli* using the FdL-1 or FdL-2 substrate peptides showed weak or no deacetylase activity (Figure 3.36). Since Vakhrusheva et. al. (Vakhrusheva et al., 2008) were able to show Sirt7 dependent deacetylation activity on the FdL-1 substrate peptide, but did not reveal the source of Sirt7 protein, we hypothesized that Sirt7 may require PTM for its activity. To this end, we used Sirt7 overexpressed in insect cells (full length Sirt7 with a 6xHis-MBP tag was expressed in insect cells (High Five) and purified at the DPF) against the FdL peptide substrates and observed (Figure 3.36) better deacetylation activity, which supports our hypothesis that PTMs play a role in Sirt7's activity. To identify the type of PTM and the residue modified in Sirt7 which leads to its higher activity, the insect cell expressed full length Sirt7 was resolved on an SDS gel and the band corresponding to the protein was isolated, followed by tryptic digest and MS analysis (Section 2.5.2). Analysis of the MS peaks against the Sirt7 sequence using the SEQUEST algorithm identified that at least Thr224 was phosphorylated (Figure 3.37).

To probe further the role of phosphorylation on Sirt7's activity, a Threonine to Aspartate (T224D) point mutant was generated in Sirt7 (full length and 81-356 constructs) by site directed mutagenesis (Section 2.3.3). The constructs were sequence verified and transformed in *E. coli* to overexpress the mutant proteins. In spite of several attempts with different conditions, there was no overexpression of T224D Sirt7 protein constructs in *E. coli*.

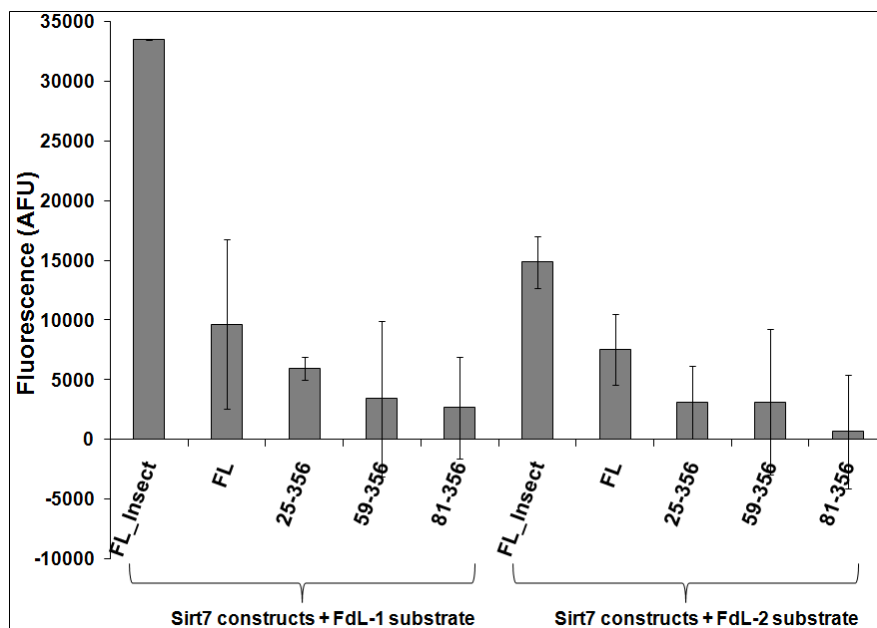


Figure 3.36: Sirt7 activity is influenced by PTM. The FdL fluorescence assay was used to measure the activity of Sirt7, using either FdL-1 or FdL-2 substrate peptide and NAD^+ . $1 \mu\text{g}$ of Sirt7 was incubated with $100 \mu\text{M}$ peptide and 2mM NAD^+ . FL_Insect represents Sirt7 overexpressed and purified from insect cells. The other Sirt7 constructs were overexpressed and purified from *E. coli* cells.

Accession	Coverage	# PSMs	# AAs	Score	Description													
6xHis-MPB-3C-Sirt7FL	62.51	316	907	1137.70	6xHis-MPB-3C-Sirt7FL													
Confidence	Sequence	# Protein	Modifications	Probability	XCorr	Δ Score	Rank	Charge	m/z [Da]	MH+ [Da]	Δ M [ppm]	RT [min]	First Scan	Last Scan	MS Orde	Ions Matched		
High	tCHKCGTQLRDTIVHFGER	1	T1(Phospho)	1.11	2.03	1.00	1	2	1140.99988	2280.99248	-19.37	166.74	31238	31238	MS2	11/72		

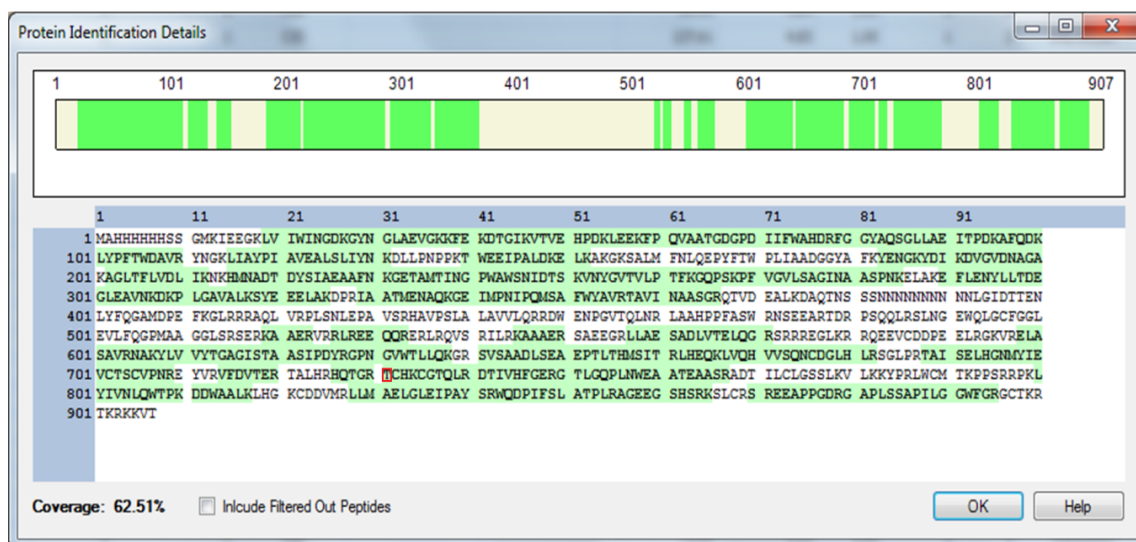


Figure 3.37: Sirt7 is phosphorylated at Thr224. MBP tagged Sirt7 overexpressed in insect cells was resolved on SDS gels, followed by tryptic digest and MS analysis. The table and screen shot (from the Proteome Discoverer software package) indicates that Sirt7 is phosphorylated at Thr224. For clarification purposes only the peptide containing Thr224 is shown in the table. The peptides identified are shaded in green and Thr224 is highlighted with a red box.

3.4.6 Investigating the modulation of Sirt7 by resveratrol and nicotinamide

Sirtuin isoforms are differently regulated by small molecules. In order to understand the regulation of Sirt7 by small molecules, we tested the full length Sirt7 expressed in both *E. coli* and insect cells for their modulation by resveratrol and NAM, widely used activator and inhibitor of Sirtuins respectively. Sirt7 activity was tested using the fluorogenic peptide FdL-1 as substrate. In our assays, neither resveratrol nor NAM modulated the activity of Sirt7 (Figure 3.38), indicating that Sirt7 might be resveratrol insensitive or have unusual substrate requirements for modulation by resveratrol (see Sirt1 results section 3.1.5) and is also insensitive to NAM under the conditions tested, similar to Sirt5.

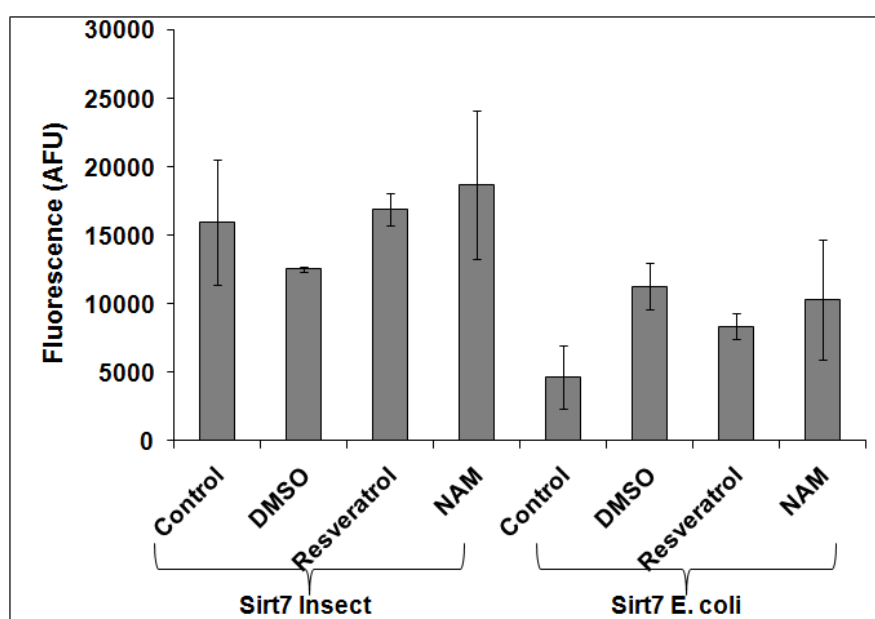


Figure 3.38: Sirt7 is insensitive to modulation by resveratrol and NAM in the FdL assay. The activity of 0.9 μg Sirt7 with 100 μM FdL-1 peptide and 1 mM NAD^+ was measured with 100 μM resveratrol or 2 mM NAM. 0.5 % DMSO was included as solvent control. Sirt7 insect represents full length Sirt7 overexpressed and purified from insect cells and Sirt7 E. coli represents full length Sirt7 overexpressed and purified from *E. coli* cells.

3.5 Studies on Sir2Tm

3.5.1 Investigating the oligomerization behavior of Sir2Tm

Expression and purification of Sir2Tm was performed as mentioned in sections 2.2.5, 2.2.6 and 2.4.4 respectively. During purification, the SEC profile of pure Sir2Tm showed a single peak eluting at 13.72 ml (Figure 3.39a), corresponding to ~ 26 kDa in agreement with Sir2Tm's monomer molecular weight of ~ 27.5 kDa. SDS-PAGE analysis of SEC fractions revealed two bands; a major specie at ~ 27.5 kDa and a minor one at almost twice the molecular weight (~ 48 kDa) (Figure 3.39b). Tryptic digest followed by MS analysis of the two bands revealed that both are in fact Sir2Tm without additional modifications. This prompted us to supplement all the buffers with 5 mM DTT (deviating from Smith et. al.'s protocol), because we suspected dimer formation due to oxidation of Cysteines present in Sir2Tm. SDS-PAGE analysis of the sample supplemented with high amounts of reducing agents (Figure 3.40a), shifted the equilibrium towards monomer, whereas BN-PAGE (Figure 3.40b) revealed that Sir2Tm runs at ~ 45 kDa. Based on these results, it can be concluded that the unusual behavior of Sir2Tm seen in PAGE analysis pertains to the conditions used in resolving the protein, but in solution Sir2Tm seems to behave as a monomer and is not affected in either in its activity or ability to crystallize.

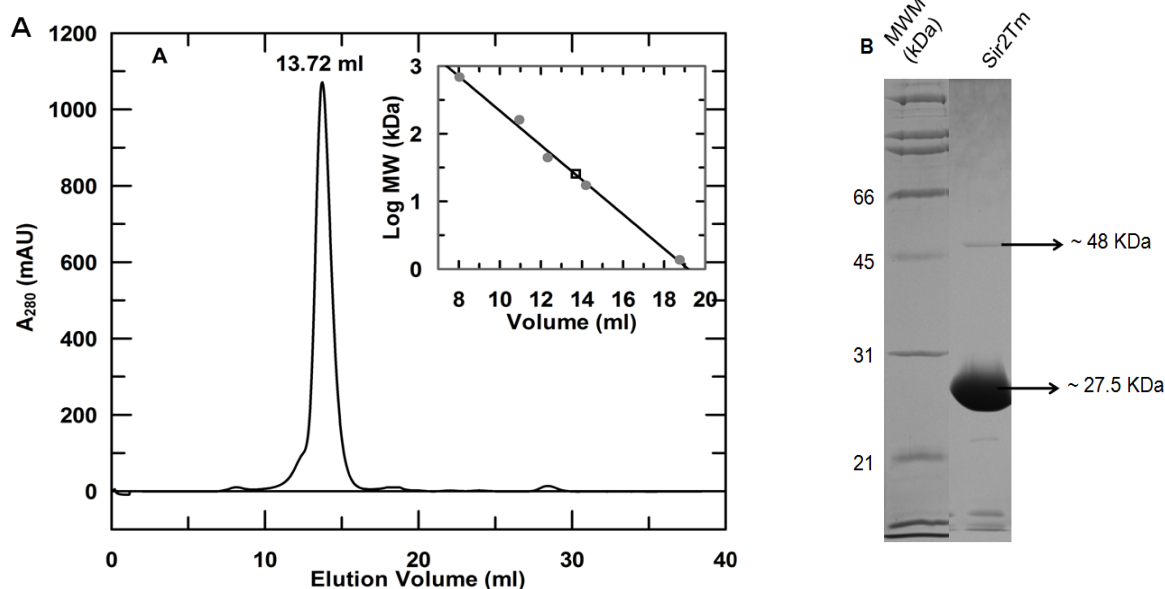


Figure 3.39: Purification of Sir2Tm. A) Size exclusion chromatography profile of full length Sir2Tm. The elution volume corresponds to monomer molecular weight of ~ 27.5 kDa. The inset shows a plot of standards (\log_{10} molecular weight versus volume (ml) in gray circles and the elution volume of Sir2Tm in black square. B) Analysis of gel filtration purified Sir2Tm on a 14 % (w/v) SDS gel shows two bands. The lower band corresponds to a monomer molecular weight of ~ 27.5 kDa and the upper band corresponds to ~ 48 kDa (close to the size of a dimer).

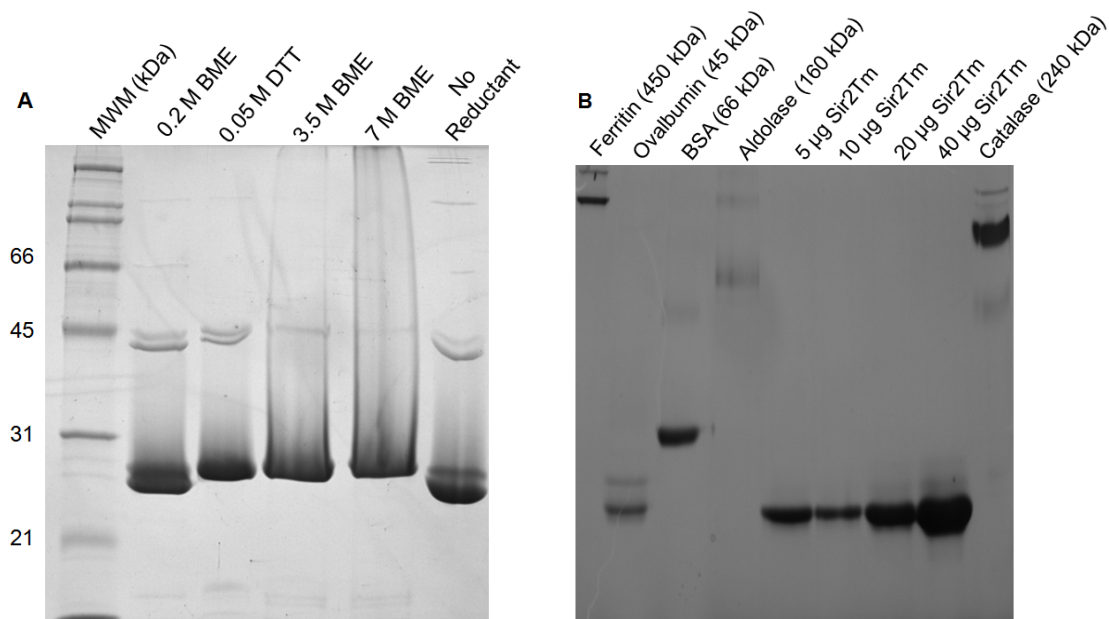


Figure 3.40: Sir2Tm exhibits oligomer like behavior in PAGE. A) 10 µg of full length Sir2Tm containing different amounts of reductants resolved on a 14 % SDS-gel. B) BN-PAGE analysis of different amounts of full length Sir2Tm indicates the protein to have a molecular weight of ~ 45 KDa.

3.5.2 Identification of substrate-modulator pairs for Sir2Tm

Understanding the mechanism of Sirt1 modulation by small molecules has been hampered by the lack of its crystal structure. Sir2Tm shares ~57 % sequence similarity with the catalytic domain of Sirt1 (Figure S1), can be modulated similarly to Sirt1 (see Ex-527 section below) and is more amenable for crystallization. Due to these reasons, Sir2Tm was chosen as a model system to structurally characterize the modulation of Sirt1 by small molecules.

Continuous assay was used to identify the substrate preference of Sir2Tm using well known peptide substrates of Sirt1. As shown in figure 3.41, Sir2Tm has a slight preference among the different substrates tested, with p53lg and HMG-B1 showing the highest and lowest activity respectively. HMG-B1 is still an interesting candidate for screening experiments, because it can reveal potential small molecule activators of Sir2Tm.

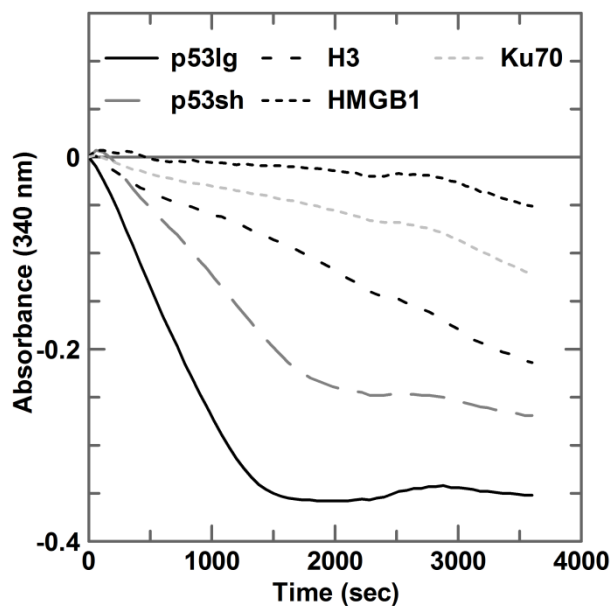


Figure 3.41: Sir2Tm preferentially deacetylates substrate peptides. A continuous assay was performed using 1 μ M Sir2Tm, 1mM of each peptide substrate and 2 mM NAD^+ . The decrease in absorbance at 340 nm was followed over time in a 96 well plate reader. The absorbance of a control (without peptide substrate) was subtracted from each peptide value, normalized and plotted over time. (p53lg = p53 long), (p53sh = p53 short).

When Sir2Tm was assayed in the presence of resveratrol using the FdL-1 substrate peptide, no activation was observed (Figure 3.42a), whereas the same substrate-modulator pair was able to activate Sirt1 (Figure 3.8, section 3.1.3). MS based assays, using polydatin (glycosylated form of resveratrol with increased solubility in aqueous solutions) and unmodified peptide substrates, p53sh (p53 short), p53lg (p53 long) and H3, also showed no change in the activity of Sir2Tm (Figure 3.42b). These results seem to indicate that activation by resveratrol and other polyphenols might have different substrate requirements.

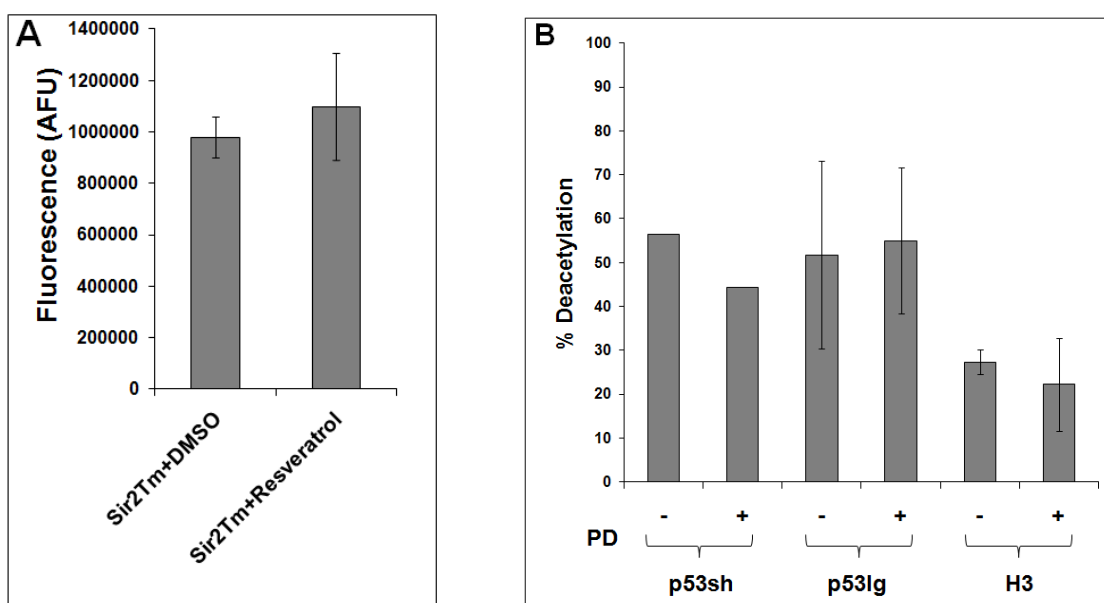


Figure 3.42: Sir2Tm modulation by polyphenols. A) The activity of 1 μg Sir2Tm with 100 μM FdL-1 peptide and 200 μM NAD^+ was measured with 100 μM resveratrol. B) 3.5 μg Sir2Tm was incubated with 500 μM respective peptides, 1 mM NAD^+ and 100 μM PD (PolyDatin) for 15 minutes at 37 $^\circ\text{C}$ and quenched with 0.05 % (v/v) FA and analyzed by MS. 2 % (v/v) DMSO was present in all the samples. p53sh peptide was analyzed only once.

Ex-527 is a potent isoform specific inhibitor of Sirt1, with IC_{50} in the nM range ((Napper et al., 2005), see below). When Ex-527 was tested against Sir2Tm using the FdL-1 substrate, inhibition was observed (Figure 3.43a). In order to avoid fluorogenic peptide substrates which can often give rise to artifacts, we also performed the same assay using unmodified H3 peptide. As shown in Figure 3.43b, Sir2Tm was completely inhibited by 100 μM Ex-527, identifying a good substrate-modulator pair for further characterization.

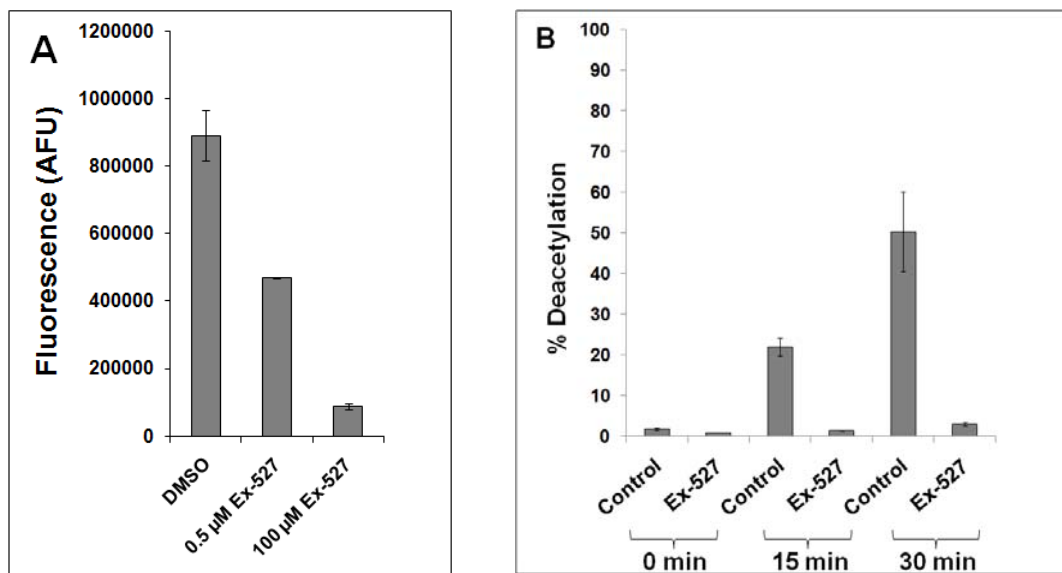


Figure 3.43: Ex-527 inhibits Sir2Tm using unmodified peptide substrates. A) 1 μg Sir2Tm was mixed with 25 μM FdL-1 substrate and 200 μM NAD^+ and incubated with various amounts of Ex-527 for 30 minutes at 37 $^\circ\text{C}$. B) 3.5 μg of Sir2Tm was mixed with 500 μM H3 peptide, 1 mM NAD^+ and 100 μM Ex-527 and incubated at 37 $^\circ\text{C}$ for various time points and quenched with 0.05 % (v/v) FA followed by MS analysis. In the control samples a time dependent deacetylation can be seen, whereas the protein sample containing Ex-527 were inactive. Control samples contained 1 % (v/v) DMSO.

3.5.3 Ex-527 is a potent inhibitor of Sir2Tm

To characterize Sir2Tm and Sirt1 inhibition by Ex-527, a dose response study was performed using unmodified peptide substrates. Since Ex-527 does not absorb at 340 nm , continuous assay was used to determine the IC_{50} values. As shown in figure 3.44, Ex-527 inhibits both Sir2Tm and Sirt1 in the nanomolar range. The IC_{50} values are $390 \text{ nM} \pm 170 \text{ nM}$ and $470 \pm 20 \text{ nM}$ for Sir2Tm and Sirt1 respectively. The IC_{50} value for Sir1 is higher in comparison to Napper et. al. who reported a value of 100 nM (Napper et al., 2005), the

difference may arise due to the peptide substrates used in the assay, because Napper et. al used the artificial FdL-1 substrate, whereas we used an unmodified substrate peptide based on the C-terminus of p53 containing acetylated Lys382.

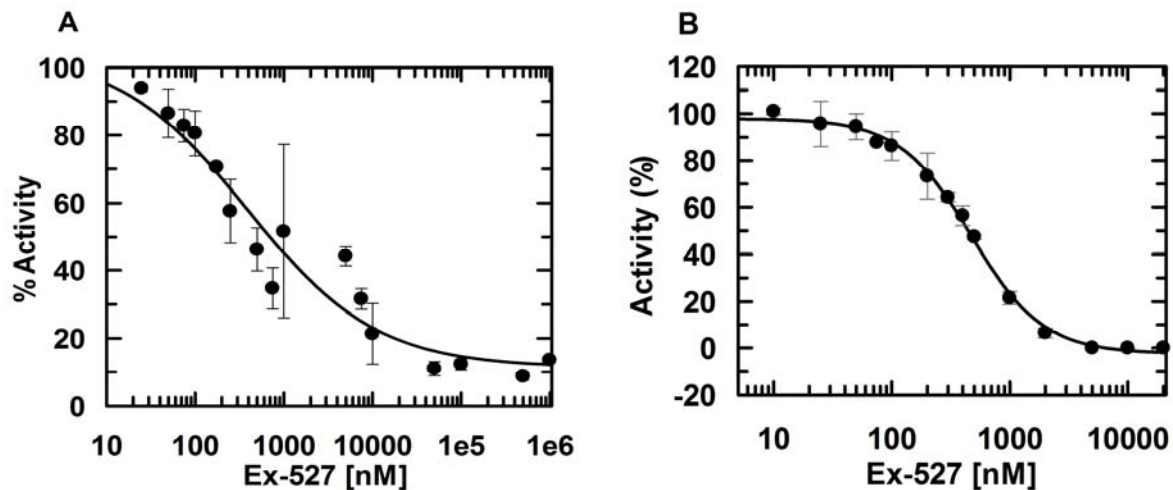


Figure 3.44: Ex-527 is a potent inhibitor of Sir2Tm and Sirt1. A) 15 μg Sir2Tm was mixed with 500 μM H3 peptide, 1 mM NAD^+ and various amounts of Ex-527 and activity was measured using the continuous assay. B) 12.6 μg human Sirt1 was mixed with 500 μM p53sh peptide, 1 mM NAD^+ and activity was measured using the continuous assay. The IC_{50} values are $390 \text{ nM} \pm 170 \text{ nM}$ and $470 \pm 20 \text{ nM}$ for Sir2Tm and Sirt1 respectively.

3.5.4 Ex-527 appears to require both the substrates to bind Sir2Tm

The exact mechanism of Sirtuin inhibition by Ex-527 is still unclear. Kinetic studies on Sirt1 showed that Ex-527 most likely inhibits in a non-competitive manner, which includes both substrates. To investigate the binding between Sir2Tm and Ex-527 and understand how the presence of substrates affects binding, microscale thermophoresis measurements were performed. No binding was observed when Ex-527 was titrated against the apoenzyme, in the presence of NAD^+ , acetylated peptide or ADPr plus acetylated peptide (Figure 3.45). This clearly indicates that Ex-527 does not bind to Sir2Tm when only one of the substrate is present or even in the presence of substrate peptide and a product mimic. Next we tried binding measurements after incubating the enzyme with both substrates (acetylated H3 peptide and NAD^+). This time binding was seen, with an affinity in the micromolar range ($K_d = 24.5 \pm 6.3 \mu\text{M}$). Since this strategy can lead to a complex mixture of events, as the reaction can proceed before the enzyme-substrate mixture encounters the inhibitor, we performed the same experiment using H3 peptide containing a thioacetyllysine. Thioacetyllysine (where the carbonyl oxygen of the acetyl group is replaced by a sulfur) has been shown to be a potent inhibitor of Sirtuins, because the s-alkylimidate intermediate formed after the release of NAM stalls the enzymatic reaction due to slow turnover and was in fact trapped in the crystals of

Sirtuins (Hawse et al., 2008; Jin et al., 2009; Smith and Denu, 2007). Binding of Ex-527 to Sir2Tm-substrate mixture was also seen in the presence of thioacetyllysine peptide with a K_d of $11.5 \pm 2.5 \mu\text{M}$, showing further that both the substrates or the product(s) are most likely required for efficient binding of Ex-527 to Sir2Tm.

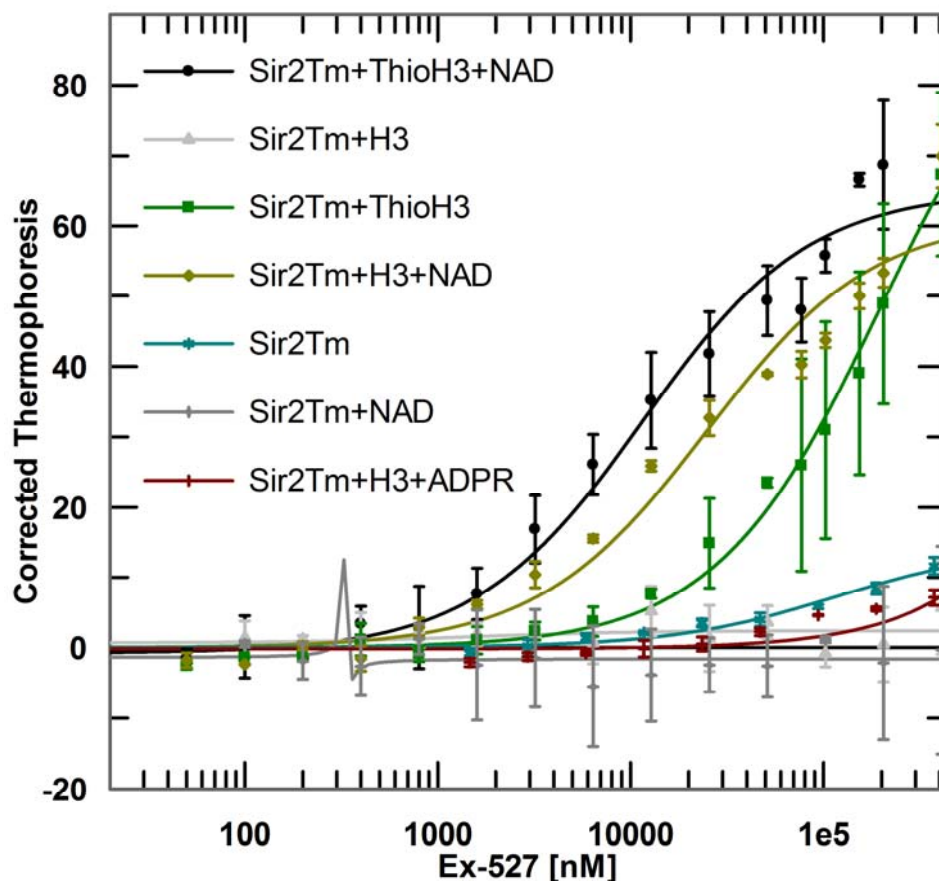


Figure 3.45: Ex-527 binds to Sir2Tm only in the presence of both substrates. 200 nM FITC labeled Sir2Tm was mixed with various compounds and titrated against Ex-527. The binding was analyzed using microscale thermophoresis. 500 μM peptide, 1 mM NAD^+ , 1 mM ADPr were used in the reaction. The reaction containing Sir2Tm, peptide and NAD^+ was incubated for 10 minutes at room temperature before adding corresponding amounts of Ex-527. The thermophoresis obtained with 17 % LASER power was used for analysis from all the measurements.

3.5.5 Sir2Tm - Crystallization and cryoprotection

To structurally elucidate the binding and mechanism of Sir2Tm inhibition by Ex-527, several crystallization screens were pursued as mentioned in section 2.6.2. Crystals were formed in many conditions as soon as 24 hours after setup and were continuously monitored for growth. The drops with Sir2Tm, peptide and Ex-527 were the most promising and out of several conditions which yielded crystals; four best conditions were selected and grid screens were setup. Figure 3.46 shows representative conditions and the appearances of the crystals

which were used for further optimization. It is interesting to note that Sir2Tm did not crystallize in the apoenzyme form and attempts to reproduce Sir2Tm crystals using published conditions proved futile.

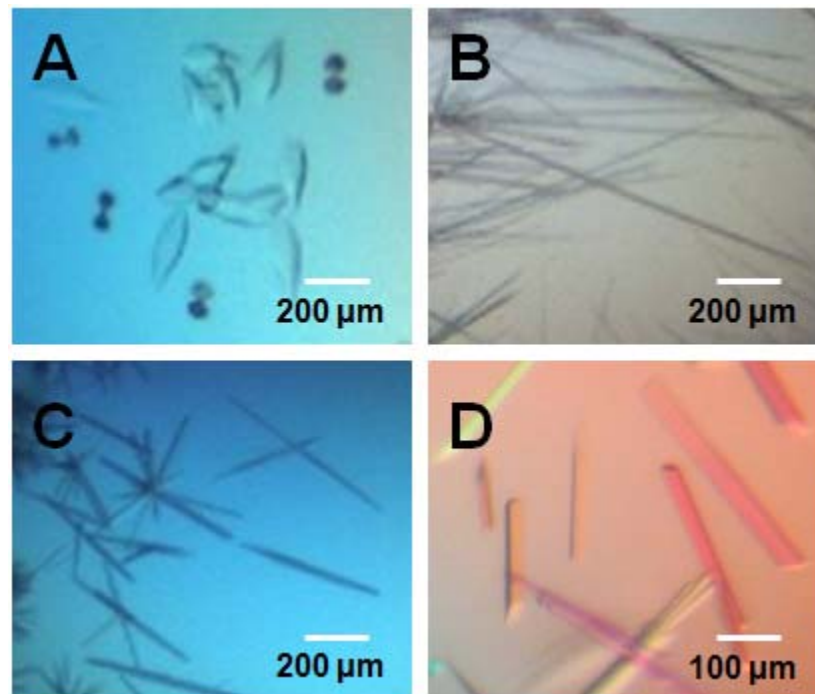


Figure 3.46: Crystallization of Sir2Tm. Representative crystals and conditions of Sir2Tm in the presence of Ex-527 and peptide substrates. A) 1M tri-sodium citrate, 0.1 M CHES (*N*-Cyclohexyl-2-aminoethanesulfonic acid), pH 9.5. B) 20 % (w/v) PEG (PolyEthylene Glycol) 6000, 0.1 M BICINE (2-(Bis(2-hydroxyethyl)amino)acetic acid), pH 8.5. C) 20 % (w/v) PEG 3350, 0.2 M di-sodium hydrogen phosphate. D) 25 % (w/v) PEG 4000, 0.1 M Tris, pH 8.5, 50 mM Li_2SO_4 .

Among the four conditions that were used in optimization process, the best looking crystals grew in 25 % (w/v) PEG 4000, 100 mM Tris, pH 8.5, 50 mM Li_2SO_4 . The crystal trays were set up using the sitting drop vapor diffusion method by mixing 1.5 μl sample and 1.5 μl reservoir and incubated at 18 °C. The sample mixture contained ~9.6 mg/ml Sirt2Tm, 1 mM H3 acetylated/thioacetylated peptide and 1.5 mM Ex-527. The peptide substrates used in the crystallization process was changed from p53 to H3-Lys116/thioacetylated H3-Lys116 peptide (thio-H3) in most setups, as H3-Lys116 peptide was used in other biophysical and kinetic studies. Long rod shaped crystals of Sir2Tm complex crystals appeared overnight and grew to a size of at least 200 μm in one of the dimension. Figure 3.46 shows crystal pictures of Sir2Tm grown in the presence of thioacetyllysine containing H3-Lys116 peptide and Ex-527.

Crystals of Sir2Tm were cryoprotected by supplementing the reservoir with 25 % (v/v)

ethylene glycol, 1 mM corresponding H3-Lys116 peptide and 1.5 mM Ex-527. After solving the crystal structure, we observed density only for the peptide (see below), therefore a cryotrapping strategy was employed where the crystals were transferred to the cryoprotectant followed by addition of 1 mM β -NAD⁺ to the solution containing the crystal and incubated for two minutes before flash freezing in liquid N₂. In the case of thioacetyllysine condition, the soaking was carried on for 5 minutes. As soon as the NAD⁺ was added, the crystals containing acetylated H3-Lys peptide started disintegrating to small needles and were fully dissolved around four minutes, whereas for the thioacetyllysine-H3-Lys116 peptide the crystals started dissolving only after roughly 3 to 4 minutes and were fully dissolved around 9 to 10 minutes, perhaps due to the stalling of the enzymatic reaction by the thioalkylimidate intermediate. Therefore the crystals were frozen at 1, 2, 3 and 4 minute time intervals for acetyllysine peptide and for 5, 8 and 9 minutes for the thioacetyllysine peptide. Since the alkylimidate/thioalkylimidate intermediate is formed between the peptide and NAD⁺, the structural rearrangements happening during the reaction and especially during the release of products may disrupt the crystal as time progresses, leading to their deterioration.

3.5.6 Data collection

Diffraction data collection was performed as mentioned in section 2.6.3. All the crystals were rotated at an oscillation range of 1° and was exposed to X-rays at different time intervals: 4 sec exposure and 120 images were collected with starting angle of 80° for Sir2Tm/H3-Lys116, 6 sec exposure and 110 images were collected with starting angle of 150° for Sir2Tm/ligand mix + Ex-527 and 5 sec exposure and 100 images were collected with starting angle of 90° for Sir2Tm/thio-H3-Lys116. The unit cell constants, data collection and processing statistics are listed in Table 3.3. The crystals diffracted at 1.72 (Sir2Tm + H3-Lys116), 1.90 (Sir2Tm/ligand mix + Ex-527) and 2.8 (Sir2Tm + Thio-H3-Lys116) Å respectively. The unit cell constants (Table 3.3) differed slightly between the two structures, which could have arisen due to changes in the crystal packing during cryotrapping.

Crystal	Sir2Tm/H3-Lys116	Sir2Tm/ p53 ligand mix + Ex-527	Sir2Tm/H3-thio-Lys116
Space group	P2 ₁ 2 ₁ 2 ₁	P2 ₁ 2 ₁ 2 ₁	P2 ₁ 2 ₁ 2 ₁
Unit cell constants	a = 58.1 Å, b = 61.3 Å, c = 75.7 Å	a = 46.8 Å, b = 59.9 Å, c = 109.0 Å	a = 45.3 Å, b = 58.2 Å, c = 105.8 Å
Resolution (Å)	47.6 - 1.72	46.8 - 1.9	19.6 - 2.8
Unique reflections	29180	24821	7264
$\langle I \rangle / \langle \sigma(I) \rangle$ ^(a)	18.0 (2.8)	20.7 (3.5)	10.8/(2.3)
Completeness ^(a) (%)	99.3 (99.5)	99.8 (100)	99.3 (99.9)
R _{merge} (%) ^{(a)(b)}	4.9 (57.3)	5.3 (41.4)	13.1 (68.3)
R _{meas} (%) ^{(a)(c)}	5.5 (64.2)	6 (46.9)	15 (78.5)

^(a) Numbers in parentheses are for the outermost shell.

^(b) $R_{\text{merge}} = \sum (I - \langle I \rangle) / \sum I$; I is the intensity of an individual measurement and $\langle I \rangle$ the corresponding mean value.

^(c) $R_{\text{meas}} = \sum [N/(N-1)]^{1/2} (I - \langle I \rangle) / \sum I$; I is the intensity of an individual measurement and $\langle I \rangle$ the corresponding mean value. N indicates multiplicity and $[N/(N-1)]^{1/2}$ the correction factor for multiplicity.

Table 3.3: Data collection and processing statistics for crystals of Sir2Tm

3.5.7 Structure solution, refinement and modeling

Structures were solved through Patterson searches as mentioned in section 2.6.4. The Patterson search yielded a unique solution with an RFZ (Rotation Function Z-score) of 22.2 and TFZ (Translation Function Z-score) of 30.4 for Sir2Tm/H3-Lys116 structure, RFZ of 26.6 and TFZ of 37.7 for Sir2Tm/ligand mix + Ex-527 and an RFZ of 20.4 and 29.3 for Sir2Tm /H3-Thio-Lys116 respectively. The high RFZ and TFZ indicate an unambiguous correct solution for all the structures.

The overall refinement of all the structures seem to proceed satisfactorily and the R_{cryst} and R_{free} values converged well during refinement and stays at a reasonable percentage appropriate for the resolution (Table 3.4). In the case of Sir2Tm/H3-thio-Lys116, the difference between R_{cryst} and R_{free} seems to be more than that observed for the other two structures, this could be due to the movement of the protein molecule in the presence of substrates or intermediate. Figures 3.47 shows a representative Ramachandran plot (ϕ and ψ backbone dihedral angles) of one of the solved structures. There were 99.2 %, 98.9 % and

98.4 % of residues in the favored region, 0.8 %, 1.1 % and 1.6 % in the allowed region and none in the forbidden region for the H3-Lys116, ligand mix+Ex-527 and H3-thio-Lys116 bound structures respectively, indicating an excellent agreement with stereochemical parameters observed for structures with similar resolution. The residues 35-40 had no electron density for the H3-Lys116, 37-43 for ligand mix + Ex-527 and 34-44 for the H3-thio-Lys116 bound structures respectively and therefore were not modeled. This is very much in agreement with majority of the crystal structures of Sir2Tm available in the PDB (protein data bank) and indicates that these residues, which are part of the co-substrate binding loop are flexible and actively participate in catalysis.

Crystal	Sir2Tm/H3-Lys116	Sir2Tm/ ligand mix + Ex-527	Sir2Tm/H3-thio-Lys116
Refinement resolution (Å)	30.6 - 1.7	40.3 - 1.9	19.6 – 2.8
Total reflections used	29177	24820	6896
Protein atoms	1893	1872	1845
Solvent atoms modeled	141	206	63
R.m.s.d. bond lengths (Å)	0.01	0.02	0.01
R.m.s.d. Bond angles (°)	1.3	2.3	1.6
Average B-factor (Å ²)	26.5	25.7	35.5
Final R _{cryst} / R _{free} (%) (a)(b)	19.49/22.69	18.00/22.71	18.67/27.08

^(a) R-factor = $\frac{\sum ||F_{obs}| - |F_{calc}|}{\sum |F_{obs}|}$, $|F_{obs}|$ is the observed and $|F_{calc}|$ the calculated structure factor amplitude.

^(b) R_{free} was calculated from 5 % of measured reflections omitted from refinement.

Table 3.4: Refinement statistics for structures of Sir2Tm

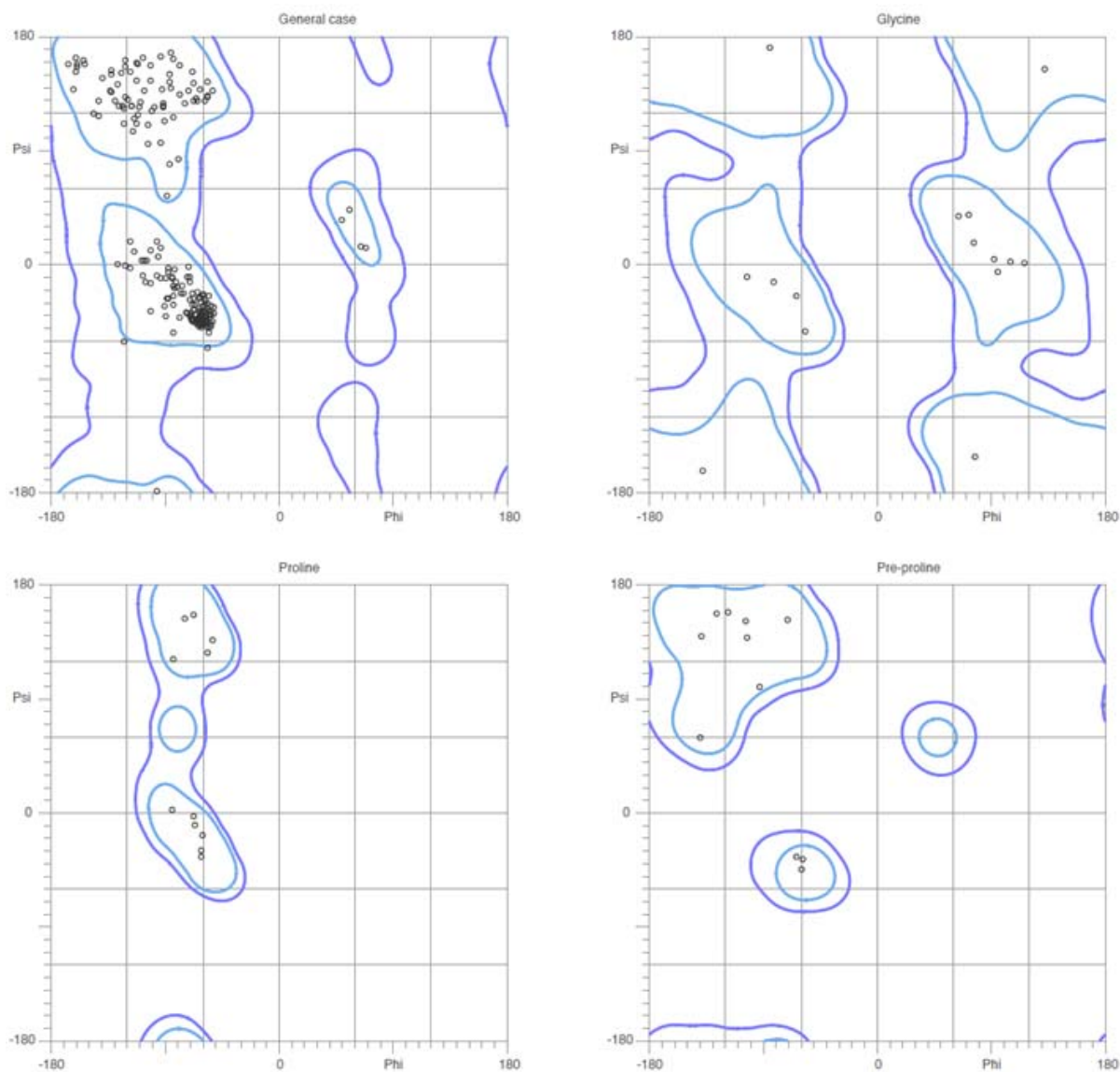


Figure 3.47: Representative Ramachandran plot of Sir2Tm crystal structures. Ramachandran plot of Sir2Tm + H3-Lys116 peptide structure. There are 99.8 % and 0.2 % residues in the favored and allowed regions respectively.

3.5.8 Analysis of crystal structures of Sir2Tm

Initial attempts to co-crystallize Ex-527 and Sir2Tm in the presence of peptide substrate resulted in a structure containing only the peptide substrate (Figure 3.48), indicating that Ex-527 binding to Sir2Tm requires either both the substrates or products, similar to our solution studies.

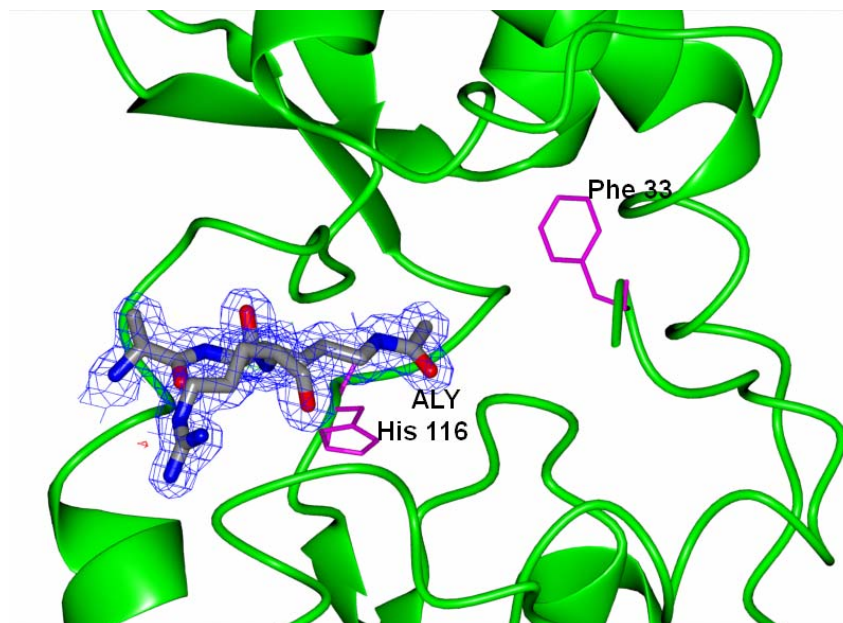


Figure 3.48: Structure of Sir2Tm co-crystallized with peptide substrate and Ex-527. The active site of Sir2Tm crystal structure, co-crystallized in the presence of peptide substrate and Ex-527 shows density only for the substrate, indicating that binding of the inhibitor may occur only in the presence of both the substrates or products. The catalytic Histidine (His 116) and phenylalanine (Phe33) which is part of the co-substrate binding loop are shown in magenta. The $2F_o - F_c$ electron density is contoured at 1σ .

We then tried soaking experiments where the cryoprotectant solution contained both the substrates (peptide and NAD^+). Initial attempts to model only the substrates (acetyllysine and NAD^+) or Ex-527 and products (lysine and OAADPR) or the intermediate and Ex-527 resulted in residual electron densities around the active sites where the ligands bind (Figure 3.49a). Crystal structure of the human Sirt3 in complex with Ex-527 solved in our laboratory (unpublished results) has clearly identified the binding site for the inhibitor. Based on this information it could be verified that Ex-527 binds to the same pocket in Sir2Tm, because placing the inhibitor at the same site results in electron density that is interpretable (Figure 3.49 A) whereas refinement of the structure without the presence of the inhibitor results in positive difference density that cannot be explained otherwise (Figure 3.49 b). Refinement of the structure in the presence of intermediate and Ex-527 (Figure 3.49 c) results in clashes, due to the close proximity between the methyl group of the acetyllysine and the part of Ex-527 that bears the chloride. Nevertheless, there seems to be continuous density between the acetyllysine and the ribose ring of NAD^+ , suggesting that a minor fraction of the structure contains the intermediate, but the clash suggests that it is likely not at the same time as when the inhibitor is present in the active site of Sir2Tm. Attempts are currently being made to account for all the observed electron density using a mixture of ligands (inhibitor, substrates or products or intermediate) and carrying out a refinement so that the sum of occupancy of all

the ligands is less than or greater than one and avoiding Van der Waals repulsions between different ligands. This can perhaps offer better information regarding the contents of the active site.

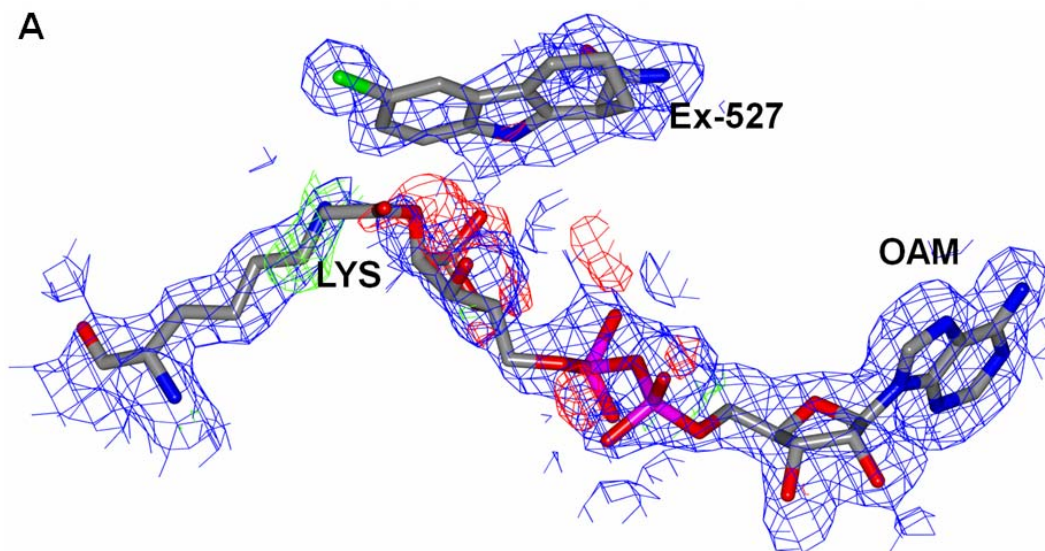
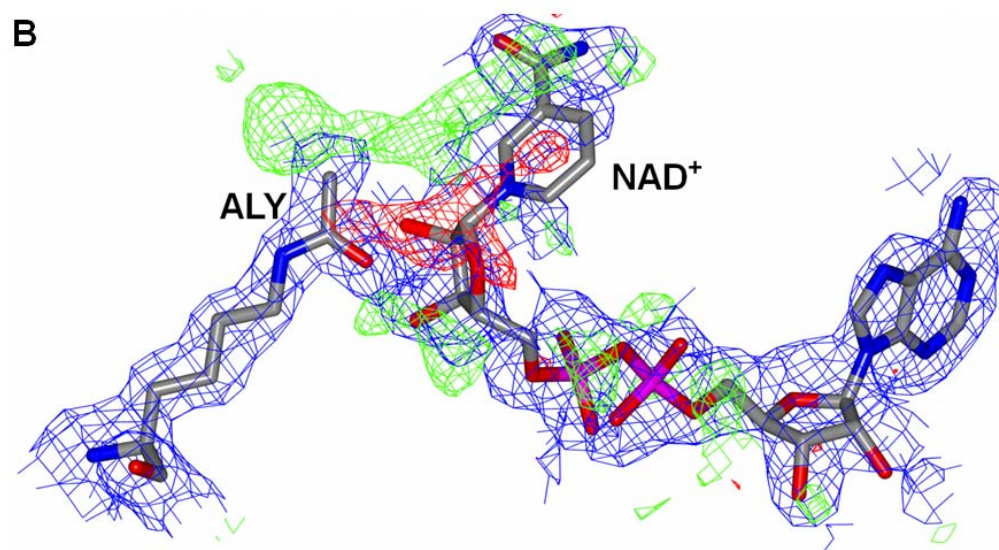
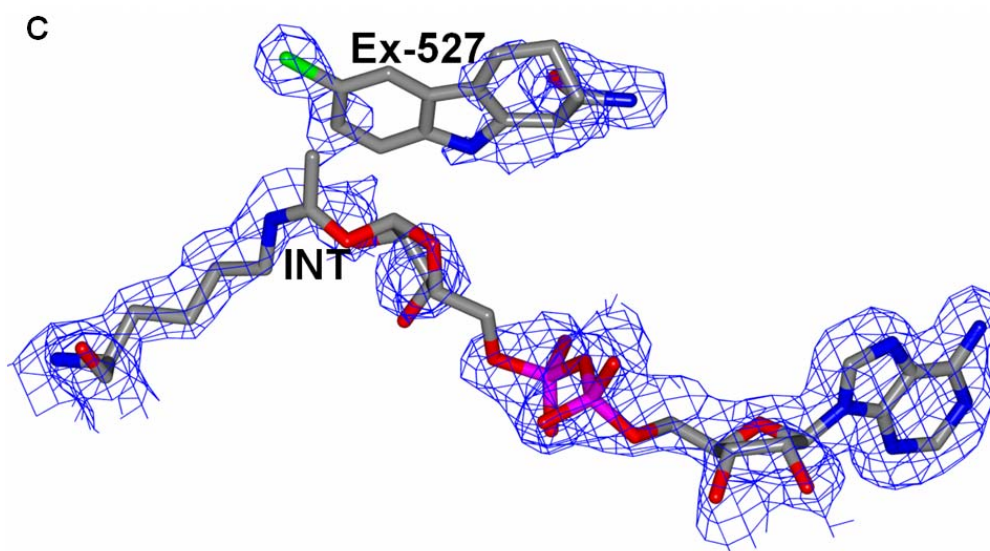


Figure 3.49: Sir2Tm complex crystal structure appears to contain a mixture of ligands. A) Refinement with products (LYS and OAM (OAADPr)) indicates incomplete fit for OAADPr and clashes between the amino group of Lys and acetyl group of OAADPr.



B) Refinement with the substrates (acetyllysine (ALY) and NAD⁺) indicates an incomplete fit for the NAM part of NAD⁺ and a clear positive difference density (green) for Ex-527 near the "C-pocket".



C) Refinement with the thioalkylimidate intermediate (INT) (40 % occupancy) and Ex-527 (35 % occupancy), gives rise to clashes between the two, indicating that they may not be present at the same time in the active site. $2F_o-F_c$ (blue) maps are contoured at 1σ and F_o-F_c maps are contoured at $\pm 3\sigma$.

When crystals grown in the presence of H3-thio-Lys116 peptide and Ex-527 were soaked with NAD^+ to form the more stable thioalkylimidate intermediate, good electron density was observed for the thioacetyllysine and some residual density was observed for the intermediate or the NAD^+ (Figure 3.50a). Refinement of the structure with varying occupancies for the substrate and the intermediate, seem to indicate that the catalytic site might be occupied with 60 % of the substrate and 40 % of the intermediate, nevertheless no density was observed for Ex-527 (Figure 3.50b). This combined with the observation for the acetyllysine substrate and NAD^+ soak indicates that the inhibitor and the intermediate may not be present in the active site at the same time, but the closure of the co-substrate binding loop and or the product might be required for efficient binding of the inhibitor to Sir2Tm.

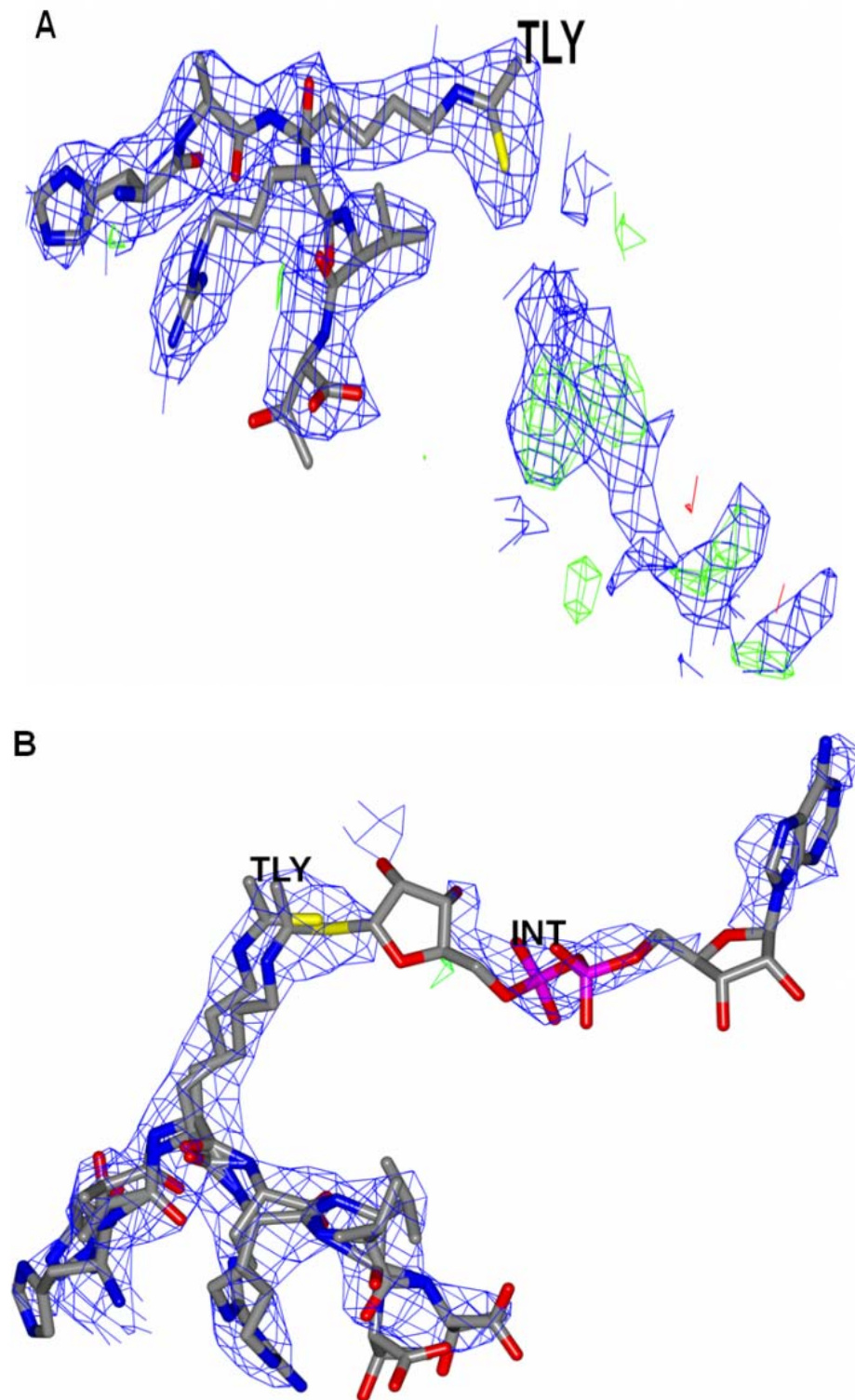


Figure 3.50: Crystal structure of Sir2Tm and thioacetyllysine. A) Refinement of the crystal structure of Sir2Tm soaked with thioacetyllysine peptide, Ex-527 and NAD^+ indicates well defined density for the substrate (TLY) and additional density that may correspond to the intermediate. B) Refinement of the structure with 60 % occupancy for the substrate (TLY) and a 40 % occupancy for the intermediate (FZN) indicates that the crystal contains mostly substrate and a small fraction of either the intermediate or NAD^+ . No density was observed for the inhibitor. The $2F_o-F_c$ maps (blue) were contoured at 1σ and F_o-F_c maps (green = positive and red = negative) were contoured at $\pm 3\sigma$.

3.5.9 EX-527 appears to bind to the “C-pocket” of Sir2Tm

Structural comparison between Sir2Tm partially bound to Ex-527 and intermediate/products and Sir2Tm bound to the peptide alone show very little difference between the two with a C α RMSD (Root Mean Square Deviation) of 0.4 Å (Figure 3.51), indicating that the protein does not undergo major conformational changes in the presence of the inhibitor. Even though the inhibitor is present with less than full occupancy, certain conclusions can still be drawn about the binding of the inhibitor. The major differences exist in the co-substrate binding loop. The peptide and ADPR part of NAD⁺ are bound in the substrate binding cleft between the Zinc binding domain and the Rossmann fold domain as seen in other substrate bound Sir2Tm structures available in the PDB (2H4F and 2H4H) (Hoff et al., 2006).

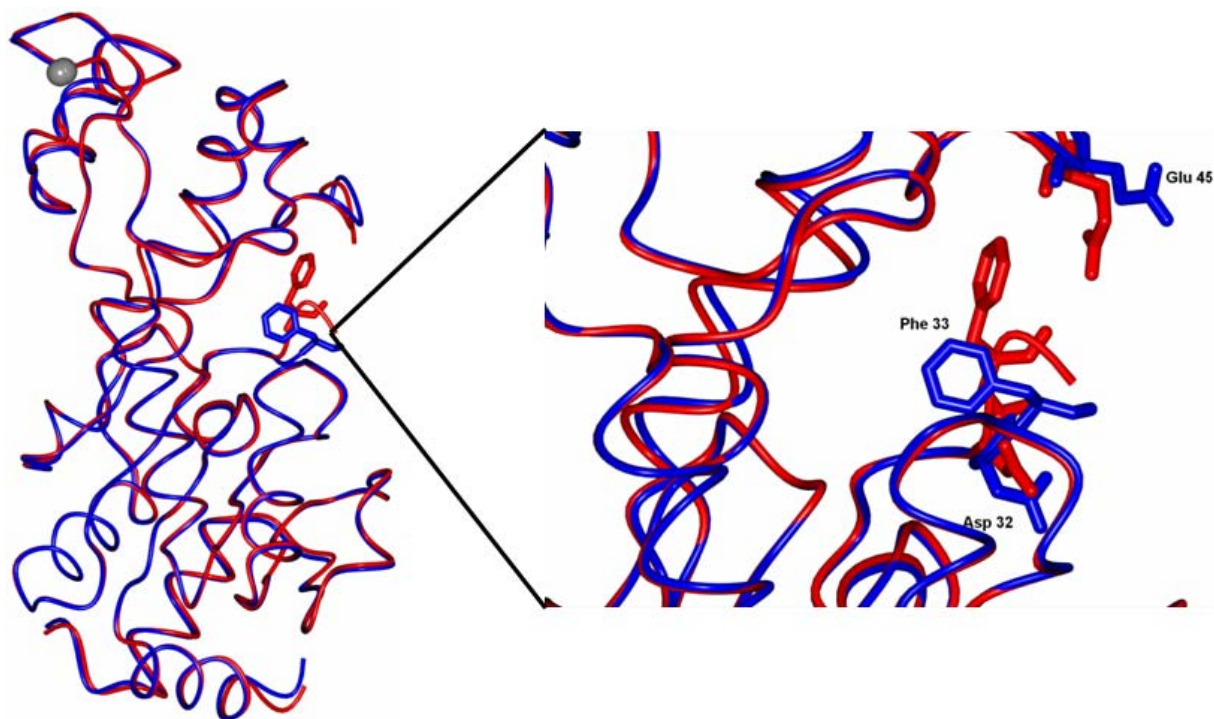


Figure 3.51: Binding of Ex-527 to Sir2Tm does not disrupt its overall structure. An overlay of crystal structures of Sir2Tm bound to ligand mix/Ex-527 (blue) (1.9 Å) and H3-Lys116 peptide (red) (1.72 Å) indicates overall similarity between the two. The blowup shows the co-substrate binding loop and residues that differ most between the two structures.

The inhibitor Ex-527 appears to bind to the so called C-pocket of Sir2Tm where the NAM of the NAD⁺ ring was shown to bind (Hoff et al., 2006). The cyclohexene ring and the carboxamide part of Ex-527 bind in the C-pocket with the carboxamide group oriented in the same direction as the carboxamide of NAM, as shown in figure 3.52. A series of hydrogen bond and Van der Waals interactions occurs between Ex-527 and the protein. The carboxamide part of Ex-527 interacts with residues Ile30, Met71, Asn99, Ile100 and Asp101,

the carbazol (B-ring) and the aromatic benzene ring (containing the Chlorine and termed A-ring) are nestled in a pocket mainly containing hydrophobic residues Phe48, Ile159, Val160 and His116 (the catalytic residue) and Gln98. The Chlorine of the A-ring is very close to and can potentially interact with Phe48, Ile159 and Val160, although the angle between the Chloride and the carbonyl oxygen of Val160 ($\sim 97^\circ$) might not be suitable for a halogen bond interaction (Metrangolo et al., 2008). The A-ring and the B-ring occupy the hydrophobic pocket that extends deep into the protein and henceforth will be called as ECP (“Extended C Pocket”). As mentioned above, the binding needs Sir2Tm in the “closed conformation”, because only in this conformation, the co-substrate loop moves closer to Ex-527, leading to contact between Phe33 (which is part of the co-substrate loop) and the B-ring of Ex-527. Since the inhibitor needs either the reaction intermediate or the products to bind Sir2Tm, it is also possible that the inhibitor interacts with the ADPr part of the intermediate/product, these interactions cannot be verified in the current structures described here, but studies are in progress to obtain better structural information regarding the binding and interactions of Ex-527.

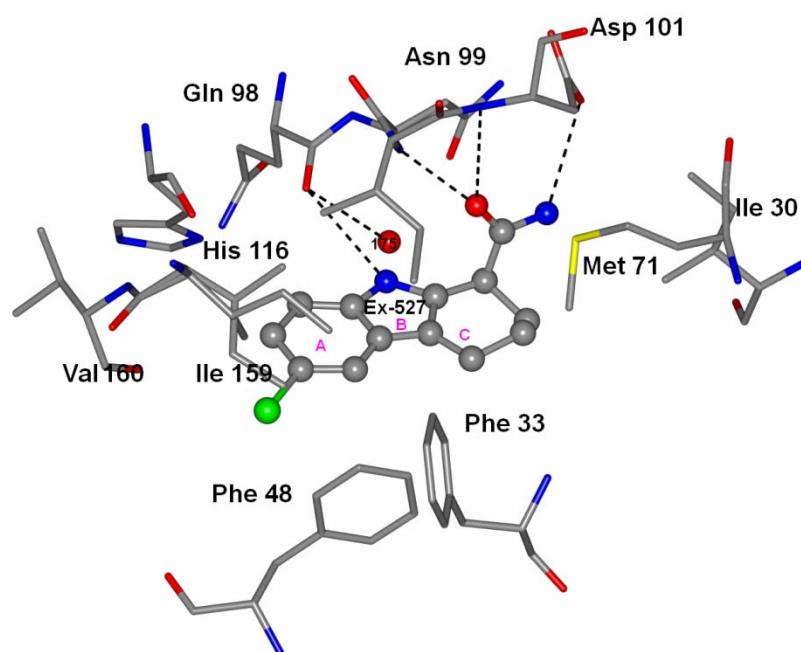


Figure 3.52: Ex-527 may interact with several residues of Sir2Tm. Ex-527 (represented as ball and stick) forms hydrogen bonds (black dashed lines) with few residues of Sir2Tm and a water molecule (shown as red balls) located near the binding pocket. The Phenylalanine (Phe 33) which forms part of the co-substrate loop is close to Ex-527 and may be involved in orienting the inhibitor towards the ECP. The catalytic Histidine (His 116) is also indicated. The A, B and C rings are indicated in magenta.

4. Discussion

Reversible lysine (de)acetylation, first described for histone proteins, is now known to be a widespread post-translational modification, with over 6800 known mammalian acetylation sites in different proteins and still counting making the proteins involved in these modifications all the more important to characterize. Although Histone deacetylases were the first set of enzymes discovered to deacetylate lysine residues, the identification of Sirtuins as PDACs created a paradigm shift, because Sirtuins require NAD^+ as a co-substrate to deacetylate lysine residues and this coupling has been proposed to link changes in cellular energy levels to deacetylation activity of Sirtuins, which would indicate them as metabolic sensors (Schlicker et al., 2008).

4.1 Purification and domain architecture of Sirt1

To analyze the role of N and C-terminal domains of Sirt1 towards its activity and structure, we expressed and purified several constructs of Sirt1 containing different regions. Human Sirt1 can be overexpressed abundantly in a stable and active form in a prokaryotic system such as *E. coli* without major problems such as host toxicity, insolubility or a need for PTMs, although it is interesting to note that mouse Sirt1 can only be expressed in Rosetta 2 (DE3) *E. coli* strain which contains tRNAs for rare codons, implying codon bias specifically in the mouse Sirt1 gene. The purification of Sirt1 turns out to be difficult when compared to other Sirtuins and required several purification and optimization strategies. Concentration of Sirt1 before complete purification (that is prior to SEC) leads to aggregation with a decrease in activity. This problem was overcome by employing a strategy where the affinity purified protein was concentrated minimally and loaded to an SEC column to remove *E. coli* contaminants and aggregates. It is possible that concentration of Sirt1 prior to SEC leads to aggregation due to the exposure of hydrophobic parts of the protein that can interact with *E. coli* proteins. CD analysis on full length Sirt1 indicates that the protein possesses secondary structure, but the amount of repetitive secondary elements (α -helices and β -strands) is higher than what is normally observed, example for other Sirtuins. The presence of unstructured/flexible parts most likely stems from the N and C-terminus of Sirt1 as indicated by disorder prediction programs (XtalPred and PHYRE), which are shown to be involved in binding to partner proteins and regulate its activity (Kang et al., 2011; Kim et al., 2007; Kim et al., 2008; Pan et al., 2011a). The presence of such flexible regions is likely the reason for the apparent oligomeric behavior of Sirt1 in SEC, as unstructured regions can often lead to extended shape for proteins and influence their migration in SEC. This is also supported by

our sedimentation velocity centrifugation and EM analysis where Sirt1 seems to behave as a monomer in the physiologically relevant concentrations. Moreover, the construct comprising only of the catalytic core (229to516) behaves as a monomer in SEC (Figure 3.5 above), providing further evidence that unstructured regions of Sirt1 at the N and C-terminus are responsible for apparent differences seen between SEC and AUC experiments. Similar to our findings Pan et. al. (Pan et al., 2011a) recently reported that a Sirt1 construct containing the catalytic core (160-665) behaves as a monomer. We thus conclude that Sirt1 is most likely a monomer in solution.

The observation that nucleic acids co-purify with Sirt1 during the affinity purification step and the fact that Sirt1 is predominantly localized to the nucleus make it tempting to speculate on an interaction between Sirt1 and nucleic acids. Programs that predict binding interactions between protein and RNA/DNA such as BindN (<http://bioinfo.ggc.org/bindn/>) and DP-Bind (<http://lcg.rit.albany.edu/dp-bind/>) in fact suggest potential binding at the N-terminus, especially for RNA with residues Lys233, Arg234 and Lys237 of Sirt1. ChIP (chromatin immunoprecipitation) assays show Sirt1 to be co-localized at the promoter region of several genes, indicating the possibility of interaction between Sirt1 and DNA, although this localization can also be due to protein/protein interactions. Sirt1, for example is known to deacetylate several transcription factors and histones. Our in vitro studies confirm that RNA is dominant in the co-purified nucleic acid mixture. Since we were not able to observe any direct binding when pure Sirt1 was incubated with either RNA or DNA, and no change in activity of Sirt1 in the presence of nucleic acids was observed, it is possible that the co-purification was either an artifact or other *E. coli* contaminants present along with Sirt1 bind to nucleic acids. However, we might have also not tested the right type of RNA, and further thorough studies with the co-purified nucleic acids will have to reveal whether Sirt1 binds RNA.

4.2 Sirt1 modulation by resveratrol

Using the different Sirt1 constructs, we were also able to show that the catalytic domain of Sirt1 is sufficient for its activation by polyphenols such as resveratrol and piceatannol, in contrast to a previous report claiming involvement of the N-terminus (Milne et al., 2007). One possible explanation for these two different results could be due to the overall activity and stability of the different protein samples used. Our assays suggest that the activity of Sirt1 is higher in presence of the termini, similar to a recent report by Pan et. al (Pan et al., 2011a) and Milne et. al. report (Milne et al., 2007). The basal activity seems to correlate, however, with the stability of these constructs (Milne et. al. and our data) indicating that the

termini are primarily important for Sirt1 stability. Nevertheless, all the constructs were equally activatable by resveratrol implying that the catalytic domain of Sirt1 is sufficient for its activation and the N-terminus might indirectly support resveratrol activation by stabilizing Sirt1.

Activation of protein or enzymatic function due to small molecules is uncommon compared to inhibition. When Sirt1 was found to be stimulated by resveratrol, it opened up an exciting opportunity for therapy. The ability of resveratrol to activate Sirt1 has been well documented (Howitz et al., 2003; Wood et al., 2004), but the mechanism and relevance has been questioned due to conflicting reports.

Sirt1 activation by resveratrol was shown to require a fluorophore modification of the substrate on the C-terminus and no activation was observed when a native peptide substrate was used (Beher et al., 2009; Borra et al., 2005; Kaeberlein et al., 2005a; Pacholec et al., 2010). We were also able to show that resveratrol binds directly to Sirt1, which suggests that the mechanism of resveratrol modulation should also involve the protein. Our findings show that the modulating effects of resveratrol is indeed substrate specific; it does not require, however, a fluorophore modification but rather depends on the local substrate sequence. This also explains data not only from previous activity assays (Kaeberlein et al., 2005a) but also the observation that resveratrol imparts positive effects in *Ceanorhabditis elegans* in a Sir2 dependent manner, which is overlapping but not identical to yeast Sir2 effects (Viswanathan et al., 2005). This leads to the conclusion that in order to analyze resveratrol specific modulation of Sirt1 it is important to consider the effects based on the substrate used, i.e. the effect depends on the substrate-modulator pair. This conclusion can be generalized for any small molecule employing the same binding site/modulation mechanism and we indeed find a similar trend in the case of the resveratrol unrelated small molecule SRT1720, which was also shown to both activate, inhibit or not affect Sirt1 (Dai et al., 2010; Milne et al., 2007; Pacholec et al., 2010). It is interesting to note that array results based on SRT1720 yielded substrate-modulator pairs that were different from the resveratrol results, clearly showing that each compound has its own set of compatible substrate sequence for activation. Our results form a basis for further studies mediated towards clarifying which of the identified resveratrol sensitive sites contribute to its in vivo effect.

Based on our observation that the catalytic core of Sirt1 is sufficient for its modulation by resveratrol, it is tempting to speculate that resveratrol might influence other Sirtuin isoforms as well, which could again depend on the substrate-modulator pair. Human Sirt1 is

implicated in several diseases such as cancer, diabetes, neuronal disorders (Haigis and Sinclair, 2010), making it an attractive drug target. Small molecules modulators of Sirt1 are in clinical trials to treat type 2 diabetes (Milne et al., 2007), even though their exact mechanism of action is still debated. We were able to show that resveratrol modulates the activity of Sirt1 in a substrate sequence specific manner. Although resveratrol and Sirt1 interaction has been extensively studied both in vitro and in vivo, it is a poor choice as a drug, because of its low solubility and bioavailability. The array experiments described here will allow us in testing and identifying different compounds that are not only more potent and specific to Sirt1 but also possess better pharmacological properties. This type of substrate-modulator pair could serve as excellent tools for Sirt1 specific drug development that preferentially targets particular Sirt1 modulated system such as histones and chromatin or a disease state which involves Sirt1.

4.3 Crystallization of Sirt1

Structure aided drug discovery efforts, which have been used successfully for identifying lead compounds for several proteins including Sirt2 (Schlicker et al., 2011), are hampered in the case of Sirt1 by the unavailability of structural information. In spite of several crystallization attempts, diffraction quality crystals of Sirt1 were not obtained. Due to high flexibility in the N and C terminal domain regions of Sirt1, efforts to solve the crystal structure of Sirt1 should focus further on the catalytic core with variable N and C-terminal extensions which might be more amenable for crystallization, an approach started in this thesis. Although structural information obtained from this type of construct would not highlight the unique features of Sirt1, it could still be used to gain valuable insights on how small molecules bind to its catalytic core and modulate its activity. Further efforts to obtain the crystal structure of full length Sirt1 could focus on overexpression and purification from insect/mammalian cells, because some PTMs occur only in eukaryotic cells and this may make the protein more amenable for crystallization. Also, physiological partner proteins of Sirt1 binding to the termini and stabilizing them could be used to co-crystallize Sirt1, as tried here with AROS. Co-crystallization attempts in the presence of non-physiological partner proteins, such as DARPinS (Designed Ankyrin Repeat Proteins) (Huber et al., 2007) or complexes with substrate-modulator pairs can also be attempted, which may “lock” the protein in a stable conformation leading to crystals. Nevertheless, our homology model of Sirt1 can at least be used to analyze the residues involved in substrate binding (via electrostatic surface potential) to understand its substrate preferences. Moreover, other Sirt1

homologs such as Sir2Tm, which are easy to purify and crystallize can serve as Sirt1 models and aid in structure based drug discovery efforts as demonstrated by our Ex-527 study.

4.4 Zinc is essential for the structural stability and activity of Sirtuins

Sirtuins contain a Zn^{2+} ion coordinated typically by four Cysteine residues. The Zinc binding domain of Sirtuins is part of the conserved catalytic core but varies among the Sirtuins in detail, both at the structural and sequence level. Unlike other HDACs, Sirtuins do not use Zinc for catalysis. Zinc in Sirtuins either is required for their structural stability or function in an indirect way. Our studies indicate that Sirt3 has an absolute requirement for Zinc for its stability. The insolubility of the Cysteine mutants indicates that the Zinc ion is most likely required during protein folding and plays an important role in the structure of Sirt3. EDTA has a high affinity towards Zinc ($K_d \sim 10^{-16}$ M) and can easily strip Zinc from Zinc binding motifs in transcription factors (K_d of $\sim 10^{-9}$ - 10^{-11} M) (Nyborg and Peersen, 2004). In our experiments, up to 2 mM EDTA was not able to affect the function (and thereby stability) of Sirt3 whereas 1,10-phenanthroline (a even more potent Zinc chelator) readily precipitated the protein, indicating an unusually high affinity for Zinc among the Sirtuins in comparison to other Zinc binding proteins. In a recent study Chen et. al (Chen et al., 2010a) also reported that Sirt1 retained activity even in the presence of 10 mM EDTA, corroborating our findings. It is interesting to note that the Cysteine to Serine mutants of Sirt1 were stable during expression and were bound to Zinc even after purification, but were inactive (Chen et al., 2010a). Based on these results it is tempting to speculate that Zinc binding might be influenced by the termini of Sirtuins (highly variable among Sirtuins) and the Zinc binding domain may also participate in events such as protein-protein interactions thereby contributing to isoform specificity among Sirtuins.

4.5 Sirt5 requires unusually high amount of NAD^+ for its deacetylase activity

Mammalian Sirtuins are localized in different organelles of the cell and deacetylate a variety of proteins. In spite of this, there are very few substrates identified for the mitochondrial isoform Sirt5. Sirt5 knockout mice did not show a clear phenotype compared to their control littermates, whereas Sirt3 knockout mice showed remarkable hyperacetylation of mitochondrial proteins (Lombard et al., 2007). A plausible reason for this finding could be that under normal conditions, the basal activity of Sirt5 might be much lower compared to its mitochondrial homolog, Sirt3 and therefore a Sirt5 knockout mouse may not show hyperacetylation. Based on our findings that high amounts of NAD^+ is required for decent

Sirt5 activity, it is tempting to speculate that Sirt5's deacetylation activity may be coupled to the amount of NAD^+ present in the mitochondria at a given time. Normal levels of NAD^+ in the mitochondria has been estimated to be $\sim 250 \mu\text{M}$, at which time there is high levels of deacetylation by Sirt3, whereas Sirt5 dependent deacetylation may be negligible in comparison. In the case of stress (CR, apoptosis, etc.) there is a chance for NAD^+ levels to rise, thus leading to increased deacetylation levels also due to Sirt5. Although the physiological levels of NAD^+ will never reach the high levels reported here, the apparent affinity between NAD^+ and Sirtuins in the presence of substrate protein is lower in general, indicating that NAD^+ could act as a metabolic sensor and lead to physiological changes in the mitochondria in a Sirt5 dependent manner. An alternative explanation for the high amounts of NAD^+ required for Sirt5's activity could be due to the technical limitations of the assay itself (ELISA and Fluorescence based assays), since a more refined MS based assay (Fisher et. al. manuscript submitted to chemical biology) indicated that NAD^+ in fact has better binding affinity for Sirt5 ($\sim 0.2 \text{ mM}$) in the presence of peptide substrate. It is also possible that the apparent affinity of NAD^+ towards Sirt5 may also be influenced by the protein/peptide substrate used in the assay. Recently Du et. al. (Du et al., 2011) reported that Sirt5 is a desuccinylase and a demalonylase and exhibits robust activity towards succinylated and malonylated lysine residues and Sirt5 deletion mice exhibited increased levels of succinylation in CPS1. It was concluded that the architecture of Sirt5 in the acyl pocket confers this type of activity to the enzyme. It would still be interesting to know if during extreme cellular conditions, whether NAD^+ levels can rise or certain PTM events can occur that can increase the affinity between Sirt5 and its substrates (acetyllysine and NAD^+), thus leading to increased Sirt5 dependent deacetylation.

4.6 Sirt5 is a NAM insensitive deacetylase among the Sirtuin family

NAM is a known physiological inhibitor of Sirtuins. Our results show that Sirt5 appears to be insensitive to NAM at physiological levels (now confirmed in our group with the more sensitive MS assay (Fischer et. al. manuscript submitted)), indicating that NAM can regulate Sirtuins in an isoform specific manner, as different Sirtuins respond differently to NAM. This isoform specific regulation by NAM could also be related to the localization of Sirtuins, as the nucleolar Sirt7 also seems to be insensitive to NAM, indicating that regulation between different Sirtuin classes can occur naturally, which could prove beneficial at various times during the cell cycle and could also be influenced by external events such as stress, pathogen attack etc. The highly conserved Asp residue among mammalian Sirtuins

which is part of the co-substrate binding loop is replaced by a Thr in the case of Sirt5. Mutating this Thr to Asp (T69D) seems to decrease the deacetylase activity of Sirt5, but still confer insensitivity towards NAM, indicating that the overall NAD⁺ binding loop and the NAM binding pocket (or orientation of NAM) are involved in the regulation by NAM. In conclusion, this lack of inhibition by NAM could very well be an interesting mechanism of mitochondrial regulation and can guide towards developing Sirt3 specific small molecule therapeutics towards acetylated protein substrates that does not affect Sirt5 dependent deacetylation.

4.7 Expression, purification and crystallization of Sirt7

In order to investigate the structure and function of Sirt7, several constructs of Sirt7 were cloned, expressed and purified. The majority of the process was performed at DPF in collaboration with Dr. Tim Bergbrede and colleagues using high-throughput technologies in a semi-automated fashion. The overall purity and yield of different Sirt7 constructs were quite satisfactory. In order to identify the best buffer and salt conditions for further studies on Sirt7, thermal denaturation shift assays were performed using varying buffer and salt conditions. The assay revealed that Sirt7 is more stable at a basic pH and with a salt concentration of at least 50 mM. Due to the basic nature of Sirt7 (calculated pI ~ 8.9 or above), a cation exchange chromatography was used for further purification from *E. coli* proteins, yielding Sirt7 with higher purity that was used in crystallization trials. An additional protein specie obtained after ion exchange chromatography was analyzed using MS and N-terminal sequencing and identified as a degradation/teolysis product. The new N-terminus starts just before the α 3 helix of the typical secondary structure topology of Sirtuins (supplemental figure S2), which is already located inside the conserved catalytic core. In order to overcome stability issues, based on the sequence alignment and bioinformatic predictions several new constructs were planned which consisted of residues 98-338, 98-342 and 98-356. Although several crystallization trials were pursued to solve the crystal structure of Sirt7, no diffraction quality crystals were obtained. Several new constructs and crystallization trials were planned to crystallize Sirt7, but so far without success. This could indicate that Sirt7 requires additional factors such as PTMs, interaction protein partners, substrates/products or small molecule regulators to make it more amenable for crystallization.

4.8 Sirt7 Phosphorylation at Thr224 increases its activity

Among all the mammalian Sirtuins, Sirt7 is perhaps the least characterized isoform in terms of structure, substrate preference and regulation. Sirt7 overexpressed in *E. coli* shows weak deacetylase activity against FdL substrates when compared to Sirt1 for example, whereas when insect cell overexpressed Sirt7 was used, better deacetylation was observed with FdL substrates, this could indicate that Sirt7 is different to other human Sirtuins in a way that expression of properly folded, active Sirt7 requires eukaryotic expression systems. However, it might also indicate that PTMs might play a role in the activity of Sirt7. In fact it has been shown that Sirt7 is phosphorylated by the CDK1-cyclin B pathway, although the exact residue phosphorylated was not identified (Grob et al., 2009). Our MS results on the insect cell overexpressed Sirt7 shows that Thr224 is indeed phosphorylated, to our knowledge this is the first time a phosphorylation/PTM site has been identified for Sirt7. Threonine to Aspartate mutation is an established procedure used to mimic phosphorylation state due to structural similarities between Aspartate and phosphorylated Threonine. Our attempts to express T224D mutants in *E. coli* to investigate whether the mutants conferred activity to Sirt7 resulted in no protein expression. This could possibly indicate that the phosphorylation mimic imparts better activity to Sirt7 resulting in toxicity to *E. coli* and therefore leading to protein degradation immediately during expression. In conclusion, we have shown that the activity of Sirt7 is influenced by PTMs and new strategies are being planned to crystallize Sirt7.

4.9 Sir2Tm as a model system for studying mammalian Sirt1

Mammalian Sirtuins play crucial roles in various processes ranging from cellular housekeeping to disease states (Haigis and Sinclair, 2010; Lavu et al., 2008). Structural elucidation of all the seven mammalian Sirtuins would be very useful in finding drug targets that can selectively modulate each Sirtuin, leading to a targeted approach towards diseases caused by a particular isoform. The lack of structural information on mammalian Sirtuins; Sirt1, Sirt4 and Sirt7 presents a challenge on the rational level, towards identifying and characterizing small molecules that target only these isoforms and modulates them against specific substrates. In spite of this, there are several small molecule modulators available for Sirt1 (Blum et al., 2011) with low specificity and potency (baring a few) compared to already marketed therapeutics, thus necessitating better drug targets. To overcome the lack of structural information on Sirt1, we have used Sir2Tm as a model system for its structural characterization due to its ease of purification and crystallizability. Numerous crystal

structures of Sir2Tm are available in the PDB and are in fact used as model systems for studying the catalytic mechanisms and regulation of Sirtuins (Avalos et al., 2005; Avalos et al., 2004; Hoff et al., 2006). Until the structure of Sirt1 is available, it would be beneficial to structurally characterize Sir2Tm with small molecules that can modulate both Sirt1 and Sir2Tm equally.

4.10 Mechanism of Sirtuin inhibition by Ex-527

The crystal structures of Sir2Tm bound partially to Ex-527 and thioacetyllysine offers possible mechanistic insights into the inhibition of Sirtuins by Ex-527. The catalytic mechanism of Sirtuins involves the formation of the alkylimidate intermediate and the release of NAM. The overall structure of Sir2Tm bound to Ex-527/alkylimidate is similar to the structure with both the substrates bound (PDB id H4F (Hoff et al., 2006), except for the co-substrate binding loop. The Phe33 which plays a role in formation of the alkylimidate intermediate and shields the intermediate from attack by NAM, is present in the closed conformation in both the structures. Despite this, there is a striking difference in the orientation of the phenyl ring. The phenyl ring of Sir2Tm bound to Ex-527 is almost perpendicular ($\sim 94^\circ$) to the phenyl ring of 2H4F (Figure 4.1) and is displaced by $\sim 2.2 \text{ \AA}$ away from the phenyl ring of 2H4F structure, towards the direction of the C-pocket. This could be due to the fact that the NAM moiety of NAD^+ is no longer present near the phenyl ring to offer steric hindrance. Since the cyclohexene ring of EX-527 is buried more deeper into the C-pocket, it may provide more freedom for the phenyl ring to move into such a position. Thus the stabilization of the inhibitor could in part be due to the closure of the co-substrate binding loop and the movement of Phe33 leading to a trapped inhibitor which prevents product release thereby rendering the enzyme inactive. Although the structure presented here does not have full occupancy for the inhibitor, the crystal structure of Sirt3 in complex with the inhibitor clearly shows that the inhibitor is bound to the same site in both the proteins, thereby allowing us to make reasonable conclusions regarding the inhibitor binding site in Sir2Tm. Because the inhibitor is close to the substrate or product molecules (close proximity between the A and B rings of Ex-527 and methyl group of acetyllysine and ribose ring) it is also possible that there is not enough room in the active site for the release of the products or reentry of fresh substrates, making the enzyme inactive. We have also shown that there exist another mechanism by which Ex-527 can inhibit Sirtuins where the IC_{50} is in the micromolar range (example $60 \mu\text{M}$ for Sirt3) using Sirt3 as a model system. In this case, Ex-527 binds to the same exact ECP as in the case of Sir2Tm, but the NAD^+ is positioned in a

different conformation, where the NAM moiety of NAD^+ is pointing towards the acetyllysine binding cleft and thereby prevents the binding of the protein/peptide substrate. In the case of Sirt3 also, the co-substrate binding loop is in the close conformation, which most likely prevents the exit of the inhibitor.

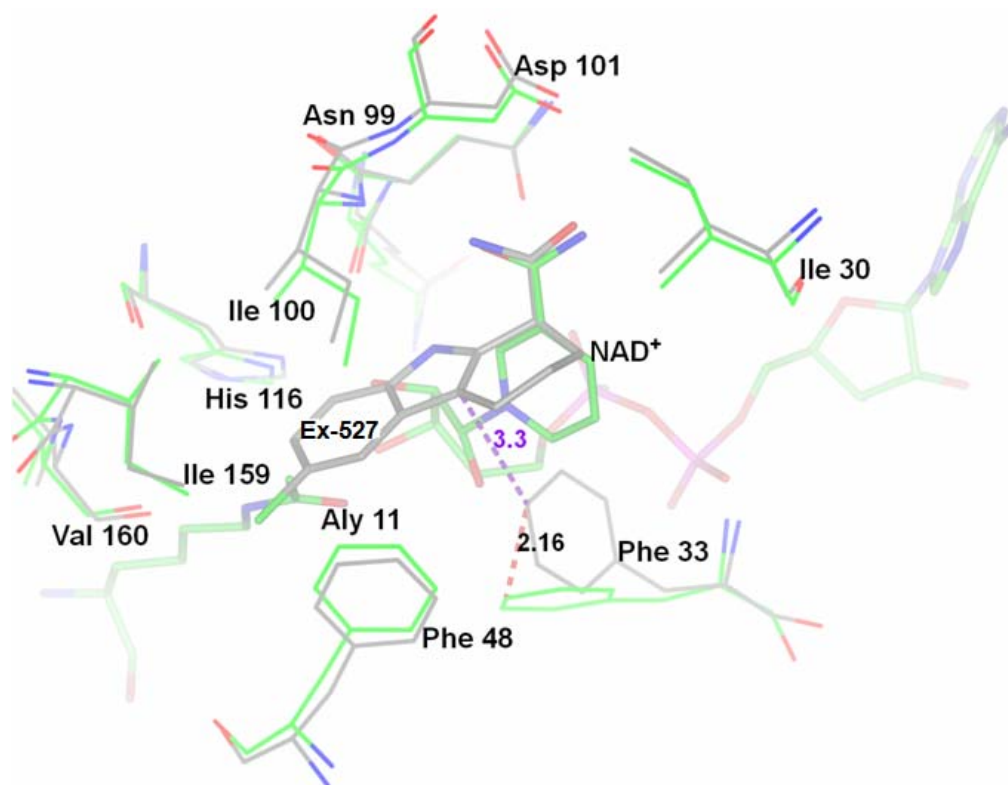


Figure 4.1: Structural comparison of the active sites of Sir2Tm in the presence and absence of Ex-527. An overlay of Sir2Tm structures bound partially to Ex-527 and peptide substrate/ NAD^+ (PDB id: 2H4F) indicates that the overall architecture of Sir2Tm active site remains unchanged when Ex-527 is bound. In both the structures the co-substrate loops exist in the closed conformation. The major difference lies in phenyl ring of Phe33. In the presence of Ex-527 the phenyl ring moves 2.2 Å away and is almost perpendicular to Phe33 without Ex-527. The phenyl ring also contacts Ex-527. The residues corresponding to Ex-527 bound structure are represented as gray cylinders and residues corresponding to 2H4F are represented as green cylinders. Aly stands for acetyllysine.

4.11 Selectivity of Ex-527 towards Sirtuins

The residues involved in binding of Ex-527 to Sir2Tm are very similar in Sirt1 and other mammalian isoforms (Supplemental figure S1). In spite of this, Ex-527 selectively inhibits Sirtuin isoforms. Sirt1 and Sir2Tm are very well inhibited by Ex-527 (IC_{50} in the nanomolar range) whereas Sirt3 and Sirt5 show moderate and no inhibition respectively. The crystal structures of Ex-527 bound to Sir2Tm and Sirt3 indicate that the inhibitor binds to the same pocket of the protein (the ECP) and is in the vicinity of similar residues, with one exception being the Met71 of Sir2Tm which contacts the cyclohexene ring that bears the

carboxamide (C-ring) where as the Sirt3 equivalent residue is Leu199. This still does not explain the selectivity of Ex-527 towards Sirt2Tm/Sirt1 and Sirt3 since Sirt1 also does not contain a Met (instead it contains Ile) at this site, moreover the residues surrounding Met71 in Sir2Tm is part of a helix that connects the Zinc binding domain and the Rossmann domain and a similar architecture exists in both Sirt1 and Sirt3. A possible explanation for the selectivity of Ex-527 towards Sirtuins could arise because of the co-substrate binding loop, as it appear to be required for binding and docking of the inhibitor at the ECP. Although this loop is conserved among all the Sirtuins, subtle differences existing between the neighboring residues surrounding this loop, and dynamics of this loop may influence EX-527 binding to the protein. In Sirt5, the Arg105 which is part of the loop was shown to confer partial insensitivity for Sirt5 towards NAM (Fisher et. al. submitted), interestingly Sirt5 is also insensitive to EX-527. Along these same lines, it would also be interesting to test if other NAM insensitive Sirtuins, such as Sirt7 is insensitive to EX-527. Another possible explanation towards isoform selectivity for Ex-527 inhibition could be due to the subtle differences on residues surrounding the ECP, as small changes in the length, size, charge of the residues etc. can alter the bonding and geometry of binding (Figure 4.2).

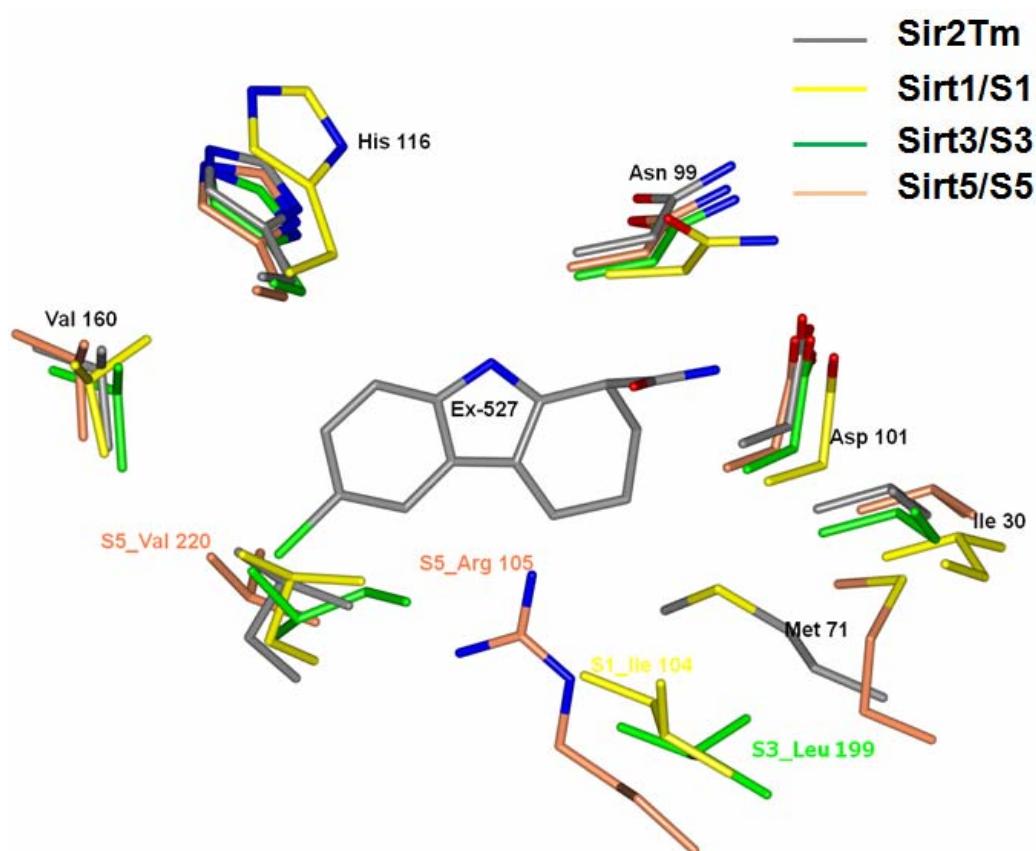


Figure 4.2: Comparison of residues surrounding Ex-527 from different Sirtuin isoforms. Superposition of Sirtuins from different isoforms on Sir2Tm bound to alkylimidate or Ex-527

indicates an overall similarity between the binding site residues, yet subtle differences exist among the isoforms. Residues that differ among the isoforms are labeled in their respective colors.

4.12 Insights for drug development

Despite the availability of structural information from various Sirtuin homologs, the only crystal structure available that shows binding of a pharmacologically active small molecule to a Sirtuin is that of Sirt5 bound to Suramin (PDB id 2NYR (Schuetz et al., 2007)). Ex-527 is one of the best characterized small molecule inhibitor of Sirtuins with high potency and selectivity. Our structural analysis on Sir2Tm shows binding details of Ex-527 to a Sirtuin at atomic level. Our structural and biophysical characterizations reveal Ex527's binding site and a probable mechanism of inhibition. Since Sir2Tm is inhibited similar to Sirt1, we conclude that they may share a similar mechanism of inhibition by Ex-527. Our results confirm the speculations of Napper et. al. (Napper et al., 2005), who proposed based on kinetic studies, that Ex-527 binds to Sirtuin near the C-pocket which accommodates NAM released after the formation of the alkylimidate intermediate. Ex-527 binds to the hydrophobic core of the protein which extends beyond the C-pocket which we call the ECP, but is incompatible with intermediate, which could indicate that product dissociation is inhibited. Sirt2 has been shown to be selectively inhibited by AGK2 in the sub-micromolar level (Outeiro et al., 2007). The authors proposed an inhibition mechanism which involved the ECP, therefore we also call compounds such as Ex-527 which binds to ECP as ECS (Extended C-Site inhibitors). The ECP serves as an excellent scaffold for identifying potential isoform selective Sirtuin inhibitors, due to the subtle differences existing between Sirtuins in and around this pocket. Similar to our studies on Sirt2 (Schlicker et al., 2011), the ECP can be exploited to perform docking calculations on Sirtuins whose structure is available, in order to screen for novel selective inhibitors. Our method of cryotrapping the inhibitor during freezing the protein crystal can also be adopted as a general strategy for structural elucidation of other Sirtuin modulators, because similar to Ex-527 other small molecules might also need the enzyme in the intermediate or product complex form for efficient binding. Our results also allow us to use EX-527 as a handle and synthesize more potent, soluble and isoform specific inhibitors of Sirtuins, which can serve as potential therapeutics. It would also be useful to synthesize Sirtuin inhibitors which can be targeted to a particular organelle such as mitochondria or nucleus for selective inhibition of different isoforms (Rajendran et al., 2010).

4.13 Outlook

The studies performed using different Sirtuins offer various interesting conclusions and exciting further avenues for research. The predominantly nuclear isoform Sirt1 is the largest member among the mammalian Sirtuins and offers plenty of potential for further characterization. It would be interesting to investigate if the sequence specific ability of resveratrol to modulate the activity of Sirt1 at the peptide level could be seen in the protein level and finally in vivo. The acetylome-chip array we established provides an excellent platform to test new Sirt1 modulators that may be both physiologically and pharmacologically relevant. Even though the physiologically relevant thyroid hormones showed no modulation on Sirt1, it would still be interesting to test them on the array, because similar to resveratrol its modulation of Sirt1 may also depend on the substrate sequence. Various attempts to crystallize Sirt1 should be pursued. For example, preparation of complexes either with physiologically relevant partner proteins or non-physiological interacting partners such as DARPins, could be used in crystallization attempts and newly identified substrate-modulator pairs can be used in crystallization trials. Structural information can offer valuable insights into the architecture of Sirt1 and help us identify how the protein differs from its isoform, especially at the termini. It would also be interesting to map the Sirt1 residues involved in resveratrol binding, for example through MS based H/D exchange studies followed by mutational studies on the identified residues to assess their influence on resveratrol binding.

One of the most important steps in understanding the function and regulation of Sirt7 is to obtain its crystal structure. Various strategies can be pursued to crystallize Sirt7. Since phosphorylation has been identified to play a role in Sirt7's activity, it would be interesting to overexpress and purify phosphorylation mimics from *E. coli* and use it for crystallization trials, because it is well known that phosphorylation can alter the structure of a protein and this might lead to a more stable form of Sirt7 leading to crystallization. Alternatively, Sirt7 overexpressed and purified from eukaryotic expression systems such as insect cells or mammalian cells can also be used in crystallization trials. Identification of better peptide substrates and modulators of Sirt7 using the acetylome chip (similar to Sirt1) may reveal substrate preferences and substrate/modulator pairs for Sirt7, which could be used to further characterize and crystallize Sirt7. Similar to Sirt5, which was recently shown to possess desuccinylase and demalonylase activity, it is possible that Sirt7 also has preference for a different substrate type, which could explain its poor deacetylase activity. Identifying such

new substrate types for Sirt7 would also be interesting.

Ex-527 binding to Sirtuins characterized in this study can be further pursued using several structural and biochemical experiments. Co-crystallization or soaking experiments of Sir2Tm in the presence of products would offer further information regarding the conditions necessary for binding of Ex-527 to Sir2Tm. Small molecules identified from docking calculations performed using the ECP scaffold of Sir2Tm or Sirt3 as template can be validated on Sirt1 to identify better inhibitors in terms of selectivity, physical and chemical property. Investigating the role of the co-substrate binding loop through mutational studies may also offer explanations as to the selectivity of Ex-527 towards Sirtuins which can then be exploited for better therapeutics.

5. Abstract

Sirtuins are NAD^+ dependent protein deacetylases involved in regulation of metabolism, age related diseases and are suggested to mediate lifespan extending effects of calorie restriction. Mammals contain seven Sirtuin isoforms with various cellular localizations and substrate preferences.

This work focuses on the structural and biochemical characterization of several mammalian Sirtuin isoforms, with main emphasis on the largest member of the family, Sirt1. Analysis of various Sirt1 constructs using analytical ultracentrifugation and electron microscopy techniques identified it to be a monomer, similar to other mammalian isoforms. Comparison of activity between different Sirt1 constructs indicates that the termini might be involved in regulating the protein's activity. It could be shown that the catalytic domain of Sirt1 is sufficient for its activation by the lifespan extending polyphenol resveratrol and that resveratrol can directly bind to Sirt1. Using a peptide array harboring all known mammalian acetylation sites several novel substrates for Sirt1 were identified and shown that resveratrol and other small molecules can modulate Sirt1 dependent deacetylation of substrate peptides and that the effect is specific for the sequence of the substrate site. This finding reveals exciting possibilities for the development of new modulators targeting only specific substrates of Sirt1. These compounds can further be used in analyzing the functions of Sirtuins in vivo and can also serve as attractive leads for developing Sirt1 specific drugs.

Studies on the mitochondrial isoform Sirt3 revealed that Zinc is essential for the structural integrity of Sirtuins. Investigations on Sirt5, also a mitochondrial Sirtuin appears to indicate that it is insensitive to nicotinamide (a physiological inhibitor of Sirtuins). Studies on the nucleolar isoform Sirt7 identified Thr224 to be phosphorylated, and play a role in the enzyme's activity.

The *thermotoga maritima* Sirtuin Sir2Tm was used as a model system for structural characterization of Sirt1. The crystal structure of Sir2Tm in complex with Ex-527, a potent Sirt1 inhibitor was solved, which combined with biophysical studies offers information about Ex-527 binding and inhibition. Close contacts between Ex-527 and some form of ADP-ribose, possibly the product O-acetyl-ADP-ribose (which is not yet fully verified) in the closed enzyme conformation prevent the release of products, thereby stalling the enzymatic reaction. These results offer insights into the isoform specific inhibition of Sirtuins by Ex-527 and provide information for further improvement of Sirt1 specific inhibitors.

6. Zusammenfassung

Sirtuine sind NAD^+ -abhängige Proteindeacetylasen, die an Stoffwechselregulation und der Entstehung altersbedingter Krankheiten beteiligt sind; zudem wird angenommen, dass sie die lebensdauerverlängernde Wirkung von „caloric restriction“ vermitteln. Bei Säugetieren kommen sieben Sirtuin Isoformen vor, die sich in ihren zellulären Lokalisierungen und Substratpräferenzen unterscheiden.

Diese Arbeit richtet sich auf die strukturelle und biochemische Charakterisierung verschiedener Sirtuin-Isoformen aus Säugern, mit Schwerpunkt auf Sirt1, dem größtem Mitglied der Sirtuinfamilie. Die Analyse verschiedener Sirt1-Konstrukte mittels analytischer Ultrazentrifugation und Elektronenmikroskopie zeigte, dass Sirt1 als Monomer vorliegt, ähnlich wie die anderen Isoformen aus Säugern. Ein Vergleich der Aktivitäten der verschiedenen Sirt1-Konstrukte weist darauf hin, dass die Termini an der Regulierung der Proteinaktivität beteiligt sein könnten. Es konnte gezeigt werden, dass die katalytische Domäne von Sirt1 ausreicht für die Aktivierung durch das lebensdauerverlängernde Polyphenol Resveratrol und dass Resveratrol direkt an Sirt1 binden kann. Unter Verwendung eines Peptidarrays, der alle bekannten Acetylierungsstellen aus Säugerproteinen beinhaltet, wurden mehrere neue Substrate für Sirt1 identifiziert und es konnte gezeigt werden, dass Resveratrol und andere Kleinmoleküle die Sirt1-abhängige Deacetylierung von Substratpeptiden modulieren können, und zwar in Abhängigkeit von der Substratsequenz. Dieses Ergebnis eröffnet außergewöhnliche Möglichkeiten für die Entwicklung neuer Modulatoren, die nur die Deacetylierung einiger der Sirt1-Substrate beeinflussen. Diese Verbindungen können dann für die Funktionsanalyse von Sirtuinen *in vivo* genutzt werden, und sie können als vielversprechende Leitstrukturen für die Entwicklung hochspezifischer Sirt1-Wirkstoffen dienen.

Studien an der mitochondrialen Isoform Sirt3 zeigen, dass Zink für die strukturelle Integrität der Enzyme notwendig ist. Untersuchungen an Sirt5, ebenso ein mitochondriales Sirtuin, scheinen darauf hinzuweisen, dass es unempfindlich ist gegen Nicotinamid (ein physiologischer Sirtuin Inhibitor). Untersuchungen an der nukleolaren Isoform Sirt7 identifizieren eine Phosphorylierung an Thr224, die die Enzymaktivität zu beeinflussen scheint.

Das *Thermotoga maritima* Sirtuin Sir2Tm wurde als Modellsystem für die strukturelle Charakterisierung von Sirt1 verwendet. Die Kristallstruktur von Sir2Tm in Komplex mit Ex-

527, einem potenten Sirt1 Inhibitor, wurde gelöst. In Verbindung mit biophysikalischen Untersuchungen ergaben sich daraus Erkenntnisse zu Bindung und Inhibitionsmechanismus von Ex-527. Eine räumlich enge Nachbarschaft zwischen Ex-527 und einer Form von ADP-Ribose, möglicherweise dem Produkt O-acetyl-ADP-Ribose (noch nicht vollständig verifiziert) in der geschlossenen Enzymkonformation verhindert die Produktfreisetzung und stoppt dadurch die enzymatische Reaktion. Diese Ergebnisse bieten Einsichten in die Isoform-spezifische Hemmung von Sirtuinen durch Ex-527 und liefern Information für die weitere Verbesserung von Sirt1-spezifischen Inhibitoren.

7. References

- Abdelmohsen, K., Pullmann Jr, R., Lal, A., Kim, H.H., Galban, S., Yang, X., Blethrow, J.D., Walker, M., Shubert, J., Gillespie, D.A., *et al.* (2007). Phosphorylation of HuR by Chk2 Regulates SIRT1 Expression. *Molecular Cell* *25*, 543-557.
- Adams, P.D., Afonine, P.V., Bunkoczi, G., Chen, V.B., Davis, I.W., Echols, N., Headd, J.J., Hung, L.W., Kapral, G.J., Grosse-Kunstleve, R.W., *et al.* (2010). PHENIX: a comprehensive Python-based system for macromolecular structure solution. *Acta Crystallogr D Biol Crystallogr* *66*, 213-221.
- Ahn, B.-H., Kim, H.-S., Song, S., Lee, I.H., Liu, J., Vassilopoulos, A., Deng, C.-X., and Finkel, T. (2008). A role for the mitochondrial deacetylase Sirt3 in regulating energy homeostasis. *Proceedings of the National Academy of Sciences* *105*, 14447-14452.
- Aquilano, K., Vigilanza, P., Baldelli, S., Pagliei, B., Rotilio, G., and Ciriolo, M.R. (2010). Peroxisome proliferator-activated receptor gamma co-activator 1alpha (PGC-1alpha) and sirtuin 1 (SIRT1) reside in mitochondria: possible direct function in mitochondrial biogenesis. *J Biol Chem* *285*, 21590-21599.
- Avalos, J.L., Bever, K.M., and Wolberger, C. (2005). Mechanism of Sirtuin Inhibition by Nicotinamide: Altering the NAD⁺ Cosubstrate Specificity of a Sir2 Enzyme. *Molecular Cell* *17*, 855-868.
- Avalos, J.L., Boeke, J.D., and Wolberger, C. (2004). Structural basis for the mechanism and regulation of Sir2 enzymes. *Mol Cell* *13*, 639-648.
- Baur, J.A., Pearson, K.J., Price, N.L., Jamieson, H.A., Lerin, C., Kalra, A., Prabhu, V.V., Allard, J.S., Lopez-Lluch, G., Lewis, K., *et al.* (2006). Resveratrol improves health and survival of mice on a high-calorie diet. *Nature* *444*, 337-342.
- Beausoleil, S.A., Jedrychowski, M., Schwartz, D., Elias, J.E., Villén, J., Li, J., Cohn, M.A., Cantley, L.C., and Gygi, S.P. (2004). Large-scale characterization of HeLa cell nuclear phosphoproteins. *Proceedings of the National Academy of Sciences of the United States of America* *101*, 12130-12135.
- Beausoleil, S.A., Villen, J., Gerber, S.A., Rush, J., and Gygi, S.P. (2006). A probability-based approach for high-throughput protein phosphorylation analysis and site localization. *Nat Biotech* *24*, 1285-1292.
- Behr, D., Wu, J., Cumine, S., Kim, K.W., Lu, S.-C., Atangan, L., and Wang, M. (2009). Resveratrol is Not a Direct Activator of SIRT1 Enzyme Activity. *Chemical Biology & Drug Design* *74*, 619-624.
- Bitterman, K.J., Anderson, R.M., Cohen, H.Y., Latorre-Esteves, M., and Sinclair, D.A. (2002). Inhibition of Silencing and Accelerated Aging by Nicotinamide, a Putative Negative Regulator of Yeast Sir2 and Human SIRT1. *Journal of Biological Chemistry* *277*, 45099-45107.
- Black, J.C., Mosley, A., Kitada, T., Washburn, M., and Carey, M. (2008). The SIRT2 deacetylase regulates autoacetylation of p300. *Mol Cell* *32*, 449-455.
- Blum, C.A., Ellis, J.L., Loh, C., Ng, P.Y., Perni, R.B., and Stein, R.L. (2011). SIRT1 modulation as a novel approach to the treatment of diseases of aging. *J Med Chem* *54*, 417-432.
- Bordone, L., and Guarente, L. (2005). Calorie restriction, SIRT1 and metabolism: understanding longevity. *Nat Rev Mol Cell Biol* *6*, 298-305.
- Borra, M.T., Smith, B.C., and Denu, J.M. (2005). Mechanism of Human SIRT1 Activation by Resveratrol. *Journal of Biological Chemistry* *280*, 17187-17195.
- Brachmann, C.B., Sherman, J.M., Devine, S.E., Cameron, E.E., Pillus, L., and Boeke, J.D. (1995). The SIR2 gene family, conserved from bacteria to humans, functions in silencing, cell cycle progression, and chromosome stability. *Genes Dev* *9*, 2888-2902.

- Brunger, A.T. (1992). Free R value: a novel statistical quantity for assessing the accuracy of crystal structures. *Nature* *355*, 472-475.
- Chen, G.J., Qiu, N., Karrer, C., Caspers, P., and Page, M.G. (2000). Restriction site-free insertion of PCR products directionally into vectors. *Biotechniques* *28*, 498-500, 504-495.
- Chen, L., Feng, Y., Zhou, Y., Zhu, W., Shen, X., Chen, K., Jiang, H., and Liu, D. (2010a). Dual role of Zn²⁺ in maintaining structural integrity and suppressing deacetylase activity of SIRT1. *J Inorg Biochem* *104*, 180-185.
- Chen, V.B., Arendall, W.B., 3rd, Headd, J.J., Keedy, D.A., Immormino, R.M., Kapral, G.J., Murray, L.W., Richardson, J.S., and Richardson, D.C. (2010b). MolProbity: all-atom structure validation for macromolecular crystallography. *Acta Crystallogr D Biol Crystallogr* *66*, 12-21.
- Choudhary, C., Kumar, C., Gnad, F., Nielsen, M.L., Rehman, M., Walther, T.C., Olsen, J.V., and Mann, M. (2009). Lysine acetylation targets protein complexes and co-regulates major cellular functions. *Science* *325*, 834-840.
- Dai, H., Kustigian, L., Carney, D., Case, A., Considine, T., Hubbard, B.P., Perni, R.B., Riera, T.V., Szczepankiewicz, B., Vlasuk, G.P., *et al.* (2010). SIRT1 Activation by Small Molecules. *Journal of Biological Chemistry* *285*, 32695-32703.
- Dephoure, N., Zhou, C., Villén, J., Beausoleil, S.A., Bakalarski, C.E., Elledge, S.J., and Gygi, S.P. (2008). A quantitative atlas of mitotic phosphorylation. *Proceedings of the National Academy of Sciences* *105*, 10762-10767.
- Derewenda, Z.S. (2004). Rational protein crystallization by mutational surface engineering. *Structure* *12*, 529-535.
- Du, J., Zhou, Y., Su, X., Yu, J.J., Khan, S., Jiang, H., Kim, J., Woo, J., Kim, J.H., Choi, B.H., *et al.* (2011). Sirt5 is a NAD-dependent protein lysine demalonylase and desuccinylase. *Science* *334*, 806-809.
- Emsley, P., Lohkamp, B., Scott, W.G., and Cowtan, K. (2010). Features and development of Coot. *Acta Crystallogr D Biol Crystallogr* *66*, 486-501.
- Engel, N., and Mahlknecht, U. (2008). Aging and anti-aging: unexpected side effects of everyday medication through sirtuin1 modulation. *Int J Mol Med* *21*, 223-232.
- Eswar, N., Webb, B., Marti-Renom, M.A., Madhusudhan, M.S., Eramian, D., Shen, M.Y., Pieper, U., and Sali, A. (2006). Comparative protein structure modeling using Modeller. *Curr Protoc Bioinformatics Chapter 5*, Unit 5 6.
- Finley, L.W.S., Haas, W., Desquirit-Dumas, V., Wallace, D.C., Procaccio, V., Gygi, S.P., and Haigis, M.C. (2011). Succinate Dehydrogenase Is a Direct Target of Sirtuin 3 Deacetylase Activity. *PLoS ONE* *6*, e23295.
- Finnin, M.S., Donigian, J.R., and Pavletich, N.P. (2001). Structure of the histone deacetylase SIRT2. *Nat Struct Biol* *8*, 621-625.
- Ford, E., Voit, R., Liszt, G., Magin, C., Grummt, I., and Guarente, L. (2006). Mammalian Sir2 homolog SIRT7 is an activator of RNA polymerase I transcription. *Genes Dev* *20*, 1075-1080.
- Ford, J., Ahmed, S., Allison, S., Jiang, M., and Milner, J. (2008). JNK2-dependent regulation of SIRT1 protein stability. *Cell Cycle* *7*, 3091-3097.
- Frye, R.A. (1999). Characterization of five human cDNAs with homology to the yeast SIR2 gene: Sir2-like proteins (sirtuins) metabolize NAD and may have protein ADP-ribosyltransferase activity. *Biochem Biophys Res Commun* *260*, 273-279.
- Frye, R.A. (2000). Phylogenetic classification of prokaryotic and eukaryotic Sir2-like proteins. *Biochem Biophys Res Commun* *273*, 793-798.
- Gauci, S., Helbig, A.O., Slijper, M., Krijgsveld, J., Heck, A.J.R., and Mohammed, S. (2009). Lys-N and Trypsin Cover Complementary Parts of the Phosphoproteome in a Refined SCX-Based Approach. *Analytical Chemistry* *81*, 4493-4501.

- Gerhart-Hines, Z., Dominy Jr, John E., Blättler, Sharon M., Jedrychowski, Mark P., Banks, Alexander S., Lim, J.-H., Chim, H., Gygi, Steven P., and Puigserver, P. (2011). The cAMP/PKA Pathway Rapidly Activates SIRT1 to Promote Fatty Acid Oxidation Independently of Changes in NAD⁺. *Molecular Cell* *44*, 851-863.
- Gertz, M., and Steegborn, C. (2010). Function and regulation of the mitochondrial sirtuin isoform Sirt5 in Mammalia. *Biochim Biophys Acta* *1804*, 1658-1665.
- Gottlieb, S., and Esposito, R.E. (1989). A new role for a yeast transcriptional silencer gene, SIR2, in regulation of recombination in ribosomal DNA. *Cell* *56*, 771-776.
- Grob, A., Roussel, P., Wright, J.E., McStay, B., Hernandez-Verdun, D., and Sirri, V. (2009). Involvement of SIRT7 in resumption of rDNA transcription at the exit from mitosis. *Journal of Cell Science* *122*, 489-498.
- Guo, X., Williams, J.G., Schug, T.T., and Li, X. (2010). DYRK1A and DYRK3 Promote Cell Survival through Phosphorylation and Activation of SIRT1. *Journal of Biological Chemistry* *285*, 13223-13232.
- Haigis, M.C., Mostoslavsky, R., Haigis, K.M., Fahie, K., Christodoulou, D.C., Murphy, Andrew J., Valenzuela, D.M., Yancopoulos, G.D., Karow, M., Blander, G., *et al.* (2006). SIRT4 Inhibits Glutamate Dehydrogenase and Opposes the Effects of Calorie Restriction in Pancreatic β Cells. *Cell* *126*, 941-954.
- Haigis, M.C., and Sinclair, D.A. (2010). Mammalian sirtuins: biological insights and disease relevance. *Annu Rev Pathol* *5*, 253-295.
- Hall, T.A. (1999). BioEdit: a user-friendly biological sequence alignment editor and analysis program for Windows 95/98/NT. *Nucleic Acids Symposium Series* *41*, 95-98.
- Hawse, W.F., Hoff, K.G., Fatkins, D.G., Daines, A., Zubkova, O.V., Schramm, V.L., Zheng, W., and Wolberger, C. (2008). Structural Insights into Intermediate Steps in the Sir2 Deacetylation Reaction. *Structure* *16*, 1368-1377.
- Hirschey, M.D., Shimazu, T., Goetzman, E., Jing, E., Schwer, B., Lombard, D.B., Grueter, C.A., Harris, C., Biddinger, S., Ilkayeva, O.R., *et al.* (2010). SIRT3 regulates mitochondrial fatty-acid oxidation by reversible enzyme deacetylation. *Nature* *464*, 121-125.
- Hoff, K.G., Avalos, J.L., Sens, K., and Wolberger, C. (2006). Insights into the sirtuin mechanism from ternary complexes containing NAD⁺ and acetylated peptide. *Structure* *14*, 1231-1240.
- Howitz, K.T., Bitterman, K.J., Cohen, H.Y., Lamming, D.W., Lavu, S., Wood, J.G., Zipkin, R.E., Chung, P., Kisielewski, A., Zhang, L.-L., *et al.* (2003). Small molecule activators of sirtuins extend *Saccharomyces cerevisiae* lifespan. *Nature* *425*, 191-196.
- Huber, T., Steiner, D., Rothlisberger, D., and Pluckthun, A. (2007). In vitro selection and characterization of DARPins and Fab fragments for the co-crystallization of membrane proteins: The Na⁽⁺⁾-citrate symporter CitS as an example. *J Struct Biol* *159*, 206-221.
- Hursting, S.D., Perkins, S.N., Donehower, L.A., and Davis, B.J. (2001). Cancer prevention studies in p53-deficient mice. *Toxicol Pathol* *29*, 137-141.
- Imai, S., Armstrong, C.M., Kaeberlein, M., and Guarente, L. (2000). Transcriptional silencing and longevity protein Sir2 is an NAD-dependent histone deacetylase. *Nature* *403*, 795-800.
- Jackson, M.D., and Denu, J.M. (2002). Structural identification of 2'- and 3'-O-acetyl-ADP-ribose as novel metabolites derived from the Sir2 family of beta -NAD⁺-dependent histone/protein deacetylases. *J Biol Chem* *277*, 18535-18544.
- Jin, L., Wei, W., Jiang, Y., Peng, H., Cai, J., Mao, C., Dai, H., Choy, W., Bemis, J.E., Jirousek, M.R., *et al.* (2009). Crystal structures of human SIRT3 displaying substrate-induced conformational changes. *J Biol Chem* *284*, 24394-24405.
- Jin, Y.-H., Kim, Y.-J., Kim, D.-W., Baek, K.-H., Kang, B.Y., Yeo, C.-Y., and Lee, K.-Y. (2008). Sirt2 interacts with 14-3-3 β/γ and down-regulates the activity of p53. *Biochemical and Biophysical Research Communications* *368*, 690-695.
- Kabsch, W. (2010). Xds. *Acta Crystallogr D Biol Crystallogr* *66*, 125-132.

- Kaeberlein, M., McDonagh, T., Heltweg, B., Hixon, J., Westman, E.A., Caldwell, S.D., Napper, A., Curtis, R., DiStefano, P.S., Fields, S., *et al.* (2005a). Substrate-specific Activation of Sirtuins by Resveratrol. *Journal of Biological Chemistry* *280*, 17038-17045.
- Kaeberlein, M., Powers, R.W., 3rd, Steffen, K.K., Westman, E.A., Hu, D., Dang, N., Kerr, E.O., Kirkland, K.T., Fields, S., and Kennedy, B.K. (2005b). Regulation of yeast replicative life span by TOR and Sch9 in response to nutrients. *Science* *310*, 1193-1196.
- Kang, H., Jung, J.W., Kim, M.K., and Chung, J.H. (2009). CK2 is the regulator of SIRT1 substrate-binding affinity, deacetylase activity and cellular response to DNA-damage. *PLoS ONE* *4*, e6611.
- Kang, H., Suh, J.-Y., Jung, Y.-S., Jung, J.-W., Kim, Myung K., and Chung, Jay H. (2011). Peptide Switch Is Essential for Sirt1 Deacetylase Activity. *Molecular Cell* *44*, 203-213.
- Kawahara, T.L.A., Michishita, E., Adler, A.S., Damian, M., Berber, E., Lin, M., McCord, R.A., Ongaigui, K.C.L., Boxer, L.D., Chang, H.Y., *et al.* (2009). SIRT6 Links Histone H3 Lysine 9 Deacetylation to NF- κ B-Dependent Gene Expression and Organismal Life Span. *Cell* *136*, 62-74.
- Kelley, L.A., and Sternberg, M.J. (2009). Protein structure prediction on the Web: a case study using the Phyre server. *Nat Protoc* *4*, 363-371.
- Khoury, G.A., Baliban, R.C., and Floudas, C.A. (2011). Proteome-wide post-translational modification statistics: frequency analysis and curation of the swiss-prot database. *Sci Rep* *1*.
- Kim, E.J., Kho, J.H., Kang, M.R., and Um, S.J. (2007). Active regulator of SIRT1 cooperates with SIRT1 and facilitates suppression of p53 activity. *Mol Cell* *28*, 277-290.
- Kim, J.-E., Chen, J., and Lou, Z. (2008). DBC1 is a negative regulator of SIRT1. *Nature* *451*, 583-586.
- Kim, S.C., Sprung, R., Chen, Y., Xu, Y., Ball, H., Pei, J., Cheng, T., Kho, Y., Xiao, H., Xiao, L., *et al.* (2006). Substrate and functional diversity of lysine acetylation revealed by a proteomics survey. *Mol Cell* *23*, 607-618.
- Koubova, J., and Guarente, L. (2003). How does calorie restriction work? *Genes Dev* *17*, 313-321.
- Laemmli, U.K. (1970). Cleavage of structural proteins during the assembly of the head of bacteriophage T4. *Nature* *227*, 680-685.
- Lagouge, M., Argmann, C., Gerhart-Hines, Z., Meziane, H., Lerin, C., Daussin, F., Messadeq, N., Milne, J., Lambert, P., Elliott, P., *et al.* (2006). Resveratrol Improves Mitochondrial Function and Protects against Metabolic Disease by Activating SIRT1 and PGC-1 β . *Cell* *127*, 1109-1122.
- Lain, S., Hollick, J.J., Campbell, J., Staples, O.D., Higgins, M., Aoubala, M., McCarthy, A., Appleyard, V., Murray, K.E., Baker, L., *et al.* (2008). Discovery, In Vivo Activity, and Mechanism of Action of a Small-Molecule p53 Activator. *Cancer Cell* *13*, 454-463.
- Lakshminarasimhan, M., and Steegborn, C. (2011). Emerging mitochondrial signaling mechanisms in physiology, aging processes, and as drug targets. *Exp Gerontol* *46*, 174-177.
- Landry, J., Sutton, A., Tafrov, S.T., Heller, R.C., Stebbins, J., Pillus, L., and Sternglanz, R. (2000). The silencing protein SIR2 and its homologs are NAD-dependent protein deacetylases. *Proc Natl Acad Sci U S A* *97*, 5807-5811.
- Lane, M.A., Ingram, D.K., and Roth, G.S. (1999). Calorie restriction in nonhuman primates: effects on diabetes and cardiovascular disease risk. *Toxicol Sci* *52*, 41-48.
- Lara, E., Mai, A., Calvanese, V., Altucci, L., Lopez-Nieva, P., Martinez-Chantar, M.L., Varela-Rey, M., Rotili, D., Nebbioso, A., Ropero, S., *et al.* (2009). Salermide, a Sirtuin inhibitor with a strong cancer-specific proapoptotic effect. *Oncogene* *28*, 781-791.
- Larkin, M.A., Blackshields, G., Brown, N.P., Chenna, R., McGettigan, P.A., McWilliam, H., Valentin, F., Wallace, I.M., Wilm, A., Lopez, R., *et al.* (2007). Clustal W and Clustal X version 2.0. *Bioinformatics* *23*, 2947-2948.

- Lavu, S., Boss, O., Elliott, P.J., and Lambert, P.D. (2008). Sirtuins [mdash] novel therapeutic targets to treat age-associated diseases. *Nat Rev Drug Discov* 7, 841-853.
- Libert, S., Pointer, K., Bell, Eric L., Das, A., Cohen, Dena E., Asara, John M., Kapur, K., Bergmann, S., Preisig, M., Otowa, T., *et al.* (2011). SIRT1 Activates MAO-A in the Brain to Mediate Anxiety and Exploratory Drive. *Cell* 147, 1459-1472.
- Lin, S.J., Kaeberlein, M., Andalis, A.A., Sturtz, L.A., Defossez, P.A., Culotta, V.C., Fink, G.R., and Guarente, L. (2002). Calorie restriction extends *Saccharomyces cerevisiae* lifespan by increasing respiration. *Nature* 418, 344-348.
- Liszt, G., Ford, E., Kurtev, M., and Guarente, L. (2005). Mouse Sir2 Homolog SIRT6 Is a Nuclear ADP-ribosyltransferase. *Journal of Biological Chemistry* 280, 21313-21320.
- Liu, X., Wang, D., Zhao, Y., Tu, B., Zheng, Z., Wang, L., Wang, H., Gu, W., Roeder, R.G., and Zhu, W.G. (2011). Methyltransferase Set7/9 regulates p53 activity by interacting with Sirtuin 1 (SIRT1). *Proc Natl Acad Sci U S A* 108, 1925-1930.
- Lombard, D.B., Alt, F.W., Cheng, H.L., Bunkenborg, J., Streeper, R.S., Mostoslavsky, R., Kim, J., Yancopoulos, G., Valenzuela, D., Murphy, A., *et al.* (2007). Mammalian Sir2 homolog SIRT3 regulates global mitochondrial lysine acetylation. *Mol Cell Biol* 27, 8807-8814.
- Louis-Jeune, C., Andrade-Navarro, M.A., and Perez-Iratxeta, C. (2012). Prediction of protein secondary structure from circular dichroism using theoretically derived spectra. *Proteins: Structure, Function, and Bioinformatics* 80, 374-381.
- Mayya, V., Lundgren, D.H., Hwang, S.-I., Rezaul, K., Wu, L., Eng, J.K., Rodionov, V., and Han, D.K. (2009). Quantitative Phosphoproteomic Analysis of T Cell Receptor Signaling Reveals System-Wide Modulation of Protein-Protein Interactions. *Sci Signal* 2, ra46-.
- McCay, C.M., Crowell, M.F., and Maynard, L.A. (1989). The effect of retarded growth upon the length of life span and upon the ultimate body size. 1935. *Nutrition* 5, 155-171; discussion 172.
- McCoy, A.J., Grosse-Kunstleve, R.W., Adams, P.D., Winn, M.D., Storoni, L.C., and Read, R.J. (2007). Phaser crystallographic software. *J Appl Crystallogr* 40, 658-674.
- McNicholas, S., Potterton, E., Wilson, K.S., and Noble, M.E. (2011). Presenting your structures: the CCP4mg molecular-graphics software. *Acta Crystallogr D Biol Crystallogr* 67, 386-394.
- Medda, F., Russell, R.J.M., Higgins, M., McCarthy, A.R., Campbell, J., Slawin, A.M.Z., Lane, D.P., Lain, S., and Westwood, N.J. (2009). Novel Cambinol Analogs as Sirtuin Inhibitors: Synthesis, Biological Evaluation, and Rationalization of Activity. *Journal of Medicinal Chemistry* 52, 2673-2682.
- Metrangolo, P., Meyer, F., Pilati, T., Resnati, G., and Terraneo, G. (2008). Halogen bonding in supramolecular chemistry. *Angew Chem Int Ed Engl* 47, 6114-6127.
- Michan, S., and Sinclair, D. (2007). Sirtuins in mammals: insights into their biological function. *Biochem J* 404, 1-13.
- Milne, J.C., Lambert, P.D., Schenk, S., Carney, D.P., Smith, J.J., Gagne, D.J., Jin, L., Boss, O., Perni, R.B., Vu, C.B., *et al.* (2007). Small molecule activators of SIRT1 as therapeutics for the treatment of type 2 diabetes. *Nature* 450, 712-716.
- Mullis, K., Faloona, F., Scharf, S., Saiki, R., Horn, G., and Erlich, H. (1986). Specific enzymatic amplification of DNA in vitro: the polymerase chain reaction. *Cold Spring Harb Symp Quant Biol* 51 Pt 1, 263-273.
- Murshudov, G.N., Vagin, A.A., and Dodson, E.J. (1997). Refinement of macromolecular structures by the maximum-likelihood method. *Acta Crystallogr D Biol Crystallogr* 53, 240-255.
- Nakagawa, T., Lomb, D.J., Haigis, M.C., and Guarente, L. (2009). SIRT5 Deacetylates carbamoyl phosphate synthetase 1 and regulates the urea cycle. *Cell* 137, 560-570.

- Napper, A.D., Hixon, J., McDonagh, T., Keavey, K., Pons, J.F., Barker, J., Yau, W.T., Amouzegh, P., Flegg, A., Hamelin, E., *et al.* (2005). Discovery of indoles as potent and selective inhibitors of the deacetylase SIRT1. *J Med Chem* 48, 8045-8054.
- Nasrin, N., Kaushik, V.K., Fortier, E., Wall, D., Pearson, K.J., de Cabo, R., and Bordone, L. (2009). JNK1 phosphorylates SIRT1 and promotes its enzymatic activity. *PLoS ONE* 4, e8414.
- Newman, J. (2005). Expanding screening space through the use of alternative reservoirs in vapor-diffusion experiments. *Acta Crystallogr D Biol Crystallogr* 61, 490-493.
- North, B.J., Marshall, B.L., Borra, M.T., Denu, J.M., and Verdin, E. (2003). The human Sir2 ortholog, SIRT2, is an NAD⁺-dependent tubulin deacetylase. *Mol Cell* 11, 437-444.
- Nyborg, J.K., and Peersen, O.B. (2004). That zincing feeling: the effects of EDTA on the behaviour of zinc-binding transcriptional regulators. *Biochem J* 381, e3-e4.
- Olsen, J.V., Vermeulen, M., Santamaria, A., Kumar, C., Miller, M.L., Jensen, L.J., Gnad, F., Cox, J., Jensen, T.S., Nigg, E.A., *et al.* (2010). Quantitative phosphoproteomics reveals widespread full phosphorylation site occupancy during mitosis. *Sci Signal* 3, ra3.
- Outeiro, T.F., Kontopoulos, E., Altmann, S.M., Kufareva, I., Strathearn, K.E., Amore, A.M., Volk, C.B., Maxwell, M.M., Rochet, J.C., McLean, P.J., *et al.* (2007). Sirtuin 2 inhibitors rescue alpha-synuclein-mediated toxicity in models of Parkinson's disease. *Science* 317, 516-519.
- Pacholec, M., Bleasdale, J.E., Chrnyk, B., Cunningham, D., Flynn, D., Garofalo, R.S., Griffith, D., Griffor, M., Loulakis, P., Pabst, B., *et al.* (2010). SRT1720, SRT2183, SRT1460, and Resveratrol Are Not Direct Activators of SIRT1. *Journal of Biological Chemistry* 285, 8340-8351.
- Pan, M., Yuan, H., Brent, M., Ding, E.C., and Marmorstein, R. (2011a). SIRT1 contains N- and C-terminal regions that potentiate deacetylase activity. *Journal of Biological Chemistry*.
- Pan, P.W., Feldman, J.L., Devries, M.K., Dong, A., Edwards, A.M., and Denu, J.M. (2011b). Structure and biochemical functions of SIRT6. *J Biol Chem* 286, 14575-14587.
- Pasco, M.Y., Rotili, D., Altucci, L., Farina, F., Rouleau, G.A., Mai, A., and Néri, C. (2009). Characterization of Sirtuin Inhibitors in Nematodes Expressing a Muscular Dystrophy Protein Reveals Muscle Cell and Behavioral Protection by Specific Sirtinol Analogues. *Journal of Medicinal Chemistry* 53, 1407-1411.
- Pervaiz, S., and Holme, A.L. (2009). Resveratrol: its biologic targets and functional activity. *Antioxid Redox Signal* 11, 2851-2897.
- Peter, S. (2000). Size-Distribution Analysis of Macromolecules by Sedimentation Velocity Ultracentrifugation and Lamm Equation Modeling. *Biophysical Journal* 78, 1606-1619.
- Rajendran, L., Knolker, H.J., and Simons, K. (2010). Subcellular targeting strategies for drug design and delivery. *Nat Rev Drug Discov* 9, 29-42.
- Riesen, M., and Morgan, A. (2009). Calorie restriction reduces rDNA recombination independently of rDNA silencing. *Aging Cell* 8, 624-632.
- Sanders, B.D., Jackson, B., Brent, M., Taylor, A.M., Dang, W., Berger, S.L., Schreiber, S.L., Howitz, K., and Marmorstein, R. (2009). Identification and characterization of novel sirtuin inhibitor scaffolds. *Bioorganic & Medicinal Chemistry* 17, 7031-7041.
- Sanders, B.D., Jackson, B., and Marmorstein, R. (2010). Structural basis for sirtuin function: What we know and what we don't. *Biochimica et Biophysica Acta (BBA) - Proteins & Proteomics* 1804, 1604-1616.
- Sasaki, T., Maier, B., Koclega, K.D., Chruszcz, M., Gluba, W., Stukenberg, P.T., Minor, W., and Scrable, H. (2008). Phosphorylation Regulates SIRT1 Function. *PLoS ONE* 3, e4020.
- Satoh, A., Stein, L., and Imai, S. (2011). The Role of Mammalian Sirtuins in the Regulation of Metabolism, Aging, and Longevity
- Histone Deacetylases: the Biology and Clinical Implication. In, T.-P. Yao, and E. Seto, eds. (Springer Berlin Heidelberg), pp. 125-162.

- Sauve, A.A. (2010). Sirtuin chemical mechanisms. *Biochimica et Biophysica Acta (BBA) - Proteins & Proteomics* 1804, 1591-1603.
- Sauve, A.A., Celic, I., Avalos, J., Deng, H., Boeke, J.D., and Schramm, V.L. (2001). Chemistry of Gene Silencing: The Mechanism of NAD⁺-Dependent Deacetylation Reactions. *Biochemistry* 40, 15456-15463.
- Sauve, A.A., and Schramm, V.L. (2003). Sir2 Regulation by Nicotinamide Results from Switching between Base Exchange and Deacetylation Chemistry†. *Biochemistry* 42, 9249-9256.
- Sauve, A.A., Wolberger, C., Schramm, V.L., and Boeke, J.D. (2006). The biochemistry of sirtuins. *Annu Rev Biochem* 75, 435-465.
- Schlicker, C., Boanca, G., Lakshminarasimhan, M., and Steegborn, C. (2011). Structure-based development of novel sirtuin inhibitors. *Aging (Albany NY)* 3, 852-872.
- Schlicker, C., Gertz, M., Papatheodorou, P., Kachholz, B., Becker, C.F., and Steegborn, C. (2008). Substrates and regulation mechanisms for the human mitochondrial sirtuins Sirt3 and Sirt5. *J Mol Biol* 382, 790-801.
- Schmidt, M.T., Smith, B.C., Jackson, M.D., and Denu, J.M. (2004). Coenzyme Specificity of Sir2 Protein Deacetylases. *Journal of Biological Chemistry* 279, 40122-40129.
- Schuetz, A., Min, J., Antoshenko, T., Wang, C.L., Allali-Hassani, A., Dong, A., Loppnau, P., Vedadi, M., Bochkarev, A., Sternglanz, R., *et al.* (2007). Structural basis of inhibition of the human NAD⁺-dependent deacetylase SIRT5 by suramin. *Structure* 15, 377-389.
- Schutzowski, M., Reimer, U., Panse, S., Dong, L., Lizcano, J.M., Alessi, D.R., and Schneider-Mergener, J. (2004). High-content peptide microarrays for deciphering kinase specificity and biology. *Angew Chem Int Ed Engl* 43, 2671-2674.
- Schuttelkopf, A.W., and van Aalten, D.M. (2004). PRODRG: a tool for high-throughput crystallography of protein-ligand complexes. *Acta Crystallogr D Biol Crystallogr* 60, 1355-1363.
- Sinclair, D.A., and Guarente, L. (1997). Extrachromosomal rDNA circles--a cause of aging in yeast. *Cell* 91, 1033-1042.
- Slabinski, L., Jaroszewski, L., Rychlewski, L., Wilson, I.A., Lesley, S.A., and Godzik, A. (2007). XtalPred: a web server for prediction of protein crystallizability. *Bioinformatics* 23, 3403-3405.
- Smith, B.C., and Denu, J.M. (2006). Sir2 protein deacetylases: evidence for chemical intermediates and functions of a conserved histidine. *Biochemistry* 45, 272-282.
- Smith, B.C., and Denu, J.M. (2007). Mechanism-based inhibition of Sir2 deacetylases by thioacetyl-lysine peptide. *Biochemistry* 46, 14478-14486.
- Smith, B.C., Hallows, W.C., and Denu, J.M. (2008). Mechanisms and Molecular Probes of Sirtuins. *Chemistry & Biology* 15, 1002-1013.
- Smith, B.C., Hallows, W.C., and Denu, J.M. (2009). A continuous microplate assay for sirtuins and nicotinamide-producing enzymes. *Anal Biochem* 394, 101-109.
- Smith, J.S., Avalos, J., Celic, I., Muhammad, S., Wolberger, C., and Boeke, J.D. (2002). SIR2 family of NAD(+) -dependent protein deacetylases. *Methods Enzymol* 353, 282-300.
- Suzuki, T., Asaba, T., Imai, E., Tsumoto, H., Nakagawa, H., and Miyata, N. (2009). Identification of a cell-active non-peptide sirtuin inhibitor containing N-thioacetyl lysine. *Bioorganic & Medicinal Chemistry Letters* 19, 5670-5672.
- Tanny, J.C., Dowd, G.J., Huang, J., Hilz, H., and Moazed, D. (1999). An enzymatic activity in the yeast Sir2 protein that is essential for gene silencing. *Cell* 99, 735-745.
- Tennen, R.I., Berber, E., and Chua, K.F. (2010). Functional dissection of SIRT6: identification of domains that regulate histone deacetylase activity and chromatin localization. *Mech Ageing Dev* 131, 185-192.

- Trapp, J., Meier, R., Hongwiset, D., Kassack, M.U., Sippl, W., and Jung, M. (2007). Structure–Activity Studies on Suramin Analogues as Inhibitors of NAD⁺-Dependent Histone Deacetylases (Sirtuins). *ChemMedChem* 2, 1419-1431.
- Vakhrusheva, O., Smolka, C., Gajawada, P., Kostin, S., Boettger, T., Kubin, T., Braun, T., and Bober, E. (2008). Sirt7 increases stress resistance of cardiomyocytes and prevents apoptosis and inflammatory cardiomyopathy in mice. *Circ Res* 102, 703-710.
- Vaquero, A., Scher, M., Lee, D., Erdjument-Bromage, H., Tempst, P., and Reinberg, D. (2004). Human SirT1 interacts with histone H1 and promotes formation of facultative heterochromatin. *Mol Cell* 16, 93-105.
- Vaziri, H., Dessain, S.K., Ng Eaton, E., Imai, S.I., Frye, R.A., Pandita, T.K., Guarente, L., and Weinberg, R.A. (2001). hSIR2(SIRT1) functions as an NAD-dependent p53 deacetylase. *Cell* 107, 149-159.
- Viswanathan, M., Kim, S.K., Berdichevsky, A., and Guarente, L. (2005). A role for SIR-2.1 regulation of ER stress response genes in determining *C. elegans* life span. *Dev Cell* 9, 605-615.
- Wood, J.G., Rogina, B., Lavu, S., Howitz, K., Helfand, S.L., Tatar, M., and Sinclair, D. (2004). Sirtuin activators mimic caloric restriction and delay ageing in metazoans. *Nature* 430, 686-689.
- Yang, H., Yang, T., Baur, J.A., Perez, E., Matsui, T., Carmona, J.J., Lamming, Dudley W., Souza-Pinto, N.C., Bohr, V.A., Rosenzweig, A., *et al.* (2007a). Nutrient-Sensitive Mitochondrial NAD⁺ Levels Dictate Cell Survival. *Cell* 130, 1095-1107.
- Yang, Y., Fu, W., Chen, J., Olashaw, N., Zhang, X., Nicosia, S.V., Bhalla, K., and Bai, W. (2007b). SIRT1 sumoylation regulates its deacetylase activity and cellular response to genotoxic stress. *Nat Cell Biol* 9, 1253-1262.
- Zhang, Z., Tan, M., Xie, Z., Dai, L., Chen, Y., and Zhao, Y. (2011). Identification of lysine succinylation as a new post-translational modification. *Nat Chem Biol* 7, 58-63.
- Zhao, K., Chai, X., Clements, A., and Marmorstein, R. (2003). Structure and autoregulation of the yeast Hst2 homolog of Sir2. *Nat Struct Biol* 10, 864-871.
- Zhao, W., Kruse, J.-P., Tang, Y., Jung, S.Y., Qin, J., and Gu, W. (2008). Negative regulation of the deacetylase SIRT1 by DBC1. *Nature* 451, 587-590.
- Zorn, J.A., and Wells, J.A. (2010). Turning enzymes ON with small molecules. *Nat Chem Biol* 6, 179-188.
- Zschoernig, B., and Mahlknecht, U. (2009). Carboxy-terminal phosphorylation of SIRT1 by protein kinase CK2. *Biochemical and Biophysical Research Communications* 381, 372-377.

8. Appendix

Table S1: A list of primers used in this study along with their start and stop positions and restriction enzymes that recognize them.

Name	Position	Stop codon	Restriction site	Sequence
hsirt1_225_ndeif	225	NA	NdeI	CGG CCG CGC CAT ATG ATT AAT ATC CTT TCA GAA CCA CC
hsirt1_664_Nostop_xhoir	664	No	XhoI	GCA AGC GCG CTC GAG GTC ATC TTC AGA GTC TGA ATA TAC
hsirt1_225_ndeif_new_f	225	NA	NdeI	CAG CTG CGC CAT ATG ATT AAT ATC CTT TCA GAA CCA CC
hsirt1_664_xhoif_new_r	664	No	XhoI	GCA ATC GCG CTC GAG GTC ATC TTC AGA GTC TGA ATA TAC
hsirt1_225_quick_chng_f	225	NA	NdeI	GA AAT AAT TTT GTT TAA CTT TAA GAA GGA GAT ATA CAT ATGATT
hsirt1_664_quick_chng_r	664	No	XhoI	CGG ATC TCA GTG GTG GTG GTG GTG GTG CTC GAG GTC ATC TTC AGA
flsirt1_sdm_xhoif		NA		GAT GGT CCC GGC CTG GAG CGG AGC CCG
flsirt1_sdm_xhoir		NA		CGG GCT CCG CTC CAG GCC GGG ACC ATC
hsirt1_fl_ndeif	1	NA	NdeI	CAG ATC ATA CAT ATG GCG GAC GAG GCG
hsirt1_fl_xhoi_Nostop_r	747	No	XhoI	GCA ATC GCG CTC GAG TGA TTT GTT TGA TGG
hsirt1_int	101	NA		GGA GAC AAT GGG CCG GGC CTG CAG GGC
hsirt1_fl_xhoir	747	Yes	XhoI	GCA GTC GCG CTC GAG CTA TGA TTT GTT TGA TGG
hsirt1_v313a_revert_f		NA		CCA TTC TTC AAG TTT GCA AAG GAA ATA TAT CC
hsirt1_v313a_revert_r				GG ATA TAT TTC CTT TGC AAA CTT GAA GAA TGG
sirt1_576-578_eek_aaa_f				CA AAA GGT TGT ATG GCA GCA GCA CCA CAG GAA GTA C
sirt1_576-578_eek_aaa_r				G TAC TTC CTG TGG TGC TGC TGC CAT ACA ACC TTT TG
hsirt1_664_stop_xhoir	664	Yes	XhoI	GCA AGC GCT CTC GAG TCA GTC ATC TTC AGA GTC
hsirt1_fl_eheif	1	NA	EheI	GTT AAA GGC GCC ATG GCG GAC GAG GCG
hsirt1_214_lic_pET15b_f	214	NA	NdeI	CAC AGC AGC GGC CTG GTG CCG CGC GGC AGC CAT
hsirt1_225_lic_pET15b_f	225	NA	NdeI	CAC AGC AGC GGC CTG GTG CCG CGC GGC AGC CAT ATG ATT AAT ATC
hsirt1_214_lic_pET21a_f	214	NA	NdeI	GA AAT AAT TTT GTT TAA CTT TAA GAA GGA GAT ATA CAT ATG GAG
hsirt1_664_lic_pET15b_r	664	Yes	XhoI	CTT TCG GGC TTT GTT AGC AGC CGG ATC CTC GAG TTA GTC ATC TTC
hsirt1_1_lic_pET15b_f	1	NA	NdeI	CAC AGC AGC GGC CTG GTG CCG CGC GGC AGC CAT ATG GCG GAC GAG
hsirt1_747_lic_pET15b_r	747	Yes	XhoI	CTT TCG GGC TTT GTT AGC AGC CGG ATC CTC GAG CTA TGA TTT GTT
hsirt1_1_lic_pET21a_f	1	NA	NdeI	GA AAT AAT TTT GTT TAA CTT TAA GAA GGA GAT ATA CAT ATG GCG

hsirt1_747_lic_pET21a_r	747	No	XhoI	CGG ATC TCA GTG GTG GTG GTG GTG GTG CTC GAG TGA TTT GTT TGA
hsirt1_183_lic_pET15b_f	183	NA	NdeI	CAC AGC AGC GGC CTG GTG CCG CGC GGC AGC CAT ATG GGT CCA TAT
hsirt1_183_lic_pET21a_f	183	NA	NdeI	GA AAT AAT TTT GTT TAA CTT TAA GAA GGA GAT ATA CAT ATG GGT
hsirt1_229_ndeifor	229	NA	NdeI	CAG GCG CAT ATG TCA GAA CCA CCA AAA AGG
hsirt1_516_xhoi_rev	516	Yes	XhoI	GAC CAC CTC GAG TCA TCG TGG AGG TTT TTC
hsirt1_h363a_f		NA		GG ATA ATT CAG TGT GCT GGT TCC TTT GCA AC
hsirt1_h363a_r		NA		GT TGC AAA GGA ACC AGC ACA CTG AAT TAT CC
hsirt1_t530d_f		NA		GAG TTG CCA CCC GAC CCT CTT CAT GTT TC
hsirt1_t530d_r		NA		GA AAC ATG AAG AGG GTC GGG TGG CAA CTC
hsirt1_245_lic_pET15b_f	245	NA	NdeI	CAC AGC AGC GGC CTG GTG CCG CGC GGC AGC CAT ATG GAT GCT GTG
hsirt1_510_lic_pET15b_r	510	Yes	XhoI	CTT TCG GGC TTT GTT AGC AGC CGG ATC CTC GAG TTA AAT TTC TGA
hS1_129_licp15F	129	NA	NdeI	CAC AGC AGC GGC CTG GTG CCG CGC GGC AGC CAT ATG GGC GAG GAG
hS1_181_licp15F	181	NA	NdeI	CAC AGC AGC GGC CTG GTG CCG CGC GGC AGC CAT ATG CGG ATA GGT
hS1_217_licp15F	217	NA	NdeI	CAC AGC AGC GGC CTG GTG CCG CGC GGC AGC CAT ATG GAT ATG ACA
hs1_527_licp15R	527	Yes	XhoI	CTT TCG GGC TTT GTT AGC AGC CGG ATC CTC GAG CTA CAA CTC TGA
hsirt1_p15_tevF	1	NA	NdeI	CAT CAT CAT CAC AGC AGC GGC GAA AAC CTG TAT TTT CAG GGA CAT
hsirt1_p15_tevR		NA	NdeI	CGC CTC GTC CGC CAT ATG TCC CTG AAA ATA CAG GTT TTC GCC GCT
msirt1_ndeifl_f	1	NA	NdeI	CAT ATA TAC CAT ATG GCG GAC GAG GTG GCG
msirt1_xhoifl_f	1	NA	XhoI	CAT ATA TAC CTC GAG ATG GCG GAC GAG GTG
msirt1_salifl_f	1	NA	Sall	CAT ATA TAC GTC GAC ATG GCG GAC GAG GTG
msirt1_xhoifl_r	737	Yes	XhoI	GCA GTC GCG CTC GAG TTA TGA TTT GTC TGA TGG
msirt1_xhoifl_Nostop_r	737	No	XhoI	GCA GTC GCG CTC GAG TGA TTT GTC TGA TGG
msirt1_206_ndeif	206	NA	NdeI	CAG CTG CGC CAT ATG GAG CTG GAT GAT ATG
msirt1_508_xhoir	508	Yes	XhoI	GCA ATC GCG CTC GAG TTA GCG TGG AGG TTT TTC
msirt1_222_ndeif	222	NA	NdeI	CAG CTG CGA CAT ATG GAA CCA CCA AAG CGG
msirt1_483_xhoir	483	Yes	XhoI	GCA GTC GCG CTC GAG TTA ATG ACA CAA CTC
msirt1_522_xhoir	522	Yes	XhoI	GTA GAT GCG CTC GAG TTA TGT TGG TGG CAA CTC
msirt1_483_Nostop_xhoi_	483	No	XhoI	GCA GTC GCG CTC GAG ATG ACA CAA CTC
msirt1_508_Nostop_xhoi_	508	No	XhoI	GCA ATC GCG CTC GAG GCG TGG AGG TTT TTC
msirt1_ndeifl_new_f	1	NA	NdeI	CAT ATA TAC CAT ATG GCG GAC GAG GTG GCG CTC GCC CTT CAG
msirt1_xhoifl_new_r	737	Yes	XhoI	GCA GTC GCG CTC GAG TTA TGA TTT GTC TGA TGG ATA GTT TAC

aros_1_lic_pET15b_f	1	NA	NdeI	CAC AGC AGC GGC CTG GTG CCG CGC GGC AGC CAT ATG TCC GCC GCC
aros_136_lic_pET15b_r	136	Yes	XhoI	CTT TCG GGC TTT GTT AGC AGC CGG ATC CTC GAG CTA GCT GCC GAA
aros_1_pGEX_f	1	NA	BamHI	GTT CCG CGT GGA TCC ATG TCC GCC GCC CTG CTG
aros_1_kpnI_f	1	NA	KpnI	GTT AAT TAT GGT ACC ATG TCC GCC GCC CTG CTG
aros136HindIII_r	136	Yes	HindIII	GCTGGACTGAAGCTTCTAGCTGCCGAAGTATTCCTGCTG
hsirt3C259Afor		NA		TGC CAC CTG CAC AGT CGC ACA AAG ACC CTT CCC AG
hsirt3C259Arev		NA		CTG GGA AGG GTC TTT GTG CGA CTG TGC AGG TGG CA
hsirt3C280Afor		NA		AGA CAG GGT TCC CCG CGC ACC GGT CTG CAC CGG CGT TGT
hsirt3C280Arev		NA		ACA ACG CCG GTG CAG ACC GGT GCG CGG GGA ACC CTG TCT
fwd_pOPIN		NA		TACGACTCACTATAGGGGAATTGTG
rev_pOPIN		NA		GATCGATCTCAGTGGTATTTGTG
hSirt7_T224D_f		NA		CAGACAGGCCGGGACTGCCACAAG
hSirt7_T224D_r		NA		CTTGTGGCAGTCCCGGCCTGTCTG

Table S2: Crystallization trials of Sirt1. The table shows various constructs of Sirt1 (both human and mouse) used in the crystallization process along with the conditions. The construct 82-664 contains Met, Ala and Asp before the N-terminus, a result of cloning artifact.

Sirt1 Construct	Protein concentration	Screen	Temperature (° C)	Sample volume (ul)	Method	Comments
Full length	9	Microlytic capillary tray	18		capillary /manual setting	
Full length	9	JCSG (Molecular Dimensions)	18	1	Sitting drop/Manual	
Full length	5	Index Screen (Hampton)	18	1	Sitting drop/Manual	
Full length	5	Index Screen (Hampton)	18	1	Sitting drop/Manual	Tag cleaved
Full length	4.6	JCSG (Molecular Dimensions)	18	1	Sitting drop/Manual	Protein + 1 mM p53 + 1 mM PCT + 1 mM ADPr
Full length	4.6	JCSG (Molecular Dimensions)	4	1	Sitting drop/Manual	Protein + 1 mM p53 + 1 mM PCT + 1 mM ADPr
Full length	8	Additive screen (Hampton)	18	1	Sitting drop/Manual	Protein+ 1 mM p53 + 1 mM NADH

Full length	10	JCSG (Molecular Dimensions)	18	1	Sitting drop/Manual	Protein + 1 mM p53 + 1 mM ADPr + 100 μ M SRT1720
Full length	10	PACT (Molecular Dimensions)	18	1	Sitting drop/Manual	Protein + 1 mM p53 + 1 mM ADPr + 100 μ M SRT1720
Full length	10	JCSG Core I (Qiagen)	18	1	Sitting drop/Manual	
Full length	8	JCSG Core I (Qiagen)	18	1	Sitting drop/Manual	In situ Proteolysis with 1000:1 Chymotrypsin
Full length	8	JCSG Core I (Qiagen)	18	1	Sitting drop/Manual	In situ Proteolysis with 1000:1 Trypsin
Full length	5	JCSG Core I (Qiagen)	20	0.5	Sitting drop/Manual	Protein + 1 mM H3 + 500 μ M Resveratrol
Full length	5	JCSG Core I (Qiagen)	20	0.5	Sitting drop/Manual	Protein+ 1 mM H3 + 500 μ M Resveratrol
1-664	5	Pentaerythritol (Jena Biosciences)	18	1	Sitting drop/Manual	
1-664	5	JCSG (Molecular Dimensions)	18	1	Sitting drop/Manual	
1-664	5	Microlytic capillary tray	18		capillary /manual setting	
1-664	4.7	Pentaerythritol (Jena Biosciences)	18	1	Sitting drop/Manual	Protein + 1 mM Resveratrol + 3 mM ADPr + 1 mM p53
1-664	4.7	Pentaerythritol (Jena Biosciences)	18	1	Sitting drop/Manual	Protein + 1 mM NADH + 1 mM p53
1-664	4.7	JCSG (Molecular Dimensions)	18	1	Sitting drop/Manual	Protein + 1 mM p53 + 3 mM ADPr + 1 mM Piceatannol
1-664	4.7	JCSG (Molecular Dimensions)	18	1	Sitting drop/Manual	Protein + 1 mM p53 + 1 mM NADH
1-664	5	Structure Screen (Molecular Dimensions)	18	1	Sitting drop/Manual	
1-664	5	PEG Ion (Hampton)	18	1	Sitting drop/Manual	
1-664	5	JCSG Core I (Qiagen)	18	1	Sitting drop/Manual	
1-664	5	JCSG Core I (Qiagen)	18	1	Sitting drop/Robot	In situ Proteolysis with 10000:1 Trypsin
1-664	10	JCSG Core IV (Qiagen)	20	0.1	Sitting drop/Robot	Protein + 1 mM NAD

1-664	10	JCSG Core IV (Qiagen)	20	0.1	Sitting drop/Robot	Protein + 1 mM EthenoNAD
1-664	10	JCSG Core IV (Qiagen)	20	0.1	Sitting drop/Robot	Protein + 1 mM EthenoNAD + 1mM p53
82-664	10	Pentaerythritol (Jena Biosciences)	18	1	Sitting drop/Manual	
82-664	10	JCSG Core I (Qiagen)	18	1	Sitting drop/Manual	
82-664	4.3	JCSG Core II (Qiagen)	20	0.1	Sitting drop/Robot	3 different Drop sizes: A). 0.1 μ l + 0.1 μ l drop ; B). 0.1 μ l + 0.15 μ l drop; C). 0.15 μ l + 0.15 μ l drop
82-664	4.3	JCSG Core III (Qiagen)	20	0.1	Sitting drop/Robot	3 different Drop sizes: A). 0.1 μ l + 0.1 μ l drop ; B). 0.1 μ l + 0.15 μ l drop; C).0.15 μ l + 0.15 μ l drop
82-664	4.3	JCSG Core IV (Qiagen)	20	0.1	Sitting drop/Robot	3 different Drop sizes: A). 0.1 μ l + 0.1 μ l drop ; B). 0.1 μ l + 0.15 μ l drop; C).0.15 μ l + 0.15 μ l drop
82-664	5	JCSG Core I (Qiagen)	20	0.5	Sitting drop/Manual	Protein + 1 mM H3 + 500 μ M Resveratrol
82-664	5	JCSG Core I (Qiagen)	20	0.5	Sitting drop/Manual	Protein + 1 mM H3 + 500 μ M Resveratrol
129-747	6	JCSG Core I (Qiagen)	20	0.1	Sitting drop/Robot	
129-747	6	JCSG Core II (Qiagen)	20	0.1	Sitting drop/Robot	
129-747	6	JCSG Core III (Qiagen)	20	0.1	Sitting drop/Robot	
129-747	6	JCSG Core IV (Qiagen)	20	0.1	Sitting drop/Robot	
181-747	6.6	JCSG Core I (Qiagen)	20	0.1	Sitting drop/Robot	
181-747	6.6	JCSG Core II (Qiagen)	20	0.1	Sitting drop/Robot	
181-747	6.6	JCSG Core III (Qiagen)	20	0.1	Sitting drop/Robot	
181-747	6.6	JCSG Core IV (Qiagen)	20	0.1	Sitting drop/Robot	

225-747	6.3	JCSG Core I (Qiagen)	20	0.1	Sitting drop/Robot	A). Protein alone; B). Protein + 1 mM p53 + 1 mM ADPr ; C). Protein + 50 μ M Ex527 + 1 mM p53 + 1 mM ADPr
225-747	6.3	JCSG Core II (Qiagen)	20	0.1	Sitting drop/Robot	A). protein alone; B). Protein + 1 mM p53 + 1 mM ADPr ; C). Protein +50 μ M Ex527 + 1 mM p53 + 1 mM ADPr
225-747	6.3	JCSG Core III (Qiagen)	20	0.1	Sitting drop/Robot	A). protein alone; B). Protein + 1 mM p53 + 1 mM ADPr ; C). Protein +50 μ M Ex527 + 1 mM p53 + 1 mM ADPr
225-747	6.3	JCSG Core IV (Qiagen)	20	0.1	Sitting drop/Robot	A). protein alone; B). Protein + 1 mM p53 + 1 mM ADPr ; C). Protein +50 μ M Ex527 + 1 mM p53 + 1 mM ADPr
183-664	5	JCSG Core I (Qiagen)	18	1	Sitting drop/Manual	
183-664	4.8	JCSG + (Molecular Dimensions)	20	0.1	Sitting drop/Robot	Protein+ 1 mM H3 + 1 mM ADPr + 500 μ M Resveratrol
183-664	4.8	JCSG + (Molecular Dimensions)	20	0.1	Sitting drop/Robot	Protein +1 mM NAM + 1 mM H3 + 1 mM ADPr + 500 μ M Resveratrol
183-664 T530D	5	JCSG Core I (Qiagen)	20	0.1	Sitting drop/Robot	A). Protein alone B).Protein + 1 mM H3 C). Protein + 1 mM H3 + 500 μ M Resveratrol
183-664 T530D	5	JCSG Core II (Qiagen)	20	0.1	Sitting drop/Robot	A). Protein alone B).Protein + 1 mM H3 C). Protein + 1 mM H3 + 500 μ M Resveratrol
183-664 T530D	5	JCSG Core III (Qiagen)	20	0.1	Sitting drop/Robot	A). Protein alone B).Protein + 1 mM H3 C). Protein + 1 mM H3 + 500 μ M Resveratrol
183-664 T530D	5	JCSG Core IV (Qiagen)	20	0.1	Sitting drop/Robot	A). Protein alone B).Protein + 1 mM H3 C). Protein + 1 mM H3 + 500 μ M Resveratrol
183-664 T530D	5	JCSG Core I (Qiagen) with Alternative reservoir 50% PEG 3350	20	0.1	Sitting drop/Robot	A). Protein alone B).Protein + 1 mM H3 C). Protein + 1 mM H3 + 500 μ M Resveratrol
HSIRT 1 183-664 T530D	5	JCSG Core II (Qiagen) with Alternative reservoir 50% PEG 3350	20	0.1	Sitting drop/Robot	A). Protein alone B).Protein + 1 mM H3 C). Protein + 1 mM H3 + 500 μ M Resveratrol
183-664 T530D	5	JCSG Core III (Qiagen) with Alternative reservoir 50% PEG 3350	20	0.1	Sitting drop/Robot	A). Protein alone B).Protein + 1 mM H3 C). Protein + 1 mM H3 + 500 μ M Resveratrol

183-664 T530D	5	JCSG Core IV (Qiagen) with Alternative reservoir 50% PEG 3350	20	0.1	Sitting drop/Robot	A). Protein alone B).Protein + 1 mM H3 C). Protein + 1 mM H3 + 500 μ M Resveratrol
214-664	5	Pentaerythritol (Jena Biosciences)	18	1	Sitting drop/Manual	
214-664	6.7	Structure Screen (Molecular Dimensions)	18	1	Sitting drop/Manual	
214-664	6.7	PEG Ion Hampton	18	1	Sitting drop/Manual	
225-664	4.86	Structure Screen (Molecularr Dimensions)	18	0.125	Sitting drop/Robot	3 drops: 1st hSirt1+p53 paptide, 2 nd hSirt1+NAD, 3 rd hSirt1+p53+ADPr
225-664	15	Pact (Molecularr Dimensions)	18	1	Sitting drop/Manual	
225-664	15	Index Hampton	18	0.125	Sitting drop/Robot	A) protein alone, B) Protein + NAD, C) Protein + ADR and p53
225-664	15	PEG Ion (Hampton)	18	0.125	Sitting drop/Robot	A) Protein + 20 % (v/v) DMSO, B) Protein + NAD, C) Protein + ADPr and p53
225-664	15	Structure Screen (Molecularr Dimensions)	18	0.125	Sitting drop/Robot	A) Protein + 20 % (v/v) DMSO, B) Methylated protein, C) Protein +
225-664	15	PEG Ion (Hampton)	18	0.125	Sitting drop/Robot	3 drops:Protein + 20 % (v/v) DMSO, B) Methylated protein, C) Protein +
225-664	10	Pact I (Molecularr Dimensions) with Alternative reservoir 1.5 M NaCl	18	0.7	Sitting drop/Manual	
225-664	5	Pact II (Molecularr Dimensions) with Alternative reservoir 1.5 M NaCl	18	0.7	Sitting drop/Manual	
225-664	10	Microlytic capillary tray	18		New capillary manual setting	Greiner Microfluidic diffusion chips
225-664	10	Structure (Molecularr Dimensions)	18	0.7	Sitting drop/Manual	In situ Proteolysis with 1000:1 Trypsin
225-664	10	Structure (Molecularr Dimensions)	18	0.7	Sitting drop/Manual	In situ Proteolysis with 1000:1 Trypsin
225-664	10	JCSG (Molecular Dimensions)	18	1	Sitting drop/Manual	
225-664	10	Crystal HARP (molecular Dimensions)	18	23 μ l total protein	capillary/manual	Capillary Diffusion Principle

225-664 H363A	5	JCSG (Molecular Dimensions)	18	1	Sitting drop/Manual	Catalytic Histidine mutant
225-664	10	Microlytic capillary tray	18		New capillary manual setting	Catalytic Histidine mutant
225-664 H363A	5	PACT I (Molecular Dimensions)	18	1	Sitting drop/Manual	Catalytic Histidine mutant
225-664 H363A	5	PACT II (Molecular Dimensions)	18	1	Sitting drop/Manual	Catalytic Histidine mutant
225-664 H363A	5	PEG Ion (Hampton)	18	1	Sitting drop/Manual	Catalytic Histidine mutant
225-664 SER	10	Pentaerythritol (Jena Biosciences)	18	1	Sitting drop/Manual	SER= Surface Entropy Reduction mutant EEK-AAA (574-578)
225-664 SER	10	JCSG (Molecular Dimensions)	18	1	Sitting drop/Manual	SER= Surface Entropy Reduction mutant EEK-AAA (574-578)
225-664 SER	5	JCSG Core II (Qiagen)	18	1	Sitting drop/Manual	SER= Surface Entropy Reduction mutant EEK-AAA (574-578)
225-664	10	JCSG Core I (Qiagen)	20	0.1	Sitting drop/Robot	Trypsinized protein
225-664	10	JCSG Core I (Qiagen)	20	0.1	Sitting drop/Robot	Trypsinized protein + 1 mM H3 + 1 mM ADPr
225-664	10	JCSG Core I (Qiagen)	20	0.1	Sitting drop/Robot	Trypsinized protein + 1 mM H3 + 1 mM ADPr + 200 μ M Resveratrol
225-664 H363A	5	JCSG Core II (Qiagen)	18	1	Sitting drop/Robot	Catalytic Histidine mutant
225-664 H363A	4.7	JCSG Core II (Qiagen)	20	0.1	Sitting drop/Robot	Catalytic Histidine mutant +1 mM p53 + 2 mM ADPr
225-664 H363A	4.7	JCSG Core II (Qiagen)	20	0.1	Sitting drop/Robot	Catalytic Histidine mutant +1 mM p53 + 2 mM NAD
225-664 H363A	4.7	JCSG Core II (Qiagen)	20	0.1	Sitting drop/Robot	Catalytic Histidine mutant +1 mM p53 + 2 mM NAD + 500 μ M Resveratrol
225-664 H363A	4.7	JCSG Core III (Qiagen)	20	0.1	Sitting drop/Robot	Catalytic Histidine mutant +1 mM p53 + 2 mM ADPr
225-664 H363A	4.7	JCSG Core III (Qiagen)	20	0.1	Sitting drop/Robot	Catalytic Histidine mutant +1 mM p53 + 2 mM NAD
225-664 H363A	4.7	JCSG Core III (Qiagen)	20	0.1	Sitting drop/Robot	Catalytic Histidine mutant +1 mM p53 + 2 mM NAD + 500 μ M Resveratrol
225-664 SER	5	JCSG Core I (Qiagen)	20	0.1	Phoenix Robot	SER= Surface Entropy Reduction mutant EEK-AAA (574-578)

225-664 SER	5	JCSG Core I (Qiagen)	20	0.1	Phoenix Robot	SER= Surface Entropy Reduction mutant EEK-AAA (574-578)
225-664 SER	5	JCSG Core III (Qiagen)	20	0.1	Phoenix Robot	SER= Surface Entropy Reduction mutant EEK-AAA (574-578)
225-664 SER	5	JCSG Core IV (Qiagen)	20	0.1	Phoenix Robot	SER= Surface Entropy Reduction mutant EEK-AAA (574-578)
229-516	5	JCSG (Molecular Dimensions)	20	0.1	Sitting drop/Robot	Tag cleaved
229-516	5	JCSG (Molecular Dimensions)	20	0.1	Sitting drop/Robot	Protein + 1mM p53
229-516	5	JCSG I Core (Qiagen)	20	0.5	Sitting drop/Manual	
229-516	5	JCSG II Core (Qiagen)	20	0.5	Sitting drop/Manual	
229-516	5	JCSG I Core (Qiagen)	20	0.5	Sitting drop/Manual	Protein + 1.5 mM Ex527 + 0.5 mM p53 +2 mM NAD
229-516	5	JCSG II Core (Qiagen)	20	0.5	Sitting drop/Manual	Protein+ 1.5 mM Ex527 + 0.5 mM p53 +2 mM NAD
229-516	5	JCSG III Core (Qiagen)	20	0.5	Sitting drop/Manual	Protein
229-516	5	JCSG III Core (Qiagen)	20	0.5	Sitting drop/Manual	Protein + 1.5 mM Ex527 + 0.5 mM p53 + 2 mM NAD
206-737	20	Index (Hampton)	18	1	Sitting drop/Manual	Mouse Sirt1
206-737	20	Structure (Molecular Dimensions)	18	1	Sitting drop/Manual	Mouse Sirt1
206-737	10	Structure (Molecular Dimensions)	18	0.125	Sitting drop/Robot	A) Mouse Sirt1 +1 mM p53, B) Protein + NAD, C) Protein +ADPr and p53
206-737	10	PEG Ion (Hampton)	18	0.125	Sitting drop/Robot	A) Mouse Sirt1 + p53, Protein + NAD, Protein + ADPr and + p53

Table S3: Crystallization trials of Sirt7. The table shows various constructs of Sirt7 used in the crystallization process along with the conditions.

Sirt7 Construct	Protein concentration (mg/ml)	Screen	Temperature (° C)	Sample volume (µl)	Method	Comments
Full length	5	JCSG Core	20	0.1	Sitting drop/Robot	
14-367	9.2	JCSG Core	20	0.1	Sitting drop/Robot	
14-367	9.2	JCSG+	18	0.7	Sitting drop/ Manual	
14-367	9.2	JCSG Core	20	0.1	Sitting drop/ Robot	
14-367	9.2	JCSG Core	20	0.1	Sitting drop/ Robot	In situ proteolysis with 1/10000th Trypsin
14-367	9.2	JCSG Core	20	0.1	Sitting drop/ Robot	In situ proteolysis with 1/10000th Chymotrypsin
59-356	5	JCSG Core	20	0.1	Sitting drop/Robot	
81-356	4.7	Pact1&2	18	1	Sitting drop/ Manual	
81-356	4.7	JCSG Core	18	1	Sitting drop/ Manual	
81-356	6.8	JCSG Core	18	1	Sitting drop/ Manual	After CEC
81-356	6.8	JCSG Core	18	1	Sitting drop/ Manual	In situ proteolysis with 1/1000th Trypsin
81-356	6.8	JCSG Core	18	1	Sitting drop/ Manual	In situ proteolysis with 1/1000th Chymotrypsin
81-356	6.8	JCSG Core	18	1	Sitting drop/ Manual	In situ proteolysis with 1/10000th Subtilisin

Table S4: List of peptides and their sequence used in this work. The Thio-H3 = thioacetyllysine.

Peptide name	Protein name	Sequence	Acetylated
p53sh (p53 short)	p53	RHKK[Ac]LMFK	Lys382
p53lg (p53 long)	p53	STSRHKK[ac]LMFKTE	Lys382
H3	Histone 3	IHAK[ac]RVT	Lys116
Thio-H3	Histone 3	IHAK[thio-ac]RVT	Lys116
HMG-B1	High Mobility Group B1	KKPRGK[ac]MSSY	Lys12
SF38A	Pre-mRNA-splicing factor 38A	PQYLVEK[Ac]IIRTRI	Lys23
TFIID	Transcription initiation factor TFIID subunit 3	DREKGKK[Ac]DKDKRE	Lys628
Ku70	Ku70	TKRK[Ac]HDN	Lys544
AAATase	Aspartate aminotransferase 2	VFLPK[ac]PTWG	Lys159

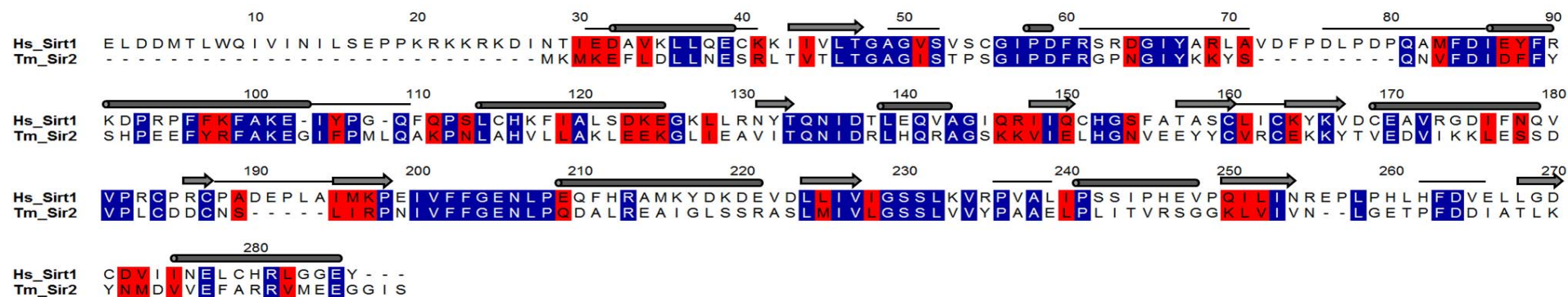


Figure S1: Sequence alignment of human Sirt1 catalytic domain (214-497) (Hs_Sirt1) and Sir2Tm (Tm_Sir2) with secondary structure elements from Sir2Tm. The alignment was created using BioEdit (Hall, 1999).

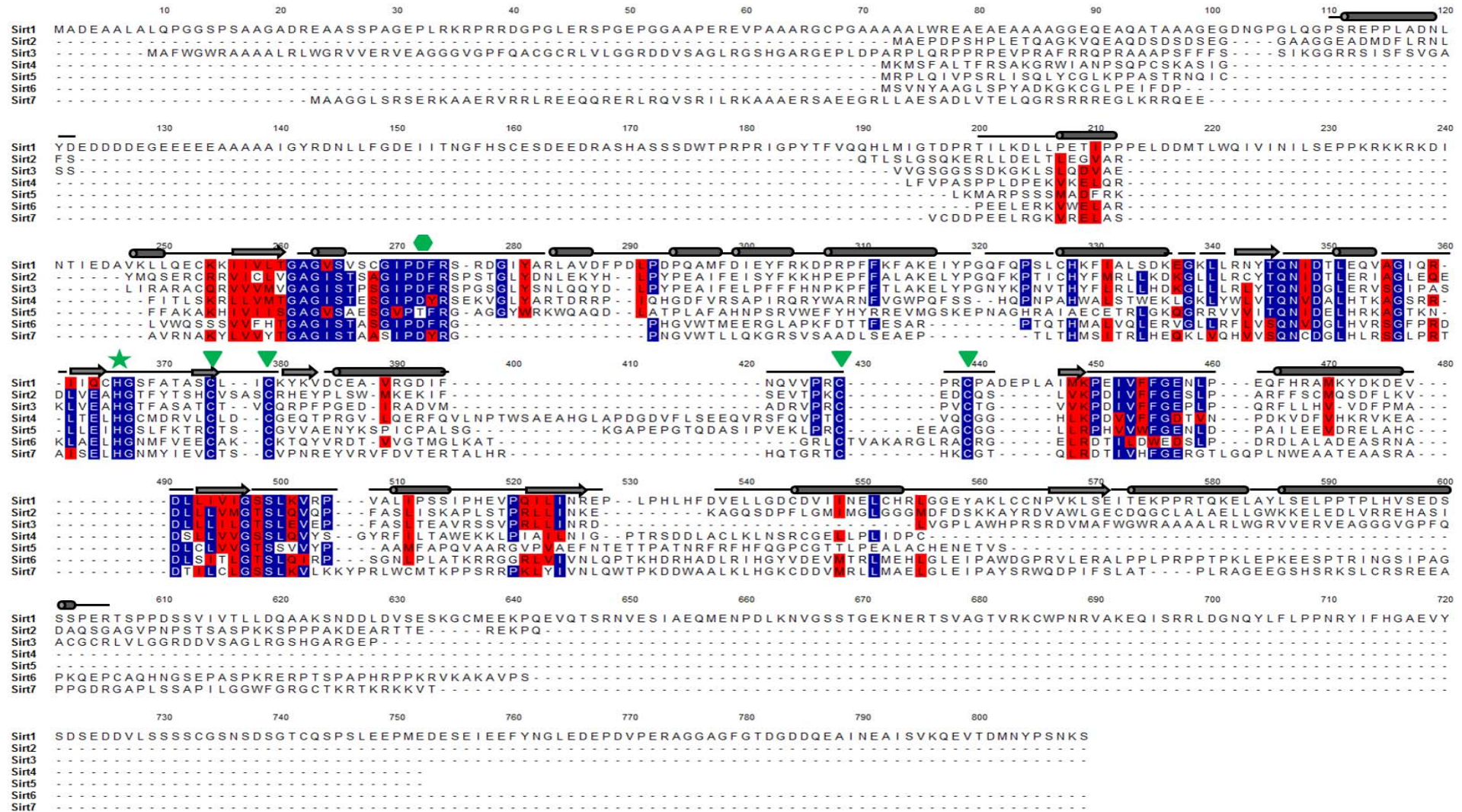


Figure S2: Multiple sequence alignment of all the seven human Sirtuin isoforms. The secondary structure elements correspond to the structure of Sirt2 (1J8F). The numbering corresponds to Sirt1. The catalytic Histidine (indicated as green star), Cysteines coordinating Zn²⁺ (green triangles) and the Thr69 of Sirt5 (green hexagon) are indicated on top of the residues. The alignment was created using BioEdit (Hall, 1999).

9. Erklärung

Hiermit erkläre ich, dass ich die Arbeit selbständig verfasst und keine anderen als die von mir angegebenen Quellen und Hilfsmittel benutzt habe.

Ferner erkläre ich, dass ich anderweitig mit oder ohne Erfolg nicht versucht habe, diese Dissertation einzureichen. Ich habe keine gleichartige Doktorprüfung an einer anderen Hochschule endgültig nicht bestanden.

Bayreuth, Date: 7th March, 2012

Mahadevan Lakshminarasimhan

Declaration

I hereby declare that this dissertation is my own original work and that I have acknowledged all sources used.

Furthermore I declare that I have not attempted, with or without success, to submit this dissertation to any other academic institution and that I have not failed a similar doctoral exam at any other academic institution.

Bayreuth, Date: 7th March, 2012

Mahadevan Lakshminarasimhan